UNIVERSIDADE da MADEIRA

N° de ordem: 9/D/07   Ano de 2007

TESE DE DOUTORAMENTO

apresentada na
UNIVERSIDADE DA MADEIRA

Para obtenção do grau de Doutor

César Esmeraldo Fernandes

Argilas Modificadas como Catalisadores Ácidos Sólidos

Júri:

Presidente:
Doutor Pedro Telhado Pereira   Reitor da Universidade da Madeira

Vogais:
Doutor Christopher Breen   Professor Catedrático da
                                               Universidade de Sheffield Hallam
Doutor Miguel Angel Vicente Rodríguez   Professor Titular da
                                               Universidade de Salamanca
Doutora Maria Manuela L. Ribeiro Carrott   Professora Associada da
                                               Universidade de Évora
Doutora Paula Cristina M. F. Castilho   Professora Associada da
                                               Universidade da Madeira
Doutor João Manuel Cunha Rodrigues   Professor Auxiliar da
                                               Universidade da Madeira

UNIVERSIDADE da MADEIRA

TESE DE DOUTORAMENTO

apresentada na
UNIVERSIDADE DA MADEIRA

Para obtenção do grau de Doutor

César Esmeraldo Fernandes

Argilas Modificadas como Catalisadores Ácidos Sólidos

Júri:

Presidente:
Doutor Pedro Telhado Pereira   Reitor da Universidade da Madeira

Vogais:
Doutor Christopher Breen   Professor Catedrático da
                                      Universidade de Sheffield Hallam

Doutor Miguel Angel Vicente Rodríguez Professor Titular da
                                      Universidade de Salamanca

Doutora Maria Manuela L. Ribeiro Carrott Professora Associada da
                                      Universidade de Évora

Doutora Paula Cristina M. F. Castilho Professora Associada da
                                      Universidade da Madeira

Doutor João Manuel Cunha Rodrigues   Professor Auxiliar da
                                      Universidade da Madeira

ACKNOWLEDGEMENTS

It is a pleasure to thank the many people who made this thesis possible.

It is difficult to overstate my gratitude to my PhD supervisors, Prof. Paula Castilho and Prof. Christopher Breen. With their enthusiasm, inspiration and great efforts to explain things clearly and simply, they helped to make 'mud' fun for me. Throughout my thesis-writing period, they provided encouragement, sound advice, good teaching and lots of good ideas. I would have been lost without them.

I would like to thank the many people who have helped me through the experimental part of my PhD project. In particular, I'm deeply grateful to Francis Clegg and Jeffrey Forsyth (Materials and Engineering Research Institute), Prof. Manuela Carrott (Centro de Química de Évora) and Cezar Catrinescu and Gonçalo Faria (Centro de Química da Madeira) for their technical and scientific support and, above all, their friendship.

I am grateful to technical and administrative staff both in Sheffield Hallam and Madeira Universities for assisting me in many different ways.

I wish to thank my friends and colleagues at the Chemistry Department of Madeira University for their support throughout this thesis. In particular, I would like to mention my international coffee group for the stress-relieving morning and afternoon breaks: Carla, Cezar, Vis and Zsolt.

To my 'real world' friends (in particular Marci, Rubina, Fernanda, Ivone, Francisco, Cath, Hywel) thank you for helping me get through the difficult times, and for all the emotional support, camaraderie, entertainment, and caring you provided.

I wish to thank my parents, Elizabete and Francisco. They bore me, raised me, supported me, taught me and loved me. Isabel, for all the reasons in the world, thank you! Lastly, and more importantly, I wish to thank Gaspar, my newborn child. He was my best achievement in 2006. To them I dedicate this thesis.

RESUMO

A ilha do Porto Santo, pertencente ao arquipélago da Madeira, possui importantes depósitos bentoníticos. Foram recolhidas e caracterizadas amostras provenientes de diversas localizações no Porto Santo e seleccionou-se a amostra proveniente da Serra de Dentro (SD) para o desenvolvimento das actividades laboratoriais subsequentes. Esta amostra foi submetida a diversos processos de purificação no sentido de obter a fracção argilosa na sua forma homoiónica sódica, o material de partida para os três tipos de modificações introduzidas na fracção fina da SD: obtenção de formas homoiónicas metálicas, activação por ácido e pilarização. Este tipo de modificações permitiu obter materiais com diferentes propriedades acídicas (e.g. acidez de Brönsted e/ou Lewis), texturais (e.g. aumento da superfície e/ou acessibilidade aos centros activos) ou estruturais (e.g. criação de estruturas porosas permanentes). A gama alargada de amostras obtidas (incluindo exemplares de argilas consideradas referenciais) foi caracterizada em termos químicos, estruturais, texturais e catalíticos. A reacção de aromatização do limoneno (importante matéria-prima produzida em Portugal) foi escolhida para aferir as potencialidades catalíticas dos catalisadores argilosos preparados neste trabalho.

ABSTRACT

Important bentonitic deposits are present in Porto Santo Island, part of the Madeira Archipelago. Several locations were selected and samples were collected and characterised. The bentonite obtained at Serra de Dentro (SD) was selected for further laboratorial work. The fine fraction of SD bentonite was purified using several methods and the sodium homoionic form was prepared. This was the starting material used in the three generic types of modifications: metal exchange, acid activation and pillaring. These modifications produce materials with markedly different acidic (e.g. Brönsted and/or Lewis acidity), textural (e.g. increase of the surface area and active site accessibility) or structural (e.g. creation of permanent porous structures) properties. The wide range of materials obtained (including reference clays counterparts) was characterised in terms of chemical, structural, textural and catalytic properties. Limonene is an important raw material produced in Portugal, and its aromatisation reaction was chosen for the catalytic characterisation of the clay catalysts prepared.

TABLE OF CONTENTS

LIST OF TABLES

LIST OF FIGURES

LIST OF SYMBOLS AND ABBREVIATIONS

a.u.	Atomic units
A	Aniline
AAC	Acid Activated clays
A_{BET}	Surface Area by application of the Brunauer, Emmett and Teller (BET) method
Al_{13}	$[Al_{13}O_4(OH)_{24}(H_2O)_{12}]^{7+}$
AlSAz	Al^{3+} exchanged SAz-1
AlSD	Al^{3+} exchanged Serra de Dentro bentonite
B	Benzene
BHT	'Butylated HydroxiToluene' or 3,5-di-tert-butyl-4-hydroxytoluene
BPYR	pyridinium ion, Brönsted acidity (VT-DRIFTS)
CEC	Cationic Exchange Capacity
CH	Cyclohexene
CHA	Cyclohexylamine
CHD	Cyclohexadiene
cps	Counts per second
CrSD	Cr^{3+} exchanged Serra de Dentro bentonite
DRIFTS	Diffuse Reflectance Infrared Fourier Transform Spectroscopy
DSC	Differential Scanning Calorimetry
DTA	Differential Thermal Analysis
DTG	Derivative ThermoGravimetry
EGA	Evolved Gas Analysis
EI	Electron Impact
Ex	Exchangeable cations
EXAFS	Extended X-ray Absorption Fine Structure

FID	Flame Ionisation Detector
FTIR	Fourier Transform Infrared
GC-MS	Gas Chromatography – Mass Spectrometry
HPYR	H-bonded pyridine (VT-DRIFTS)
IEC	Ion Exchanged Clay
K10	commercially available acid activated clay
LPYR	pyridine co-ordinately bound to Lewis acid sites (VT-DRIFTS)
m/z	mass to charge ratio
MCP	Methylcyclopentene
NaSAz	Na^+ exchanged SAz-1
NaSD	Na^+ exchanged Serra de Dentro bentonite
NiSAz	Ni^{2+} exchanged SAz-1
NiSD	Ni^{2+} exchanged Serra de Dentro bentonite
O	octahedral sheet (clay layer)
PAF6.1	Pico Ana Ferreira, Outcrop 6, Sample 1
PCab1.1	Pico Cabrita, Outcrop 1, Sample 1
PCas9.2	Pico Castelo, Outcrop 9, Sample 2
PILC	Pillared InterLayered Clays
PZC	Point of Zero Charge
QPA	Quantitative Phase Analysis
RIR	Reference Intensity Ratio method
rpm	Rotations per minute
SapCa-1	Saponite (reference clay from Source Clays Repository)
Sap-PILAl$_x$Cr$_{1-x}$y	Pillared SapCa-1 obtained from a hydrolysed solution with variable initial proportions of Al^{3+} and Cr^{3+} ions, calcined at y ºC.
SAz-1	Ca-montmorillonite (reference clay from Source Clays Repository)
SAz-xM-y-z	Acid activated SAz-1 (xM HCl solution, y ºC; z time in minutes)

SD	Serra de Dentro Bentonite
SD3.1	Serra de Dentro, Outcrop 3, Sample 1
SD4.1	Serra de Dentro, Outcrop 4, Sample 1
SD-PILAl$_x$Cr$_{1-x}$y	Pillared SD obtained from a hydrolysed solution with variable initial proportions of Al^{3+} and Cr^{3+} ions, calcined at y ºC.
SD-xM-y-z	Acid activated SD (xM HCl solution, y ºC; z time in minutes)
SF3.1	Serra de Fora, Outcrop 3, Sample 1
SF9.1	Serra de Fora, Outcrop 9, Sample 1
T	tetrahedral sheet (clay layer)
TGA	ThermoGravimetric Analysis
TG-MS	Thermogravimetry – Mass Spectrometry
TIC	Total Ion Count
US	ultrasound
VT8.1	Vale do Touro, Outcrop 8, Sample 1
VT8.2	Vale do Touro, Outcrop 8, Sample 2
VT-DRIFTS	Variable Temperature Diffuse Reflectance Infrared Fourier Transform Spectroscopy
wt%	weight percentage
wt	weight
XRD	X-Ray Diffraction
XRF	X-Ray Fluorescence
XRPD	X-Ray Powder Diffraction

CHAPTER 1. INTRODUCTION

1. INTRODUCTION

1.1 OVERVIEW

Clays have been used by Man over more than 25000 years in ceramics manufacture and building construction. Besides these classic applications, clays are used in the paper industry, as drilling muds, foundry sands, pharmaceuticals, etc. They also can be used as adsorbents, catalysts or catalyst supports, ion exchangers or decolourising agents. All these applications are dependant upon the clay's specific properties. Currently, clays are receiving considerable attention, due to the international need to implement less polluting industrial processes. These minerals are convenient, cheap and environmentally friendly alternatives to many expensive manufactured catalysts (Kloprogge, 1998; Vaccari, 1998; Murray, 1999).

Porto Santo Island, part of the Portuguese Madeira Archipelago has several bentonite deposits, which are, to the best of the author's knowledge, unique in Portugal in terms of genesis and composition. Natural untreated clays possess a very low ability to catalyse reactions in either polar or non-polar media. However, the structural properties of these materials can be modified by various activation methods in order to produce catalysts with high acidity, surface area, porosity and thermal stability. In this thesis, ion exchange, acid activation and pillaring have been employed in order to improve the catalytic potential of the chosen parent bentonite (Serra de Dentro). The resulting catalysts, together with other bentonites obtained at Porto Santo have been characterised by several techniques, including X-Ray diffraction (XRD), thermogravimetric analysis (TGA), X-Ray Fluorescence (XRF), infrared spectroscopy (IR), real time thermogravimetry-mass spectrometry (TG-MS) and isothermal N_2 adsorption.

The use of renewable feedstocks from natural sources is a growing field in which heterogeneous catalysis can offer considerable improvement. The conversion of cheaply

available limonene to the more commercially valuable p-cymene is a good example. This conversion requires the migration of the exocyclic double bound into the ring followed by a further ring dehydrogenation. Limonene, an abundant raw material in Portugal is available from pine gum, for which Portugal is the main European producer. The turpentine spirit produced by distillation of the pine gum may contain up to 80% limonene, when the *Pinus Pinea* species is considered. P-cymene, this project's target molecule, has many uses in the chemical industry; namely as a solvent in the ink and varnish industry, in the production of p-cresol and carvacrol, as an intermediate in the synthesis of antioxidants (e.g. BHT: 3,5-di-*tert*-butyl-4-hydroxytoluene), in the production of synthetic resins, in perfumery and as a thermal fluid in heat exchanging systems. It is produced industrially via the alkylation of toluene, which is cheap, but operating conditions are harsh and the product mixture difficult to purify. By contrast, the dehydrogenation of limonene, which already possesses the required carbon skeleton, is very attractive.

Therefore, the main aim of this project was to produce indigenous clay based active catalysts for the aromatisation of limonene, a strategy to derive value from natural products of vegetable and mineral origin.

1.2 CLAY MINERALOGY

In geology, the designation 'clay' has a double meaning: it may designate a finely divided rock, composed of a limited number of crystalline minerals (clay minerals), that develops plasticity on mixing with a limited amount of water or it may refer to a group of particles with a fixed maximum size (originally under 4 µm – Grim, 1962 – and nowadays, under 2 µm – Guggenheim and Martin, 1995).

Clay minerals are the most abundant sedimentary mineral group. They predominate in the colloidal fractions of soils, sediments, rocks and waters and are classified as phyllosilicates

(usually hydrous aluminosilicates). Clays present a wide range of potential applications and properties, dependant on the clay and non-clay mineral compositions, the presence of organic mater, the type and quantity of exchangeable cations and texture (Murray, 1998). The first recorded application of clay as a catalyst was reported by Bondt *et al.* (1797) who investigated the dehydration of alcohol. The first industrial applications of clays as catalysts appeared in 1915. In the 1930's and 1940's, acid activated catalysts were extensively used in cracking reactions (Houdry process), but were rapidly replaced by amorphous aluminisilicates (more consistent results) and, in 1964, by zeolites (more active and selective). Nowadays, the industrial applications derived from clay minerals science is very diverse (e.g. drilling mud, oil adsorbents, emulsion stabilizers, paint, fillers, paper, medical formulation, catalysts, food additives, etc.) (Murray, 1999).

1.2.1 BASIC STRUCTURE OF CLAYS

Clay minerals are laminar silicates that belong to the phyllosilicate family (i.e. silicates based on the two dimensional structure); the basic building blocks are $Si(O,OH)_4$ tetrahedra (Figure 1.1) and $M(O,OH)_6$ octahedra (M = Al^{3+}, Mg^{2+}, Fe^{3+} or Fe^{2+}) (Figure 1. 2). These structures are grouped in tetrahedral and octahedral sheets, respectively, connected in two perpendicular directions.
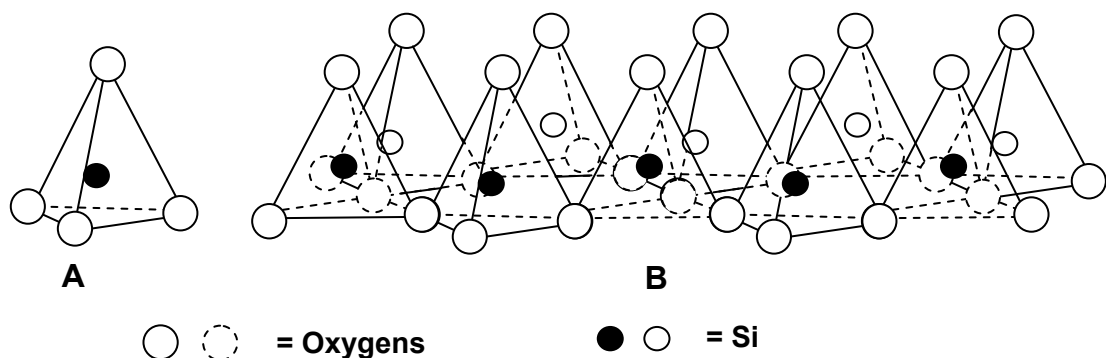
Figure 1.1 Diagrammatic representation of A. single tetrahedral unit and B. the sheet of tetrahedral units.
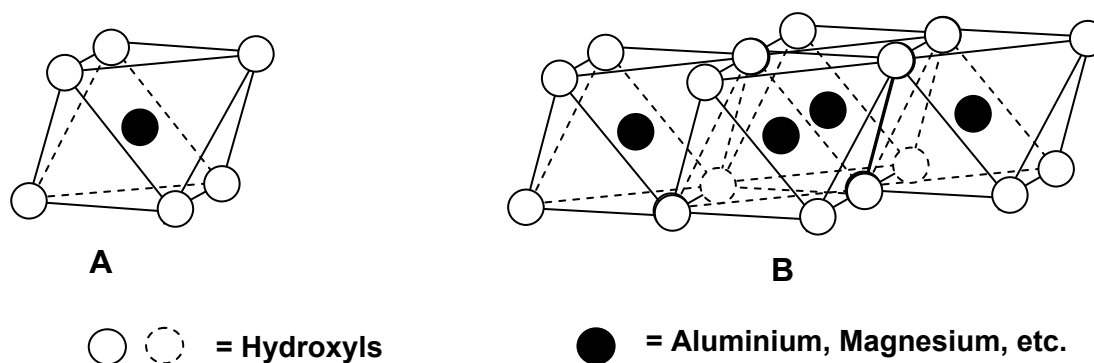
Figure 1.2 Diagrammatic representation of A. single octahedral unit and B. the sheet of octahedral units.

Clay minerals may be triooctahedral or dioctahedral, as a result of the total or partial (2 thirds) occupancy of the octahedral cationic positions. The 'degree' of occupancy depends, basically, of the type of octahedral cation (Mg^{2+} for the former and Al^{3+} for the latter) (Gomes, 1988; Santos, 1989; Vaccari, 1998).

Due to symmetry and dimensional similarities of the tetrahedral and octahedral sheets, they can be combined in different structural arrangements resulting in a variety of clay mineral sub-groups. Condensation of one tetrahedral (T) sheet with one octahedral (O) sheet results in a structure referred to as 1:1. The combination of a further tetrahedral sheet on the opposite side of the octahedral sheet results in a 2:1 structure (Figure 1.3) (Hoffmann *et al.*, 1933, Marshall, 1935; Maegdefrau and Hoffmann, 1937; Hendricks, 1942), the most important from a catalysis point of view. The octahedral and tetrahedral sheets are linked together mainly by covalent bonds (Gomes, 1988; Santos, 1989; Vaccari, 1998).

In the 2:1 clay minerals (Figure 1.3), the adjacent layers each face a plane of oxygens, which results in appreciable repulsive forces. The intensity of these forces is not compensated totally by Van der Waals interactions. The equilibrium distance is maintained by two additional factors: the presence of adsorbed cations in the interlayer region and the possibility of hydrogen bond formation between the water molecules present in this region

(adsorbed or present in the hydration sphere of the exchangeable cations and O^{2-} ions of the tetrahedral sheets) (Santos, 1989).
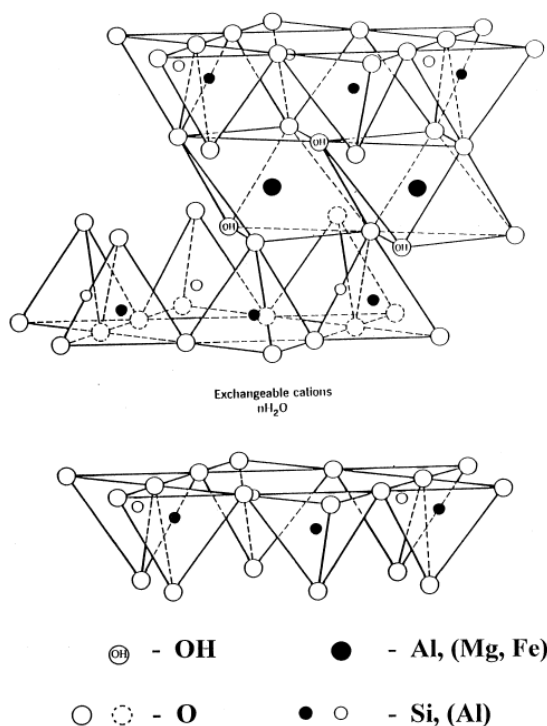
Figure 1.3 2:1 layer of smectites (Madejová et al., 1998)

The tetrahedral sheet Si^{4+} and octahedral sheet Al^{3+} ions are frequently replaced by lower valence ions, such as Al^{3+} (tetrahedral sheet) and Mg^{2+}, Li^+ or Fe^{2+} (octahedral sheet). This type of ion replacement is denoted isomorphic substitution (cf. Section 1.2.3.3) and results in an electrical charge imbalance of the crystal structure (Grimshaw, 1971).

The different combinations of octahedral and tetrahedral sheets, different degrees of octahedral sheet occupation and different types and degrees of isomorphic substitution produce a wide variety of members of the clay family. The main characteristics of these species are summarised in Table 1.1. The ideal composition formulas reflect the structural organisation of the species (octahedral sheet composition, tetrahedral sheet composition, oxygen and hydroxyl ions, exchangeable cation, water content when applicable).

Table1.1 Classification Scheme of Phyllosilicate Clay Minerals (Carrado, 2004)

Structure type	Charge per unit cell	Group	Mineral examples	Ideal composition	Notes
1:1 (TO)	0	Kaolin-serpentine	Kaolinite, dickite, nacrite	$Al_4Si_4O_{10}(OH)_8$	Kaolin subgroup, dioctahedral, nonswelling
			Halloysite	$Al_4Si_4O_{10}(OH)_8 \cdot 4H_2O$	Kaolin subgroup, dioctahedral, swelling
			Chrysotile, antigorite, lizardite	$Mg_6Si_4O_{10}(OH)_8$	Serpentine subgroup, trioctahedral, nonswelling
2:1 (TOT)	0	Pyrophyllite-talc	Pyrophyllite	$Al_4Si_8O_{20}(OH)_4$	Dioctahedral, nonswelling
			Talc	$Mg_6Si_8O_{20}(OH)_4$	Trioctahedral, nonswelling
	0.5-1.2	Smectite	Beidellite	$[(Al_4)(Si_{7.5-6.8}Al_{0.5-1.2})O_{20}(OH)_4]Ex_{0.5-1.2}$	Dioctahedral, swelling
			Montmorillonite	$[(Al_{3.5-2.8}Mg_{0.5-1.2})(Si_8)O_{20}(OH)_4]Ex_{0.5-1.2}$	
			Nontronite	$[(Fe_4)(Si_{7.5-6.8}Al_{0.5-1.2})O_{20}(OH)_4]Ex_{0.5-1.2}$	
			Saponite	$[(Mg_6)(Si_{7.5-6.8}Al_{0.5-1.2})O_{20}(OH)_4]Ex_{0.5-1.2}$	Trioctahedral, swelling
			Hectorite	$[(Al_{5.5-4.8}Li_{0.5-1.2})(Si_8)O_{20}(OH)_4]Ex_{0.5-1.2}$	
	1.2-1.8	Vermiculite	Vermiculite	$[(Al_4)(Si_{6.8-6.2}Al_{1.2-1.8})O_{20}(OH)_4]Ex_{1.2-1.8}$	Dioctahedral, swelling
			Vermiculite	$[(Mg_6)(Si_{6.8-6.2}Al_{1.2-1.8})O_{20}(OH)_4]Ex_{1.2-1.8}$	Trioctahedral, swelling
		Illite	Illite	$[(Al_4)(Si_{7.5-6.5}Al_{0.5-1.5})O_{20}(OH)_4]K_{0.5-1.5}$	Dioctahedral, nonswelling
			Glauconite	Illite rich in Fe	
	2	Mica	Muscovite	$[(Al_4)(Si_6Al_2)O_{20}(OH,F)_4]K_2$	Dioctahedral, nonswelling
			Celadonite	$[(Fe_2Mg_2)(Si_8)O_{20}(OH,F)_4]K_2$	
			Phlogopite	$[(Mg_6)(Si_6Al_2)O_{20}(OH,F)_4]K_2$	Trioctahedral, nonswelling
			Taenolite	$[(Li_2Mg_4)(Si_8)O_{20}(OH,F)_4]K_2$	Trioctahedral, lithium mica
	4	Brittle mica	Margarite	$[(Al_4)(Si_4Al_4)O_{20}(OH,F)_4]Ca_2$	Dioctahedral, nonswelling
2:1 channels or inverted ribbons	Variable	Palygorskite-sepiolite	Palygorskite	$[(Mg,Al)_4(Si_{7.5-7.75}Al_{0.5-0.25})O_{20}(OH)_2(OH_2)_4]Ex_{var}$	
			Sepiolite	$[(Mg,M)_8(Si,M')_{12}O_{30}(OH)_4(OH_2)_4]Ex_{var}$	Trioctahedral M=Al, Fe(III); M´= Fe(II), Fe(III), Mn(II)
2:1:1	Variable	Chlorite	Clinochlore		[TOT]O[TOT] structure

Ex: exchangeable cations

1.2.2 THE HYDRATION AND SWELLING CAPACITY OF CLAYS

The basal spacing of smectites is not constant; it depends on the type of intercalating species (cation type, other species present in the interlayer region) and the hydration state (hence the designation 'expanding clays') – Figure 1.4. The presence of several layers of water molecules causes the basal spacing to increase up to 90% of its initial value, depending on the type of clay and exchangeable cation (Low *et al.*, 1970; Velde, 1995).
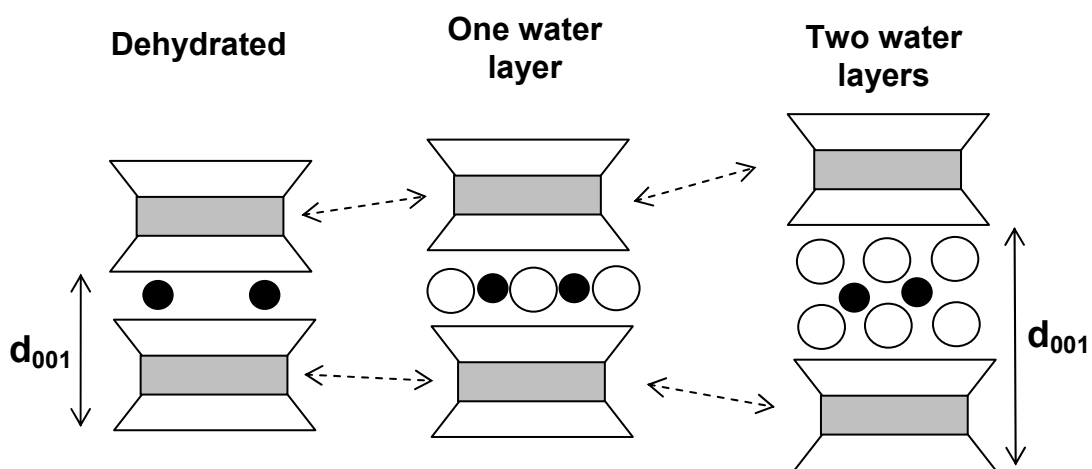
Figure 1.4 Diagrammatic representation of the swelling of a clay (e.g. montmorillonite)

The heating process, at a regular temperature rate, affects the weight loss of clays. These temperatures depend on the type of clay and the rate and time of heating. According to Bradley and Grim (1951), below 300 ºC, water and other molecules are adsorbed reversibly between the clay layers. Above 500 ºC the structural water associated with the structural hydroxyls are removed and the laminae collapse irreversibly (Bradley and Grim, 1951; Serratosa, 1960). After calcination at 600 ºC no water is adsorbed in the interlamellar space.

1.2.3 CLAY MINERAL ACTIVE BONDING SITES

Seven predominant active sites are normally available on clays, which result from the surface features illustrated in Figure 1.5 (Johnston, 1996):

1. Neutral siloxane surface (basal surfaces of the silica tetrahedra)

2. Hydroxyl groups

3. Isomorphic substitution sites

4. Metal cations occupying exchange sites

5. Water molecules surrounding exchangeable cations

6. Hydrophobic sites

7. Broken edge sites including exposed silanol and aluminol groups
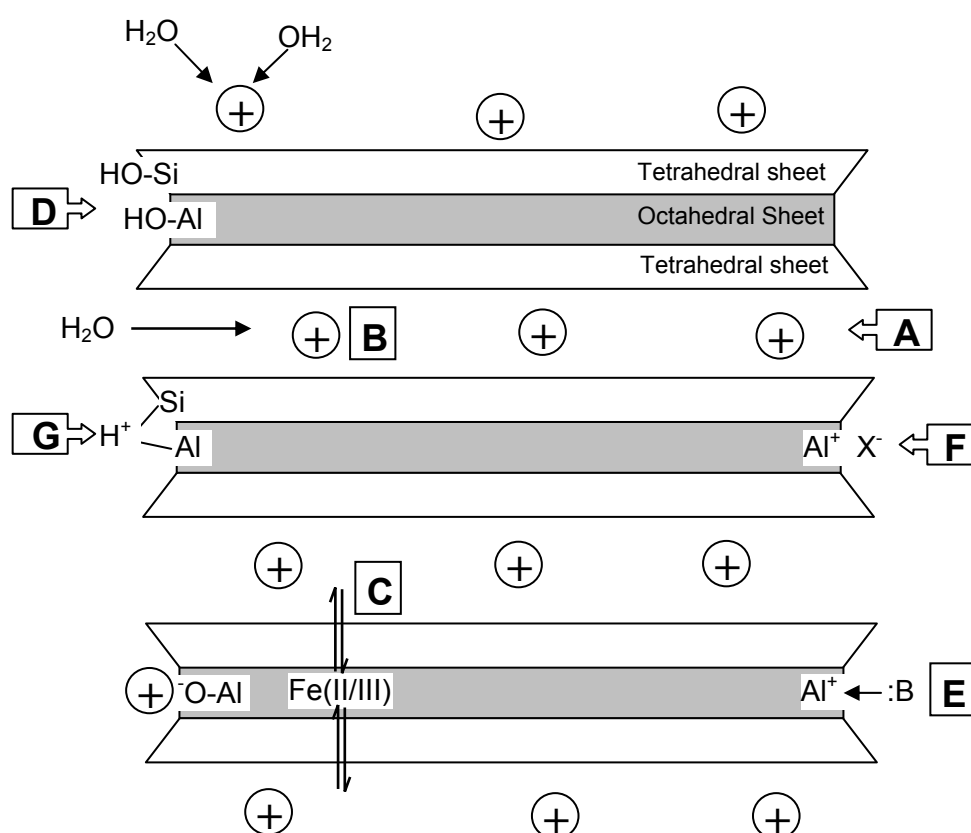
Figure 1.5 Principal surface features on a clay (A. Interlayer space; B. Hydratable exchange cations; C. Single electron transfer with structural ions; D. Reactive hydroxylic species; E. Lewis acid sites; F. Anion exchange sites; G. Bridged hydroxyl sites)

1.2.3.1 NEUTRAL SILOXANE SURFACE

This type of surface only occurs for neutral 2:1 (no isomorphic substitution) and 1:1 (e.g. kaolinite) layer silicates or by modification of 2:1 layer silicates by exchange with alkylammonium

ions or organic cations. The surface is hydrophobic in character and is considered to be inert and unreactive due to the strong bonds formed between Si and O atoms.

1.2.3.2 HYDROXYL GROUPS

Hydroxyl groups located at external edge positions may be of two types, bridging and non-bridging, depending on the degree of hydration. These hydroxyl groups may in turn act as a source of Brönsted acidity (cf. Section 1.2.4) or external binding sites for metal ions.

1.2.3.3 ISOMORPHIC SUBSTITUTION

The tetrahedral sheet Si^{4+} and octahedral sheet Al^{3+} ions are frequently replaced by lower valence ions, such as Al^{3+} (tetrahedral sheet) and Mg^{2+}, Li^+ or Fe^{2+} (octahedral sheet). This type of ion replacement is called isomorphic substitution and results in an electrical charge imbalance on the crystal structure (Grimshaw, 1971). Substitution in the octahedral sheet creates a de-localised charge deficiency (spread over 10 basal oxygen ions), whereas when substitution occurs in the tetrahedral layer, the charge imbalance is more localised (spread over only 3 oxygens of the basal layer) (Johnston, 1996).

1.2.3.4 EXCHANGEABLE METAL CATIONS & EXPOSED UNDERCOORDINATED METAL ATOMS

In order to compensate the excess negative charge mentioned in the previous section, the clay mineral crystals retain cations in the interlayer region[1] and on the exterior surface. The amount of retained ions (normally H^+, Na^+, K^+, NH^{4+}, Ca^{2+}, Mg^{2+} and Al^{3+} - Brindley and Brown, 1984) depends on the degree of isomorphic substitution. The interlayer cations are much less strongly bound than the layer cations and will thus easily exchange with cations from an aqueous solution (Grim and Kulbicki, 1961). Due to the exchangeable character of

---

[1] The interlayer space is the distance between two consecutive layers. The basal spacing of a clay mineral is the distance between the bases of two consecutive layers and therefore includes the interlayer space and the thickness of one layer).

these ions, it is possible to obtain homoionic clays, materials with only one type of charge compensating cation (Gomes, 1988; Bain and Smith, 1994; Thomas and Thomas, 1997), by a simple exchange process (sorption from a solution).

The exchangeability of cations present in the clay by cations of a particular aqueous solution is determined by the natures of both the clay and cation (hydration energy, size, and valence), the concentration of the electrolyte and pH of the exchange solution and the population of exchange sites on the clay. Solutions of small size/high valence metal cations are very effective at displacing the interlayer exchangeable cations of a clay (Bar and Tenderloo, 1936; Grim and Bray, 1936). The ease of replacement of interlayer cations follows the reverse order (McCabe, 1996). In smectites, the exchangeable cations in the gallery account for 80% of the total Cation Exchange Capacity (CEC).

Coordinatively unsaturated Al^{3+} and Mg^{2+} are easily formed at the edges and should behave as Lewis acidic centres.

1.2.3.5 POLARISED WATER MOLECULES SURROUNDING EXCHANGEABLE CATIONS (OR UNCOORDINATED METAL CATIONS AT BROKEN EDGES)

The structure of sorbed water on smectites is influenced primarily by the nature of the exchangeable cations. Two types of water sorption occur: i) direct coordination to exchangeable cations and ii) physisorption, where water molecules occupy interstitial pores, interlayer spaces between exchangeable cations or polar sites on external surfaces.

The sites generated become sources of surface Brönsted acidity and are mainly concerned with site A (Figure 1.5). The polarised water molecules surrounding exchangeable cations and undercoordinated surface atoms can donate protons to adjacent organic solutes more readily than bulk water and therefore have the ability to promote a variety of chemical reactions (cf. Section 1.2.4).

1.2.3.6 HYDROPHOBIC SITES

It is known that smectite surfaces have a high selectivity for organic cations. Sorption of organic molecules on clay surfaces can impart an organophilic nature to the clay surface (e.g. exchange of alkylammonium cations for inorganic cations on montmorillonite – Lee *et al.*, 1990; Jaynes and Boyd, 1991; Bujdák and Slosiariková, 1992).

1.2.3.7 BROKEN EDGE SITES (PH DEPENDENT ACTIVE SITES)

Undercoordinated metal ions (Si^{4+}, Al^{3+}, Fe^{3+}) at the broken edges, terraces, kinks or holes on the surface of the clay can react with water molecules to form surface hydroxyl groups in an attempt to complete their coordination sphere. The undercoordinated metal ions can also form inner sphere complexation (OH groups formed) with metal species and can undergo hydrogen bonding. The overall contribution of these edge sites to the CEC is approximately 20% and depends strongly on the size and shape of the clay particle. As the particle size decreases, the contribution of broken sites to the reactivity of the clay particle becomes significant.

At low pH, these sites develop a positive charge due to the adsorption of protons, which favours strong interactions with organic acids and oxyanions. As pH increases, these sites become more neutral and ultimately acquire negative charge when the pH value is greater than the point of zero charge (PZC).

1.2.4 ACIDITY

As noted previously, the most used clay minerals for catalytic purposes are the 2:1 type, in particular species with high electrical charge (and, consequently, high CEC values): smectites and vermiculites. These clay minerals are intrinsically acidic, exhibiting Lewis and Brönsted acidity. Structural and environmental factors govern the degree to which each type

of acid site is present and normally one predominates for a given set of conditions (Mortland and Raman, 1968). For example, montmorillonites present both Brönsted and Lewis acidic centres, whereas Lewis acidic centres are predominant in saponites (Ohtsuka, 1997).

Lewis acidity is attributed to the presence of exposed Al^{3+}, Fe^{3+} and Mg^{2+} at the broken crystallite edges and such acidity can be increased by heating the clay to above 300 ºC. Altogether, although the edge surface constitutes only about 10% of the total clay surface, it is sufficient to impart significant acidic properties to smectite clays (Theng, 1974; Lambert and Poncelet, 1997).

Brönsted acidity arises from the strong polarisation imposed on interlayer water molecules due to the presence of exchangeable cations (Mortland and Raman, 1968; Clark, 1994; Thomas and Thomas, 1997; Vaccari, 1998) and from the presence of external OH groups (Clark, 1994; Thomas and Thomas, 1997; Vaccari, 1998). Acidity is maximised when the water content in the clay is low and when highly polarizing species such as Al^{3+} cations replace the natural Na^+ and Ca^{2+} ions (Mortland and Raman, 1968; Frenkel, 1974; Benesi and Winquist, 1978).

1.3 CLAY CATALYSTS

Acid or basic heterogeneous catalysis (solid/liquid and solid/gas) has received increasing interest due to the advantages that it presents when compared to liquid Brönsted and Lewis acid catalysts. The former are non corrosive, environmentally friendly and relatively easy to eliminate. They may be reused and the separation from the liquid phase is simpler. Furthermore, they may be prepared or fine tuned in order to increase their activity, selectivity and/or usability. However, some disadvantages coexist, namely the cost of catalyst preparation and inclusion of an extra component in the reaction, the difficulties of ensuring a good solid-liquid or solid-gas dispersion and the possibility of irreversible retention of organic

molecules (reactants, intermediates or reaction products) in the pores of the catalysts. The main solid catalysts presently used include zeolites, metallic oxides, complex oxides, ion exchange resins, phosphates, supported enzymes and sulfonated polysiloxanes (Clark, 1994; Thomas and Thomas, 1997; Cheng, 1999; Tanabe and Hölderich, 1999). Tanabe and Hölderich (1999) listed 127 industrial processes that use acid and/or basic solid catalysts in at least one of the production phases. This number is probably underestimated because the information on many industrial processes is not easily accessible.

Clay minerals comply with all the advantages of heterogeneous catalysis. The high natural availability, the small average particle size and high surface areas are important favourable characteristics of this type of mineral (Santos, 1989; Thomas and Thomas, 1997).

In section 1.2, the main structural and chemical features of clay minerals were noted. The potential of clays as catalysts arises from those properties and the possibility to enhance them by correct modification of the parent materials. The most important variable properties from a catalysis point of view are:

- Possibility of intercalating a wide diversity of species;
- Possibility of replacement of the exchangeable cations by a wide range of inorganic and organic cations;
- Intrinsic and increasable/tuneable acidity;
- Variable surface area.

Thomas and Thomas (1997) listed some reactions catalysed by clays, namely: conversion of primary amines and alcohols into their secondary counterparts, isomerisations, alkylations and cyclisations, hydration, alkene alkylation and acylation to produce alcohols, ethers and esters, alcohol dehydrations, dimerisations, oligomerisations and polymerisations, decarboxylations, polycondensations and hydrothermal decompositions of hydrocarbonates.

Adams (1987), Foucaud (1987), Kellendonk *et al.* (1987), McKillop and Clissod (1987), Pinnavaia (1987), Clark *et al.* (1992), and Clark (1994) present extensive lists of alkylation, cyclisation, Friedel-Crafts, isomerisation, oxidation, hydrogenation and anionic or cationic activation reactions catalysed by clays.

Some properties of untransformed clays prevent their use in a wider range of applications, particularly at higher temperatures. It was previously noted that when the clay mineral is heated at high temperatures, it looses its hydration water and the basal spacing diminishes drastically and eventually, irreversible collapse occurs. Another negative feature is a low activity due to an insufficient acidity of the clay catalyst. In order to overcome these drawbacks, widening the range of possible applications several modifications may be performed on the parent material. The following are, presently, the most popular (Vogels *et al.*, 2005):

− "Normal" smectite clays with acid sites generated by isomorphous substitution in the tetrahedral or octahedral sheets. Montmorillonite clays are most frequently used. The catalytic activity can be enhanced by replacement of the interlayer cations (usually Na^+, Ca^{2+}) with acidic cations, such as H^+, Al^{3+} and Fe^{3+};

− The catalytic properties of smectites can be enhanced by acid treatment of the smectite surface with sulphuric or hydrochloric acid to remove ions from the octahedral sheet, to increase the layer charge and the pore volume;

− Organometallic compounds, such as metal chelate complexes or inorganic polyoxocationic pillars have often been intercalated to increase the acidity and/or the specific surface area, which results in an increase of the catalytic performance;

− The smectite surface is often doped with high-valence Lewis acids, such as Fe^{3+}-chloride or with metallic nitrates to increase the performance in acid-catalysed reactions.

The first three types of modification were used in this work.

1.3.1 ION EXCHANGE

Acid strengths of some common ions decrease in the order of polarisation capacity (decreasing size and increasing charge) as: Fe^{3+}, Al^{3+}, Ni^{2+}, Mg^{2+}, Ca^{2+}, Ba^{2+}, Li^+, Na^+, K^+ (Yariv and Michaelian, 2002). Since acid strength increases with increasing polarisation ability of the cations, then as the amount of water decreases the polarisation (and therefore the ability to donate protons) increases. Fully dehydrated interlayer cations then behave as Lewis acids (Carrado, 2004).

As mentioned before, the intercalated cation in naturally occurring clays is Na^+ or Ca^{2+} and occasionally K^+. Such clays are at best weakly catalytic. However, when these ions are exchanged by others that increase the acidity and/or change the nature of acidic sites, they become active.

The native hydrated exchangeable cations are replaced by highly polarising species of small radius, such as aluminium, chromium or iron (Ballantine et al., 1981[a]; Vaccari, 1998), by a simple ion exchange process in solution. Trivalent homoionic clays are active in many organic reactions and in reactions were an active source of protons is required. Al^{3+} saturated clays are normally more active than other ion exchanged clays, due to enhanced polarisation of water molecules in the primary co-ordination sphere of the Al^{3+} cation (Atkins et al., 1983; Gregory et al., 1983; Tennakoon et al., 1983). Divalent ions also possess

polarising power and several examples of active Mg^{2+}, Cu^{2+}, Ni^{2+}, Co^{2+} and Zn^{2+} clays have been reported (Mitre and Sindhu, 1971; Purnell *et al.*, 1991; Breen, 1991[a]). The order of activity of ion-exchanged clays with these cations was $Cu^{2+} > Zn^{2+} \geq Ni^{2+} \geq Co^{2+} \approx Mg^{2+}$, for both Brönsted and Lewis acid catalysed reactions (Brown and Rhodes, 1997).

Ni^{2+} and Al^{3+} -exchanged montmorillonites are considered "model" Lewis and Brönsted acids, respectively. The nature of the active sites has been probed using FTIR spectra of adsorbed pyridine (Breen, 1991[a]; Brown and Rhodes, 1997) and supported by catalytic data. The most common test reactions in the current context are: (a) Brönsted acid catalysed rearrangement of α-pinene (Brown and Rhodes, 1997; Breen and Moronta, 2001; Hart and Brown, 2004); (b) Lewis acid catalysed rearrangement of camphene hydrochloride (Brown and Rhodes, 1997); (c) Lewis acid catalysed alkylation of toluene with benzyl chloride (Hart and Brown, 2004). Cr based catalysts are frequently reported as being used in several catalytic applications. It has been shown (Breen *et al.*, 1987) that Cr containing clays offer a combination of both Lewis and Brönsted acid sites and that they may present higher acidities than their Al counterparts (Cañizares *et al.*, 1999).

Ion exchanged clays have been shown to be efficient catalysts for a variety of organic reactions, which include formation of di-alkylethers from alcohols (Ballantine *et al.*, 1981[a]), protonation of amines (Breen, 1991[a]), transformation of alkenes (Adams *et al.*, 1981; 1982), hydration of ethylene (Gregory *et al.*, 1983) and esterification of organic acids (Ballantine *et al.*, 1981[b]), among others.

1.3.2 ACID ACTIVATION

The activation of mineral clays by inorganic acids (normally HCl or H_2SO_4) involves lixiviation and consequent depletion of the metallic cations present in the octahedral sheets.

The first use of acid activated clays was as petroleum-cracking catalysts, back in the 1950's (Ryland *et al.*, 1960). They were used in industry until the mid-1960's, when they were replaced by more thermally stable and selective zeolite catalysts. Acid-activated montmorillonite clays find wide applications in chemical, foodstuff, beverage, and paper industry as well as for cleaning and detergents usage (Christidis *et al.*, 1997). Several acid treated clays are used in industrial applications such as phenol alkylations and the dimerisation of unsaturated hydrocarbonates and polymerisation reactions (Kaplan, 1966; Hojabri, 1971) and in research with their role as high-surface-area supports for environmentally benign catalysts in isomerisation (Yadav *et al.*, 2004) and Friedel Crafts alkylation (Rhodes *et al.*, 1991; Rhodes and Brown, 1993; Hart and Brown, 2004) and acylation reactions (Brown, 1994; Clark *et al.*, 1994; Jasra, 2003).

The main aim of acid activating a clay is to increase the accessible surface area (up to 730 $m^2.g^{-1}$ – Yang, 1999) by disaggregation of clay particles, elimination of several mineral impurities and removal of metallic structural cations (Mendioroz and Pajares, 1987; Jovanović *et al.*, 1996; Vicente *et al.*, 1996[a]; Christidis *et al.*, 1997; Falaras *et al.*, 1999; Valenzuela-Diaz and Santos, 2001; Vuković *et al.*, 2005) and to increase the Brönsted acidity. Acid treatment of clays results in two major outcomes: the substitution of the exchangeable cations by protons and the dissolution of metals ions from the clay structure, by depopulating the octahedral sheet (Figure 1.6) (Mills *et al.*, 1950; Heyding *et al.*, 1960; Kaviratna and Pinnavaia, 1994).
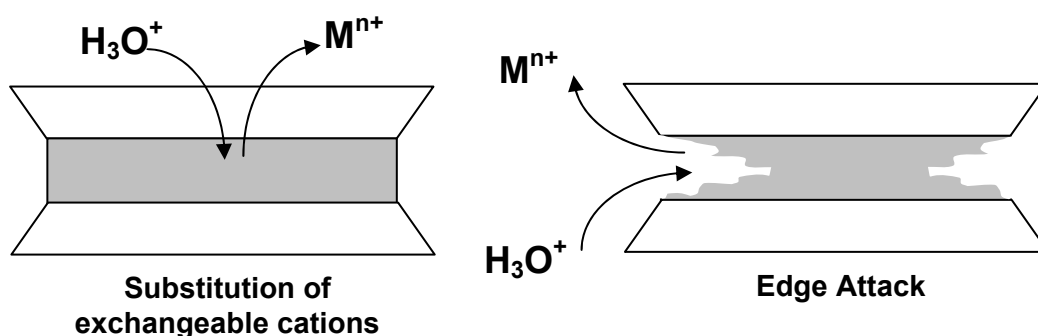
Figure 1.6 Diagrammatic representation of the effect of acid activation (Kaviratna and Pinnavaia, 1994)

The acid activated materials produced are not stable in the H^+-form, due to gradual exsolution of metal ions (mainly Al^{3+}, Mg^{2+} and Fe^{3+}), from the octahedral sheet which displace the H^+ ions on the cation exchange sites. This process is known as autotransformation (Janek and Komadel, 1993).

Acid activation alters the number, strength and, probably, also the type of acid sites on the clay. It has been shown that octahedral Fe and Mg rich bentonites are leached more readily than those containing a higher proportion of octahedral aluminium (Osthaus, 1955; Norvak and Gregor, 1969; Novák and Čičel, 1978; Janek and Komadel, 1993; Vicente *et al.*, 1994; Komadel *et al.*, 1996; Breen *et al.*, 1995[a,b], 1997[a,b]).

Removal of ions from the octahedral sheet leads to an increase in surface area in the early stages of the process. Subsequently, both the cation exchange capacity and the surface area decrease in parallel (Lagaly, 1981; Kheok and Lim, 1982; Taylor and Jenkins, 1986). The choice of conditions of acid treatment[2] depends on the reaction of interest. Reactions that involve polar molecules require mildly acid treated clays, which enhance the numerous acidic centres present on the internal surfaces. On the other hand, the accessible surface for non-polar molecules is restricted to the external exposed surfaces. These reactions are better catalysed by clays activated in severe conditions, because the resulting open porous structure can offer a higher number of acid sites (in comparative terms) to reagents that are not sufficiently polar to enter the gallery and swell the untransformed part of the clay beyond the frontier of acid attack (Rhodes and Brown, 1992, 1994[a]; Brown and Rhodes, 1997; Vaccari, 1998).

---

[2] Treatment temperature, acid strength, acid-to-clay ratio, water-to-acid ratio, duration of the treatment

1.3.3 PILLARED CLAYS

Pillared clays, PILCs, are obtained by replacement of the interlayer exchangeable cations by bulky inorganic polyoxocations, followed by calcination. These bulky polycations increase the basal spacing and, upon heating, they are stabilised due to dehydration and, eventually dehydroxylation reactions. The metallic oxide pillars are thermally stable and prop the layers permanently apart, avoiding the collapse of the clay structure. A two dimensional porous network is created, with interlayer spacings compatible with molecular dimensions (Gil *et al.*, 2000). The pillaring process is schematically represented in Figure 1.7.
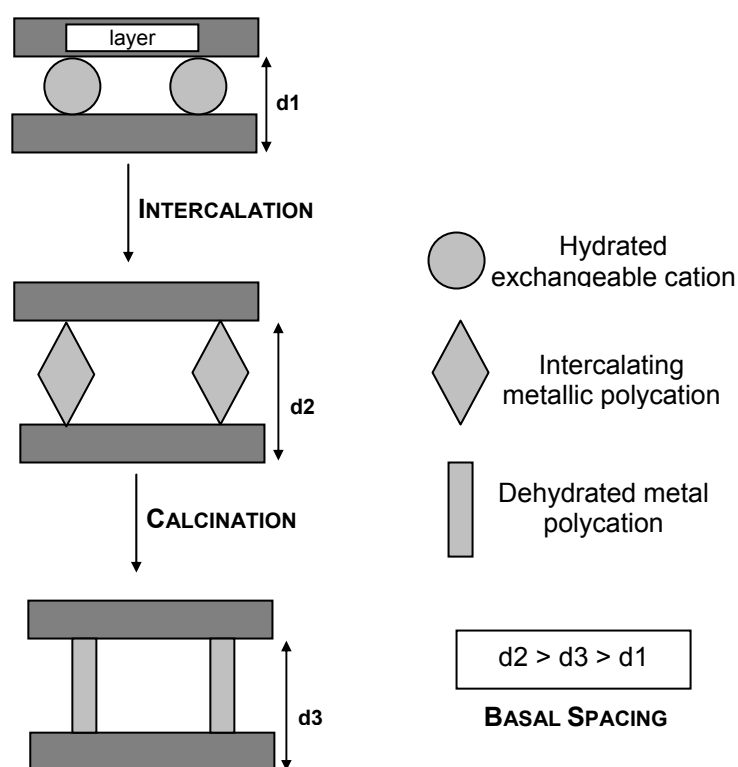
Figure 1.7 Schematic representation of the pillaring process (Gil et al., 2000)

When compared to other porous solids, pillared clays present several advantages. Clays are abundant raw materials and the preparation methods of PILCs are simpler than the methods used for synthesizing zeolites. Some PILCs exhibit large pores (1 nm or higher), markedly higher than zeolites (between 0.3 and 0.7 nm); therefore, PILCs may be used as shape

selective catalysts for a wider range of molecular dimensions. Moreover, several additives (e.g. transition metals) may be introduced into the PILCs (pillaring with mixed metallic oxides and/or doping of PILCs). The incorporation of specific cations in the pillared structure proved to be very useful in the improvement of the adsorbent and catalytic properties of PILCs (Zhu and Lu, 1998).

Numerous types of reactions are catalysed by PILCs, including primary amine conversion, cracking of hydrocarbons, Friedel-Crafts alkylations, oxidations, hydrogenations and dehydrogenations, isomerisations, alcohol dehydrations, photo-degradations, disproportionation, etc. (Adams, 1987; Kellendonk *et al.*, 1987; Santos, 1989; Clark, 1994; Lambert and Poncelet, 1997; Kloprogge, 1998; Yang *et al.*, 1998; Cheng, 1999; Gil *et al.*, 2000).

1.3.3.1 FACTORS THAT INFLUENCE THE PILCs

The nature of the clay and intercalating solutions and the experimental procedures employed greatly influence the properties of the obtained materials.

A. Nature of the parent clay

Several clays may be used as hosts for the intercalating species. Montmorillonites are, by far, the most regularly used clay mineral; the high natural occurrence of this mineral and its favourable expandability and CEC are, possibly the reasons for this popularity. The pillaring of saponites has received increased interest over the last years due to its excellent intercalating capacity and the better structural properties for infrared and NMR intercalation mechanisms studies (Chevalier *et al.*, 1994; Lambert *et al.*, 1994; Molina *et al.*, 1994; Bergaoui *et al.*, 1995; Vicente and Lambert, 1999; Vicente *et al.*, 2002, Louloudi, 2003).

Beidellites, vermicullites, hectorites, micas and laponites have also been used in pillaring studies (Shabtai, 1979; Pinnavaia, 1983, 1995; Figueras, 1988; Vaughan, 1990; Thomas and Theocharis, 1992; Occelli *et al.*, 1995; Lambert and Poncelet, 1997; Othsuka, 1997; Solin, 1997).

Besides different clay members, substantial differences occur between clays that belong to the same species, namely chemical composition, crystallinity, degree of isomorphic substitution, nature and amount of exchangeable cations and the presence of impurities. Synthetic clays (hydrothermal synthesis) have been used to overcome these differences, which result from the natural origin of these minerals (Bergaoui *et al.*, 1995; Kloprogge, 1998; Michot *et al.*, 1998; Catrinescu *et al.*, 2003).

The acidity and the intrinsic oxidative properties of the clays, as well as their expanding capacity are other important variables that may influence the material produced (Vaccari, 1998).

B. Nature of the pillaring solution

The intercalating solution used also influences the properties of the materials obtained. Aluminium (III) is the most used cation in pillaring processes (Gil *et al.*, 2000). Zr^{4+} (Burch and Warburton, 1986; Figueras *et al.*, 1989; Baksh *et al.*, 1992; Pereira *et al.*, 1998), Ti^{3+} (Bernier *et al.*, 1991; Tsai *et al.*, 1994), Cr^{3+} (Pinnavaia *et al.*, 1985; Maireles-Torres *et al.*, 1991; Toranzo *et al.*, 1997), Fe^{3+} (Barrault *et al.*, 2000; Catrinescu *et al.*, 2003), Ga^{3+} (Bellaoui *et al.*, 1990; Bradley *et al.*, 1990; Bradley and Kydd, 1991) and Ce^{3+} (Booij *et al.*, 1996; Valverde *et al.*, 2000) have also been thoroughly studied. The use of solutions containing mixtures of metals increases the range of materials produced (Gil *et al.*, 2000). The properties of Al- and Cr-PILCs will be further explored in sections 1.3.3.2 to 1.3.3.4.

C. Experimental procedures

The choice of parameters is dependant on the potential use of the material (e.g. increase of acidity for Brönsted acidity driven reactions, increase of the pore size in shape selective reactions or increase of the surface area in gas adsorption applications). Besides the nature of the metallic cation, other important factors must be taken into account: hydrolysis conditions, concentration, maturation time and conditions of the intercalating solutions, contact time, temperature, mixing speed and washing, drying and calcination procedures (Ohtsuka, 1997; Gil *et al.*, 2000). The effect of experimental variables will be explored for Al-PILCs (the most studied materials) in the following section.

1.3.3.2 AL-PILCs

The aluminium pillared clays are, by far, the most regularly studied (Ohtsuka, 1997). The solution chemistry of aluminium has been thoroughly investigated and the polymerisation mechanisms are better understood than those of other cations (Gil *et al.*, 2000). Furthermore, aluminium oxides are stable in both oxidative and reductive media, and present high thermal stability and surface areas (Ohtsuka, 1997).

Generically, most Al pillaring procedures are based on the partial hydrolysis of $AlCl_3$ or $Al(NO_3)_3$ solutions, during different time intervals and at variable temperatures, by controlled addition of powder Al or hydrated Al^{3+} salt (Kloprogge, 1998). The solutions prepared in such a way exhibit high concentrations of $[Al_{13}O_4(OH)_{24}(H_2O)_{12}]^{7+}$ (Ohtsuka, 1997), a Keggin structure described by Johansson (1960) and commonly represented by Al_{13}. The Al_{13} structure is composed of 12 Al octahedral, assembled as 4 groups of 3 octahedra, arranged around a central AlO_4 tetrahedron. The average diameter is 8.6 Å (Ohtsuka, 1997).

The intercalation of the Al_{13} ions is performed by careful addition of the oligomer solution to a clay suspension, under stirring; the contact period is variable. Several authors concluded that the saturation of the negative charges by small aluminium species is the first step, followed by Al_{13} diffusion and that the ion exchange rate is controlled by the diffusion of the latter (Plee *et al.*, 1987; Suzuki *et al.*, 1988; Figueras *et al.*, 1990; Katdare *et al.*, 2000). The excess is removed by washing (dialysis or several consecutive water additions and centrifugations). The samples obtained are dried at 60ºC or lyophilised. The last step is the calcination at temperatures normally above 400 ºC (Kumar *et al.*, 1997; Toranzo *et al.*, 1997; Cañizares *et al.*, 1999; Gandía *et al.*, 1999). It is often stated that calcination of the pillars results in their transformation into aluminium oxide. This formulation is imprecise and misleading because the stoichiometry of Al_2O_3 cannot be obtained in Al_{13} moieties and the environment of Al^{3+} in pillared materials is not the same as in classical forms of Al_2O_3 (Fripiat, 1988; Lambert and Poncelet, 1997). During calcination at 500 ^{o}C, the Al_{13} ions undergo dehydration and pillar/layer anchoring reactions, but the Al/O/OH skeleton remains intact (Lambert and Poncelet, 1997). The Al-PILCs obtained by these methods exhibit basal spacings of about 18 Å and surface areas that reach 300 $m^2.g^{-1}$ (Ohtsuka, 1997; Cheng, 1999).

Several factors affect the pillaring processes and they have been thoroughly studied. The amount of Al_{13} species depends on the preparation method, the nature of the reactants and their initial concentration, the degree of hydrolysis (OH/Al ratio) and the hydrolysed solutions maturation time (Vaccari, 1998). In order to exemplify the effect of these parameters, some selected examples are presented as follows.

Kumar *et al.* (1997) studied the effect of the OH/Al ratio (between 1.5 and 1.9) on the texture and acidity of Al-PILCs. The PILC prepared with the Al solution hydrolysed with OH/Al = 1.7 exhibited a higher concentration of Brönsted acid sites.

Moreno *et al.* (1997) studied the influence that different pillaring solutions had on the structural, textural and acidic properties of pillared saponites and montmorillonites. Basically, the different pillaring methodologies varied in terms of the source of Al^{3+} cations. Structurally, the PILCs prepared with solutions containing 'exclusively' Al_{13} ions exhibited better thermal stabilities, due to increased pillar density. Additionally, the pillared saponites (but not the montmorillonites) prepared with the commercial and the 'pure' Al_{13} solutions exhibited higher surface areas and stronger acidic sites.

When dilute solutions are used, the Al_{13} ions may be excessively hydrolysed which generates smaller species (Harris, 1988; Schoonheydt *et al.*, 1993). The pillared materials may incorporate high amounts of Al, but the species distribution is irregular, due to the faster diffusion of the smaller species. With more concentrated solutions, the Al_{13} molecules may associate, which produces materials with a smaller uptake of aluminium (Harris, 1988). Other authors refer to the necessity of heating the Al^{3+} solutions in order to accelerate their maturation. However, this procedure may gradually produce an Al_{13} dimer (Ohtsuka, 1997).

Vicente *et al.* (1996[b]) studied the influence of the Al concentration-to-mass of clay ratio on the properties of an iron rich saponite. The amount of aluminium incorporated did not change significantly nor did the basal spacings or acidity values, but the material prepared with the highest Al/mass of clay ratio exhibited the highest surface area and porosity.

Normally, the pillaring procedures are carried out in dilute conditions, which requires the manipulation of large volumes of water. Moreover, the pillaring solution and clay suspension maturation steps are time consuming. Schoonheydt and Leeman (1992) and Schoonheydt *et al.* (1993) analysed the effect of the concentration of the Al solutions and clay dispersions on pillared saponites. These authors used concentrated Al^{3+} and NaOH solutions, matured at high temperatures for short periods and mixed the hydrolysed solution obtained with air-dried

clay samples during 12 h. The materials obtained exhibited basal spacings comparable to conventionally prepared materials.

The intercalation step is very time consuming, because the pillaring solutions have to be added drop-wise and the resultant mixture needs time and energy to reach maturity. Katdare and co-workers (1997, 1999, 2000) intercalated a Ca-montmorillonite using ultrasonic treatment over a number of time periods and different Al^{3+}/clay ratios. The PILCs prepared using ultrasound presented better thermal stability than the conventionally prepared material, which was attributed to the more uniform pillaring obtained by the use of ultrasonic's. The ultrasound route did not alter properties such as acidity and catalytic activity. Fetter *et al.* (1996, 1997) also looked at a way to speed up the intercalation step by using microwave irradiation. They prepared clay/aluminium chlorohydrate slurries and subjected the sealed mixtures to microwave irradiation. These samples gave surface areas some 20-30% higher than samples prepared by conventional methods.

The washing and drying steps also influence the properties of the materials obtained, mainly in terms of structural properties (former) and textural properties (later). Two procedures are commonly used to remove the excess pillaring solution: i) dialysis and ii) consecutive water addition and centrifugation steps. The first procedure requires large amounts of water and long realisation periods and the second is more aggressive for the solid (Gil *et al.*, 2000). Despite the method used, the removal of the excess intercalating solution seems to play an essential role on the intercalation step.

Schoonheydt and Leeman (1992) followed the structural changes that occurred in an intercalated saponite after each washing step using XRD. After the third washing step, a symmetrical and unchanging peak appeared in the trace of the material. Similar results were obtained by Thomas and Occelli (2000). Moreno *et al.* (1997) prepared an intercalated montmorillonite and removed the excess of Al_{13} solution by the two different procedures

noted above. The dialysed material exhibited a smaller initial basal spacing (non heated sample), but calcination at 400 ºC inverted this behaviour. Bergaoui *et al.* (1995) obtained diffractograms of a natural saponite intercalated with Al_{13} after successive dialysis treatments. The non dialysed material exhibited two peaks, assigned to the presence of layers intercalated with Al_{13} and hydrated Na^+ (thus, incomplete intercalation had occurred). After, the first dialysis, complete intercalation occurred and upon subsequent dialysis, the organisation of the intercalated layers improved. Aceman and co-workers (2000) examined how the use of dialysis compared to conventional washing methods using several types of clay. They verified that initially Al is adsorbed into the layer space either in a monomeric state or as small oligomers and that several days were needed for the species to undergo hydrolytic oligomerisation to form Keggin-like ions. Dialysis improved the intercalated beidelitte and saponite properties when compared to the washed materials but the dialysed and non-dialysed montmorillonite, hectorite and laponite materials exhibited similar properties.

The drying procedure employed (air-dried or lyophilised) decisively influences the textural properties of the products obtained. In the first case, materials with a lamellar aggregation (face-to-face orientations – Figure 1.8A) are obtained, whereas in the second case, a 'house of cards' like structure (edge-to-edge and edge-to-face orientations – Figure 1.8B) predominates. The first type of materials is essentially microporous, whereas the second offers a combination of micro- and macroporosity (Kloprogge, 1998; Vaccari, 1998). Although this is a common tendency, it does not necessarily occur all the time (de Carvallho *et al.*, 1996). These authors characterised the texture of three pillared montmorillonites which had been dried in air or lyophilised. One of the materials exhibited lower surface area when lyophilised than its air-dried counterpart. The authors explained these results based on the smaller particle size of the parent material, a factor that favours the face to face aggregation and overcomes the lyophilisation effect.
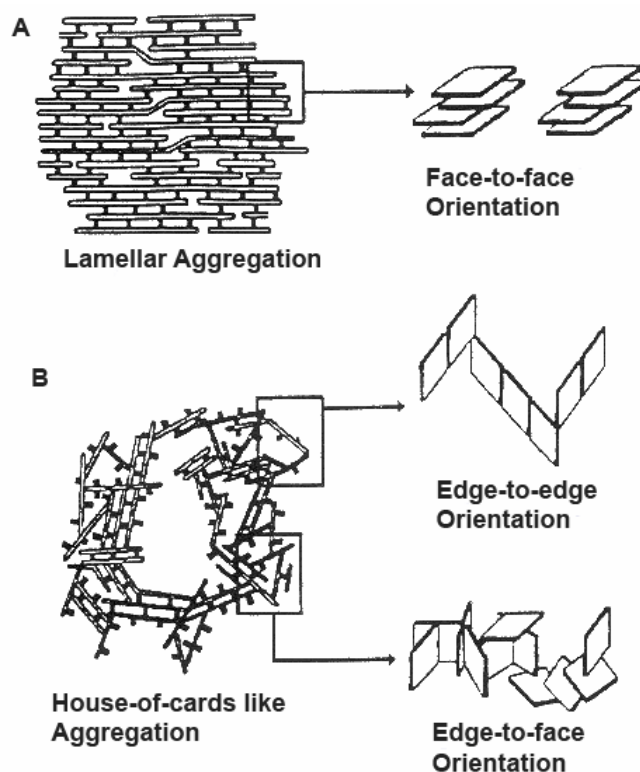
Figure 1.8 Schematic representation of A: lamellar aggregation and B: 'house of cards' like aggregation (Kloprogge, 1998)

Several authors used ^{27}Al and ^{29}Si NMR techniques to study the thermal transformations that occur in the pillars and their bonding to the clay layers (tetrahedrally substituted beidellite and saponite) (Plee *et al.*, 1985[a]; Lambert *et al.*, 1994; Bergaoui *et al.*, 1995). The proposed model involves the inversion of an Al tetrahedron from the tetrahedral sheet and implies the formation of new Si-O-Al^{IV} bonds, in which a negative charge is exposed in the interlayer space. The mechanism involved in the pillaring of smectites without tetrahedral Al is less clear. Kloprogge *et al.* (1999) extended the study of the pillaring mechanisms with Al$_{13}$ to montmorillonites, using infrared spectroscopy. These authors confirmed the existence of structural modifications of the tetrahedral sheets of saponites due to bonding with pillars. However, no evidence of interaction between the pillars and the montmorillonite structure was obtained for the pillared montmorillonites, despite the structural modifications detected in the pillars.

The shelf life of Al-PILCs (and of their uncalcined counterparts) was studied by Chevalier *et al.* (1994). After 5 months, the surface areas of the uncalcined materials did not change significantly (minus 9%) and the basal spacings remained constant, but the subsequent heating at 500 ºC produced a material with a 30% decrease in surface area. Aging produced more significant alterations in the Al-PILC in terms of surface area (-41%) and basal spacing (broader and less intense d_{001} peak). These changes may be attributed to partial hydrolysis of the aluminium pillars, therefore two types of basal spacings coexisted i.e. those produced by unaltered and hydrated pillars. This result proves that calcination at 500 ºC does not stabilize permanently the aluminium pillars (at least when saponite hosts are considered).

The Al interlayer uptake per unit cell is restricted to a narrow range (2.78-3.07), which corresponds to approximately one pillar of Al_{13} per 4.2-4.6 unit cells, and shows no correlation with the structural charge (Kloprogge, 1998). Chevalier *et al.* (1994) and Bergaoui *et al.* (1995) studied the effect of clay charge on the mechanism of intercalation/pillaring of natural and synthetic saponites and found out that the Al uptake never exceeded the equivalent of one Al_{13} per 6 unit cells. These authors concluded that this was the maximum possible density, related to steric hindering of Al_{13}, when confined in tight spaces. They demonstrated that the layer charge influenced the competition between flocculation and intercalation: low charge saponites flocculated easily, directly related to the decrease in the intercalation rate. Although the layer charge does seem to not influence the maximum pillar density, Al-PILCs with specific pillar densities may be obtained by controlling the CEC of the parent material (Suzuki and Mori, 1989) or using competitive ion exchange procedures (Figueras *et al.*, 1990).

Al-PILCs exhibit increased Brönsted and Lewis acidity, when compared to the parent materials. Bergaoui *et al.* (1995) assigned the Lewis acidity to pentacoordinated Al, formed by loss of remaining terminal H_2O ligands from 6-coordinated Al in the pillars. The origin of Brönsted acidity is less clear, but results suggest contributions from the pillar OH groups and

from other acidic species formed in the clay layers (Lambert and Poncelet, 1997). Normally Al-PILCs exhibit a higher proportion of Brönsted than Lewis acid sites, when calcined at moderate temperatures. The number of acidic centres in Al-PILCs (based on NH_3 adsorption data) increases with the number of incorporated pillars and it is comparable with the acidity of certain zeolites (ca. 2.8 mol $NH_3.m^{-2}$). When treated under the right conditions, the acid strength of an Al-PILC is similar to the acid strength of zeolite-Y (Cheng, 1999).

1.3.3.3 CHROMIUM PILLARED CLAYS

Chromium (III) ions are among the few that can be extensively hydrolysed in order to produce bulky polyoxocations (Kloprogge, 1998). Cr-PILCs exhibit interesting properties and have proven to be active in several reactions, including cyclohexene dehydrogenation, n-decane hydrolytic decomposition and butane hydrogenation (Sychev *et al.*, 2000). Probably, the greatest potential for Cr-PILCs is related to their use as active catalysts in oxidation reactions, namely epoxidation (important regio- and stereo-selectivities) and mild oxidation (e.g. alcohols) reactions. Cr_2O_3 does not present inherent catalytic activity and, therefore, requires a reactant that promotes (and maintains) Cr in a high valence state (e.g. organic peroxides). Unfortunately, these chemicals are expensive and may be hazardous (Clark, 1994; Toranzo *et al.*, 1997).

Cr polyoxocations are prepared, normally, by basic hydrolysis, in a similar fashion to their Al counterparts. The oligomerisation reaction is slow at room temperature, but quite fast at 100 ºC. During maturation, the initial $Cr(NO_3)_3$ purple solutions change to blue (due to the presence of the dimer $[Cr_2(OH)_2(H_2O)_8]^{4+}$) and then to green (larger oligomers) (Kloprogge, 1998). Thus, the maturation of Cr solutions may be monitored by UV-vis spectroscopy (Toranzo *et al.*, 1997).

Two generic methods were developed for the preparation of Cr-PILCs: i) intercalation with polynuclear Cr(III) species generated by basic hydrolysis with heating and ii) intercalation of hydrolytic Cr(III) species, e.g. dimers, trimers and tetramers (Drljaca *et al.*, 1997).

In opposition to Al-PILCs, many questions remain unanswered about the species that participate in the intercalation. The existence of the cation $[CrO_4Cr_{12}(OH)_{24}(H_2O)_{12}]^{7+}$, analogous to Al_{13} was considered, but quickly ruled out due to the lack of experimental evidence (infrared and UV-vis spectroscopy) to support a tetrahedrally coordinated Cr(III) atom, similar to the central Al atom in Al_{13} (Bradley *et al.*, 1993; Kloprogge, 1998). Actually, there are very few structures where Cr(III) exhibits a tetrahedral coordination (Bradley *et al.*, 1993; Palinkó *et al.*, 1997). These authors proposed, based on UV-vis and infrared spectroscopy, the existence of a dodecameric Cr structure $[Cr_{12}(OH)_{28}(H_2O)_{12}]^{8+}$, structurally similar to Al_{13}, but with a vacant central position. To reinforce this hypothesis, Bradley and co-workers (1993) draw attention to the similar basal spacings of the materials intercalated with hydrolysed solutions of Cr and Ga (Ga coordinates in a Ga_{13} structure, equivalent to Al_{13}). Toranzo *et al.* (1997) studied several hydrolysed chromium solutions, used in saponite intercalation studies, and suggested that the predominant (but not unique) species present was the trimer $[Cr_3(OH)_4(H_2O)_9]^{5+}$. In his review article, Kloprogge (1998) referred to several studies aimed at clarifying the oligomeric species present suggested of the presence of linear trimers built of three octahedra, a result that reinforces Toranzo and co-workers (1997) suggestion.

Vijayakumar *et al.* (1994) studied the effect of Cr concentration on the structural, textural and acidic properties of montmorillonites and vermiculites, pillared with this metal. When montmorillonites were used, the surface increased with increasing Cr^{3+} concentration, but the basal spacing did not follow the same trend, remaining constant at 15.6 Å for all PILCs. The surface areas of the Cr pillared vermiculites did not change significantly. In terms of acidity, the pillared montmorillonites were clearly more acidic (Brönsted and Lewis) than the

unpillared material. As noted by Kloprogge (1998), the Lewis acid centres of Cr-PILCs are stronger than the corresponding acidic sites in Al- and Zr-PILCs, and that acidity, together with an increased macroporosity, may produce more catalytically active materials.

Toranzo *et al.* (1997) obtained Cr pillared saponites with basal spacings of 16.5 Å stable up to 200 ºC. The non heated intercalated material exhibited a basal spacing of 18.9 Å, compatible with the presence of dimeric, trimeric and/or tetrameric Cr species. The calculated oligomer density per unit cell was 0.548. The authors attributed this somewhat high value to the small size of the trimer, when compared to Al_{13} oligomers. The surface area of the material heated at 200ºC was higher than that of the parent clay, but heating the material at 300ºC, or above, destroyed the pillared structure and the surface area values decreased back to the initial value or lower.

Sychev and co-workers (2000) prepared Cr pillared bentonites and verified that the increase in Cr uptake produced materials with higher surface areas, but with lower pore volume, which would be expected due to the higher pillar density. These authors concluded that an important part of the porous volume of the Cr-PILCs arises from ultramicropores (diameters under 0.7 nm) and that the contribution of these increased with increasing Cr content.

Cañizares *et al.* (1999) compared several properties of two bentonites pillared with Cr and obtained large basal spacings for intercalated materials (23-24 Å) and those calcined at 300 ºC (20 Å). The pillared structure collapsed above this temperature. The acidity of the Cr materials (NH_3 TPD) was higher than the Al counterparts (ca. 0.5 mmol $NH_3.g^{-1}$ vs. 0.3-0.4 mmol $NH_3.g^{-1}$, respectively). Surface areas and micropore volumes of the samples calcined at 200ºC were comparable to the Al-PILCs.

The low thermal stability of the Cr-PILCs is related to the oxidation in air of Cr(III) and subsequent formation of volatile oxides (Ohtsuka, 1997; Kloprogge, 1998). Some doubts

remain about the nature of the oxide obtained by calcination of the materials intercalated with Cr oligomers. The exclusive presence of Cr_2O_3 was proposed, as well as a Cr(III) and Cr(V) mixed oxide (Cr_5O_{12}) (Toranzo *et al.*, 1997).

The prolonged maturation of chromic solutions, at room temperature, may induce the dissociation of the bigger agglomerates and, hence, using recently prepared heat maturated solutions is probably more reliable. Calcination in an inert atmosphere seems to prevent, to some degree, structural collapse (Kloprogge, 1998).

1.3.3.4 MIXED AL-CR PILCS

One of the attractive features of pillared clays is the possibility of modifying the materials produced in order to improve certain properties; these modifications may be performed before, during or after the intercalating/pillaring process. The increasing interest in modified versions of monometallic PILCs (mainly Al-PILCs) is clearly demonstrated by the number of review articles that focus on this issue (Kloprogge, 1998; Zhu and Lu, 1998; Gil *et al.*, 2000).

Cr-Al-PILCs have caught the attention of several investigators due to the intrinsic acidic properties of Cr and its use in several catalytic processes.

Zhao and co-workers (1995) produced an Al/Cr-PILC using $CrCl_3$ and $AlCl_3$ in Na_2CO_3 solution. Basal spacings of around 18 Å were achieved when calcined at 500 ºC with surface areas around 230 $m^2.g^{-1}$.

Toranzo *et al.* (1997) pillared a saponite with solutions containing different Al/Cr ratios. Al^{3+} polymerised to form exclusively Al_{13}, whereas Cr^{3+} formed trimers $[Cr_3(OH)(H_2O)_9]^{5+}$, dimers $[Cr_2(OH)_2(H_2O)_8]^{4+}$ or did not polymerize, depending on the Al^{3+}/Cr^{3+} ratio of the intercalating solution. The mixed metal PILCs obtained presented intermediate properties between Al-

PILC (d_{001} = 18 Å and stable up to 600 ºC) and Cr-PILC (d_{001} = 19 Å, but unstable above 200ºC). The thermal stability was strongly dependant on the Al uptake, reaching 500 ºC when Al^{3+}/Cr^{3+} > 1. The values of surface areas and the porous structures were intimately related to the evolution of the thermal stability. On the other hand, the catalytic activity in the deep oxidation of acetone depended, strongly, on the amount of Cr present. For a given quantity of Cr, the activity was higher in samples with increased accessibility of acetone to the active phase, which reflects the porous structure of the PILC (dependant on the pillar density).

Palinkó *et al.* (1997) and Kiricsi *et al.* (1997) prepared Cr-Al-PILCs by co-hydrolysis of $CrCl_3$ and $AlCl_3$ in the presence of a sodium montmorillonite. They used several Al/Cr ratios and obtained materials with basal spacings ranging between 18.4 and 19.1 Å and surface areas between 152-265 $m^2.g^{-1}$. These authors investigated the presence of Cr in the pillars and concluded that Cr^{3+} ions do not incorporate into the Al_{13} structure and that co-hydrolysis and co-pillaring took place.

Cañizares *et al.* (1999) prepared single Cr- and mixed Al/Cr-PILCs using three types of intercalating strategies: i) incorporation of Cr^{3+} into the calcined Al-PILC by impregnation, ii) pre-swelling of the clay with the Al_{13} ions, followed by addition of the oligomeric Cr solution and iii) intercalation of mixed Al/Cr hydrolysed solutions. The latter method produced better materials. The authors concluded that the pillar structure varies with the Al/Cr ratio of the intercalating solutions; higher ratios produced PILCs where the Keggin structure predominates, whereas in those with lower Al/Cr ratios, the resultant structure approaches that of the monometallic Cr-PILC.

1.3.3.5 OTHER PILC MODIFICATIONS

Further modifications may be performed on PILCs in order to improve or fine tune their properties for specific applications, namely substitution of the exchangeable cations by

relevant cations, prior to or after the pillaring process (Li^+, Na^+, Mg^{2+}, Al^{3+}, Cu^{2+}, Fe^{3+}, Cr^{3+}, etc.) and acid activation of the PILCs (Pillared Acid Activated Clays, PAAC). (Mokaya and Jones, 1994; 1995; Zhu and Lu, 1998; Zhu *et al.*, 2000; Gil *et al.*, 2000).

A. M^{n+}-doped Pillared Clays

A different approach for modifying single oxide PILCs is doping (prior to or after the pillaring process) with small quantities of metallic cations. The materials obtained may present clearly different properties than the ones obtained by co-hydrolysis (Lenarda *et al.*, 2000).

Normally, sodium homoionic forms of the clays are used for the pillaring process. However, PILCs have low CECs after being calcined. During heating, while the pillaring precursors undergo dehydration and dehydroxylation, protons are released. The released protons (positively charged and with reduced size) migrate into the clay layers and become quite inaccessible for subsequent cationic exchange processes. If these migrant protons are enticed back out of the clay layer in the PILCs, they can be substituted by bulkier cations that are unable to migrate into the layer through the small ditrigonal cavity. Thus, the PILCs will reassume appreciable CECs (treatment with bases such as K_2CO_3, NaOH, KOH and ammonia may recover up to 80% of the initial CEC). The positive counter ions of the base used (frequently NH_4^+) are retained by the PILC in order to compensate the inherent clay layers negative charge. The bases may react with the acidic centres of the pillars, responsible for the Lewis acidity of the PILCs. (Zhu and Lu, 1998; Zhu *et al.*, 2000). An alternative doping method consists in the replacement of the sodium ions by relevant ions prior to the pillaring process. The new homoionic form of the clay is then pillared in a controlled fashion and some of the substitute ions remain in the pores of the final material. The amount of fixed cations is generally higher than when post pillaring doping techniques are used. On the other hand, the materials tend to exhibit low porosity values and the number of fixed ions is difficult to control (Zhu *et al.*, 2000).

The inclusion of transition metals with catalytic properties is possible using these two step techniques. Other useful properties that result from doping are: modifying the hydrophobic character of Al-PILCs into hydrophilic (selective adsorbents) and rigorous adjustment of the pore dimensions (catalytic and separation applications) (Hutson *et al.*, 1998; Yang *et al.*, 1998, Zhu and Lu, 1998; Lenarda *et al.*, 1999; Zhu *et al.*, 2000).

B. Acid Activated PILCs

The pillaring of clays previously submitted to acid treatments permits the combination of the attractive features of both types of materials. Several studies performed on acid activated pillared clays showed that the physical and chemical properties of these materials are a mixture of the properties of normal PILCs and acid activated clays. The acid activated PILCs were tested in several reactions, namely pentanol and butanol dehydration and cumene conversion and generally exhibited higher catalytic activities than PILCs or acid activated materials. Brönsted acidity is highly accentuated in these materials. Their adsorption properties also improved (e.g. adsorption of chlorophyll from edible oils) (Mokaya *et al.*, 1993; Mokaya and Jones, 1994; 1995; Bovey and Jones, 1995; Kooli and Jones, 1998).

1.4 TERPENE CONVERSION

1.4.1 RENEWABLE FEEDSTOCKS

Depleting reserves and rising prices of oil, together with the need for sustainable production, has led to an emerging necessity to produce chemicals from renewable feedstocks. Recently, Okkerse and van Bekkum (1999) showed that the production of top eight organic materials (polyethylene, polypropylene, polyvinylchloride, polyethyleneterephthalate, polystyrene-butadiene copolymers, phenol resins and polyamines) from renewable sources is technologically feasible, though novel synthetic routes need to be developed. On the other

hand, around 95% of all industrial heterogeneous catalysts are used in the production of bulk chemicals and only 3–5% in the synthesis of fine chemicals, yet this seemingly low percentage delivers approximately 20% of the profit (Hölderich, 2000).

The use of renewable feedstocks from natural sources is a growing field in which heterogeneous catalysis can offer considerable improvement. The conversion of cheaply available limonene to the more commercially valuable p-cymene (for use in fine and speciality chemicals) is a good example.

World production of turpentine oils in 1995 was around 330,000 tons. Crude sulfate turpentine accounted for 230,000 tons with the remainder being from gum turpentine. The flavour and fragrance industry consumes approximately 30,000 tons per year of pinenes used to produce a diverse range of products. Limonene production is around 30,000 tons per year, making it a valuable and renewable feedstock for the flavour and fragrance industry and others (Swift, 2004).

1.4.2 LIMONENE AND P-CYMENE

Limonene - 1,8(9)-p-menthadiene (Figure 1.9A), a cyclic monoterpene, is the major component present in pine gum (*Pinus Pinea, L.*) with contents between 75 and 90% (Costa and Lourenço, 1982). Recently, Lourenço (1999) reported average limonene compositions of 92% in 30 samples of pine gum obtained from *Pinus Pinea, L*. However, despite being an abundant raw material that is easy to obtain and purify, limonene is not highly valued even though it does have several applications in industry (Lourenço and Casquilho, 1988), namely in the ink and varnish industries (Shimakava and Sasami, 1993; Williams, 1993; Takahashi and Mizoguchi, 1994; Vlasbom and Dotolo, 1994), in cosmetics and perfumery production (Kolomai, 1990; McGee *et al.*, 1993), in pharmaceutical preparations (Matsuda *et al.*, 1993[a]), as an intermediate in organic synthesis, aromatising agents in the food industry and

detergent addictives (Yokusuka *et al.,* 1992; Matsuda *et al.*, 1993[b]; Shirato and Inoe, 1994).

P-cymene (1-isopropyl-4-methylbenzene) – Figure 1.9B - finds many applications in the chemical industry including its use as a solvent in the ink and varnish industry, for the production of carvacrol, as an intermediate in the synthesis of anti-oxidants (e.g. BHT), in the production of synthetic resins, in perfumery and as a thermal fluid in heat exchanging systems (Booth and Autentrieth, 1969; Fiege, 1987; Sato *et al.*, 1993).
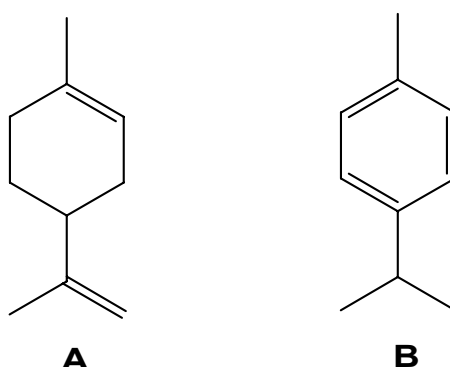
Figure 1.9 Structures of A. limonene and B. p-cymene

The main use of p-cymene is its transformation to p-cresol. At the moment, p-cresol is mainly produced industrially via the alkylation of toluene with propylene or 2-propanol (BASF, 1967), followed by oxidation and hydroperoxide cleavage. The alkylation and isomerisation steps (over Friedel–Crafts catalysts, e.g. hydrochloric acid containing $AlCl_3$, BF_3 or H_2SO_4) produce a mixture of cymenes rich in m- and p-isomers, which is difficult and energetically demanding to separate by distillation due to the number of components present in the mixture, the proximity of their boiling points and the possibility of azeotrope formation (Fiege, 1987; Roberge *et al.*, 2001). In addition, the use of acid gives rise to many problems regarding handling, safety, corrosion and treatment of the disposed catalyst. In contrast, the dehydrogenation of limonene, which already possesses the required carbon skeleton, promoted by solid catalysts, is very attractive.

1.4.3 LIMONENE CONVERSION TO P-CYMENE

Limonene has been transformed into cymene using a variety of catalytic systems; nickel, palladium on coal or alumina, platinum on coal, chromium oxide with or without oxides of copper or zinc, Fuller's earth, copper–nickel, activated alumina, and the heteropolyacid $H_5PMo_{10}V_2O_{40}$ (Swift, 2004).

1.4.3.1 HOMOGENEOUS CATALYSIS

Baeyer and Villiger (1898) described a method for aromatizing limonene based on its complete bromination, followed by reductive HBr removal. Another halogen based method involves the known capacity of iodine to promote the migration of double bonds throughout the carbon skeleton of olefins. Although little information about the process was available by the time of his findings, Ho (1987) reported that heating limonene with catalytic quantities of iodine, for several hours produced a mixed with 65% of p-cymene. Several organometallic compounds were reported as catalysts in hydrogen transfer reactions, including for example, lithium-, sodium- and potassium-ethylenediamine (Reggel *et al.*, 1958; Brown, 1973; Mitchel and Sasser, 1993).

1.4.3.2 HETEROGENEOUS CATALYSIS

It was first proposed that acid centres are required to isomerise the double bonds into the cyclohexene ring. Once these ring conjugated bonds are formed aromatisation can proceed rapidly over the dehydrogenation function of the catalyst. The function can be either based on Cr_2O_3 (Krishnasamy and Yeddanapalli, 1976; Hercules Powder Co. U.S., 1946; Am. Cyanamid Co., 1942) or Pd (Buhl *et al.*, 1998; 1999). The major challenge is the precise control of the acid site strength necessary to minimise secondary reactions, such as polymerisation and/or further isomerisation of p-cymene. Krishnasamy and Yeddanapalli (1976) have shown that an optimum amount of K^+ ions is required in the Cr_2O_3/γ-alumina catalyst, to neutralize the strong acid sites. Weyrich *et al.* (1997[a,b]) have used a Ce-promoted Pd/ZSM-5 catalyst which offered

both enhanced selectivity towards p-cymene and slower catalyst deactivation. The acidity of the host zeolite also had a very significant impact on both the catalytic activity, and the selectivity for p-cymene. Lopes (1996) used commercial Y-zeolites as catalysts for the limonene conversion reaction, both in batch and flow conditions. The author tested several parameters including temperature, solvent effect, and limonene-to-zeolite ratio and found that the zeolites exhibited poor selectivity for p-cymene and were rapidly deactivated.

The second approach is the use of a purely hydrogenation/dehydrogenation catalyst under reducing conditions. For this process Pd supported on a low-acidity silica carrier turned out to be the most appropriate catalyst. At temperatures of ca. 300°C the yield of p-cymene is > 99%.The catalyst has been tested with commercial mixtures of terpenes (dipentene) and the yield remained high (> 95%). The process is now being tested in a scale-up unit and preliminary results have been published (Buhl *et al.*, 1998, 1999).

The conversion of α-limonene to p-cymene was also performed using solid acid and solid base solid. Two early papers have shown that heating limonene in the presence of Japanese acid clay, results in various mixtures of products with predominance of p-cymene, depending on the reaction conditions (Balogh and Laszlo, 1993). Na^+, Mg^{2+}, Al^{3+} and H^+-exchanged forms of montmorillonite have been used at selected temperatures in the range of 80-175 °C and the amount of p-cymene produced was reported to be inversely related to the surface acidity of the clay (Frenkel and Heller-Kalai, 1983). More recently, de Stefanis *et al.* (1995) have compared the catalytic behaviour of alumina-pillared clays (Al-PILC) with that of layered phosphates and zeolites for the conversion of various terpenes. The large-pore zeolite USY was the most active and selective towards p-cymene, followed by the most acidic of the Al-PILCs catalysts. The order of reactivity was explained in terms of both surface acidities and shape selectivity.

All these studies emphasize the important role of the acidity and active site accessibility, in controlling both the reaction rate and the selectivity towards the desired product.

CHAPTER 2. EXPERIMENTAL

2. EXPERIMENTAL

This chapter is divided into two parts. In the first part, summarised descriptions of the main characterisation techniques used in this thesis will be provided, with the main focus directed towards the information that can be obtained from their application to clay minerals. The second part of this chapter will be dedicated to the description of the actual procedures used for the catalysts characterisation, including the catalytic tests.

2.1 THEORY AND APPLICATIONS

2.1.1 X-RAY FLUORESCENCE (XRF)

XRF is a technique used to determine the quantity of elemental oxides present in a sample. X-rays are directed towards a sample and elements present in the sample produce characteristic fluorescence radiation at specific, characteristic wavelengths. The incoming X-rays eject core shell electrons and electrons from higher energy levels drop down to fill the vacancy. As the electron drops from the outer shell to the inner shell a frequency characteristic of the element is emitted because the energy difference between the two quantised electron shells is a fixed quantity. The amount of fluorescence at a specific wavelength is then related to the concentration of the element in the sample.

XRF is a very popular technique for geological materials analysis, because it is possible to identify and quantify a wide range of elements, present in quantities as low as a few ppm. Both major (Na, Mg, Al, Si, P, K, Ca, Ti, Mn and Fe) and trace elements may be analysed in a quick routine manner.

To obtain XRF data the samples have to be homogeneous, because the grain sizes and shapes may significantly influence the intensities of the fluorescence lines. The usual method to homogenize the material is the $Li_2B_4O_7$ (or $Na_2B_4O_7$) fusion method. The vitreous phase

obtained presents a homogeneous distribution of the chemical elements. In order to overcome the matrix effect (variation of the fluorescence lines of certain elements under the influence of others) a matrix matched calibration curve is used (Gomes, 1988; Bain *et al.*, 1994).

2.1.2 X-RAY DIFFRACTION (XRD)

XRD is a powerful technique used to identify the crystalline phases present in materials - Figure 2.1 (Brindley and Brown, 1984). Figure 2.2 shows the basic features of an XRD experiment.
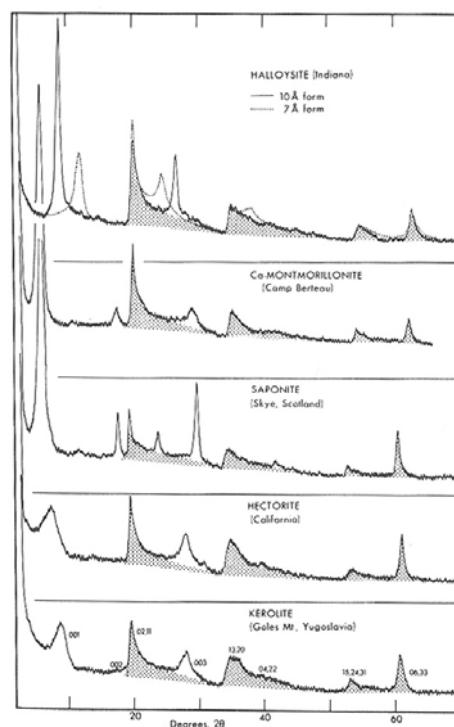
Figure 2.1 X-Ray diffractomer patterns of halloysite, 7 Å and 10 Å forms, of three smectites, Ca-montmorillonite, saponite, and hectorite, and of kerolite. The two dimensional diffraction bands are stippled to emphasize their similarity. Cu Kα radiation. (Brindley and Brown, 1984)

X-rays are produced, as in XRF, when high speed electrons strike the atoms of any substance. A modern X-ray tube consists of a heated filament (source of electrons) and a metal target (e.g. Cu) in an evacuated chamber.
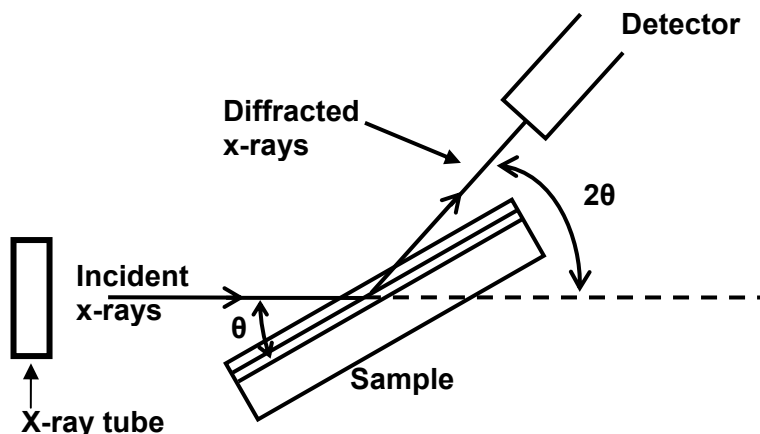
Figure 2.2 Basic features of a XRD experiment

In a typical experiment the diffracted intensity (of the scattered X-rays that obey Braggs Law) is measured as a function of the diffraction angle (2θ) and the orientation of the sample, which yields the diffraction pattern. Diffraction will occur if a beam of X-rays falls on a series of atom-bearing planes, each a distance d apart, at an angle θ, if the Bragg Law is obeyed:

$$n\lambda = 2d \sin \theta$$

(where λ is the wavelength of the rays and n is an integer).

During an experiment the detector and sample are rotated by a goniometer in order to cover the required angle ranges (3-75°). Samples can be offered as a deposited film or as a powder. Deposited films are obtained by smearing a solution of the clay on a glass slide and allowing the film to dry. The use of powder samples involves compacting a finely ground sample into an aluminium sample holder.

The two most useful XRD regimes for clay characterisation are the basal spacing region (2-10° 2θ, Cu radiation) and the (060) reflection (near 60° 2θ), which is diagnostic for several structural and compositional types. For PILCs, for example, the basal spacing is essential to

confirm the success of the experimental procedures. In the case of AAC, the depletion of the material may be followed by changes in intensity of the (060) reflection peak. Two standard polar molecules are used to determine the swelling properties of clays: water yields a 5 Å^3 increase in basal spacing and ethylene glycol expands layers by 7° 2θ (Carrado, 2004).

2.1.2.1 QUANTITATIVE XRD

In order to obtain quantitative information from XRD data, the use of internal standards is a common procedure. A standard substance S is added to the mixture to be analysed in a known weight proportion. Reflections from S and from the components of the mixture are compared using (a) S in the unknown mixture and (b) S in a known mixture.

The internal standard should have a low attenuation coefficient, preferably only a few reflections and at least one conveniently located strong reflection. Then a small proportion of S can be used, with a minimum interference between the reflections from S and those from the components of the mixture. The intensities of the mixture components will be diminished only slightly by the addition of S. Corundum, α-Al_2O_3, has been adopted by the *Joint Committee on Powder Diffraction Standards* as a suitable standard for comparing the diffraction intensities from powdered materials. The Reference Intensity Ratio (RIR) method is often used for quantification purposes and it is based on the ratio of intensities of the strongest line of the sample to that of the reference phase for a 1:1 mixture (the standard values are listed on the *International Centre for Diffraction Data*) (Brindley and Brown, 1984).

2.1.3 SURFACE AREA DETERMINATION, PORE VOLUME AND PORE SIZE DISTRIBUTION

Surface area determination of unmodified and modified clay catalysts and absorbents is an essential characterisation feature. This parameter is determined normally from physical

---

[3] Depending on the exchange cation and relative humidity

adsorption equilibrium isotherms of a vapour (frequently nitrogen). The 5 types of adsorption isotherms according to Brunauer are displayed schematically in Figure 2.3.
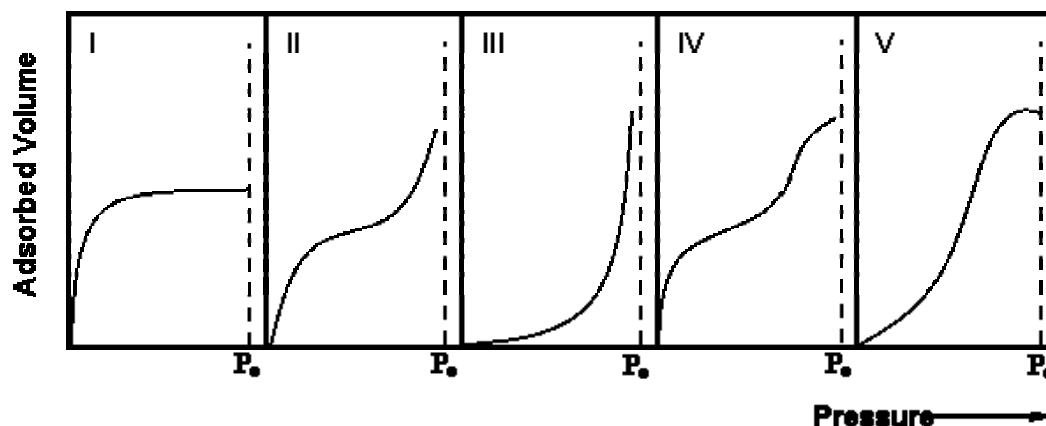
Figure 2.3 Adsorption isotherms types according to Brunauer's classification (Thomas and Thomas, 1997)

The ype I isotherm is characteristic of microporous solids with a small external surface. This isotherm is also representative of chemical adsorption, where the sorption limit value is related to the formation of a monolayer. In isotherms of types II and III, the adsorbed quantity tends to ∞, when the p/p0 ratio tends to 1, and corresponds to superimposed multilayer adsorption, typical of non porous and macroporous solids. If the solids are mesoporous (pore diameters between 2 and 50 nm) isotherms of the types IV and V are obtained (derivations from isotherms II and III, respectively) due to the capillary condensation phenomenon. The adsorbed quantity tends to a fixed maximum value, corresponding to the complete filling of the capilliaries with the adsorbate in the liquid state (Figueiredo and Ribeiro, 1989). Unmodified clays normally exhibit, type I or II isotherms (microporous solids); pillaring and harsh acid activation produces mesoporous materials resulting in type IV isotherms (mesoporous solids).

The hysteresis phenomenon (the desorption curve is not collinear with the adsorption curve) present in the physical adsorption isotherms is associated with capillary condensation in mesoporous structures. PILCs and acid activated clays normally exhibit type H3 (IUPAC

classification) hysterisis loops reflecting behaviour characteristic of aggregates of platelike particles giving rise to slit-shaped pores. It is characterised by 2 assymptotic isotherm branches relative to the vertical at $p/p_0=1$.

The most direct and universally used method for determining the surface area of finely divided solids from the gas or vapour adsorption isotherm was developed by Brunauer, Emmett and Teller (1938). The BET equation is based on the analysis of the multilayer gas adsorption on a solid process and may be written in the following way:

$$\frac{x}{n(1-x)} = \frac{1}{cm} + \frac{(c-1)x}{cm}$$

where x is the relative pressure p/p_0, n is the mass of adsorbed vapour at a given vapour pressure, m is the mass of adsorbed vapour for monolayer formation per unit mass of the solid and c is a constant related with the first layer adsorption energy. For relative pressures between 0.1 and 0.3, the graphical representation of x/n(1-x) as a function of x is linear and the values of m and c may be calculated. Given the known value of the surface area covered by one vapour molecule in the monolayer (calibration with surfaces of known area), the total area per unit mass may be calculated from m (van Olphen, 1977). The typical BET surface areas of smectites (external surface) range between 50 and 150 $m^2.g^{-1}$ (Vaccari, 1998), whereas 300 $m^2.g^{-1}$ is an average value for PILCs (Clark, 1994) and ca. 730 $m^2.g^{-1}$ has been reported for AA clays (Yang, 1999).

The BET surface areas are considered to be underestimates of the actual surface area, due to the important fraction of surface present inside the micropores of the materials. One of the presumptions of the BET equation is not observed, because multilayer adsorption is not possible inside these confined galleries. Roughly two molecules may enter the gallery, but nitrogen molecules, when confined in volumes comparable to their own molecular

dimensions will pack differently from what happens on the external surface. Therefore, the packing densities fluctuate significantly as a function of the interlayer spacing (Chevalier *et al.*, 1994). The use of nitrogen, considered to be an inert gas, is also controversial. Nitrogen is, in fact, a weak Brönsted base and may form acid-base adducts with OH groups. For example, when Al-PILCs are considered, the strongest Brönsted acid sites are the H_2O ligands of the pillars octahedral Al. Hence, nitrogen will bond preferentially to these centres and the adsorption process becomes a pillar titration instead of a simple measurement of exposed area (Michot *et al.*, 1998). Despite these drawbacks, the BET surface area, together with basal spacing data, are the most widely disseminated pieces of information. Hence, although it cannot be considered a real area measurement, it does represent an important comparison value.

Total pore volume and, mainly, pore size distribution are important solid catalyst characterisation data. Pores may be divided in three types according to their diameter d (Campbell, 1988):

- Micropores: d < 2 nm;
- Mesopores: 2 nm ≤ d ≤ 50 nm;
- Macropores: d > 50 nm.

Experimentally, two ways coexist for pore volume and pore size distribution determinations: from gas adsorption data (gas condensation inside narrow pores at lower pressures than the adsorbate saturation pressure) and the Hg porosimetry method (measure of the volume of Hg that penetrates the solid as a function of the hydrostatic pressure applied) (Thomas and Thomas, 1997). Multiple methods have been developed to determine the porous structure of solids from the isothermal adsorption data. Due to their simplicity and the relevance of the information obtained, the α_s and t methods are the most popular (Sychev *et al.*, 2000).

The t-method is used to obtain the micropore volume and the external surface area of microporous solids. It is based on the comparison of the adsorption isotherm data for a porous sample and that for a non porous sample of identical chemical composition and surface character (reference isotherm). When the adsorbed N_2 volume is plotted against the statistical thickness t of the adsorbed N_2 layer (V_{ads} vs t), a linear relation can be obtained (Figure 2.4). If both reference and sample isotherms are identical, i.e. if a straight line passing through or close to the origin is obtained; the microporous volume is obtained from a straight line extrapolated to a positive intercept on the ordinate. The choice of the standard t function and the part of the V-t curve used for linear fitting drastically affect the values of the external surface and micropore volume. In order to overcome these complications, the α_s method was introduced, in which the normalised adsorption, α_s (= $n/n_{0.4}$) is derived from the isotherm of a reference material by using the amount adsorbed at a relative pressure of 0.4 ($n_{0.4}$) as the normalisation factor (Cool and Vansant, 2004).
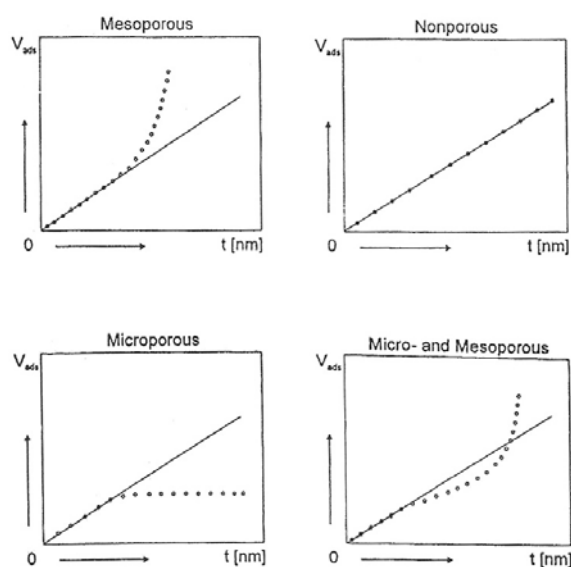
Figure 2.4 t-Plots of mesoporous, nonporous, microporous and combined micro-mesoporous solids (Cool and Vansant, 2004).

2.1.4 THERMOGRAVIMETRIC ANALYSIS (TGA)

There are several different types of water and hydroxyl groups associated with a clay matrix that are liberated with increasing temperature. Upon thermal treatment, clay minerals normally lose water in three distinct regions (Figure 2.5, Guggenheim and van Groos, 2001):

- 80-90 ºC: loss of adsorbed water in defect sites or at broken edges (ca. 1 wt%);

- 100-200 ºC: loss of interlayer water, associated with exchangeable cations in smectites (there is a linear loss of weight between 200 and 500 ºC which is attributed to loss of the inner shell water of hydration. The slope of this line has been shown to be proportional to the polarising power of the exchange cation. The more polarising the cation the steeper the slope).

- 500-700 ºC: dehydroxylation of the inner 2:1 and 1:1 lattice hydroxyl groups, lost also as water (Kaisersberger and Post, 1997).

Thermal analysis is often used to qualitatively determine the binding energies of these different types of water, which can then be used to help characterize a mineral. Three techniques are normally used for thermal analysis purposes:

- **Thermogravimetric Analysis (TGA)**: the mass of a sample is monitored vs. temperature while it is heated according to a program in a specific atmosphere (oxidizing, reducing, or inert). The first derivative of the TG curve may be plotted against temperature (Derivative thermogravimetry – DTG), which allows a more practical manipulation of the data but fails to report weight losses in which the weight loss is linear and unchanging;

- **Differential Scanning Calorimetry (DSC)**: the heat flow rate to a sample is monitored against temperature during programmed heating;

- **Differential Thermal Analysis (DTA)**: the difference in temperature between a sample and a reference material is monitored against temperature while the temperature of the sample in a specific atmosphere is programmed.
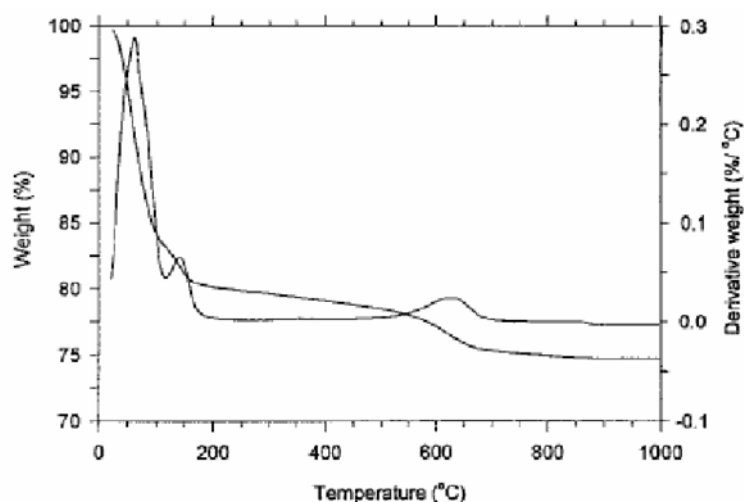
Figure 2.5 TG/DTG curves for SAz-1 (from Guggenheim and van Groos, 2001)

2.1.4.1 TG/DTG OF CLAY/ADSORBED BASES SYSTEMS

Thermogravimetric analysis of the desorption/decomposition of bases such as cyclohexylamine (CHA), butylamine and pyridine can be used for a rapid semi-quantitative determination of the number of acid centres in the clays (Ballantine *et al.*, 1987; Breen *et al.*, 1987; Breen, 1991[a]). The thermal desorption of CHA has been frequently used to evaluate the number of acid sites on clay catalysts (Ballantine *et al.*, 1987).

The technique requires the determination of the weight loss between 280 and 440 ºC (Figure 2.6, Breen *et al.*, 2000) and its conversion to the number of mmol of CHA desorbed. The

relative ease of obtaining this quantity has popularised its use even though the value

obtained does not distinguish between cyclohexylamine bound to Brönsted or Lewis acid

sites. Moreover, the method often reports high acidity values which are not substantiated by

the yields obtained in the associated tests of catalytic activity. For example, the presence of

Ca^{2+}-ions, which retain CHA to temperatures at which thermal C-N bond cleavage occurs,

can lead to a spurious acidity value (Komadel *et al.*, 1997).
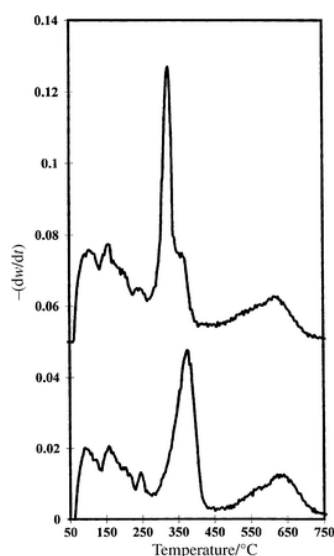
Figure 2.6 Derivative thermograms for the desorption of CHA from Al^{3+}- (top) and Ni^{2+}- (bottom) exchanged SWy-2 (Breen et al., 2000)

2.1.5 THERMOGRAVIMETRY – MASS SPECTROMETRY (TG-MS)

The TGA records the weight loss of a sample, whilst the MS detects the evolved gases

corresponding to those weight losses in real time. This is known as real time analysis, where

time/temperature related weight losses observed in TG are related to spectroscopic features

seen in MS (MS breaks up a molecule and identifies it from the diagnostic fragmentation

pattern.). The method presents clear advantages over the simple thermogravimetric analysis,

because it is possible to identify the decomposition products that are released during thermal

desorption.

2.1.5.1 BASICS

A. Mass Spectrometer

The Mass spectrometer used in this work is a ATI Unicam Automass System 2 quadrupole mass spectrometer which was operated in the Electron Impact (EI), positive ionisation mode.

In Real Time MS the TG-MS transfer line is directly interfaced with the ion source. The charged particles (ions) for mass analysis are formed by Electron Impact (EI) ionisation. The sample passes through an electron beam (70ev) and ionisation occurs when an electron strikes a molecule and imparts enough energy to remove another electron from that molecule.

EI ionisation usually produces singly charged ions containing one unpaired electron. The charged ion, which remains intact, is called the molecular ion. Energy imparted by EI is more than that required to produce the molecular ion, this excess energy causes instability in the molecular ion, causing it to break into smaller fragments to give a characteristic mass spectrum. A typical EI fragmentation pattern of cyclohexylamine (CHA) is shown in Figure 2.7.
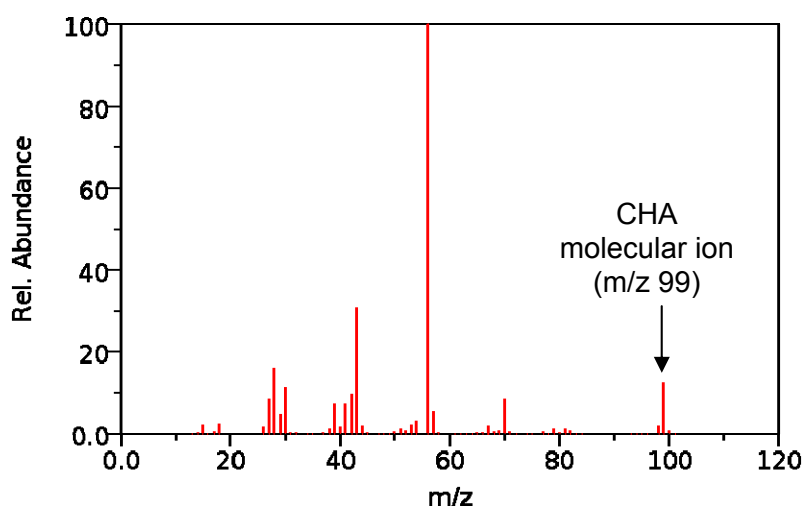
Figure 2.7 EI mass spectrum of cyclohexylamine
(from NIST Chemistry Web Book, **http://webbook.nist.gov/chemistry**)

From an analytical (qualitative) viewpoint, the important features of this type of spectrum are:

- The ions produced are normally singly charged and the m/z ratio corresponds to the combined 'weight' of the elements in the fragment involved. Not only is the elemental composition of each fragment ion accessible, but so are the molecular weight and molecular formula;

- The ions produced may be related in most cases to the structure of the intact molecule using well-understood principles;

- The mass spectra so produced are reproducible. This is of crucial importance when libraries of reference spectra are used to aid structure determination.

Fragmentation reactions may reduce the utility of EI spectrum by reducing the intensity of the molecular ion to a level that is not detectable. In these cases the molecular weight may not be determined and one of the single most valuable pieces of analytical information is lost. The optimisation of transfer line temperature and introduction of the sample into the MS source is therefore of utmost importance and has been studied for the particular system used in this work (Forsyth, 2001).

B. TG/ MS interface

Traditionally, due to the differing flow requirements of the two instruments (TG/MS), there have been limitations on the quality of real-time data acquisition via the simultaneous use of both techniques. The two instruments (TG and MS) are interfaced via a sniffer component, made of a high temperature alloy tube, placed in a position just above the sampling cup (Figure 2.8). The sniffer interface allows sampling of the evolved gases before they diffuse

through the entire volume of the TG reaction cell, due to the vacuum of operation of the MS unit which draws the evolved gas.
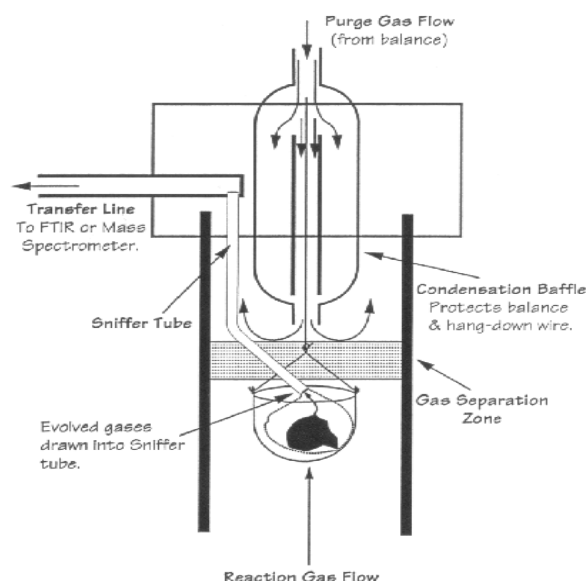
Figure 2.8 Sniffer Interface (from Czarnecki and Thumin, 1995)

2.1.5.2 EVOLVED GAS ANALYSIS OF THE CLAY/CHA SYSTEM

Breen *et al.* (2000) showed that real time TG-MS of the decomposition products derived from CHA provides pertinent information regarding the transformation properties of the catalyst. Generally, CHA decomposition can be represented by scheme 2.1.

Binding to a Brönsted acid site produces protonated CHA. Deamination generates unbound cyclohexene (CH) leaving NH_4^+ ions occupying some of the exchange sites. Successive dehydrogenation reactions result in the subsequent formation of cyclohexadiene (CHD) and then benzene (B). The formation of methylcyclopentene (MCP) cannot be disregarded. The presence of dehydrogenation sites can be further confirmed by the appearance of aniline (A), which arises from the aromatisation of untransformed CHA.

In order to identify the temperature range over which the degradation products are released,

single representative ions for each product species need to be selected. The main concerns are to avoid interference from common ionisation fragments arising from chemically distinct compounds and to choose those ions that provide appropriate profiles, neither too intense (to avoid saturation) nor very weak (to avoid sensitivity issues).
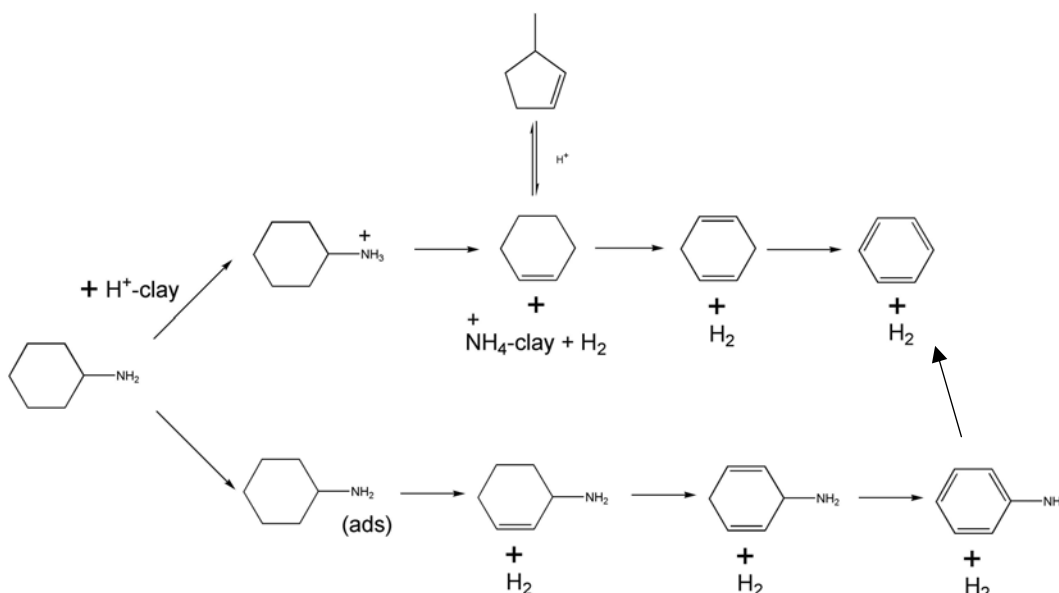
Scheme 2.1 Decomposition mechanism for acid controlled CHA degradation

2.1.6 INFRARED SPECTROSCOPY (IR)

Mid-Infrared spectroscopy (4000-400 cm^{-1}) is frequently used for the characterisation of solid catalysts, in general, and clay-based catalysts, in particular. An IR spectrum can serve as a fingerprint for mineral identification, but it can also give unique information about the mineral structure, including the family of minerals to which the specimen belongs and the degree of regularity within the structure, the nature of isomorphic substituents, the distinction of molecular water from constitutional hydroxyl, and the presence of both crystalline and non-crystalline impurities (Farmer, 1979; Russel and Fraser, 1994; Madejová and Komadel, 2001; Madejová, 2003). The use of nitrogen containing probe molecules extends the application of IR spectroscopy to acidity evaluation of the solid materials (cf. Section 2.1.6.3 - Ward, 1968).

2.1.6.1 BASICS

A. Absorption of Infrared radiation

Infrared radiation is electromagnetic radiation with a wavelength between approximately 10^{-3} and 10^{-6} m. Absorption of particular frequencies of infrared radiation by polyatomic chemical species gives rise to a characteristic infrared spectrum.

There are two fundamental types of vibration that occur in polyatomic molecules:

    i) stretching of the interatomic bonds, where the length of a bond changes

    ii) bending, where the angle between two bonds changes.

If a chemical specie is to absorb infrared radiation it must undergo a net change in dipole moment due to its vibrational motion. A dipole moment is the product of the magnitude of the localised electrical charges within any molecule and the distance separating the positive and negative components of these charges (i.e. atoms). If the frequency of the incident radiation is the same as the frequency of the molecular vibration then a net transfer of energy occurs which results in a change in the amplitude of the molecular vibration, and absorption of the radiation occurs.

B. Fourier Transform Infrared Spectroscopy (FTIR)

FTIR spectroscopy is now the preferred method of infrared spectral analysis and has several advantages over the traditional dispersive methods. In a dispersive instrument a prism or grating is used to resolve the radiation into separate components whereas in a Fourier transform instrument a Michelson interferometer is used. A Michelson interferometer allows all the infrared frequencies of the source to be recorded in the time domain as an

interferogram. A Fourier transform (i.e. a mathematical formula) is then used to convert this to the frequency domain.

C. Transmission Spectroscopy

In the classical method of infrared spectroscopy, radiation passes completely through the sample. This is known as transmission spectroscopy. A range of appropriate sampling techniques have been developed, which include mulls (difficult to obtain a good dispersion), KBr discs (may cause structural damage) and free standing films (can be difficult to prepare).

D. Diffuse Reflectance Infrared Fourier Transform Spectroscopy (DRIFTS)

During a DRIFTS[4] experiment the incident radiation is reflected off the surface of the sample. DRIFTS spectra are calculated by measuring the single beam reflectance spectrum of a sample and ratioing this against a reference single beam reflectance spectrum of a good diffuse reflector. The reflectance spectrum is therefore calculated in a manner that is analogous to transmittance:

% Reflectance = (Reflectance sample/Reflectance reference) x 100

There are three main modes in which the incident radiation can be reflected from a powdered sample (Figure 2.9). The first mode is where the incident beam is reflected from the sample as if from a mirror (i.e. the angles of incidence and reflectance are equal) - true specular reflectance. In the second mode (diffuse specular reflectance) the beam undergoes multiple reflections off particle surfaces without penetrating into the particle. The resulting beam emerges from the sample and is distributed in all directions. The third mode of reflection is true diffuse reflection, where the beam passes into the bulk of the material and undergoes

---

[4] Griffiths and Fuller (1982)

absorption, reflection, refraction and/or scattering before re-emerging at the sample surface. The light reflected in this manner is distributed in all directions.
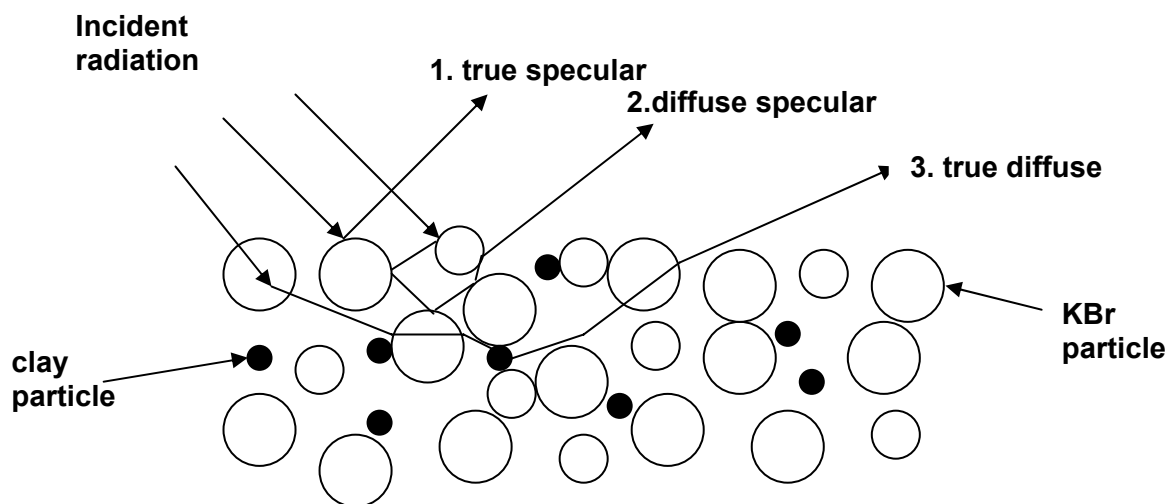
Figure 2.9 Schematic diagram showing the three modes of reflection during a DRIFTS experiment

There are many factors that govern the amount of each type of reflectance collected during an experiment, including the optical arrangement of the accessory and the physical and chemical characteristics of the sample. The major drawback with the DRIFTS technique arises from the specular component (true specular and diffuse specular) of the reflected radiation. When the specularly reflected component is small, the DRIFTS spectrum is similar in appearance to that of a transmittance spectrum. However, when the specularly reflected component is high, distortions appear in the spectrum as either anomalous dispersions or complete band inversions (Restsrahlen bands). During a DRIFTS experiment all the factors that produce specular reflectance are minimised in order to collect the maximum ratio of true diffuse to specular reflection. There are many preparation factors which can affect the true spectral data, namely:

- Choice of reference powder (good diffuse reflector, non absorbing and a highly scattering material – Fuller and Griffiths, 1978);

– Particle size (with samples dispersed in a non-absorbing matrix, a decrease in particle size results in an increase in band height and decrease in band width - Fuller and Griffiths, 1978);

– Absorptivity and refractive index (n) (diffusely reflected energy increases from 0 for n=1, to a maximum for n close to 2, and then decreases for higher refractive index values - Moradi *et al.*, 1994);

– Depth of sample matrix (as the depth of any absorbing sample is increased a subsequent increase in its absorption bands will be observed until a certain depth is reached - Fuller and Griffiths, 1978; Fraser and Griffiths, 1990);

– Sample packing (as the pressure increases the variability in the scattering coefficient decreases from sample to sample - Yeboah *et al.*, 1984; Krivacsy *et al.*, 1994);

– Sample homogeneity (thorough mixing is required, because simply mixing two materials together does not lead necessarily to a homogeneous mixture – Hamadeh *et al.*, 1984);

E. Variable Temperature - Diffuse Reflectance Infrared Fourier Transform Spectroscopy (VT-DRIFTS)

Basically, VT-DRIFTS allows diffuse reflectance spectra to be obtained at a range of temperatures and can provide information regarding the changes in the solid sample as it is heated. The information can also be correlated with information obtained by conventional thermal analysis techniques, for example, TG, DTA and DSC.

Two types of VT-DRIFTS may be performed:

- Stepped VT-DRIFTS: samples are heated to selected temperatures and infrared spectra are obtained after equilibration at each temperature.

- Ramped VT-DRIFTS: samples are heated at a constant rate and each infrared spectrum is collected over a temperature range.

Ramped VT-DRIFTS results are more easily correlated with TGA and DSC measurements than stepped VT-DRIFTS results, but the latter generally yield spectra with fewer baseline distortions.

VT-DRIFTS spectra are highly susceptible to baseline artefacts, but these may be eliminated by measuring sample and reference single beam spectra at the same temperature (White, 1992).

2.1.6.2 CLAY STRUCTURAL CHARACTERISATION BY INFRARED SPECTROSCOPY

Since the introduction of Fourier transform instrumentation the application of IR spectroscopy has greatly increased in many spheres of clay research. The improved performance of the FTIR spectrometers (enhanced frequency accuracy, high signal-to-noise ratios and high data acquisition speed) made it possible to design sample-handling accessories that were impractical or difficult to implement on older instruments. Madejová (2003) recently reviewed the application of FTIR spectroscopy to clay mineral studies, which include identification of the clay mineral type (Figure 2.10) and presence of admixtures, determination of the octahedral sheet composition (950-700 cm^{-1}, highlighted in Figure 2.10B) and analysis of the structural effects of acid activation (Figure 2.11).
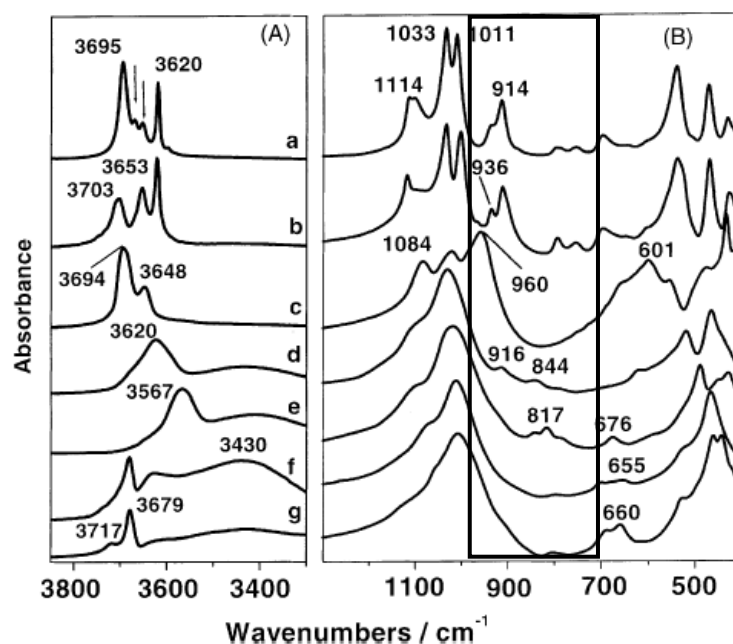
Figure 2.10 IR spectra of (a) kaolinite, (b) dickite, (c) chrysotile, (d) SAz-1 montmorillonite, (e) nontronite, (f) hectorite and (g) saponite in the (A) OH stretching and (B) 1300-400 cm^{-1} regions (Madejová, 2003)
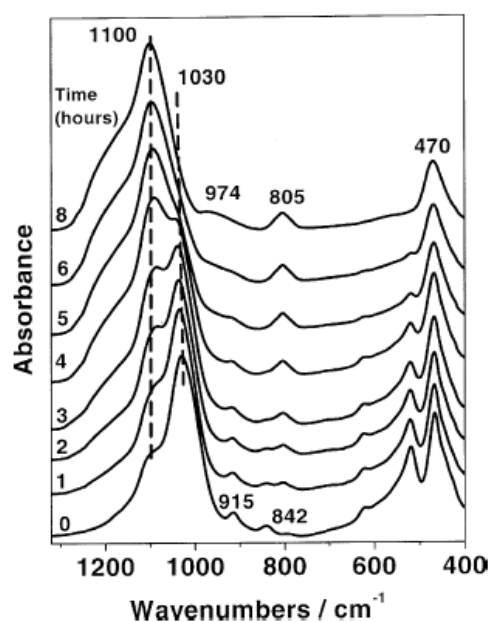
Figure 2.11 Transmission IR spectra of SAz-1 montmorillonite treated in 6 M HCl at 80 ºC for different time intervals (Madejová, 2003)

2.1.6.3 ACIDIC CENTRES CHARACTERISATION BY IR SPECTROSCOPY

The first determination of surface acidity was reported by Walling (1950) who found that an acid treated clay imparted colour to p-nitrobenzene-azo diphenylamine. The author incorrectly attributed the acidity to the presence of residual acid from the acid treatment.

Several techniques have been used to measure the acidity of catalysts and catalyst supports, namely the use of indicators (Benesi, 1956; Benesi and Winquist, 1978), measurement of the quantity of chemisorbed ammonia at various temperatures (Barth and Ballou, 1961; Kubokawa, 1963), the determination of the IR spectrum of chemisorbed ammonia (Pliskin and Eischens, 1955; Mortland *et al.*, 1963), carbocation formation of arylmethanol (Helsen, 1970) and adsorption of pyridine by IR (Parry, 1963; Swoboda and Kunze, 1964; Connerton *et al.*, 1995). The results obtained by application of these methods to the same material often return significantly different results.

Only the pyridine adsorption method can readily distinguish between pyridine bound to Brönsted (1635 and 1540 cm^{-1} infrared bands; pyridinium ion) and Lewis (1613 and 1440-1460 cm^{-1} bands – coordination of pyridine to Lewis acid sites) acid sites (Figure 2.12) (Parry, 1963; Ward, 1968). Peaks at 1596 and 1440 cm^{-1} may report the presence of H-bonded pyridine. It also has been suggested (Emeis, 1993) that the determination of the number of Brönsted and Lewis acid sites may be obtained by dividing the integrated absorbances in the two regions by the weight of the wafer and by the molar extinction coefficients (1.67 and 2.22 cm µmol^{-1} for Brönsted and Lewis acid sites, respectively).
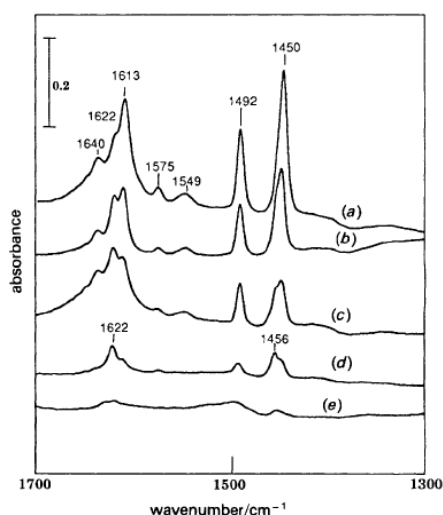
Figure 2.12 IR spectra in the 1700-1300 cm^{-1} range of a pillared saponite after pyridine adsorption and subsequent desorption at (a) 150, (b) 250, (c) 350, (d) 450 and (e) 520 ºC (Chevalier et al., 1994)

2.2 Techniques Used in this Thesis

2.2.1 XRF

XRF was utilised in this study to estimate the chemical composition of clays. Beads for XRF analysis were prepared using the $Li_2B_4O_7$ fusion method. Each sample was ground into a powder and dried at 120 ºC. The dried material (1g) was then mixed with 10 g of $Li_2B_4O_7$, put into a platinum crucible and heated at 125 ºC/min for 6 minutes (maximum temperature 750 ºC). The mixture was then swirled to improve the mixing process, heated for a further 6 minutes, poured into a mould and allowed to solidify before analysis. The sample was analysed using a Phillips PW 2400 XRF spectrometer.

2.2.2 XRD

In the context of this thesis, XRD was used:

1. to identify crystalline phases present in the Porto Santo bentonites (cf. Chapter 3);

2. to quantify the crystalline phases present in the Serra de Dentro bentonite (which was the parent material used for catalyst preparation (cf. Chapter 3)[5];

3. to evaluate the effect of acid treatment on the structure of the clay minerals (cf. Chapter 5);

4. to evaluate the d(001) spacing of intercalated and pillared clays in order to determine if the experimental procedures had been successful (cf. Chapter 6).

---

[5] performed by Macauley Analytical Services

X-ray diffraction profiles of pressed powder samples were obtained using a Philips PW1830 X-ray diffractometer (CuKα; λ = 1.542 Å) operating at 40 kV and 35 mA. Diffractograms were recorded at 2º (2θ) min^{-1}. For preliminary identifications of clay minerals (Chapter 3) and PILCs evaluation (Chapter 6), scans were collected from 2-35 º2θ, whereas for the acid activated materials characterisation, scans were obtained over 2-70 º2θ. (Chapter 6).

Quantitative X-Ray powder diffraction was performed on the sodium exchanged Serra de Dentro bentonite. The bulk sample was wet ground and spray dried to produce a random powder to which 30 wt% corundum was added to act as an internal standard for quantitative phase analysis (QPA). X-ray powder diffraction (XRPD) patterns were recorded from 2-75°2θ using Cobalt Kα radiation. QPA was done using the reference intensity ratio (RIR) method. Additionally, the sample was prepared as an oriented mount using the filter peel transfer technique and scanned from 2-45°2θ in the air-dried state, after glycolation, and after heating to 300°C for one hour. Clay minerals identified were quantified using a mineral intensity factor approach based on calculated XRPD patterns.

2.2.3 SURFACE AREA

The analysis were performed by M. R. Carrott and P. Russo at the facilities of Centro de Química de Évora. Nitrogen adsorption isotherms were determined at −196 ºC on a CE Instruments Sorptomatic 1990, using helium (for dead space calibration) and nitrogen of 99.999% purity. Prior to the determination of the adsorption isotherms, the samples were outgassed for 8h at 423K, achieved using a heating rate of 1 ºC min^{-1}.

2.2.4 TG

TG data (simple and CHA saturated samples) were recorded on a Mettler TG50 thermobalance equipped with a TC10A processor.

TG of simple clay samples (~20 mg) were recorded at a heating rate of 20ºC under a nitrogen flow of 25 cm^3 /min, following a 15 min conditioning time, under flowing nitrogen.

CHA saturated samples (~10mg) were transferred directly out of CHA vapour into the thermobalance and the desorption traces were recorded at a heating rate of 20ºC / min under a nitrogen flow of 25 cm^3 /min. Samples were conditioned for 15 min under flowing nitrogen to reduce the amount of physisorbed CHA. The weight loss (from TG) observed between 240 and 350 ºC was used to monitor acidity. The number of acid sites was calculated on the assumption that one molecule of base reacts with one acid site (Breen, 1991[b]).

2.2.5 EVOLVED GAS ANALYSIS (TG-MS)

The TG data obtained from the clay/CHA system (cf. previous section) does not provide information on the distribution of acid sites and only gives an average of acid strength. Additionally, the samples were analysed on the TG-MS apparatus. Evolved gas analysis (EGA) was conducted using a ATI Unicam Automass System 2 quadrupole mass spectrometer (operated in the Electron Impact (EI), positive ionisation mode) connected with a Cahn TG 131 thermobalance. Clay-CHA samples (ca. 20 mg) were placed in a quartz crucible and pre-treated for 15 minutes at 25 ºC under a flow of nitrogen at atmospheric pressure before being heated from 25 to 800 ºC at 20 ºC/ min in the same nitrogen flow. This removed the entire physisorbed base, which is why there was no weight loss or mass spectral response below 50 ºC. The evolved gases were then transferred from the TG to the MS (Automass System 2, Unicam) via a silica-lined stainless steel, transfer line, maintained at 200 ºC, which ensured immediate sampling and minimised dilution effects. During "real time" TG-MS analysis, the mass spectrometer scanned 4-500 u every 1.5 s.

The following ion fragments were selected: cyclohexylamine, CHA – m/z 99, aniline, A – m/z 93, benzene, B – m/z 78, cyclohexadiene, CHD – m/z 77 and cyclohexene, CH – m/z 54. Water (m/z 18) and CO_2 (m/z) 44 were also monitored.

2.2.6 IR

Infrared spectra were obtained on Nicolet Avatar 360 FTIR ESP. For each sample 256 scans were recorded in the 4000–400 cm^{-1} spectral range in the transmittance mode with a resolution of 4 cm^{-1}. The KBr pressed disc technique (0.4 mg of sample and 200 mg of KBr) was used.

2.2.7 VT-DRIFTS

KBr Backgrounds: Before the KBr (Aldrich >99%) was used to prepare any background (or clay) samples it was ground and then heated at 200 ºC to remove bound water. The excess KBr was removed by scraping a razor blade over the surface so that it was level with the sides of the cup. Before a spectrum was collected, the background or sample was purged, in the sample chamber, for three minutes with nitrogen.

Clay Samples: For VT-DRIFTS the samples were dried in air at 60 °C overnight, prior to exposure to vapour phase pyridine for periods in excess of 72 h. The samples were thoroughly blended with the previously grounded dry KBr, using a pestle and mortar, creating a 10% dispersion in KBr and transferred to the environmental chamber (Graseby-Specac; maximum operating temperature 500 ºC), and the spectra were collected. The first spectrum was collected before purging at 25 °C then after purging for at least 15 min. The sample was then heated to 50 °C and allowed to equilibrate for 15 min before collecting the spectrum. This process was repeated up to 200 °C at 25 °C increments and then up to 500 °C at 50 °C increments. Background spectra, collected using KBr under the same conditions, were used

to ratio against the respective sample spectra. The spectrometer used was a Mattson Polaris operating at 4 cm^{-1} resolution and 256 scans.

2.2.8 UV-Visible Spectroscopy

The Cr containing intercalation solutions were analysed by UV-vis spectroscopy. This technique was also used for the NaSD CEC determination. In both cases, the instrument used was a Perkin-Elmers Lambda 2 UV/VIS Spectrometer.

Cation Exchange Capacity (CEC): This parameter was obtained using the method suggested by Rhodes and Brown (1994[b]), which consists of mixing a 0.25 mol.dm^{-3} CoSO$_4$ solution with 0.5 g of the clay (twice), filtering the suspension, washing the clay and measuring the absorbance at 511 nm of the resulting solution (filtrate and washings). The spectrometer was previously calibrated with standard Co^{2+} solutions. The quantity absorbed was determined from the concentration of cobalt (II) ions that remained in solution. This procedure was repeated three times.

2.2.9 Catalytic Tests

The materials obtained were tested in the limonene conversion reaction.

It is well documented that clays are easily deactivated by residual amounts of water. Madeira Island exhibits reasonably high levels of humidity throughout the year and, therefore, catalyst activation and reaction procedures needed to be controlled in very strict terms, in order to obtain reproducible results.

The catalyst activation time was defined as 2 hours at the designated temperatures, although some systematic studies proved that 1 hour was equally efficient for activation purposes.

The following activation/reaction procedures were tested and ruled out before systematic, reproducible catalytic runs were performed.

1. Catalyst activated in oven and left to cool in a desiccator for 15-30 minutes; the catalyst was added into the hot reaction mixture. The results reflected the wetting of the catalyst during the transfer process, as proven by the exothermic, violent reaction that took place during the addition.

2. A process similar to the one described above, but the catalyst was added to the hot reaction mixture whilst still hot. The reaction was highly exothermic, with violent effervescence; the temperature increased instantaneously by 60ºC.

3. In situ activation of the catalyst in the reaction vessel placed in the oil bath, under dry $CaCl_2$ protection. The apparatus was cooled down to the reaction temperature (150 ºC) and both limonene and internal standard were added. The reaction vessel was, in this case, a 3 necked round bottom flask, equipped with a reflux condenser. The reactant/internal standard mixture were added with a syringe via a Teflon septum, but the plastic o-ring junction used dissolved in the hot limonene, forming a viscous blend with the reaction mixture. Interestingly, all the catalysts acquired, during activation, a dark colour which, apparently, did not affect their catalytic activity; the reason for this colour change is not clear. Despite the drawbacks mentioned, the results obtained with this experimental procedure were reproducible, which indicated that the water content of the catalyst was an essential feature and that, at this stage, this variable was under control.

4. Virtually identical to the approach described except that during the cooling cycle, a dry air flow was forced throw the reaction vessel (air forced through a drying

tube). Again, the results were reproducible, but the drying tubes were quickly deactivated due to the high levels of atmospheric humidity.

In all the methods described, all the glassware was carefully dried (dried in the oven at 150ºC overnight and cooled in the desiccator) prior to use. When applicable, the Pasteur pipettes used for sampling were dried over a flame before being introduced in the reaction mixture. The frequent opening of the reaction system in order to obtain samples often proved to be a source of humidity for the catalytic system, causing the reaction to clearly slow down or, in extreme cases, reach a halt.

The methods described below proved to be the most reliable. Differences between the catalytic testing of IEC (open system) and AAC (closed system) arose from significantly different reactions rates and the relative resilience of AAC behaviour towards humidity. PILCs were tested both in closed and open systems.

2.2.9.1 IEC CATALYTIC TESTS

Limonene and n-dodecane (internal standard) were dried over anhydrous magnesium sulphate prior to use. Reactions were performed in a stirred 25 mL batch reactor, equipped with a reflux condenser, under drying tube ($CaCl_2$) protection. The stirrer speed was chosen to ensure that reaction rates were not under diffusion control. Before the test reaction, 100 mg of catalyst was thermally activated at the prescribed temperature, under air, in the reaction vessel before being allowed to cool. This operation was performed under dry conditions to avoid any contact with atmospheric humidity. A limonene/internal standard mixture comprising 10 mL of limonene and 2 mL of n-dodecane, was injected over the dried catalyst. The reaction conditions were 15 min at 150 ºC. Samples were taken at selected time intervals, separated using a syringe filter and stored in dry sample vials. The filter had no influence on the reaction products and no further reaction occurred during storage. The

products were identified by GC–MS (Varian Saturn 3) and quantified by capillary GC with FID detection (Hewlett Packard 5890 Series II).

2.2.9.2 AA CATALYTIC TESTS

Limonene and n-decane were dried over anhydrous magnesium sulphate prior to use.

The optimum time and temperature for the catalytic process were identified after studying a wide range of potential conditions. The product yields reported here were obtained after 15 min at 80 ºC in 10 mL glass vials. The stirrer speed was chosen to ensure that reaction rates were not under diffusion control.

Before reaction, 100 mg of catalyst was thermally activated at 150 ºC for 16 h, under air, in the reaction vessel. To avoid the introduction of water, the activated clays were suspended in dry n-decane, and the glass vials were closed and transferred to an oil bath, preheated at 80 ºC. After being cooled to the reaction temperature over a period of 15 min, 0.5 mL limonene was injected into the vial and this marked the start of the reaction. At the end of the reaction the vials were cooled, opened, and the catalyst was separated using a syringe filter. The filter had no influence on the reaction products and no further reaction occurred during storage. This method allowed good extraction ratios for limonene and reaction products, rendering better mass balances than the method employed for IEC, although it did not allow samples to be collected at different reaction times. The products were identified by GC-MS (Varian Saturn 3) and quantified by capillary GC with FID detection (Hewlett Packard 5890 Series II) with the n-decane acting as the internal standard.

CHAPTER 3. PORTO SANTO BENTONITES

3. SERRA DE DENTRO BENTONITE

3.1 INTRODUCTION

Madeira archipelago is located in the Atlantic Ocean between parallels 32º 31' N and 33º 31' N and meridians 16º 30' W and 17º 30' W (between the Canary and the Azores archipelagos) (de Carvalho and Brandão, 1991). The archipelago is situated at about 310 miles from the African coast and 620 miles from the European continent.

The archipelago is constituted by Madeira (763.7 km^2) and Porto Santo (43.2 km^2) islands, both inhabited and by two groups of uninhabited small islands: Desertas (3 islands, 14.2 km^2) and Selvagens (3 islands, 3.6 km^2), both of which are natural reserves[6].

Porto Santo Island (Figure 3.1) is located at 21 miles NE from Madeira (between parallels 33º 00' N and 33º 07' N and meridians 16º 17' W and 16º 25' W). Climatologically[7], Porto Santo is characterised by the data presented in Table 3.1.

Porto Santo has several bentonite deposits, which are, for the best of the author knowledge, unique in the Portuguese territory. These deposits occur mainly in the oriental part of the island, below and above sea water level. They were probably formed by alteration of the acidic or neutral volcanic tuffs rich in glass; the tuffs were deposited successively (but not continuously) on the island platform, in shallow and warm water, during several phases of explosive volcanism (Miocene) (Ferreira and Serrano, 1971).

---

[6] Instituto Geográfico e Cadastral (Delegação Regional da Madeira)
[7] This data refers to the period 1940-1970 and was collected at the meteorological station located at the local airport.

Figure 3.1 Aerial view of Porto Santo Island (and surrounding islets)[8]

Table 3.1 Climate data for Porto Santo Island

Variable	Value
Minimum Temperature (monthly average)	15.6 ºC (February)
Maximum Temperature (monthly average)	22.6 ºC (August)
Maximum Temperature	33 ºC
Minimum Temperature	7 ºC
Air Temperature (annual average)	18.7 ºC
Sea Water Temperature (annual average)	19.7 ºC
Annual Thermal Amplitude	7 ºC
Relative Humidity (annual average)	75.6 %
Rain (annual average)#	361.5 mm

significant differences from year to year

Over the years, several studies on clay sciences have been published supporting the characterisation of Porto Santo clays (Antunes *et al.*, 1998, 1999[a,b]; Silva *et al.*, 2000) and their pillared derivatives to be used as catalysts for organic reactions or as adsorbants for pollutants (de Carvalho *et al.*, 1996; Pires and de Carvalho, 1997; Pires *et al.*, 1997, 1998, 2003; Pereira *et al.*, 1998; 2001; Guil *et al.*, 2002). Chemical composition, surface area and mineralogical composition results show great variation (Table 3.2) which suggests that the

---

[8] www.madeiraarchipelago.com

disparity in the data is not due to several methods being used for property determination but that the nature of the starting materials are probably very dissimilar. In fact, although the authors refer to Porto Santo clay, the exact points of collection are not always mentioned nor are the conditions of sample collection.

Table 3.2 Comparisons between referenced characterisation results of Porto Santo bentonites

	Sample A (de Carvalho *et al.*, 1996)	Sample B (Antunes *et al.*, 1999)	Sample C (Antunes *et al.*, 1999)
SiO_2 / %	50.1*	48.7*	54.8*
Al_2O_3 / %	16.8	20.2	18.5
Fe_2O_3 / %	9.1	10.8	8.3
TiO_2 / %	1.8	2.2	0.9
CaO / %	2.0	1.2	0.6
MgO / %	4.1	4.1	4.3
K_2O / %	0.58	0.75	0.87
Na_2O / %	0.15	3.56	2.53
Clay minerals / %	93*	94#	49#
Impurities	Main: calcite Traces: feldspar, quartz	Main: --- Traces: siderite, hematite, magnetite-maghemite	Main: plagioclase, opala CT, magnetite-maghemite Traces: quartz, calcite, hematite
CEC / meq.100g^{-1}	120.3 ± 2.3	98. 3	92.9
Surface area / m^2.g^{-1}	142	108	87.0

\# < 63 µm fraction; dry sieving.
* < 2 µm fraction; wet sedimentation

3.2 EXPERIMENTAL

3.2.1 SAMPLE COLLECTION AND PURIFICATION

Six Porto Santo bentonite deposits were selected (Table 3.3). The samples[9] were collected after discarding the top 10 cm of superficial materials to avoid weathering contamination. At least 3 kg of bentonite was collected from each location, quartered, coned and sieved. The <0,125 mm

---

[9] Kindly supplied by Dr. Domingos Rodrigues, member of the Biology Department of Madeira University.

fraction was decarbonated with hydrogen peroxide, 30 vol%, at 80ºC to remove all organic mater, centrifuged at 6000 rpm, washed with deionised water and centrifuged again. The solid was suspended in deionised water, sonicated for 5 minutes in order to promote dissaggregation and the < 2μm fraction was collected after 8h sedimentation (application of Stokes Law for <2 μm spherical particles settling time) (Sheldrick and Wang, 1993). This procedure does not promote the separation of the clay minerals from other insoluble contaminants with similar particle sizes which commonly coexist, namely quartz, feldspar, calcite, carbonates, plagioclase, etc. (Chipera *et al.,* 1993, Komadel, 2003). The percentages of the < 2 μm fractions were not determined analytically, but the "yields" varied substantially. SD4.1 and both Serra de Fora bentonites provided the best results, whereas VT8.2, PAF6.1 and PCab1.1 rendered low portions of the < 2 μm fraction. All bentonitic materials were analysed using XRD, XRF, isothermal nitrogen adsorption/desorption and infrared spectroscopy techniques.

Table 3.3 Location of bentonite deposits and ID of the materials collected

Location	Outcrop	Sample	ID
Pico Ana Ferreira	6	1	PAF6.1
Pico Castelo	9	2	PCas9.2
Pico da Cabrita	1	1	PCab1.1
Serra de Dentro	3	1	SD3.1
Serra de Dentro	4	1	SD4.1
Serra de Fora	3	1	SF3.1
Serra de Fora	9	1	SF9.1
Vale do Touro	8	1	VT8.1
Vale do Touro	8	2	VT8.2

SD4.1 was selected for further work, a decision based on the characterisation data obtained for these bentonites (cf. Section 3.3).

3.2.2 SODIUM EXCHANGED SERRA DE DENTRO BENTONITE (SD4.1)

The < 2µm fraction of the SD4.1 bentonite was obtained by standard sedimentation procedures, as described above. The Na$^+$-exchanged form (**NaSD**) was prepared by thoroughly stirring a 1% suspension of the fine fraction of SD4.1 (10 g of bentonite/1 L 1M NaCl solution) overnight. The supernatant liquid was removed and the procedure was repeated twice. Excess Cl$^-$ was removed initially by several washing and centrifuging steps (deionised water) and subsequently by dialysis, until a steady, low conductivity was achieved. Chemical composition data for the material obtained revealed a substantial amount of calcium, which could not be attributed entirely to an external calcium phase. Further Na-exchange was achieved by mixing Na$_{3.5}$EDTA with the clay, stirring the suspension overnight, followed by several washing and centrifuging procedures and finally submitting the material to dialysis until a stable, low conductivity was obtained in the supernatant liquid. NaSD was characterised using XRD, XRF, nitrogen isothermal adsorption and desorption, thermogravimetric and spectroscopic techniques.

3.3 CHARACTERISATION OF PORTO SANTO BENTONITES

Figure 3.2 summarizes the main characterisation data obtained for the bentonites collected[10]. The DRIFTS spectra presented refer to samples that where submitted to a mild acid washing procedure (HCl 0.1 M, 60 minutes, room temperature), in order to eliminate the strong infrared absorption bands at ca. 1450 and 878 cm^{-1}, attributed to the presence of a calcium phase (normally calcite). The latter superimposes the diagnostic AlFeOH deformation band which provides information on the substitution of Al for Fe in the octahedral

---

[10] All characterisation runs were repeated at least twice with different samples in order to verify the homogeneity of the materials.

sheet. This treatment promptly removed the calcium impurity without (noticeably) affecting the clay mineral structure (Figure 3.3). The remaining data shown in Figure 3.2 was obtained prior to the acid washing step referred above.

DRIFTS, XRD and XRF data helps distinguish the samples based on the type and relative amounts of contaminants; moreover, the data confirms the high smectite content of the materials. The range of surface areas (BET method applied do nitrogen adsorption at 77K), 71-115 $m^2.g^{-1}$ and the high Si/Al ratio (XRF) fall within the expected region for montmorillonites and thus confirms the predominant clay character of the materials (de Carvalho *et al.*, 1996; Gomes, 1988; Vaccari, 1998).

Globally, it can be seen (XRF, XRD, surface area and DRIFTS data – Figure 3.2) that the nature and quantity of impurities vary significantly not only within samples from different locations but also when comparing samples collected in close proximity to each other. This aspect will be explored in more detail in the following sections (based on the analytical data presented). However, a simple visual inspection of the different materials (compare images of the bentonites in Figure 3.2) provides enough evidence of clear dissimilarities between materials. The range of different brownish colours reflects, probably, variable contents in iron, which can be present either as part of the clay mineral's structure or as external phases. During the purification procedures of some of the materials, the presence of particles magnetically attracted to the stirring rods used was detected, which provides evidence of the presence of external magnetic phase(s) (e.g. iron).
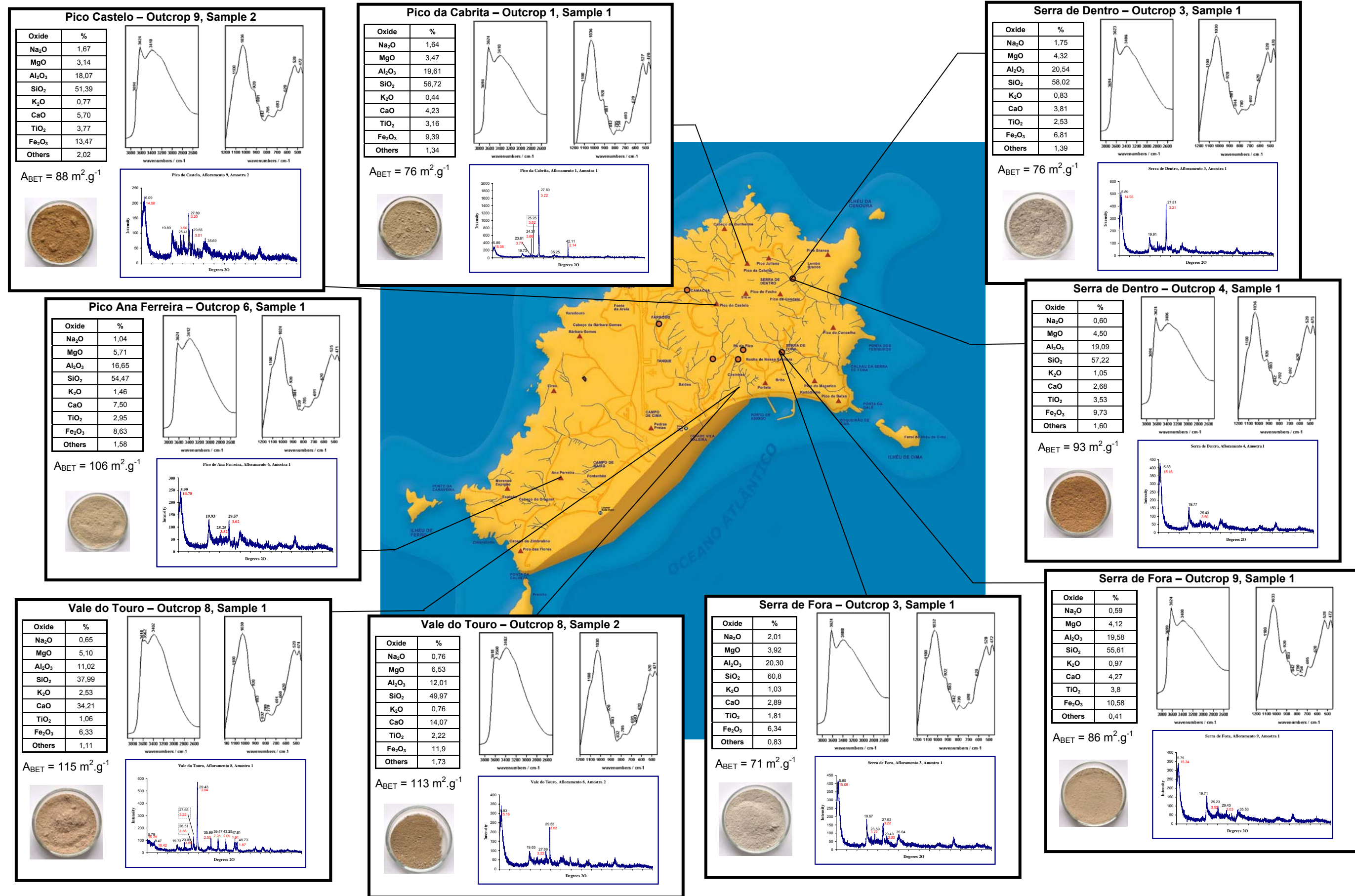
Figure 3.2 Summary of main characterisation results of the Porto Santo bentonites analysed (XRF composition, DRIFTS, XRD traces, surface area)
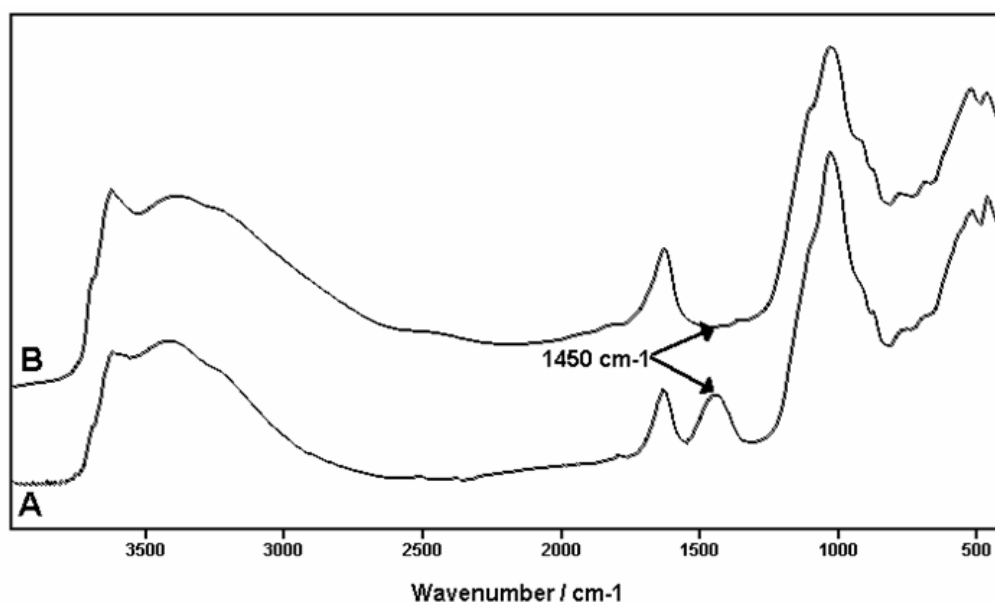
Figure 3.3 DRIFTS spectra of PCas9.2 before (A) and after (B) acid washing (HCl 0.1M, 60 minutes)

3.3.1 CHEMICAL COMPOSITION (XRF DATA)

XRF data presented in Figure 3.2 shows marked differences between the different materials analysed (e.g., calcium oxide content of VT8.1 and VT8.2 or titanium oxide content of SF3.1 and SF9.1).

XRF data can lead to misleading conclusions if one is not aware of the relative amounts of non structural impurities (higher contents in contaminants generally lead to more significant degrees in uncertainty). This means that the XRF data presented in Figure 3.2 (all the elements present, whether they are part of the clay structure or not) does not present a clear picture regarding the relative weights of the structural ions present in the sample. In order to obtain more relevant information from the chemical composition data, an internal reference was established within each sample, therefore 'normalizing' the metal oxide contents. The 'internal standard' chosen was Si, because it is normally the major element present in bentonitic materials (hence, the presence of external silica minerals, e.g. feldspar or quartz, probably will not affect significantly the normalised values) and the infrared spectra/XRD traces did not reveal major contamination by other silica bearing minerals. The "normalised"

results[11] are shown in Table 3.4 (together with images of the bentonite materials before and after their calcination at 500ºC together with the DRIFTS spectra of the 1200-400 cm^{-1} region) and Figure 3.4. It is important to note that this empirical method is fallible and no absolute conclusions should be drawn from its use. However, it is possible to visually infer the clear differences in terms of chemical composition between the materials obtained from different sources. Figure 3.4 enhances the heavy calcium contamination (calcite) of the Vale do Touro samples. It can also be seen that the iron content varies significantly throughout the materials (hence the colour changes referred above). Titanium, which was identified as being present as anatase (cf. infra), also is present in variable amounts.

3.3.2 XRD ANALYSIS

All XRD traces (Figure 3.2) exhibit the typical reflections of smectites (e.g. d(001) 14.5-15.5 Å and d(002) at ca. 4.5 Å); the basal spacing values are characteristic of Ca^{2+}-clays. (Brindley and Brown, 1984; Moore and Reynolds, 1989).

The diffractograms provide further evidence of the presence of different types of contaminants in the materials analysed (and, in a qualitative matter, that those contaminants are present in substantially different amounts). The main contaminants are calcite, feldspar and, in some cases, anatase (Figure 3.2). Figure 3.5 combines the XRD traces of three bentonites (SD4.1, VT8.1 and PCab1.1) that exhibit representative differences in terms of type and amount of impurities. It can be seen that the main impurity present in the PCab1.1 sample is feldspar (probably plagioclase, $NaAlSi_3O_8$ to $CaAl_2Si_2O_8$) whereas VT8.1 is heavily contaminated with calcite (good agreement with XRF composition data, as referred in the previous section). SD4.1 seems to exhibit a bigger range of impurities, but the intensity of the feldspar (PCab1.1) and calcite (VT8.1) peaks tend to obscure the presence of the other non-clay associated minerals. The XRD trace for SD4.1 exhibits peaks at 33.0, 35.9, 49.7 and

---

[11] (% Metal oxide/ % SiO_2) * 100

57,9 ° 2θ, attributed to hematite (Brindley and Brown, 1984; Moore and Reynolds, 1989), which confirms the supposition that not all the iron identified by XRF belongs to the clay structure.
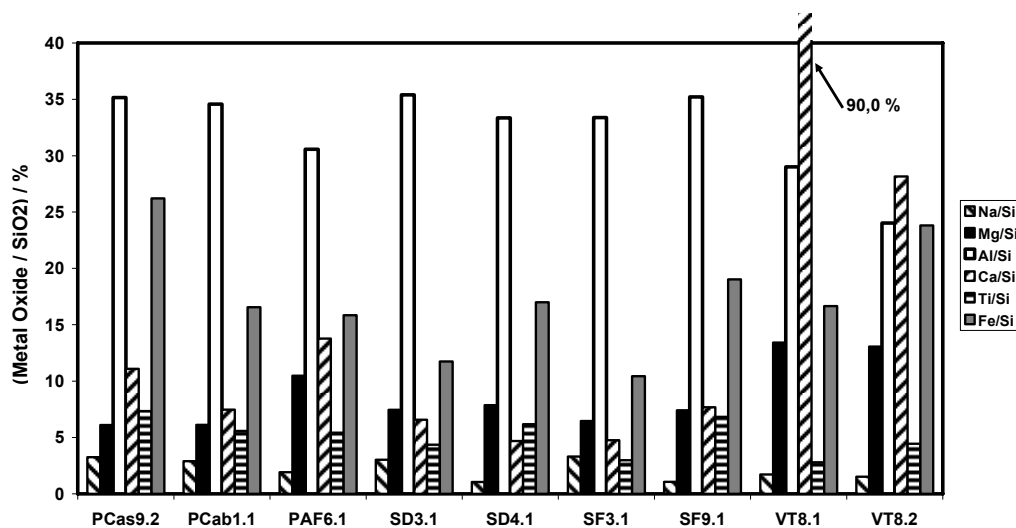
Figure 3.4. "Normalised" chemical composition of Porto Santo bentonitic materials
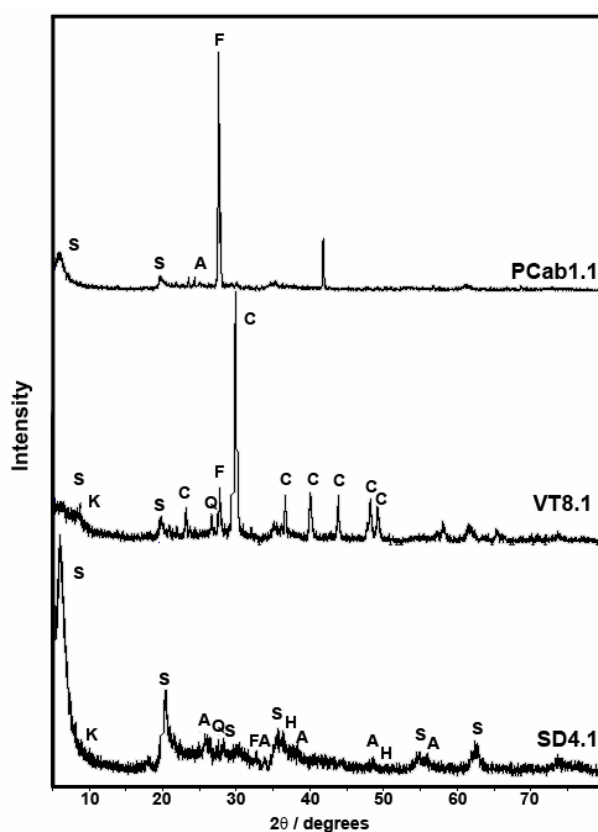
Figure 3.5 Main contaminants identified in SD4.1, VT8.1 and PCab1.1 bentonites (S: smectite; K: kaolin; C: calcite; Q: quartz; F: feldspar (plagioclase); A: anatase; FA: fluorapatite; H: hematite)

3.3.3 SURFACE AREA (N$_2$ ADSORPTION ISOTHERMS AT 77 K)
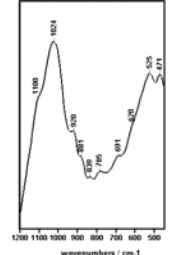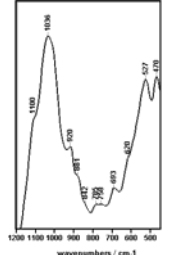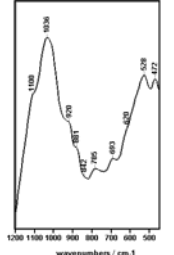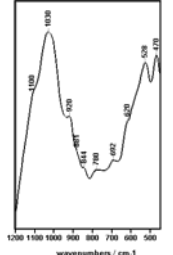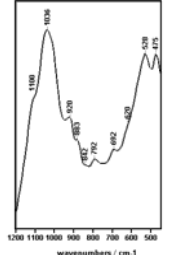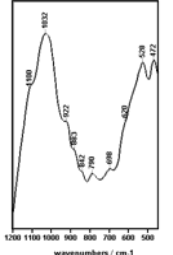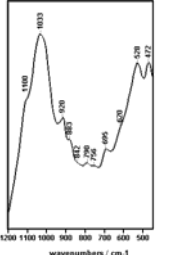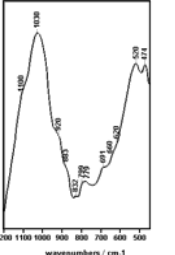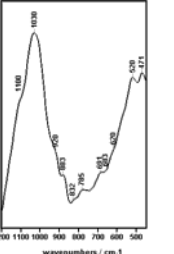
The measured surface areas (calculated by application of the BET method to the adsorption isotherms of N$_2$ at 77K, Figure 3.2 and Table 3.4) vary between 71 m^2.g^{-1} (SF3.1) and 115 m^2.g^{-1} (VT8.1). These values are not conclusive because they are clearly affected by the presence of the contaminants. Calcite seems to affect the isotherms the most (PAF6.1, VT8.1 and VT8.2 exhibit, simultaneously, the highest levels of calcite contamination and the biggest surface areas).

3.3.4 INFRARED ANALYSIS

As stated above, all samples were submitted to mild acid treatment, in order to remove the carbonate contaminant and, therefore removing the 878 cm^{-1} peak that would obscure the important diagnostic band correspondent to AlFeOH deformation (ca. 880 cm^{-1}), that arises from octahedral substitution of Al by Fe. DRIFTS spectra confirmed that the clay structure was not affected by this treatment (Figure 3.3). Further confirmation was obtained by analyzing the chemical composition of the most heavily contaminated sample, VT8.1. It can be seen (Table 3.5) that the normalised values of the metal oxides remain roughly the same, with the clear exception of MgO (probable external magnesium carbonate phase, e.g. dolomite) and CaO (which was the purpose of the acid treatment).

The infrared spectra (Figure 3.2 and Table 3.4) confirm the montmorillonitic character of the clay minerals present in the samples; all bentonitic samples exhibit typical smectites bands (Table 3.6) (Farmer 1974; 1979; Russell and Fraser, 1994; Madejová *et al.*, 1995; Madejová and Komadel, 2001; 2005; Madejová, 2003; Gates, 2005).

Table 3.4 Normalised metal content[12], images before and after calcination and DRIFTS spectra in 1200-400 cm^{-1} region of the bentonite samples

	PAF6.1	PCab1.1	PCas9.2	SD3.1	SD4.1	SF3.1	SF9.1	VT8.1	VT8.2
Na/Si	1,91	2,89	3,25	3,02	1,05	3,31	1,06	1,71	1,52
Mg/Si	10,48	6,12	6,11	7,45	7,86	6,45	7,41	13,42	13,07
Al/Si	30,57	34,57	35,16	35,40	33,36	33,39	35,21	29,01	24,03
K/Si	2,68	0,78	1,50	1,43	1,84	1,69	1,74	6,66	1,52
Ca/Si	13,77	7,46	11,09	6,57	4,68	4,75	7,68	90,05	28,16
Ti/Si	5,42	5,57	7,34	4,36	6,17	2,98	6,83	2,79	4,44
Fe/Si	15,84	16,56	26,21	11,74	17,00	10,43	19,03	16,66	23,81
Non heated									
Heated (500ºC)									
DRIFTS (1200-450 cm^{-1})									

---

[12] (% Metal oxide/ % SiO2) * 100

Table 3.5 Chemical composition of VT8.1 prior to and after mild acid washing
(between brackets, the metal oxide-to-SiO_2 ratio, in percentage)

	VT8.1	**VT8.1 (acid washed)**
Na_2O	0.65 (1.71)	0,58 (1.20)
MgO	5.10 (13.42)	3,62 (7.5)
Al_2O_3	11.02 (29.01)	14,48 (29.90)
SiO_2	37.99 (---)	48,42 (---)
K_2O	2.53 (6.66)	3,28 (6.77)
CaO	34.21 (90.05)	1,38 (2.85)
TiO_2	1.06 (2.79)	1,6 (3.30)
Fe_2O_3	6.33 (16.66)	8,64 (17.84)
Others	1.11 (2.92)	0,33 (0.68)

In addition to the different levels of calcite contamination, already mentioned, kaolin was also detected in all the samples (695 cm^{-1}). The more contaminated samples also exhibited a band at ca. 3695 cm^{-1}. It has been proven (Joussein *et al.*, 2001; Madejová *et al.*, 2002) that the absorption coefficient of the OH stretching vibration of kaolinite is higher than that of smectites. Hence, the presence of minor amounts of kaolinite in the bentonitic sample produces relatively strong 3699 cm^{-1} bands and leading, therefore, to misguided conclusions about the weight of kaolin in the mixture. Based on Madejová and co-workers (2002) results, it is possible to estimate that, even for the most kaolin contaminated material (SF9.1, cf. 3700 cm^{-1} band, Figure 3.2 and Figure 3.6A), the content of kaolin does not exceed 2-3 % wt of the smectite.

PCab1.1 does not exhibit the 1455 cm^{-1} band already attributed to the presence of a calcite admixture, although the XRF composition data (Figures 3.2 and 3.4) show the presence of an important amount of calcium (ca. 4.2% / 8% Ca/Si). This result correlates well with the plagioclase peak detected in the XRD trace of this bentonite (Figure 3.5) and is indicative of the presence of the calcium end member of this mineral ($CaAl_2Si_2O_8$).

Table 3.6 Tentative assignment for IR bands

Assignment	PAF6.1	PCab1.1	PCas9.2	SD3.1	SD4.1	SF3.1	SF9.1	VT8.1	VT8.2
OH stretching of inner-surface hydroxyl groups (kaolin)	---	3694	3694	3694	3694	---	3699	---	---
OH stretching of structural hydroxyl groups	3624	3624	3624	3623	3624	3624	3624	3610	3618
Nontronite fraction?	---	---	---	---	---	---	---	3562 (br)	3560 (br)
OH stretching of water (broad)	3412	3410	3410	3406	3406	3408	3408	3402	3402
OH deformation of water	1636	1634	1635	1635	1635	1635	1635	1635	1635
Carbonate phase (removed by acid wash)	1455	---	1455	1455	1455	1455	1455	1455	1455
Si-O stretching (longitudinal mode), shoulder	~1100	~1100	~1100	~1100	~1100	~1100	~1100	~1100	~1100
Si-O stretching	1024	1036	1035	1030	1036	1032	1033	1030	1030
AlAlOH deformation	920	920	921	920	920	922	920	920 (sh)	920 (sh)
AlFeOH deformation	881	883	883	881 (sh)	883	883	883	883	883
AlMgOH deformation	839	842 (sh)	840 (sh)	844	842 (sh)	842	841 (sh)	---	---
Nontronite fraction?	---	---	---	---	---	---	---	832 (br)	832 (br)
Si-O stretching of sílica	785	784	785	780	792	790	790	799; 779	785
Si–O, perpendicular (kaolin)	---	758	---	---	---	---	756	---	---
Si–O, perpendicular (kaolin)	692	693	693	692	692	698	695	691	691 (sh)
Nontronite fraction?	---	---	---	---	---	---	---	~660 (sh)	683
Coupled Al-O and Si-O, out-of-plane (sh)	~620	~620	~620	~620	~620	~620	~620	~620	~620
Al-O-Si deformation	525	527	528	528	528	528	528	520	520
Si-O-Si deformation	471	470	472	470	475	472	472	474	471

sh: shoulder; br: broad
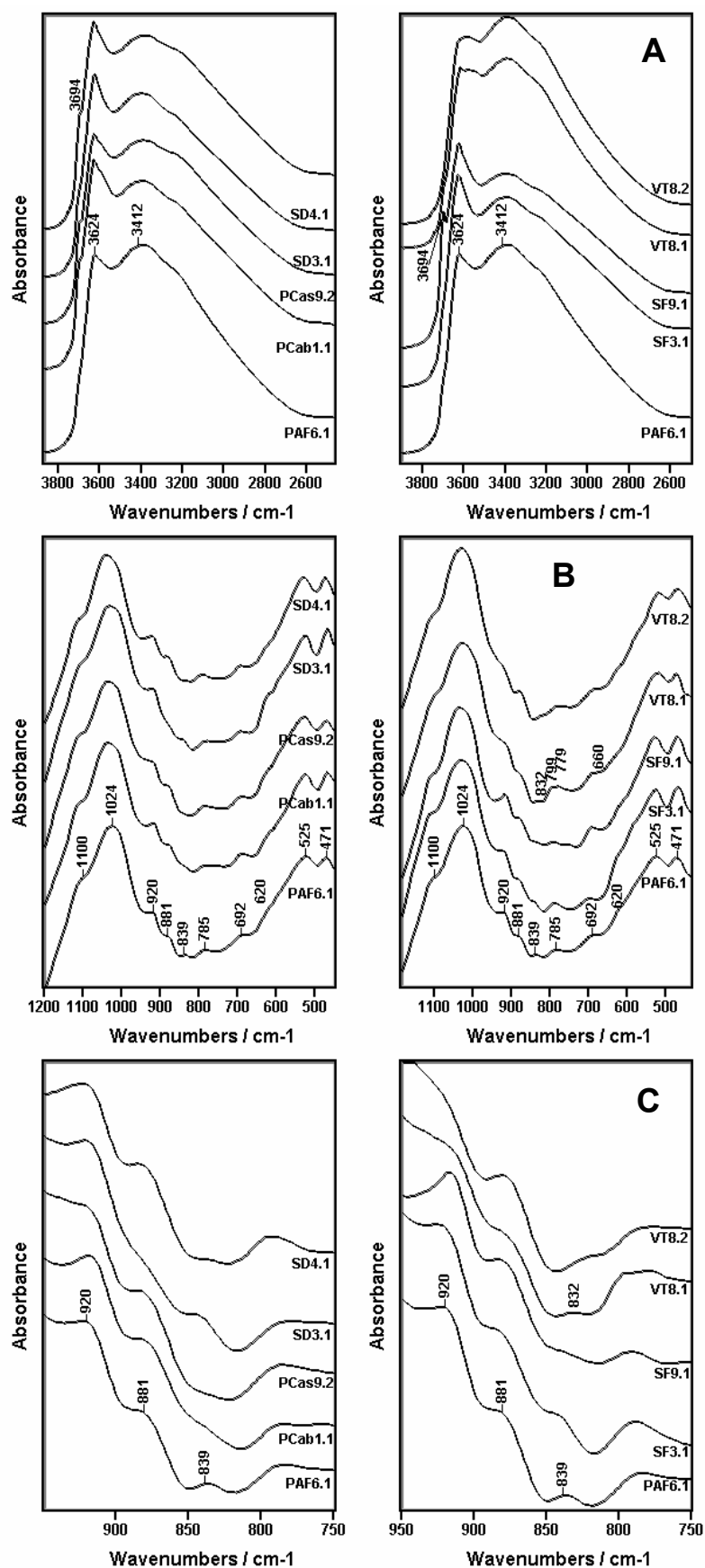
Figure 3.6 DRIFTS spectra of Porto Santo bentonitic materials (A: 3900-2500 cm^{-1}; B: 1200-500 cm^{-1}; C: 950-750 cm^{-1} regions)

VT8.2 introduces a new feature to the characterisation of the Porto Santo bentonites. Although not totally conclusive, there is some infrared evidence (Table 3.6) of the possible existence of a second type of smectite in the material, with nontronitic character. The bands at 3580 (very broad), 820 and 680 cm^{-1} are representative of the nontronite family (Madejová et al., 1995) and were reasonably well detected in VT8.2 which also exhibits one of the highest Fe/Si ratios (Table 3.3). VT8.1 infrared spectrum (Table 3.6) also exhibits typical nontronite bands, although in this case they are not as well defined neither is the iron content particularly high.

The type of isomorphic substitutions that occur in the smectite fraction of the bentonites may be deduced from the bands in the region 950-750 cm^{-1} (metal-metal-OH deformation region, Figure 3.6B). All samples exhibit relatively well defined peaks at 920 cm^{-1}, attributed to the AlAlOH deformation mode, 880 cm^{-1} (AlFeOH) and 840 cm^{-1} (AlMgOH) (Wilson, 1994). The data show that the smectite fractions of the materials analysed contain octahedral substitution of Al by Fe or Mg, with different degrees of substitution. As noted above, the VT samples (in particular VT8.2) exhibit an 830 cm^{-1} band, attributed to the FeFeOH deformation, which confirms the presence of "pure" iron domains in these bentonites.

There is no direct correlation between the intensity/resolution of the AlFeOH bands in the infrared spectra (Table 3.4 and Figure 3.6B) and the amount of iron present in the samples (Figures 3.2 and 3.3). For example, SF3.1 exhibits the lowest Fe to Si ratio (10.4 %, Table 3.4) but still exhibits a reasonably well defined AlFeOH peak, whereas SD3.1 (11.7% Fe/Si, Table 3.4) does not display a clear 880 cm^{-1} band and the corresponding band in the spectrum of PCas9.1 does not reflect (neither in intensity nor in resolution) the highest Fe to Si ratio (26.2 %, Table 3.4) of all materials analysed. These observations reinforce the idea of the presence of non-structural iron in the materials analysed, already deduced by analysis of the XRD data (cf. section 3.3.2) and visual inspection[13] of the bentonite samples (Figure 3.2 and Table 3.4).

---

[13] Empirical observation: the stirring magnets exhibited magnetic materials attached after stirring bentonite suspensions.

In addition to the images of the unheated bentonites (Figure 3.2 and Table 3.4), images of heated samples at 500 ºC are presented in Table 3.4. The idea was to infer, based on the colour developed by the bentonitic materials, the possible existence of iron admixtures. As expected, all heated samples exhibited more intense colours than their unheated counterparts. Apparently, the existence of non structural iron (proved by the IR spectra of SD3.1 and PCas9.2, Table 3.4) produces, upon heating, stronger colour changes than samples with lesser amounts of non-clay iron phases (e.g. SF3.1, Table 3.4). Based on these very empirical (and probably unreliable) observations, one could assume the presence of important non-clay iron phases in PCas9.2 and SD4.1 and that the iron content of the bentonites PAF6.1 and PCab1.1 is largely present in the layers of the smectite fraction of these materials.

3.3.5 CONCLUSIONS

The characterisation data hereby presented clearly shows that the designation "Porto Santo bentonite" is, for many applications, too general to define the range of materials collected at the island's bentonitic deposits (even those in close proximity) due to the following reasons:

1- The yield of the < 2 μm fraction varied significantly within the samples collected;

2- The samples collected exhibited major differences in terms of the type and, mainly, the amount of impurities present (e.g. the major contaminant of VT8.1 is calcite, whereas PCab1.1 exhibits an important plagioclase admixture). These disparities will affect the percentage of clay minerals present in the fine fractions;

3- The clay minerals present in the fine fractions exhibit important differences in terms of composition, namely the degree of octahedral isomorphic substitution of Al by Fe. There was evidence of a second member of the smectite family in the Vale do Touro materials, nontronitic in character.

The differences detected within these Porto Santo bentonite samples suggest that proper sample and collection point should be recorded and reported. The Porto Santo bentonite deposits are important both in geologic and chemical senses, because they differ substantially, when the area of their location is considered.

Within the materials analysed, SF and SD materials proved to possess the lower amount of contaminants, which makes them the most appropriate choice for further work. The high surface areas and high iron and titanium contents of the samples obtained at these locations reinforced their eligibility for further catalytic work. Due to material availability, SD4.1 was chosen for all the subsequent catalyst preparation and characterisation. From this point forward **SD4.1** will be referred to as **SD**.

3.4 Na-SD

3.4.1 Characterisation

Chemical composition analysis by X-Ray Fluorescence (Table 3.7) shows that the sodium exchange procedure was successful. It can also be seen that Na-SD presents a high percentage of iron and titanium, as well as a relevant amount of magnesium.

Table 3.7 Chemical composition, surface area, basal spacing and CEC of NaSD

Chemical composition / oxide %									A_{BET} $(m^2.g^{-1})$	d_{001} (Å)	CEC (meq/100 g)
Na	Mg	Al	Si	K	Ca	Ti	Fe	Others			
2.6	3.4	20.5	57.4	0.9	0.5	3.3	10.3	1.1	130	14.9	81.4 ± 1.2

Nitrogen adsorption data[14] (Russo and Carrott, 2004) revealed that SD exhibits higher surface area (ca. 130 m^2 g^{-1}, Table 3.7) than the normal 20 - 65 m^2 g^{-1}, observed for

---

[14] The analysis were performed by M. R. Carrott and P. Russo at the facilities of Centro de Química de Évora.

smectites (Dogan *et al.*, 2006). These features may be attributed in part to the small size of the constituent particles and their microscopic aggregation (de Carvalho *et al.*, 1996). The nitrogen adsorption isotherm at 77 K of NaSD is a mixture of types I and IIb according to the IUPAC classification (Rouquerol *et al.*, 1999): at low p/pº, the adsorbed quantity is high (type I character) which indicates primary microporosity; after filling the micropores, adsorption continues to occur (multilayer), which means that the solid exhibits external area associated with microporosity. The isotherm exhibits a H4 hysteresis loop; hence, the increase of adsorbed material in the multilayer region is due, also, to adsorption on the mesopore walls formed between adjacent stacks of lamellar particles. The fact that the isotherm is not perfectly vertical at the low pressure region shows that the material exhibits secondary microporosity.

The Cationic Exchange Capacity (CEC), was measured in triplicate using the method suggested by Rhodes and Brown (1994[b]), and the value of (81.4 ± 1.2) meq.100g^{-1} was obtained (Table 3.7).

Thermoanalysis was performed on NaSD. The TG curve (not shown) was obtained under nitrogen up to 800 ºC and three weight loss regions were identified. The first (100-200 ºC) corresponds to the loss of water physically adsorbed between the silica sheets and depends on the nature of the exchangeable cations and the nature of surface chemistry. Na-SD exhibits a very pronounced band which is probably related to the degree of hydration of the material. The second weight loss (attributed to dehydroxylation – Grim, 1968), which normally occurs in the 450-750 ºC temperature interval for montmorillonites with moderate degrees of octahedral isomorphic substitution (Al by Fe or Mg), occurs at a slightly lower temperature range for NaSD (400-600 ºC). This reflects the high iron content of the bentonite revealed by the chemical composition data (Table 3.7) (Grim, 1968). A third transformation starts to occur near 800 ºC, which has been attributed to the collapse of the clay structure

(Grim and Bradley, 1940) or the loss of OH groups bonded to tetrahedral Si (McConnell, 1943; Page, 1943) or to Mg in the octahedral sheets (Page, 1943). Both possibilities correlate well with chemical composition data presented in Table 3.7.

XRD data (Figure 3.7 and Table 3.8) confirmed the presence of important amounts of smectite minerals in the NaSD bentonite and allowed the identification of the main impurities present in the bentonitic material. The peak at 6.84º 2θ (12.92 Å) is indicative of the beidellitic character of the smectite fraction of NaSD (Brindley and Brown, 1984). The relative intensities of the other typical smectite peaks (Table 3.8) provide evidence of the high content of clay minerals in the sample analysed. It can be seen that anatase is an important contaminant; this finding correlates well with the TiO_2 fraction identified by XRF chemical composition analysis (Table 3.7). Quartz, feldspar and possibly apatite admixtures were identified. Small, but discernible hematite peaks are present in the trace, which reinforces the earlier point regarding the existence of external iron phases.
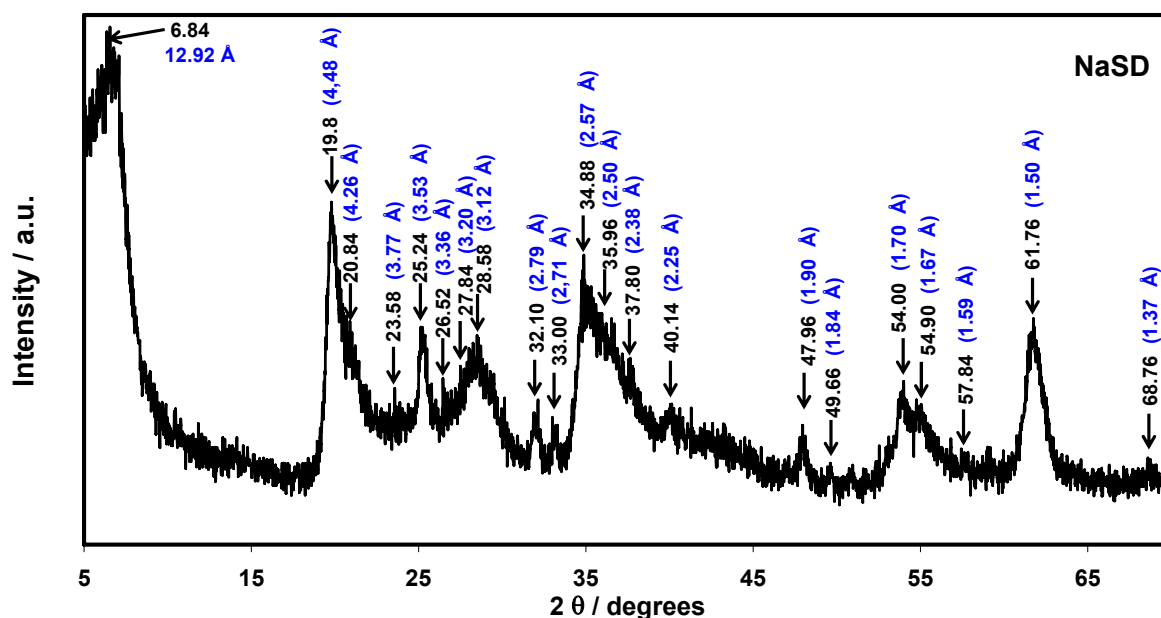
Figure 3.7 XRD trace of NaSD (between brackets in blue, d spacing values)

Table 3.8 Tentative assignment of the XRD trace peaks of NaSD (Brindley and Brown, 1984)

d / Å	2 θ / degrees	Assignment
4.48	19.80	
3.54	25.24	
3.12	28.50	
2.57	34.88	Smectite
2.25	40.14	
1.70	54.00	
1.50	61.76	
3.53	25.24	
2.38	37.80	
1.90	47.96	Anatase
1.67	54.90	
1.37	68.76	
4.26	20.84	Quartz
3.36	26.52	
2.71	33.00	
2.50	35.96	Hematite
1.84	49.66	
1.59	57.84	
3.77	23.58	Feldspar
3.20	27.84	(plagioclase)
2.79	32.1	Fluorapatite (?)

Quantitative X-Ray powder diffraction was performed on Na-SD (by Macauley Analytical Services; data not shown) and results, obtained using the reference intensity ratio (RIR)[15] method, show that NaSD presents a high content in clay minerals (ca. 92%, endmember smectite, with no indication of mixed-layering) and small amounts of quartz (4.6%), plagioclase feldspar (1.5%), anatase (2.7%) and apatite (2.0%). There is some evidence of the presence of traces of kaolin (ca. 1%), which was confirmed with FTIR spectra of the material (cf. infra). Glycolation indicated that the sample was monominerallic in terms of the swelling clays present, although the fact that the "060" peak is quite broad could indicate that

---

[15] The mineral abundances reported are semi-quantitative, providing nonetheless a reasonable estimate of the "purity" of NaSD.

there is a range of octahedral compositions. Anatase exhibited rather broad peaks indicating poor crystallinity due, possibly, to the fact that his phase can accommodate some Fe in its structure (eventually responsible for the material observed to stick to a magnetic stirring rod).

The DRIFT spectrum of Na-SD (Figure 3.8) confirmed the presence of kaolin (peaks at 3691 and 692 cm^{-1}). The peak at 3626 cm^{-1} is typical of an aluminium rich dioctahedral sheet. The OH bending bands at 918, 883 and 840 cm^{-1} (very weak) may be attributed to Al_2OH, AlFeOH and AlMgOH groups, respectively, reflecting the partial octahedral substitution of Al by Fe and Mg. The shoulder near 618 cm^{-1} may be attributed to an Al-O-R (R = Al, Mg) vibration of octahedral atoms. The band at 790 cm^{-1} may be attributed to the Si-O stretching of silica. The strong bands at 1019 cm^{-1} (Si-O stretching vibrations) and 516 and 466 cm^{-1} (Si-O-Al and Si-O-Si bending vibrations, respectively) are representative of the strong Si-O absorption of the tetrahedral layer. Broad bands at 3440 and 1631 cm^{-1} are attributed to the OH vibrations of molecular water. The rigorous Na-exchange procedures employed resulted in a very low CaO content (Table 3.7) but the presence of a calcium carbonate phase cannot be completely discarded (Madejová *et al.*, 1995) – cf. 1450 cm^{-1} region in Figure 3.8.
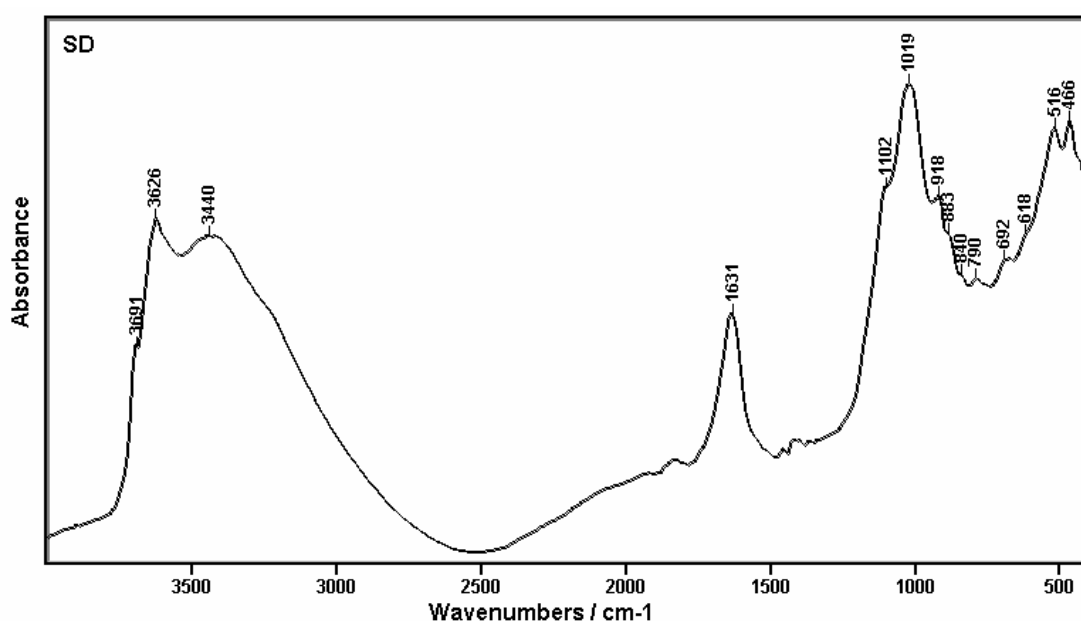
Figure 3.8 DRIFTS spectrum of NaSD

3.4.2 FINAL REMARKS

The DRIFTS spectrum together with the XRD profiles are consistent with a material containing a high percentage of an aluminium rich dioctahedral smectite, with partial isomorphic substitution of Al by Mg and Fe and Si by Al or Fe on the octahedral and tetrahedral sheets, respectively, contaminated with anatase, kaolin, quartz, plagioclase and apatite. The peaks assigned to anatase in the XRD diffractogram are quite broad, which is consistent with the possible presence of some iron in its structure. This possibility is reinforced by the results obtained by Raman and Mössbauer spectroscopy performed on NaSD and raw SD (not shown), in order to identify the magnetic phase present. Results, although not absolutely conclusive, allowed discarding the presence of substantial amounts of pure iron oxides. The majority of the iron was present as two ferric doublets which remained at low temperatures. One, or perhaps two, magnetic phases were present but were too weak to identify clearly even at 77K (Oh *et al.*, 1998).

CHAPTER 4. ION EXCHANGED CLAYS

4. Ion Exchanged Clays

4.1 Introduction

The aim of the work described in this chapter was to evaluate how different interlayer cations (Al^{3+}, Ni^{2+}, Cr^{3+}, Na^+), selected for their known influence on the acidity and the catalytic activity, influenced the activity of two clays of different origin: the low-charge SD with high structural iron content and a high-charge clay (SAz-1) which contains only a small amount of structural iron. A particular focus of the work is to explore how the combination of the transition metals in the clay structure and the exchange cations influence the activity towards p-cymene production.

4.1.1 Choice of the Reference Clay

Clay minerals are versatile, environmentally friendly catalysts that can be quite easily tailored to suit a wide variety of organic reactions (Varma, 2002). Clays are natural minerals that present a range of chemical compositions, locations and density of charge. Consequently, the nature of the clay plays an important role in maximizing the catalytic activity for the precise reaction of interest.

SAz-1 is a Ca-montmorillonite, obtained at the Bidahochi formation (pliocene), County of Apache, State of Arizona, USA and is part of the Source Clay Minerals collection (Clay Minerals Society) which is housed in the Source Clays Repository at the University of Missouri. The collection comprises representative samples of kaolinite (KGa-1b, KGa-2), palygorskite (PFl-1), montmorillonite (SAz-1, STx-1, SWy-2), hectorite (SHCa-1), and synthetic mica-montmorillonite (Syn-1). The Source Clays are collected from large, commercial, reasonably homogeneous deposits that have been carefully selected to be both representative of the clay mineral and to minimize variation. These materials have been

recently characterised[16] in terms of geological origin, composition (major, minor, trace and rare earth elements), powder X-ray diffraction patterns, layer charge, infrared spectra, thermal behaviour, cation-exchange capacity and colloid and surface properties. The main characterisation data obtained for SAz-1 follows next.

SAz-1 contains a low amount of structural iron and, when compared to NaSD, exhibits a higher CEC and a lower surface area (Table 4.1). The calculated structural formula proposed for SAz-1 (Mermut and Cano, 2001) reveals very little tetrahedral isomorphic substitution of Si by Al, an important Mg content in the octahedral sheet and an almost exclusive presence of exchangeable Ca^{2+} ions.

Table 4.1 Chemical composition, surface area and CEC of NaSD and CaSAz-1[17]

Clay	Chemical composition / oxide %									A_{BET} (m^2.g^{-1})	CEC (meq/100 g)
	Na	Mg	Al	Si	K	Ca	Ti	Fe	Others		
NaSD	2.6	3.4	20.5	57.4	0.9	0.5	3.3	10.3	1.1	130	81.4 ± 1.2
SAz-1	0.06	6.73	19.98	59.65	0.19	3.15	0.25	1.77	0.01	60	120 ± 3

The infrared spectrum of SAz-1 (Figure 4.1) reflects the lower Fe and higher Mg content of this smectite in comparison with NaSD (compare bands at 880 and 842 cm^{-1}, Figure 3.7, Chapter 3). A weak band at 792 cm^{-1} indicates traces of poorly crystalline silica.

SAz-1 based modified catalysts were prepared from the "as-shipped" material. XRD semi-quantitative analysis data for this material (Chipera and Bish, 2001) confirmed a high content in smectite minerals (ca. 98%) and traces of quartz (ca. 1%) and other minerals (e.g. feldspar, quartz, mica, magnetite; ca. 1%).

Most of this characterisation data was "confirmed" with the SAz-1 material actually used in

---

[16] *Clays and Clay Minerals* (2001), 49 (5)
[17] Mermut and Cano, 2001; Borden and Giese, 2001; Dogan et al., 2006

the experiments and the results obtained are in good agreement with the referenced data.
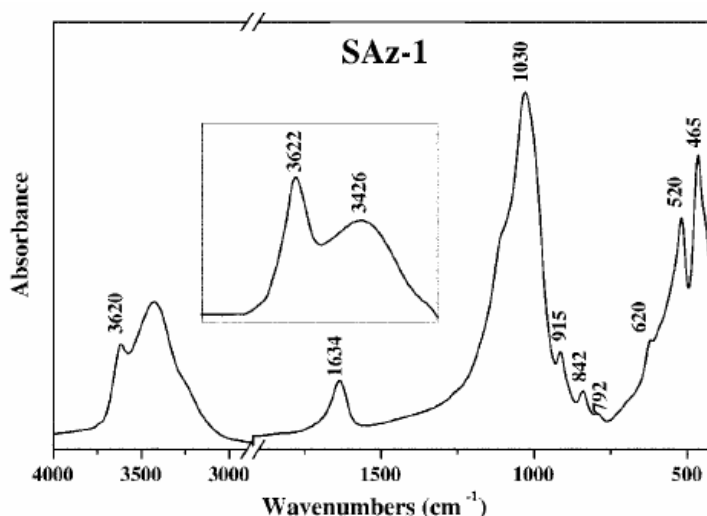
Figure 4.1 IR spectra of SAz-1 (montmorillonite) using 0.5 mg sample/200 mg KBr for 4000-400 cm^{-1}. Insert: 2.0 mg sample/200 mg KBr disk heated overnight at 150 ºC (Madejová and Komadel, 2001)

The nitrogen surface area of SD is ca. 130 m^2.g^{-1} (cf. Chapter 3) which is markedly higher than that of SAz-1 which, at 60 m^2.g^{-1} (Dogan *et al.*, 2006), is more representative of most clays. Furthermore, the possibility that the selectivity towards p-cymene could be increased by using a catalyst with substantial Lewis acid character, as suggested by the work of de Stefanis *et al.* (1995), and Crocket and Roduner (1994), has been considered. Besides acidity and site accessibility, the presence of some transition metal ions (especially Fe^{3+} for SD) in the clay structure offers the potential for redox activity. These sites may provide the required dehydrogenation activity and hence play an important role in the overall process.

4.1.2 CHOICE OF EXCHANGEABLE CATIONS

Both Lewis and Brönsted acidity are dependant upon the clay's hydration state. Strong Brönsted acidity in smectites is derived primarily from the dissociation of water that coordinates exchangeable cations. Hydrogen ion dissociation from hydration water under the polarizing effect of a metal ion occurs as follows:

$$\left[M(OH_2)_x\right]^{n+} \rightarrow \left[M(OH)(OH_2)_{x-1}\right]^{(n-1)+} + H^+$$

where M is the cation of n^+ charge and x is the number of coordinating water molecules (Carrado, 2004). Protons are much more mobile in the interlayer than in bulk water because the dielectric constant of interlayer water is less than that of bulk water. Acid strengths of some common ions decrease in the order of polarisation (decreasing size and increasing charge) as: Fe^{3+}, Al^{3+}, Ni^{2+}, Mg^{2+}, Ca^{2+}, Ba^{2+}, Li^+, Na^+, K^+ (Yariv and Michaelian, 2002). Since acid strength increases with the polarisation of cations, as the amount of water decreases the polarisation (and therefore the ability to donate protons) increases. Fully dehydrated interlayer cations then behave as Lewis acids (Carrado, 2004).

Na^+ ions do not exhibit any catalytic properties, therefore the sodium homoionic forms of SD and SAz were prepared in order to obtain materials with no added catalytic activity due to exchangeable cations; hence, these materials are considered the reference materials to which all the catalytic results will be compared.

The properties of clays can be readily modified by ion-exchange, and Ni^{2+} and Al^{3+} -exchanged montmorillonites are considered "model" Lewis and Brönsted acids, respectively. The nature of the active sites has been probed using FTIR spectra of adsorbed pyridine (Breen, 1991[a]; Brown and Rhodes, 1997) and supported by catalytic data (Brown and Rhodes, 1997; Breen and Moronta, 2001; Hart and Brown, 2004). Evolved Gas Analysis (EGA) of the thermally desorbed products, arising from the degradation of the adsorbed cyclohexylamine (CHA), demonstrated different decomposition pathways over Al^{3+}- and Ni^{2+} - exchanged SWy-2 clays which could be correlated with the different nature of the active sites (Breen *et al.*, 2000).

Cr based catalysts are frequently reported as being used in several catalytic applications. It has been shown (Breen *et al.*, 1987) that Cr containing clays offer a combination of both

Lewis and Brönsted acid sites and that they may present higher acidities than their Al

counterparts (Cañizares *et al.*, 1999).

4.2 EXPERIMENTAL

NaSD and the "as received" form of SAz-1 were used as starting materials for the preparation

of the remainder of the homoionic cation-exchanged clay catalysts (Al^{3+}, Ni^{2+} and Cr^{3+}).

Samples of NaSD and SAz-1 were ion-exchanged with Al^{3+}, Ni^{2+} and Cr^{3+}, by stirring 1%

suspensions of the clays in 0.3 (Al^{3+} and Cr^{3+}) and 0.6 (Ni^{2+}) $mol.dm^{-3}$ solutions of the metal

chlorides or nitrates overnight. In each case the clay was separated from the solution and the

procedure was repeated twice. The suspensions were centrifuged and the resulting materials

thoroughly washed, dialysed until the conductivity was low (< 30 μS), dried and ground. The

materials obtained are subsequently referred to as Na-, Al-, Ni- and CrSD or SAz.

Chemical Composition (XRF), variable temperature diffuse reflectance infrared Fourier

transform spectroscopy (VT-DRIFTS), thermal desorption of cyclohexylamine (CHA) and real

time thermogravimetry-mass spectrometry (TG-MS) of the evolved gases were used to

evaluate the properties of the prepared catalysts.

4.3 RESULTS AND DISCUSSION

4.3.1 ACIDITY MEASUREMENTS

4.3.1.1 DRIFTS STUDIES

VT-DRIFTS of pyridine treated samples still remains the only routine way to unequivocally

distinguish between Brönsted and Lewis acid sites on the surface of solid acid catalysts

(Breen, 1991[a]). It has been shown (Ward, 1968) that peaks at 1635 and 1540 cm^{-1} can be

assigned to the pyridinium ion (Brönsted acidity, BPYR), whereas peaks at 1613 and 1450 cm^{-1} are diagnostic for pyridine co-ordinately bound to Lewis acid sites (LPYR) while peaks at 1596 and 1440 cm^{-1} may report the presence of H-bonded pyridine (HPYR). All these species contribute intensity to the 1490 cm^{-1} band although the largest contribution at higher temperatures (> 120 ºC) is from BPYR.

In accordance with previous studies on a different bentonite (Breen *et al.*, 1987) Al homoionic clays exhibited bands associated with BPYR (and some LPYR), Ni-exchanged materials exhibited bands associated with LPYR whereas the spectra for pyridine treated CrSD contained bands for both BPYR and LPYR. Figure 4.2 presents the VT-DRIFTS spectra of the air-dried $M^{n+}SD$ and SAz clays, following exposure to pyridine and subsequent heating to higher temperatures. The pyridine-treated NiSD sample (Figure 4.2A), heated at 50 ºC provided evidence for significant amounts of physisorbed pyridine (1440 cm^{-1} and 1596 cm^{-1}). Degassing at 100 ºC caused a marked reduction in the intensity of both the 1440 and 1596 cm^{-1} bands, which by 150 ºC had disappeared. A weak, broad band at 1540 cm^{-1}, diagnostic for BPYR, appeared as an unresolved shoulder at 50 ºC, which remained present up to 200 ºC but became increasingly weaker above this temperature. In contrast, high temperature activation of the pyridine-treated NiSD, did not remove the bands at 1450 cm^{-1} and 1613 cm^{-1} which are considered diagnostic for LPYR.

The spectrum recorded at 50 ºC for the pyridine-treated Al^{3+}-form of SD (Figure 4.2B), exhibited a much broader envelope of peaks in the 1570-1650 cm^{-1} region, together with a weak band at 1450 cm^{-1} but there was little evidence for large amounts of physisorbed pyridine (1440 cm^{-1} and 1596 cm^{-1}). In contrast to NiSD, a well-defined, intense BPYR band at 1539 cm^{-1}, together with the 1488 cm^{-1} band, dominated these spectra. The generation of Lewis acid sites, subsequent to heating above 150 ºC, was supported by the presence of two distinct bands at 1450 and 1613 cm^{-1}, typically attributed to LPYR. The VT-DRIFTS spectra

of Al- and Ni-SAz (Figures 4.2C and D) followed the trends exhibited by SD in terms of relative intensities of the BPYR and LPYR diagnostic bands; however the bands present in the spectra of the former are less broad and generally better defined than the equivalent bands exhibited in the spectra of the SD materials. The reason for this is probably related to particle size and homogeneity aspects that distinguish both parent clays, in general, and a more uniform distribution of the acid site strength on SAz than on SD, in particular.

Despite the difficulty of obtaining quantitative information, the truly remarkable feature of these spectra was the overall dominance of bands associated with LPYR in NiSD and NiSAz in contrast to Al exchanged materials in which well-defined, intense BPYR bands appeared at 1540 cm^{-1}. Indeed, the fact that the 1540 and 1490 cm^{-1} bands were still present at 350 ºC emphasises the strength of the Brönsted acid sites on AlSD.

The homoionic Na-exchanged forms presented different results: NaSAz showed little to no evidence of BPYR or LPYR (not illustrated), whereas NaSD (Figure 4.2E) exhibited small but discernible bands assigned to BPYR and LPYR. This is consistent with both the thermogravimetric and catalytic studies referred to below.

CrSD spectra (Figure 4.2F) revealed two well defined peaks at 1540 (BPYR) and 1450 cm^{-1} (LPYR) together with the 1490 cm^{-1} band, indicative of the presence of significant amounts of both Brönsted and Lewis acid sites.

Figure 4.2G (combination of spectra of selected metal exchanged materials at 200 ºC) provides a direct comparison of the differences between these materials in terms of relative amounts of Brönsted and Lewis acid sites.
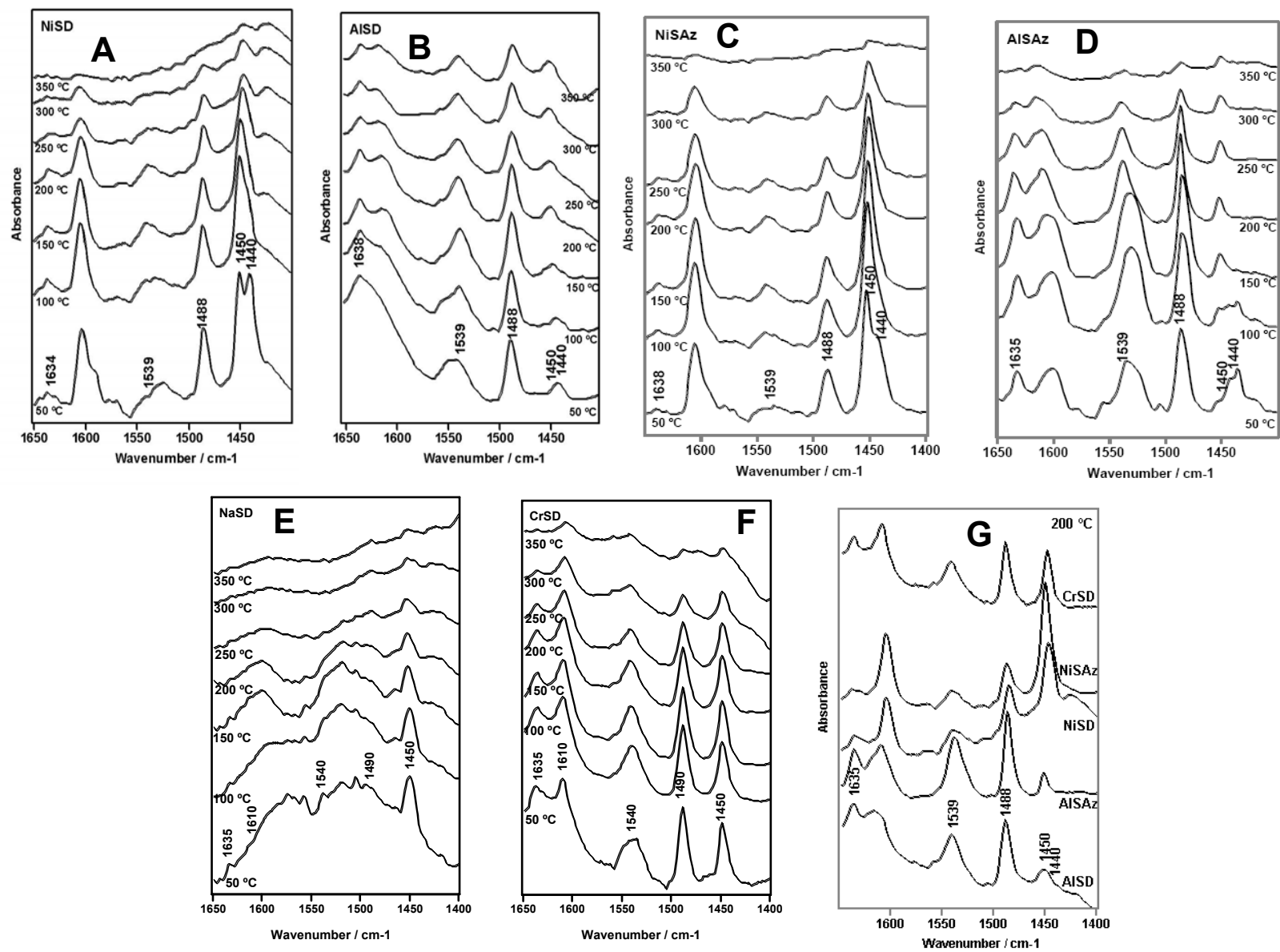
Figure 4.2 DRIFTS spectra of air-dried, following exposure to pyridine A. NiSD, B. AlSD, C. NiSAz, D. AlSAz, E. NaSD and F. CrSD heated to the temperatures indicated and G. M^{n+}-SD heated to 200 ºC, after pyridine exposure.

Figure 4.3 is a graphical representation of the intensities of the 1540, 1490 and 1450 cm^{-1} bands, normalised using the intensity of the 1030 cm^{-1} band at 150 and 300 ºC[18]. Several observations can be drawn from the data presented. It can be seen that the Al^{3+}-exchanged materials retain pyridine mainly on Brönsted sites (1540 cm^{-1}) and that LPYR is predominant in the Ni^{2+} homoionic clays (1450 cm^{-1}). As expected, the presence of Lewis bound pyridine is still discernible at 300 ºC (Figure 4.3B), whereas the intensities of the 1540 cm^{-1} bands undergo a sharp decrease when the materials are heated at 300 ºC. As anticipated, the presence of relatively strong 1540 and 1450 cm^{-1} bands in the CrSD spectra provide evidence of the existence of both Brönsted and Lewis acidic sites on the surface of this material. The amounts of pyridine adsorbed by the SAz homoionic materials (Al^{3+}- and Ni^{2+}-exchanged) are clearly higher than the amounts retained by the equivalent ion exchanged SD clays. This probably reflects the different CEC of the parent clays[19]. The decrease in intensity of the bands upon heating is more pronounced for the SAz materials than for SD catalysts, which suggests that the acidic sites present in the latter are stronger than those in the former. Another reason for this behaviour could be related to the pyridine desorption pathways out of both materials, arguably simpler on the reference clay (smaller surface area, homogenous site distribution, etc.).

4.3.1.2 THERMOGRAVIMETRIC (TG) STUDIES

It has been suggested that the thermal desorption of cyclohexylamine can be used to quantify the number of acid sites on a clay catalyst (Ballantine *et al.*, 1987). The technique requires the determination of the weight loss between 280 and 440 ºC and its conversion to the number of mmol of CHA desorbed (cf. Section 2.1.4.1). The quantities of CHA desorbed in the appropriate temperature interval are presented in Table 4.2.

---

[18] This band was chosen based on the supposition that its intensity is not severally affected by the variation of temperature.
[19] This is not an infallible conclusion because the VT-DRIFTS preparation procedures differ slightly from sample to sample. However, all the preparation steps (incubation time with pyridine, sample weighing and mixing with KBr, heating rates, etc.) were carefully performed in order to minimize the extrinsic factors.
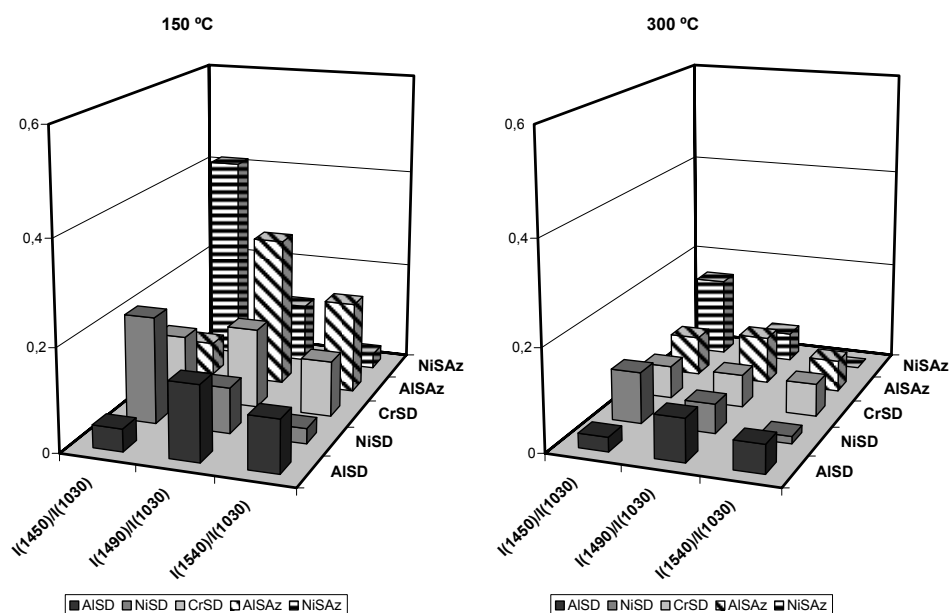
Figure 4.3 Normalised intensities of the 1450, 1490 and 1540 cm^{-1} DRIFTS spectra of AlSD, AlSAz, CrSD, NiSD and NiSAz at A: 150 ºC and B: 300 ºC (reference band: 1030 cm^{-1})

Table 4.2 Quantities of CHA desorbed in the 280 and 440 ºC temperature interval together with the temperature of the maximum in the derivative thermogram

Clay	CHA desorbed / mmol g^{-1}	DTG Maximum / º C
AlSD	1.35	350
CrSD	1.33	350
NiSD	1.21	350
CaSD	1.15	350
NaSD	0.54	350
AlSAz	1.42	320
NiSAz	1.28	360
CaSAz	1.27	310
NaSAz	0.13	350

As expected, NaSAz exhibited a very weak peak at 350ºC (0.13 mmol CHA g^{-1}), but NaSD presented a more intense peak than expected for a Na^{+}-exchanged clay (0.54 mmol CHA g^{-1}). This relatively high amount of CHA desorbed by the NaSD sample concurs with the DRIFTS spectra and is further supported by the catalytic test results. With the exception of the Na^{+} forms, the SD clays generally desorb lower quantities of CHA than the equivalent SAz-1 samples, which correlated well with the difference in CEC between SAz-1 (120 meq 100 g^{-1}) and SD (80 meq 100g^{-1}).

4.3.2 CATALYTIC RESULTS

In the presence of acid or, in this case, acidic centres existing on the clay surface, limonene reacts to form a mixture of products (Scheme 4.1), which were identified and quantified using chromatographic techniques (Figure 4.4). Figure 4.5 uses the catalytic test results obtained over Al-SD, following pre-treatment at 150 °C, to illustrate how the total conversion and the product distribution varied with time. The overall shape of the curves was the same, although differing in time and yield, over clay exchanged with other cations or activated at different temperatures.
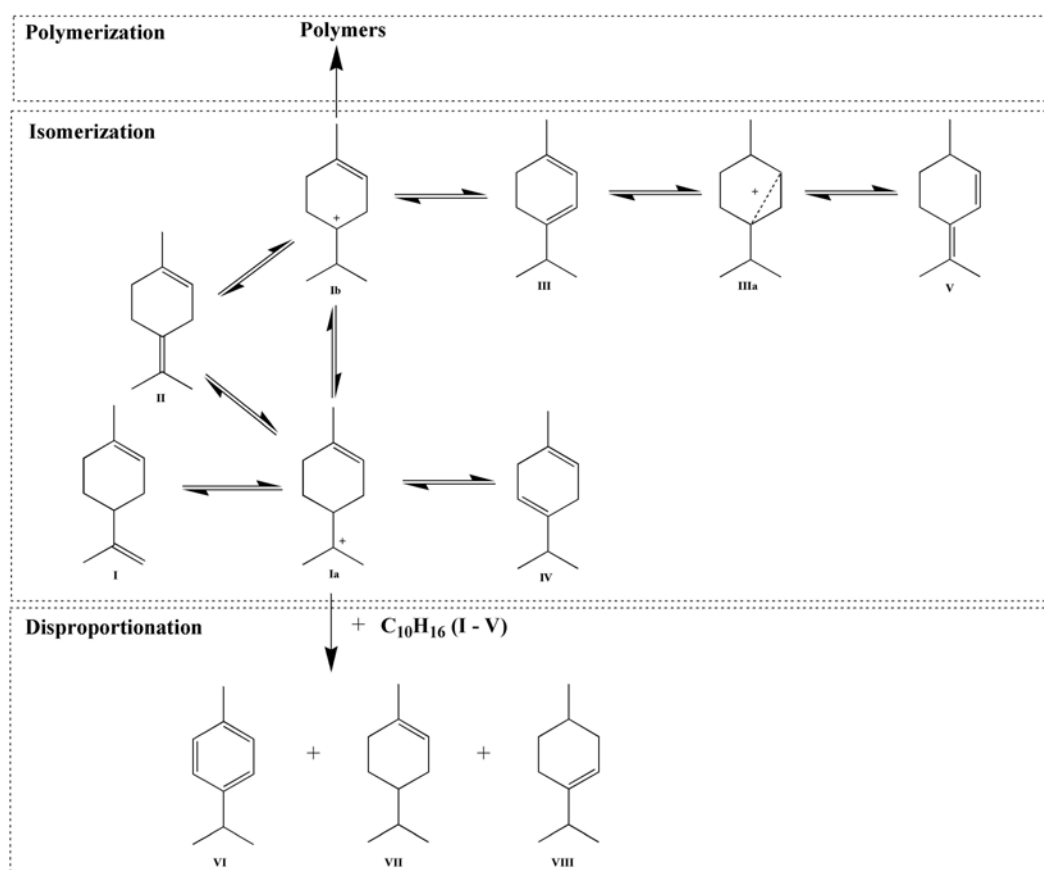
Scheme 4.1 Limonene isomerisation/aromatisation mechanisms I.- Limonene, II- Terpinolene, III-α-Terpinene, IV- γ-Terpinene, V- iso-Terpinolene, VI – p-Cymene, VII-1-p-Menthene, VIII- 3-p-Menthene

Under these reaction conditions, three competitive reactions take place (Figure 4.5): (1) isomerisation, (2) disproportionation to equimolar quantities of p-cymene's and p-menthene's

and (3) polymerisation. Examination of the hydrogen shift reactions reveals that the process could be formally divided into three stages. In the early part of the reaction (stage I) there was a steep decrease in limonene concentration (zero-order kinetics) accompanied by the production of the main reaction intermediates. The initial reaction rates decreased in the order: terpinolene > α-terpinene > γ-terpinene > isoterpinolene. The linear decrease in limonene concentration terminated as the concentration of terpinolene reached a maximum (end of stage I, 70 % limonene conversion), after which the consumption of terpinolene followed zero-order kinetics whereas the concentrations of α-terpinene and γ-terpinene remained essentially constant (stage II). During stage III, which occurred at ≥ 90% limonene conversion, the content of all dienes in the mixture decreased continuously, until their complete disappearance at prolonged reaction time (≥ 10 h). Figure 4.5b presents the distribution of the products arising from a more extensive (than isomerisation) transformation of the p-menthadienes. Clearly, both the disproportionation and polymerisation processes began during stage I but, unlike the isomerisation products which reached a plateau, the yields of p-cymene, menthenes and polymeric species continued to increase throughout stages II and III.
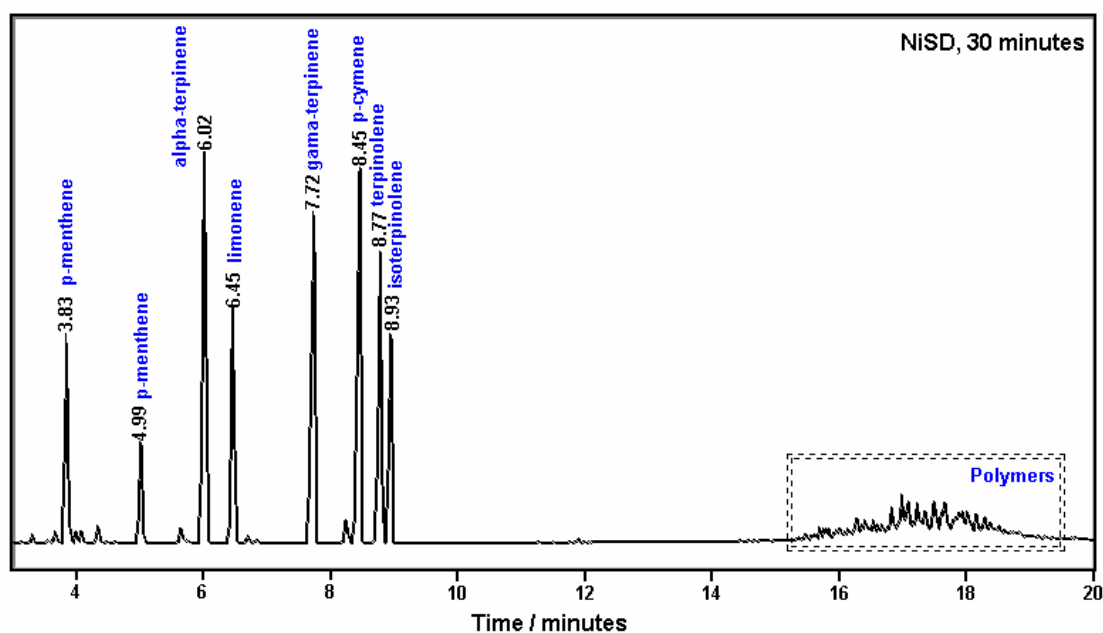
Figure 4.4 Typical chromatogram of a reaction mixture (NiSD, 30 minutes reaction time, fused silica polar capillary column BP21)
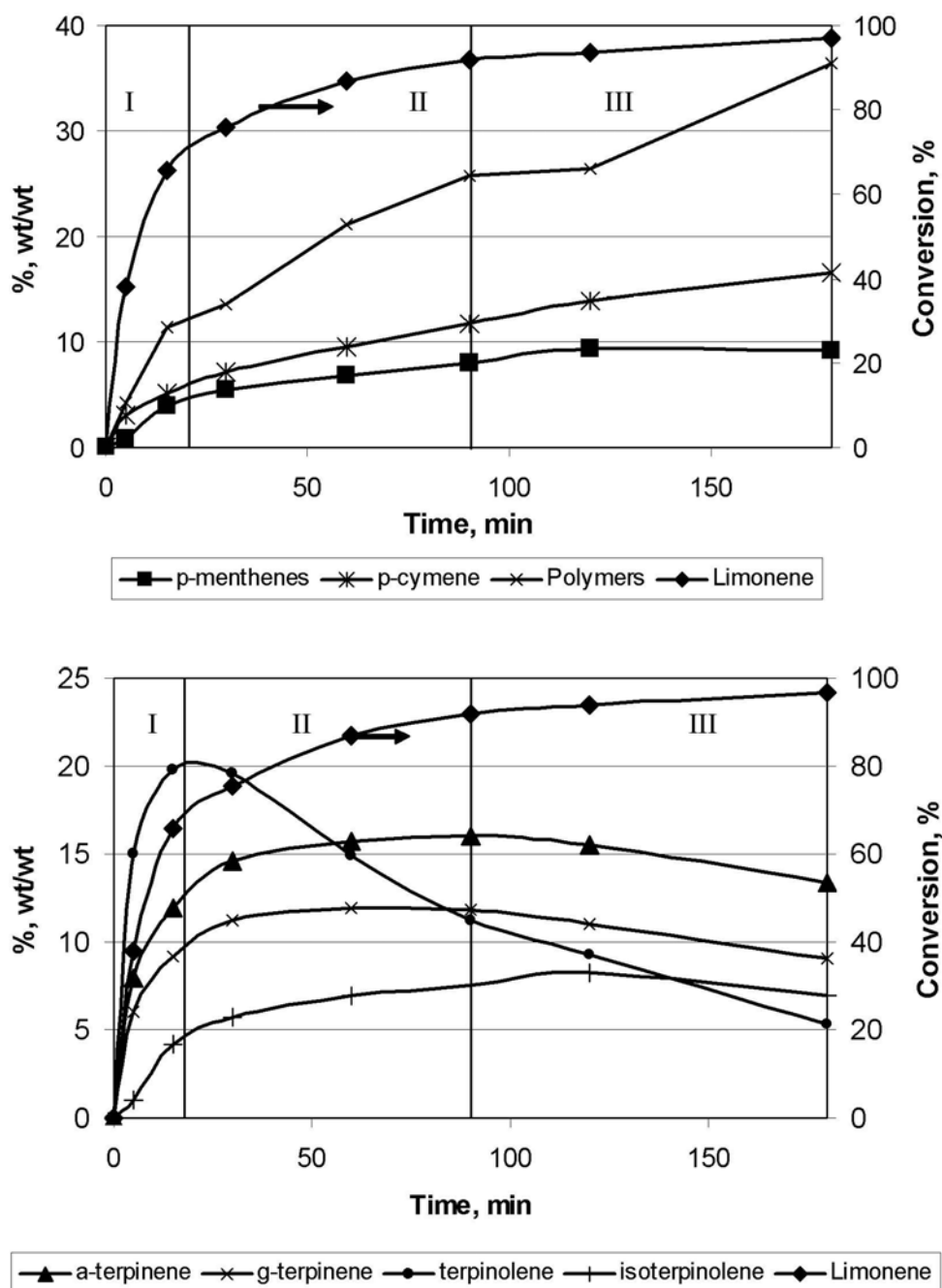
Figure 4.5 Product distribution during the conversion of limonene at a reaction temperature of 150 °C using AlSD. (a) isomerisation products, (b) other products (disproportionation, polymerisation).

The formation of similar amounts of p-cymene and p-menthenes suggested that p-cymene was formed mainly via the disproportionation of hydrogen in the dienes. In the late stages of the reaction, the concentration of p-cymene increased slightly, while the p-menthenes content remained almost constant. This increase in p-cymene/p-menthenes molar ratio could indicate that hydrogen redistribution was taking place between a p-methadiene and a

polymeric species or that the aromatic molecule was produced through an additional oxidation mechanism (on acid Lewis sites). The polymerisation process dominated stage III, as the content of the dienes with conjugated double bonds (α-terpinene and isoterpinolene) reached a maximum. Their condensation, via a Diels-Alder or radical cation processes, led to the formation of high molecular weight products, reaching up to 60 % (wt/wt) at the end of the process.

Figure 4.6, which presents the distribution of products (15 min at 150 ºC) over AlSD pre-treated at different temperatures, reinforces the generally accepted view that the acid character of an Al^{3+}-exchanged montmorillonite is strongly dependent on the thermal activation procedure. The filled diamonds present the limonene conversion values which provide a visual indication of the progress of the reaction (in conjunction with Figure 4.5). The low conversion of limonene over AlSD (hydrated) indicates that the rate over this catalyst was quite slow and thus positions these results in the early part of stage I in Figure 4.5, whereas a limonene conversion of 80% indicates that the reaction over AlSD (250 ºC) had progressed much further during the 15 minute time period and was entering stage II. Hence, the reaction rate over the individual catalysts increased from left to right across Figure 4.6. The deliberately hydrated sample (AlSD (hydrated); Figure 4.6) displayed a very low catalytic activity, suggesting that the acid sites were blocked by water making them inactive towards the reactants. Increasing the pre-treatment temperature to 100 ºC, caused a marked increase in activity, whereas only a slight increase in activity was observed between 100 and 150 ºC. Increasing the thermal activation temperature above 150 ºC, caused a reduction in the Brönsted acidity and an increase in the Lewis acidity in accordance with the model in which the exchange ions become Lewis acidic, as the directly coordinated water is driven off (Figure 4.2C). Therefore, a pre-treatment temperature of 150 ºC was selected to avoid the uncertainty regarding the Brönsted/Lewis acid balance and to take advantage of the reduced amount of polymer production.
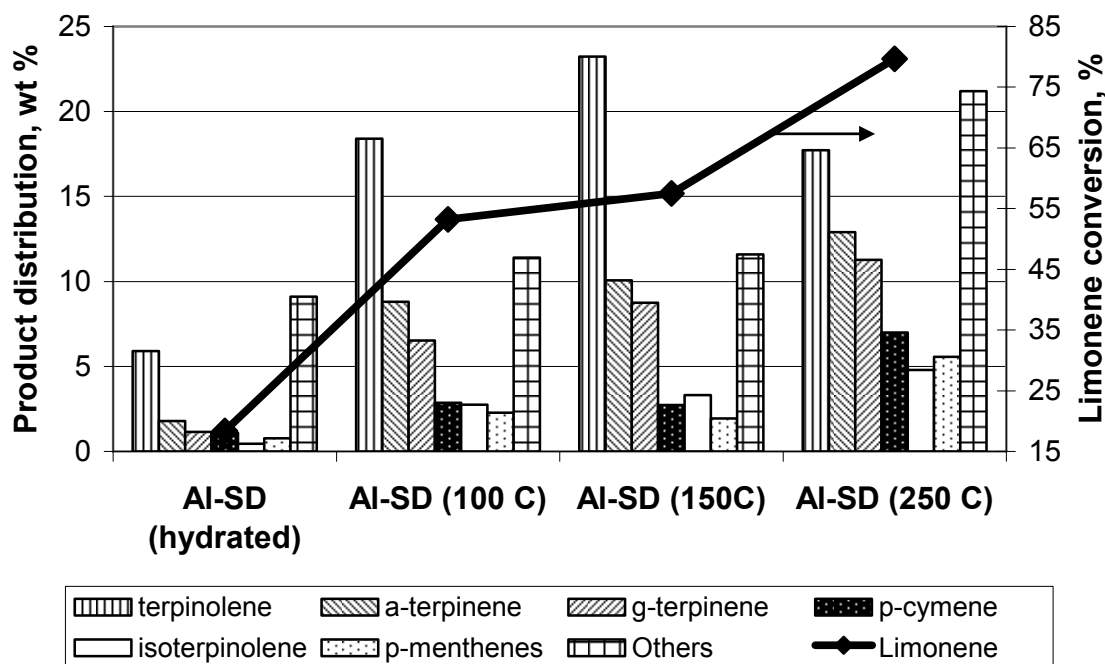
Figure 4.6 Influence of activation temperature on the product distribution over AlSD

Figure 4.7A illustrates the distribution of products obtained over Ni^{2+}-, Al^{3+}- and Cr^{3+}-exchanged SD in comparison with the benchmark (nominally inactive) NaSD after 15 min reaction at 150 ºC. The low conversion of limonene over NaSD indicated that the rate was quite slow, placing the results in the early part of stage I (Figure 4.5), whereas the limonene conversion of 70% indicated that the reaction over NiSD had entered stage II. Hence, the reaction rate over the individual catalysts increased from left to right across Figure 4.7A. It is important to note that the polymer yield after 15 min over Al^{3+}-, Cr^{3+}- and Ni^{2+}-exchanged SD did not exceed 12 wt% and the maximum yield of p-cymene, as well as α- and γ-terpinene, was obtained over NiSD.

Figure 4.7B reports the dramatically reduced activity over Al^{3+}- and Ni^{2+}-exchanged SAz-1. Once again, the Ni^{2+}-exchanged form was more active than the Al-form but it produced a significantly higher relative yield of polymeric products. Overall, the rate of limonene conversion over SD and SAz-1 was low compared with that observed over acid-activated SD which produced >90% conversion after 15 minutes at 80 ºC (cf. Chapter 5). The yields of p-cymene were also higher over the acid clays reaching 14% with the optimised acid-activated

SD. However, the yield of polymeric species was also greatly enhanced when the acid treated clays were used, reaching 50% of the total conversion. In general, the cation-exchanged forms of SD used here produced yields comparable with mildly acid activated SD, but offer the advantage of significant reductions in the production of polymeric species and therefore a cleaner product liquor.
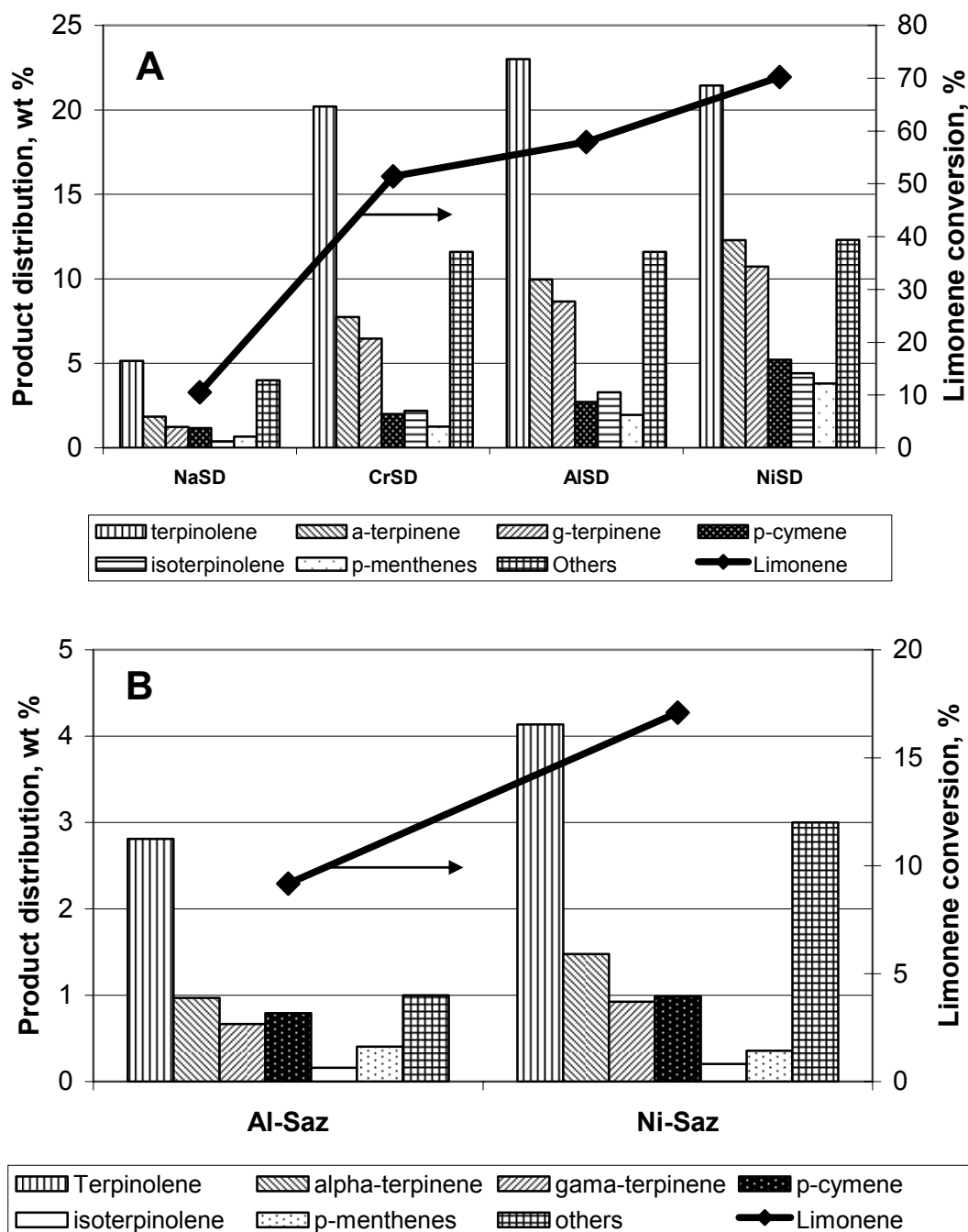
Figure 4.7 The influence of the exchange cation on limonene conversion and product distribution for A. SD and B. SAz derived catalysts

Catalytic activities over clays, whether they arise from Brönsted or Lewis acidity, generally correlate with the exchange capacity of the base clay, provided the reactant can enter the gallery. Consequently, it is reasonable to anticipate that SAz-1 would provide more acid sites than similarly exchanged SD samples, although a valid counter argument would identify the potential lack of space to accommodate the limonene in the gallery of SAz-1 due to the greater density of exchange cations required to compensate the higher exchange capacity of SAz-1. Thus, the extremely low activities reported for Ni^{2+}- and Al^{3+}-exchanged SAz-1 in Figure 4.7B indicate that, although the SAz-1 clays should have a higher acidity than the SD clays, only a very small fraction of these sites was accessible to the reactant, limonene. A realistic rationalisation of this observation is that only the sites located at the periphery of the gallery or on the external surface of the clay are accessible to the non clay-swelling reactant whilst the interlamellar regions would be more readily accessed by more polar species capable of entering the gallery.

The much enhanced activity of the SD derived catalysts may result from their high surface areas, which approach 130 $m^2.g^{-1}$. Moreover, the acidity and the catalytic activity displayed by Na^+-exchanged SD suggest that non-exchangeable acid sites (defect sites or edge sites) on SD are more active than those on SAz, and could play an important role in the sequence of catalytic events. It is also possible that the high iron content of SD provides the opportunity for electron transfer reactions, which may contribute to the overall activity.

Although these results support the fact that accessibility to the active site is an important feature for reactions involving non-polar reagents, the nature of the catalyst's acidity should also be considered to arrive at a more detailed understanding of the process. The evolution of the reaction products in time (Figure 4.5) is typical for acid catalysts and was comparable to results reported for several liquid and solid acids (silica and acid forms of ion-exchange resins) (Thomas and Bessiere, 1989). The transformation of limonene (and other terpenes) is usually attributed to Brönsted sites, which protonate the unsaturated molecule, thus initiating

a network of reactions (Scheme 4.1), including dehydrogenation and polymerisation. Weyrich *et al.* (1997[a]) studied the conversion of limonene at 200-300 ºC, over acidic H-ZSM-5 and USY zeolites. They identified the same reaction products, pointing out that, for acidic catalysts, many side and consecutive reactions occur, forming Diels-Alder products, polymers and coke. Furthermore, the presence of strong acid sites was considered critical for the formation of the aromatic moiety. Frenkel and Heller-Kallai (1983) have reported similar trends over H^+- and Al^{3+} - exchanged montmorillonite from Makhtesh Ramon (Israel). However, these authors only provided a simplified picture of the process, considering the sum of all menthadienes instead of the individual isomers and seemingly underestimating the extent of the polymerisation process. Although no information regarding the thermal activation procedure for the ion-exchanged clays was given, and the acidity was evaluated using Hammett indicators, some trends could be discerned. Thus, as the surface acidity increased, (i) the rate of limonene consumption increased and (ii) the concentration of isomerisation and disproportionation products reached a maximum after shorter reaction times.

There is evidence (Crockett and Roduner, 1994) that the conversion of some terpenes (α-pinene, trans-isolimonene and α-terpinene) over zeolites may not be catalysed by Brönsted acid sites. These authors used deuterated mordenite as the catalyst but were unable to find any deuterium incorporated in the starting terpene leading them to suggest that the rearrangements occurred over Lewis acid sites. Moreover, electron paramagnetic resonance (EPR) studies, have shown that the incorporation of the three terpenes (listed above) in mordenite give rise to the same radical cation, i.e. that of α-terpinene. Thus, a Lewis acid site could behave as an "electron hole" and accept one electron from the electron-rich terpene, giving rise to the corresponding radical cation, which undergoes further conversion to the more stable α-terpinene radical cation. Furthermore, de Stefanis *et al.* (1995) have also shown that α-pinene and limonene are readily converted over zeolites and PILCs, under Lewis acid conditions, with USY exhibiting a high selectivity (>40 %) towards p-cymene, the

oxidation product of limonene. This suggestion of Lewis acid catalyst prompted a study to consider the evidence for and evaluate the possibility that the selectivity towards p-cymene could be enhanced by using clays with Lewis acid character.

The product distribution for SD clays (Figure 4.7A), exchanged with Al^{3+}, Ni^{2+}, Cr^{3+} and Na^+, show that the conversion decreased as $Ni^{2+} > Al^{3+} > Cr^{3+} > Na^+$. This trend, which was also observed for the SAz based catalysts (Figure 4.7B), is different to that observed in Brönsted acid catalysed reactions, where ions with a high charge-to-radius ratio (Al = 0.021) are more active that those with lower ratios (e.g., Ni = 0.016). It has been previously demonstrated (Breen, 1991[a]) and further confirmed by the VT-DRIFTS data presented here (Figure 4.2) that Al^{3+}-exchanged clays, activated between 120 and 150 ºC, display a high concentration of Brönsted acid sites, and are often considered to be model Brönsted catalysts. This is due to the high polarisation of water molecules in the primary coordination sphere of the small, highly polarising Al^{3+} cations which results in the generation of acidic protons. However, it is important to note that a significant number of Lewis acid sites were also present on the surface of AlSD after heating the sample to 200 ºC, as revealed by DRIFTS spectra of adsorbed pyridine (Figure 4.2), although they may not be accessible to limonene. In contrast, Ni^{2+} - exchanged clays exhibit considerable Lewis acid character, even after low–temperature activation. Under these conditions, Ni^{2+} ions on the clay surface retain vacant coordination sites, allowing them to coordinate Lewis bases. More precisely, Velghe *et al.* (1977) found that, after activation at 140 ºC, a portion of the exchangeable Ni^{2+} cations were completely dehydrated and coordinated to three surface oxygens of the tetrahedral sheets. Indeed, Muller *et al.* (1997) have elegantly confirmed, using EXAFS data, that Ni^{2+} exchange cations continue their migration into the clay layer as the pre-treatment temperature increases from 150 to 250 ºC, eventually taking up residence in the vacant cis-octahedra of the 2:1 layers, neutralizing the negative charge on the layer and imparting a charge-neutral, talc-like nature to the product.

The limonene conversion data in Figure 4.6 show that the results for AlSD activated at 100 and 150 ºC were directly comparable whereas the yield over the sample pre-treated at 250 ºC was higher indicating that the conversion over this catalyst, in the same period, was more rapid and the system was in stage II, i.e. beyond the maximum in terpinene yield and into the region where α- and γ-terpinene production levels off and the p-cymene yield gradually increases. This enhanced activity over AlSD (250 ºC), together with the higher yield over NiSD, provide support for the involvement of Lewis acid sites in the production of p-cymene.

Unfortunately, it is difficult to assess whether the Lewis and Brönsted acid sites are situated at the edges of the clay and/or in the gallery because all the probe molecules used are able to enter the gallery and access all the available sites, whereas the partition of limonene and its transformation products, between the edges and the gallery is unknown. Consequently, the variation of p-cymene yield with the extent of limonene conversion was scrutinised. AlSD and NiSD were selected to provide a direct comparison between a Brönsted and Lewis acid functionality. The data in Figure 4.8 clearly illustrates that the gallery cation, and hence the nature of the acidity, exerted little influence on the yield of p-cymene. The amount of p-cymene produced by both cation-exchanged forms at the different limonene conversion values was identical thus testifying to the thermodynamic control of the process. Therefore, while the nature of the exchange cations significantly influenced the reaction rate, the selectivity toward p-cymene was not influenced by the nature of the exchange cation. Consequently, the catalytic activity data collected in this study cannot be used to determine whether Lewis or Brönsted acid sites offer a preferred route to p-cymene.

4.3.2.1 NA-EXCHANGED CLAY

A slightly different catalytic run was performed on NaSD, by prolonging the reaction time (24 h) at a higher temperature (185ºC). In this case, the evolution of the products is similar in the early stages of the reaction, when little disproportionation occurs. In time, the concentration of p-cymene increases, while the quantity of p-menthenes tend to decrease (Figure 4.9).
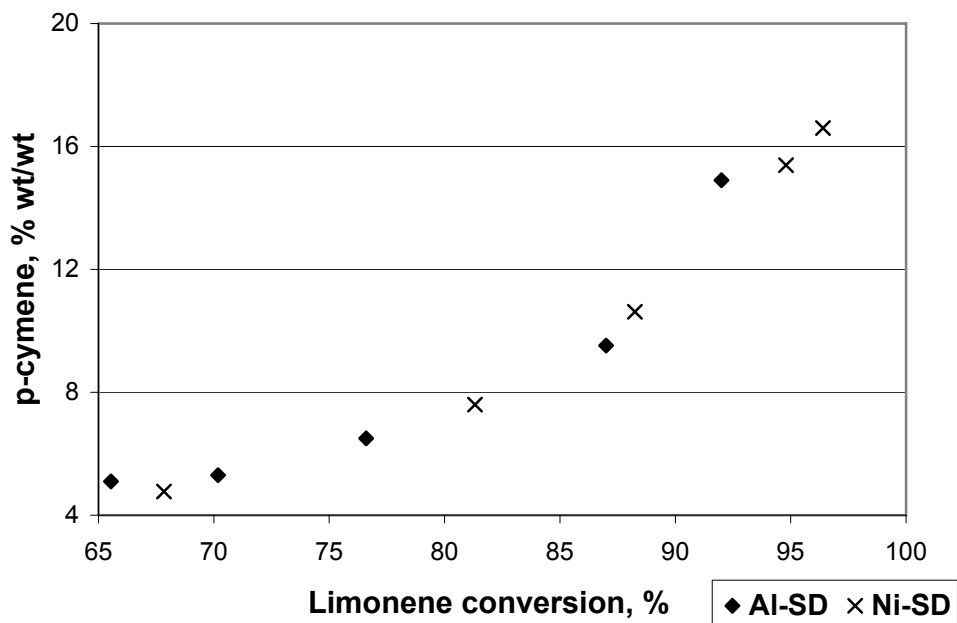
Figure 4.8 p-Cymene content in the final mixture over AlSD and NiSD presented as a function of limonene conversion
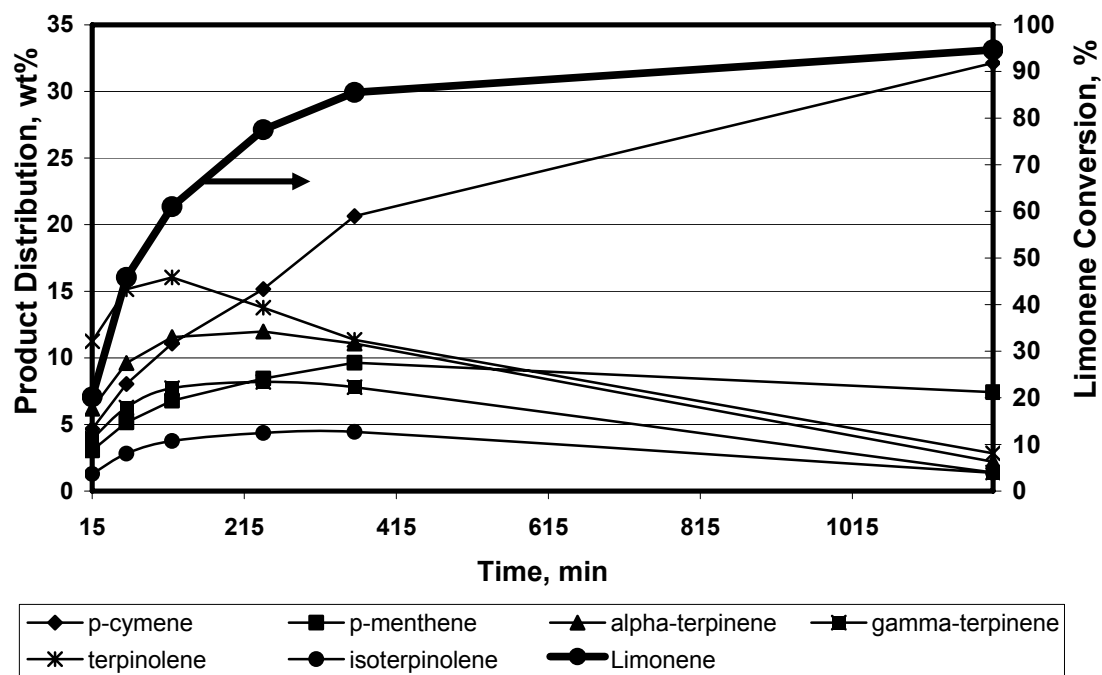
Figure 4.9 Product distribution during the conversion of limonene at a reaction temperature of 185 ºC using 25 mg NaSD and 10 mL limonene

Thus, the most surprising aspect was the formation of a low percentage of $C_{10}H_{18}$ terpenes (reduction products), suggesting that p-cymene in not only formed via disproportionation (hydride transfer process) but through an alternative pathway.

The mechanism for this oxidation process is difficult to establish. One possibility is based on the recent findings (Garcia and Roth, 2002), showing that Lewis acids can accept a single electron from an electron rich molecule of low oxidation potential (e.g., dienes) to generate the corresponding radical cation. Thus, a acid Lewis site could behave as an "electron hole" and accept one electron from the electron-rich α-terpinene, giving rise to the radical cation of α-terpinene. Afterwards, the radical cation dehydrogenates to p-cymene via an allylic radical. This is further supported by an electron paramagnetic resonance (EPR) study (Crockett and Roduner, 1994), that demonstrated the formation of the radical cation of α-terpinene, upon loading some terpenes (α-pinene, trans-isolimonene and α-terpinene) in mordenite. This single electron abstraction process has been confirmed to occur only on Lewis acid sites.

Although the formation of radical cations was only demonstrated for zeolites, we could postulate that a similar process, involving one electron transfer, could occur on some Lewis sites that exist on the external surface of NaSD.

Concerning the acidity of Na-exchanged clays, it is generally believed that this is associated with non-exchangeable sites that exist on the clay surface. They would be defect sites or coordinatively unsaturated edge sites and it is reasonable to suppose that they would be electron-deficient, and therefore behave as Lewis acids after thermal activation. A recent study (Hart and Brown, 2004) confirmed that a Na-exchanged commercial clay (K10) does show some activity in the Lewis acid catalysed Friedel-Crafts reactions. The presence of Lewis acid sites on the surface of Na-SD was also confirmed (cf. Section 4.3.1.1). The small, but discernible peaks present on the VT-DRIFTS of pyridine treated NaSD proved the existence of both Brönsted and Lewis sites, the later being more obvious. Additional characterisation of the acidity by thermal desorption of CHA showed that a significant proportion of the acid sites in SD clay are due to lattice defects, which are not removed when the clay is ion-exchanged with Na^+ ions. Moreover, these sites possess a ring dehydrogenation activity, capable of producing aniline and benzene from CHA (TG-MS studies – cf. following section).

It is also possible that the high iron content of SD provides the opportunity for electron transfer reactions, which may contribute to the overall activity.

4.3.3 THERMOGRAVIMETRY - MASS SPECTROMETRY (TG-MS)

Simple thermogravimetric CHA desorption profiles provide an estimate of the number of acid sites, but they do not reveal the differences in the decomposition pathways that can occur over different materials. Breen *et al.* (2000) showed that real time TG-MS of the decomposition products derived from CHA provides pertinent information regarding the transformation properties of the catalyst. Generally, CHA decomposition can be represented by scheme 2.1 (cf. Chapter 2). Binding to a Brönsted acid site produces protonated CHA. Deamination generates unbound cyclohexene (CH) leaving NH_4^+ ions occupying some of the exchange sites. Successive dehydrogenation reactions result in the subsequent formation of cyclohexadiene (CHD) and then benzene (B). The formation of methylcyclopentene (MCP) cannot be disregarded. The presence of dehydrogenation sites was further confirmed by the appearance of aniline (A), which must arise from the aromatisation of untransformed CHA either in the gallery or as it diffuses out of the sample.

Figure 4.10 illustrates the information obtained from a typical real time mass spectrum for the desorption of CHA from AISD[20]. The total ion count (TIC) is assigned to the left hand axis and the single ion intensities to the hand right axis.

Generally two peaks were present in the TIC profile. The peak at lower temperature (peak I) is attributed to the loss of physisorbed CHA (major component) and water and is not usually associated with clay acidity. Very small amounts of aniline were also released under peak I. The peak at higher temperature (peak II) has been routinely related to the acidity and hence the catalytic activity (Ballantine *et al.*, 1987; Komadel *et al.*, 1997; Breen and Moronta, 2000, 2001). Peak II encompasses the release of a number of decomposition/transformation products together with a little unmodified CHA. CH evolved first followed by CHD and then

---

[20] Selected ion fragments: CHA – m/z 99, A – m/z 93, B – m/z 78, CHD – m/z 77, CH – m/z 54, water - m/z 18 and CO_2 - m/z 44.

benzene at a slightly higher temperature. This delay in the time/temperature of CHD and B desorption may reflect the diffusion of CH to the ring dehydrogenation sites, transformation and then diffusion away from those sites. Significant amounts of aniline and benzene appeared at the same temperature and they both continued to be evolved to much higher temperatures than CH and CHD. Nevertheless, the dehydrogenation of CH to benzene and CHA to aniline occurred in the same, relatively low, temperature interval. This provides some evidence for ring dehydrogenation sites which may contribute to the production of p-cymene. Benzene (and aniline) was also evolved at a higher temperature (peak III) probably from the deamination of aniline, which was released at the same temperature. This will receive further consideration below.
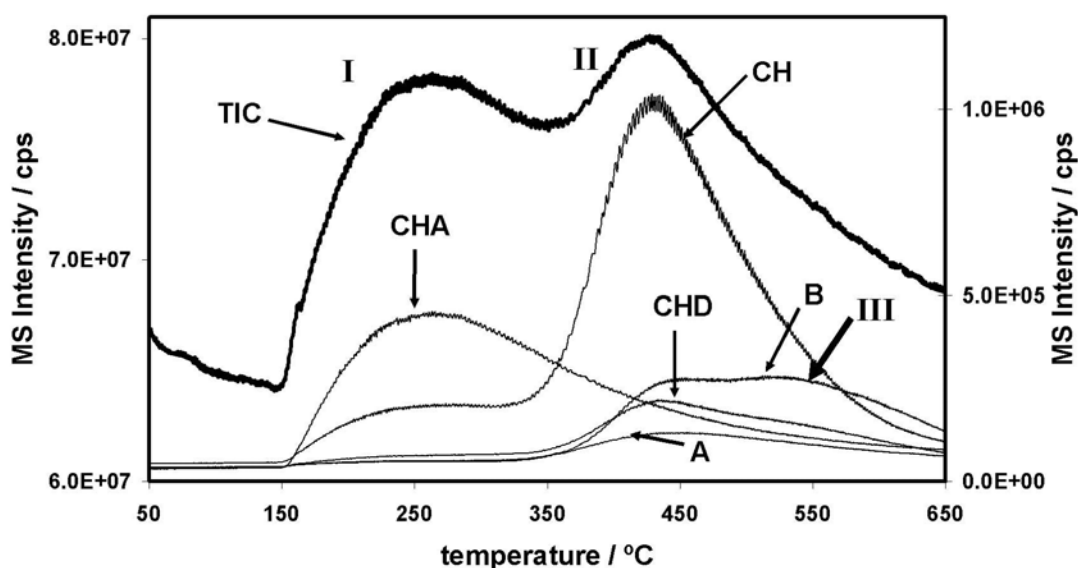
Figure 4.10 Real time MS ion chromatograms for the desorption of CHA (m/z = 99), CH (m/z = 54), CHD (m/z = 77), B (m/z = 78) and aniline (m/z = 93) from AlSD after a 7 day incubation period with CHA[21]

Direct quantification of the amount of products obtained was not possible due to the non linear response to different fragment ions. Nevertheless, a semi-quantitative, empirical method was devised, which used several synthetic mixtures containing appropriate amounts

---

[21] The comparative data presented hereafter could be affected by differences in sample sizing or incubation time. The "normalised" chromatograms (obtained by dividing the MS intensities by the mass of sample remaining after each run, not illustrated) showed that the conclusions presented in this chapter are not affected by the inclusion of this correction factor.

of CHA, CHD, CH, B and A. TG-MS data for the synthetic mixture was obtained under the same conditions as the clay samples. Subsequently, the selected ion data obtained from the CHA saturated clay was compared with the responses of the selected ions obtained from the individual components of the synthetic mixtures. This approach revealed that equal amounts of CHA and CH were produced whereas the amount of benzene and CHD produced was about one fifth that of the CHA released. The amount of aniline produced was very low (about 5% of the amount of CHA released).

The TG-MS data for the Na^+-exchanged samples (Figure 4.11) show that the MS ion intensities for the degradation products were lower than for Al^{3+}- and Ni^{2+}-exchanged counterparts. NaSD released more CH and CHD but also more benzene and aniline than SAz, suggesting the presence of more ring dehydrogenation sites on SD than on SAz. Since acidity alone in not sufficient for the clay to act as a dehydrogenation catalyst, the structural iron (and perhaps other transition metals) could provide SD with more inherent dehydrogenation activity.

The quantities of the different degradation products desorbed from AlSD and AlSAz were very dissimilar (Figure 4.12). Considerably more CH emerged from AlSAz than from AlSD and AlSD clearly generated much more benzene and aniline than AlSAz. CH is generated directly from the rupture of the N-C bond in CHA. Then CH is transformed into CHD over ring dehydrogenation (oxidation) sites followed by further dehydrogenation to benzene which emerges under peak II. The greater dehydrogenation activity of AlSD is supported by the enhanced production of aniline over AlSD compared to AlSAz. Of course, it is also conceivable that a small number of dehydrogenation sites with a high turnover number would provide a similar result, but the current data set is unable to distinguish between these alternate interpretations. In particular, it is important to note that aniline was produced under peak II and peak III. Aniline is produced via ring dehydrogenation of cyclohexylamine but it is not clear whether the aniline was released immediately upon its formation or whether, once

formed, it is retained to higher temperature and then released. Intuitively, the latter seems more likely particularly as the galleries would have collapsed by these temperatures and the aniline was probably trapped in the space produced by adjacent ditrigonal cavities in the siloxane surface. The benzene produced under peak III was considered to arise from the deamination of a portion of the trapped aniline.
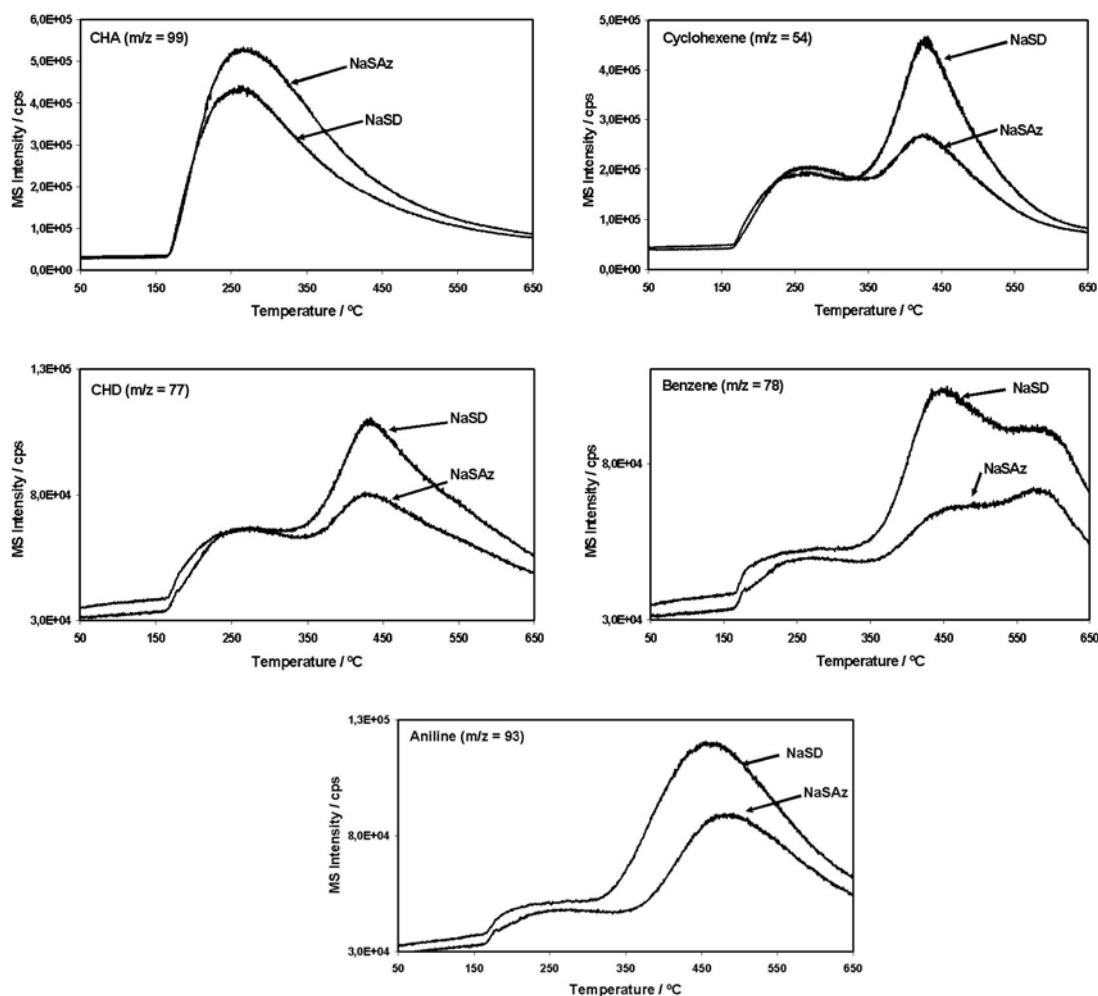
Figure 4.11 Comparative MS ion chromatograms for NaSD and NaSAz

The evolution of CH and CHD from the homoionic Ni^{2+}-clays (Figures 4.13 & 4.14) followed similar trends to those for the Al-exchanged counterparts (Figure 4.12) except that similar amounts of benzene were formed over NiSD and NiSAz. It is unclear why Ni^{2+}-saturation should work in opposite directions on SAz and SD.
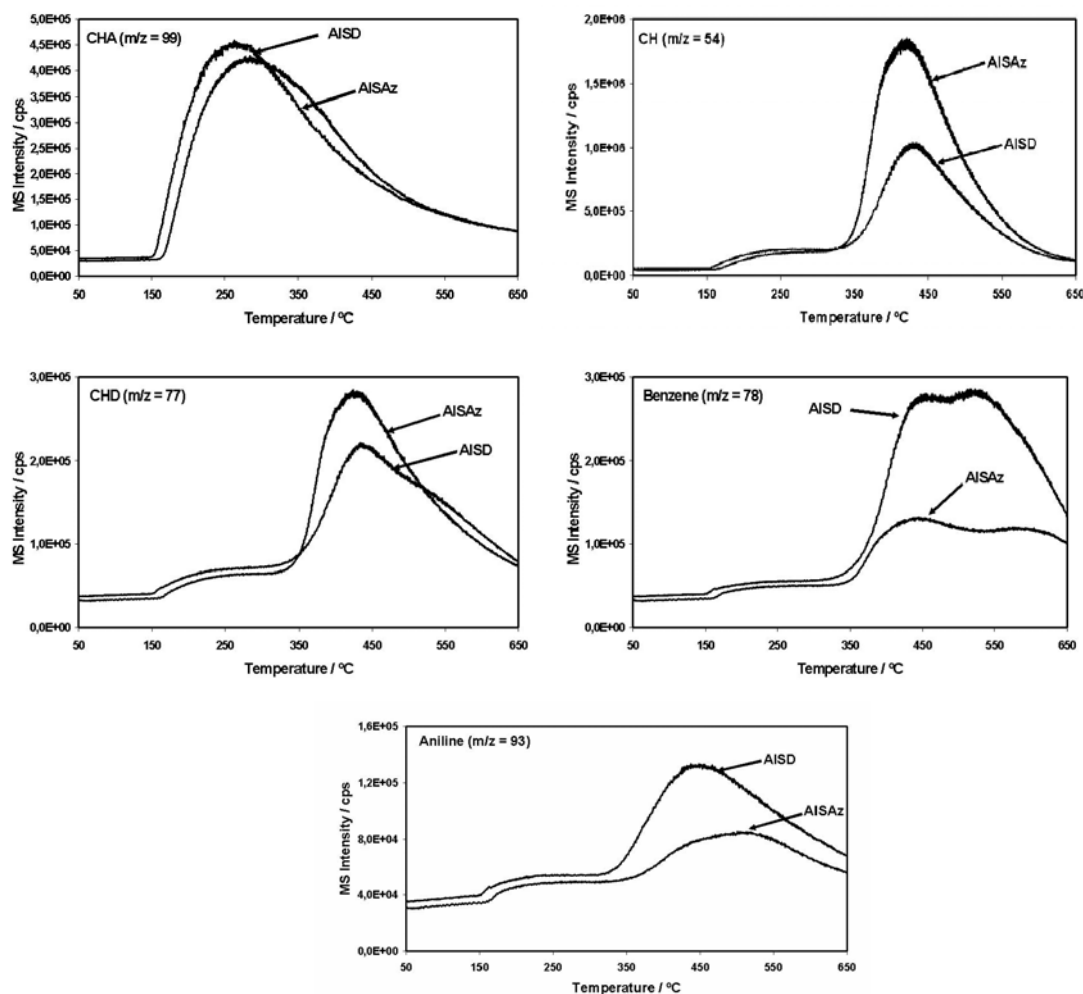
Figure 4.12 Comparative MS ion chromatograms for AlSD and AlSAz

Comparison of the MS ion chromatograms for the desorption of CHA from homoionic SAz (Figure 4.13) shows that AlSAz produced more CH and CHD than NiSAz and about 10 times more than NaSAz, which agrees with the higher number of Brönsted sites present on AlSAz. However, NiSAz produced more benzene and aniline than AlSAz.

The TG-MS data provides considerable support for there being a larger number of inherently active sites, including ring dehydrogenation sites, on SD than on SAz. Subsequent modification of the two clays by ion exchange does not remove this difference but the nature of the exchange cation does alter the detailed balance between the transformation products generated by the clays. However, the transformation products are identical despite the

significant differences in the nature of the acidity on the Al^{3+}- and Ni^{2+}-exchanged clays. It is interesting to note that NiSAz produced more benzene and aniline than its Al^{3+}-exchanged counterpart which may help to explain why NiSAz was more active than AlSAz for limonene conversion. The apparent contradiction in that AlSD produces more benzene than NiSD can be explained by the fact that the sum of the amounts of benzene and aniline produced was very similar and the increased benzene production over AlSD represents a more extensive Hofmann deamination of the trapped aniline in AlSD than in NiSD. This could explain why the Al^{3+}- and Ni^{2+}-exchanged forms of SD have similar activities in the transformation of limonene.
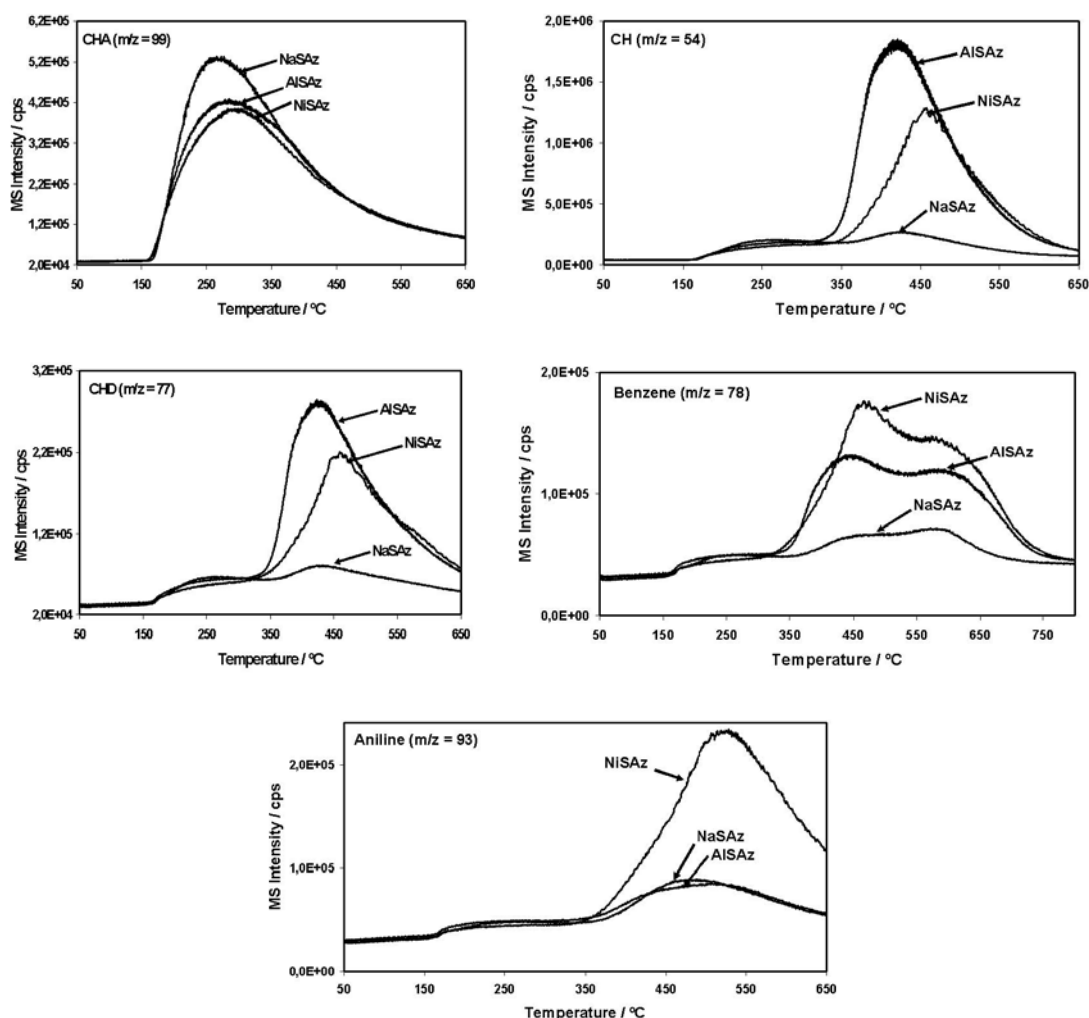
Figure 4.13 Comparative MS ion chromatograms for metal exchanged SAz clays
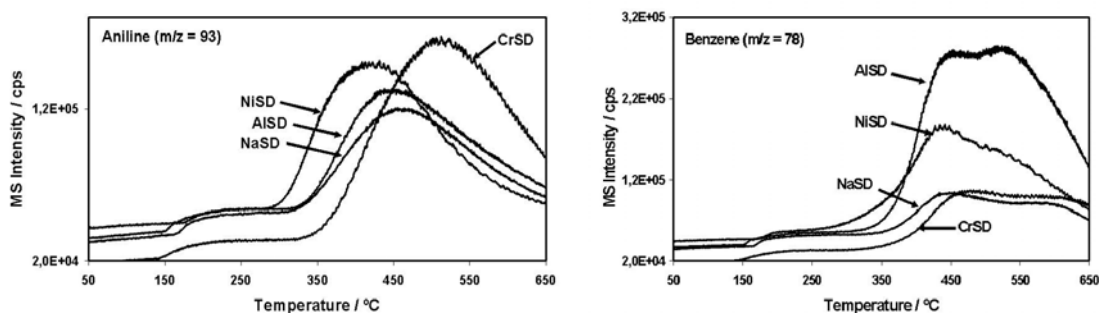
Figure 4.14 Comparative MS ion chromatograms for benzene and aniline production over metal exchanged SD clay

4.4 FINAL COMMENTS

The ion exchange procedures were successful and the materials obtained exhibited the desired Brönsted and/or Lewis acidic properties. The number of acid sites, determined by CHA desorption data, reflect the CEC of the two parent materials and the acidic strength of the exchangeable cations, with the noticeable exception of NaSD. Surprisingly, the acidity value obtained for NaSD is higher than anticipated; however the result is consistent with the catalytic test results and the infrared data.

Three competitive reactions occur during limonene conversion over the clay catalysts: isomerisation, disproportionation and polymerisation and three stages were identified during the conversion process: I – steep decrease of limonene concentration and production of the main reaction intermediates; II – sharp consumption of terpinolene and stabilisation of the amounts of α- and γ-terpinene and III – continuous decrease of the content in all dienes until their complete removal. The content of disproportionation and polymeric species increases throughout all stages.

The conversion of limonene to p-cymene over M^{n+}-SD decreased in the order Ni > Al > Cr > Na but, while this trend continued with NiSAz being more active than AlSAz, the overall activity over catalysts derived from SAz was significantly lower than over the SD counterparts. The relative inactivity of the SAz-based catalysts was attributed to the

inaccessibility of the active sites on SAz and a greater inherent activity of SD, which also has a greater nitrogen surface area. No evidence was found to support the possibility that the ratio of the amount of p-cymene produced to the extent of limonene converted was influenced by the nature (Lewis/Brönsted) of the acid sites.

The rate of production of polymeric side products over the cation-exchanged clay catalysts, which retain their lamellar character, appears to be less than that when using acid-activated clays in which the lamellar nature has been severely disrupted (cf. Chapter 5).

Mass spectral analysis of the transformation products released from the cyclohexylamine treated catalysts provided evidence that SD offered more inherent active sites than SAz. In particular the ring dehydrogenation activity over the SD derived catalysts was greater than that over those derived from SAz.

The information presented in this chapter was published under the following references:

− Catrinescu, C., Fernandes, C., Castilho, P. and Breen, C. (2006) Influence of exchange cations on the catalytic conversion of limonene over Serra de Dentro (SD) and SAz-1 clays: Correlations between acidity and catalytic activity/selectivity. *Appl. Catal. A Gen.*, **311**, 172-184.

− Catrinescu, C., Fernandes, C., Castilho, P., Breen, C. and Carrott, M. R. (2006) Porto Santo clays as environmentally friendly catalysts for the conversion of renewable limonene feedstocks. Limonene aromatisation to p-cymene. *Environ. Eng. Management J.*, **5**(3), 275-284.

CHAPTER 5. ACID ACTIVATED CLAYS

5. ACID ACTIVATED CLAYS

5.1 INTRODUCTION

In this chapter the characterisation data of the Serra de Dentro acid activated derivatives is presented, including the activity and selectivity towards the aromatisation of limonene to p-cymene.

Acid activation of montmorillonite, the main component of interest in bentonite ores, is frequently used for both scientific and industrial purposes and the products were used for the cracking of hydrocarbons (Houdry process) until their replacement by the more active and selective zeolites in the 1960s. The current drive to establish environmentally friendly technologies means that clay minerals, in general, and acid activated clays, in particular, are experiencing an increased interest with regard to their properties as catalysts for industrially important processes such as isomerisation or Friedel-Crafts alkylation (Vaccari, 1998).

As mentioned before, acid treatment of clays results in two major outcomes: the substitution of the exchangeable cations by protons and the dissolution of metals ions from the clay structure, by depopulating the octahedral sheet (cf. Figure 1.6). The rate of depletion is higher in materials with important amounts of iron and/or magnesium in the octahedral sheet. The choice between mild or harsh acid treatment depends on the specific reaction to be catalysed. Polar reactants, which can access the active sites in the interlayer region, are better catalysed by mildly activated clays, whereas non polar molecules require severely depleted clays, with important exposed surface areas.

5.2 EXPERIMENTAL

Acid Activated (AA) samples were prepared by mixing 10g of NaSD with 300 cm^3 aliquots of aqueous HCl (with selected concentrations) at 25ºC or 95ºC, for different periods of time. The samples were then diluted with a large quantity of cold water to effectively terminate the leaching process, centrifuged and washed successively until a stable pH was achieved. The samples were air-dried for 24 h. Samples are labelled as follows: acid concentration – temperature of activation – contact time in minutes. For example, SD-6M-25-120 is the material obtained when a 10g sample of NaSD was treated with 6M HCl at 25ºC, for 120 minutes. The same procedures were applied to SAz-1.

XRD, XRF, thermal desorption of cyclohexylamine (CHA) followed by evolved gas analysis by mass spectrometry, IR spectroscopy and BET surface area analysis were used to evaluate the properties of the prepared catalysts.

5.3 RESULTS AND DISCUSSION

5.3.1 CHARACTERISATION OF ACID ACTIVATED SAMPLES

5.3.1.1 XRF ANALYSIS

XRF data obtained for the solid products, reported as metal/Si ratios, as a function of contact time and acid concentration are presented in Figures 5.1 and 5.2. Si is known to be only marginally depleted by acid attack (Mills *et al.*, 1950; Novak and Gregor, 1969; Breen *et al.*, 1997[a]) and was thus chosen as an internal reference. As expected, longer contact times (Figure 5.1) and higher acid concentrations (Figure 5.2), caused more extensive metal depletion with Fe and Mg being removed at a initial faster rate than Al, which is probably related to the presence of non structural Fe and Mg phases[22].

---

[22] Cf. Chapter 3 for a discussion on the probable presence of non structural iron.
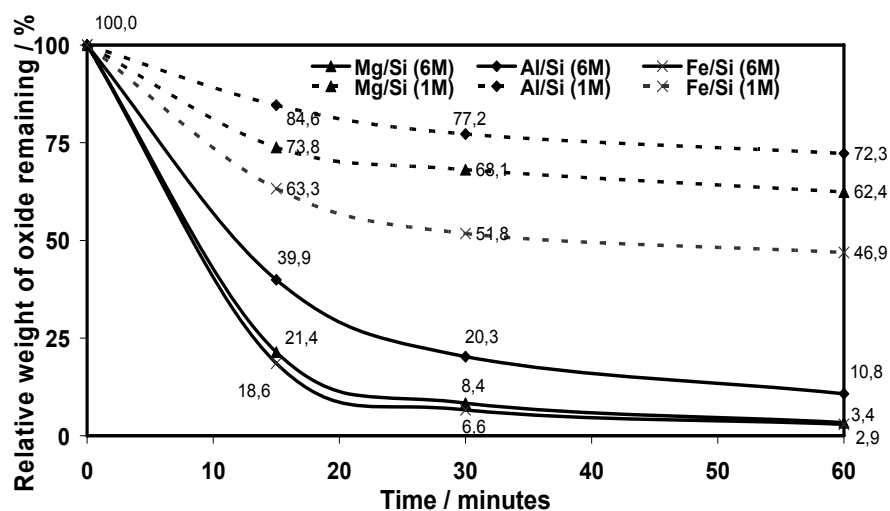
Figure 5.1 Relative weight % of Al, Mg and Fe oxides remaining after acid treatments at 95ºC (full line: 6 M series; dotted line: 1M series)
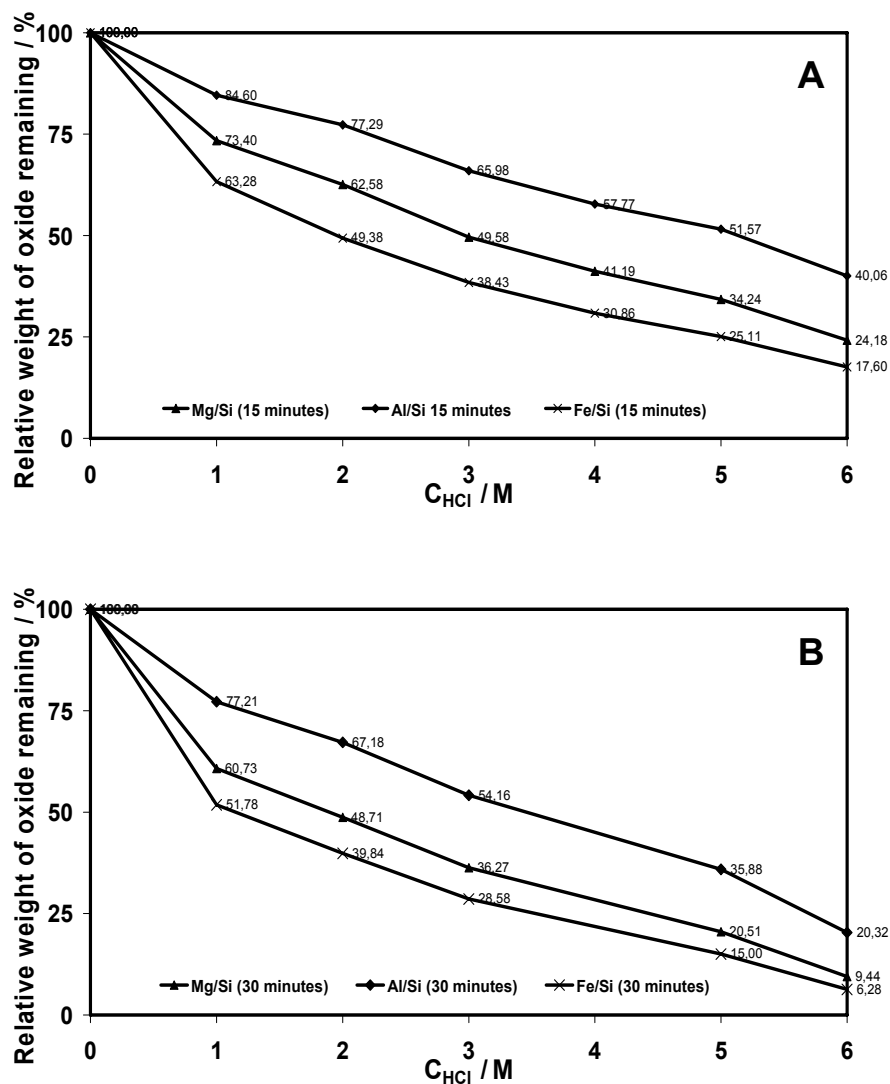
Figure 5.2 Relative weight % of Al, Mg and Fe oxides remaining after acid treatments at 95ºC with HCl solutions of different concentration during A:15 minutes and B: 30 minutes

The chemical composition data of the materials acid treated at 25 ºC (not illustrated) proved that virtually no metal depletion occurred in these materials, even after contact with 6M HCl solutions for 2 hours. Furthermore, even the sample produced by the most severe treatment (SD-6M-95-60, Figure 5.1) retained detectable quantities of the octahedral cations (10.8, 3.4 and 2.9% of the initial Al/Si, Mg/Si and Fe/Si ratios, respectively), which suggests that some portion of the clay structure was retained. XRD and IR spectroscopic data confirmed this supposition (cf. sections 5.3.1.2 and 5.3.1.3).

5.3.1.2 XRD ANALYSIS

The XRD traces of the catalysts prepared by mixing Na-SD with HCl solutions of different concentrations, at 25 ºC or 95 ºC, during different contact times are displayed in Figures 5.3-5.5.

It can be visualised (Figures 5.3 and 5.4, traces A and B) that room temperature acid treatments cause negligible structural alterations on the clay structure, even when concentrated HCl solutions were used. As expected, the contact with acid solutions in these mild temperature conditions promotes the exchange of the interlayer metal cations by the protons from the acid and the chemical washing of the clay in terms of removal of certain admixtures (namely calcite and non structural iron oxides), depleting little or none of the structural metal ions. With the increased treatment temperature (Figures 5.3 and 5.4, traces C, D and E), major changes in the clay structure are detectable, especially when the more concentrated acid solution is used (Figure 5.4). The 001 (ca. 6.5º 2θ), 110, 020 (at 19.7º 2θ) and 060 (ca. 62.5º 2θ) peaks decrease in intensity, which is directly related to the depletion of the octahedral sheets of the clay minerals.
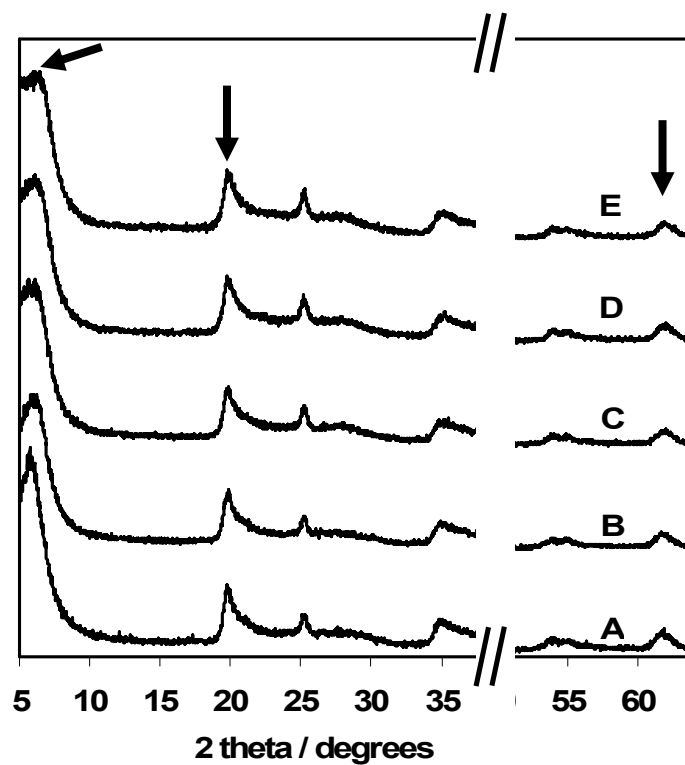
Figure 5.3 XRD traces of SD treated with 1M HCl solutions at 25 ºC during A: 60 minutes and B: 120 minutes and at 95 ºC during C: 15 minutes, D: 30 minutes and E: 60 minutes
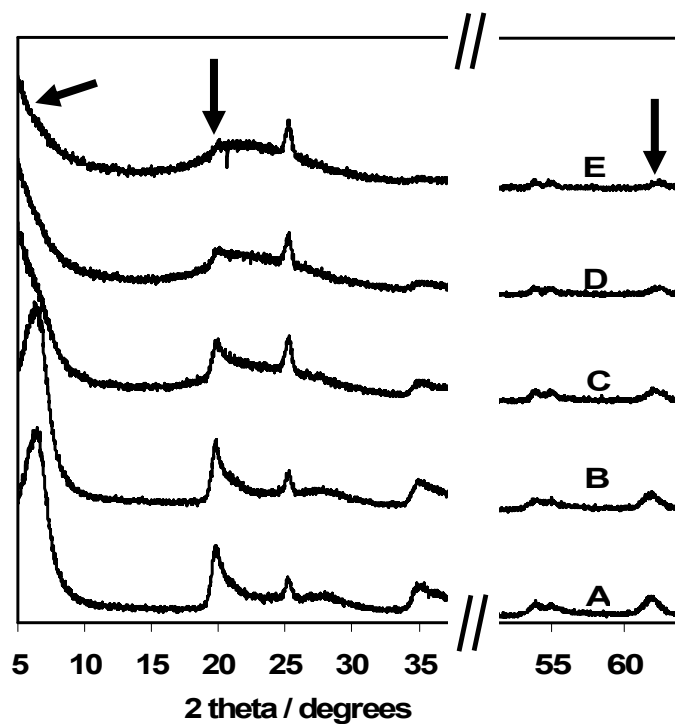
Figure 5.4 XRD traces of SD treated with 6M HCl solutions at 25 ºC during A: 60 minutes and B: 120 minutes and at 95 ºC during C: 15 minutes, D: 30 minutes and E: 60 minutes

Besides temperature, the concentration of the acid solution also plays a very important role on the degree of structural disruption of the clay minerals present in NaSD. The traces of the materials treated with acid solutions of increasing concentration displayed a regular decrease in intensity of the 001, (110, 020) and 060 peaks (Figure 5.5).
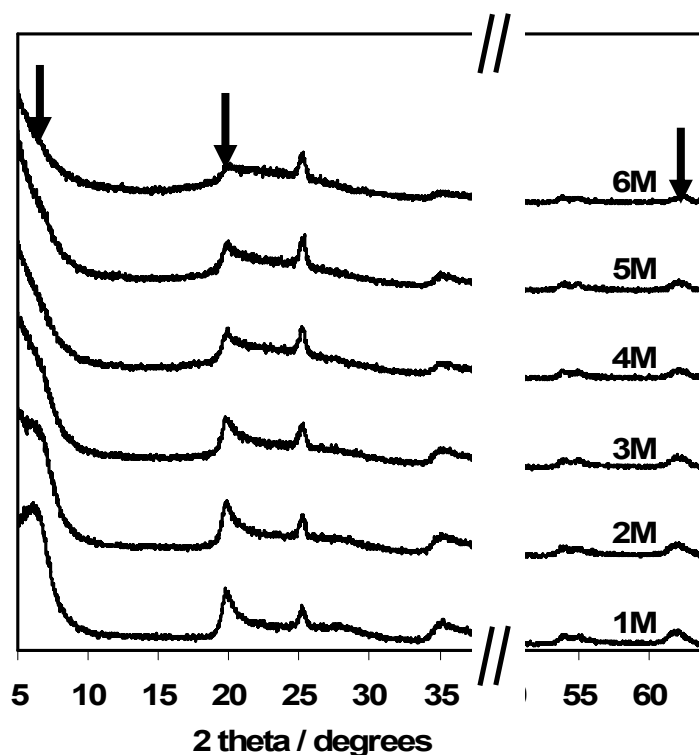
Figure 5.5 XRD traces of SD treated for 30 minutes at 95 °C with xM HCl solutions (x=1-6) [23]

The data revealed that even for the most harshly treated sample (SD-6M-95-60, Figure 5.4, trace E) some evidence for the presence of the 001, 110, 020 and 060 peaks remained, proving the incomplete destruction of the clay structure, which is consistent with the chemical composition data referred to previously (cf. Section 5.3.1.1).

5.3.1.3 INFRARED SPECTRA ANALYSIS

The most obvious effects of the acid attack on the FTIR spectra of acid activated SD bentonite (Figures 5.6-5.8) were the changes in position and shape of the main band at ca.

---

[23] Samples treated in the same conditions during 15 minutes (not illustrated) exhibited a less pronounced, yet similar behaviour.

1035 cm^{-1} and the reduction in intensity of the 526 cm^{-1} band. With increasing severity of acid treatment the 1035 cm^{-1} band shifted to higher wavenumbers and a band at ca. 1100 cm^{-1}, attributed to the Si-O vibrations of three-dimensional amorphous silica (Madejová *et al.*, 1998), increased in intensity. The other diagnostic band for amorphous silica appeared at 800 cm^{-1} and progressively grew in intensity, whereas the bands characteristic of the octahedral population (920, 878 and 839 cm^{-1} for Al$_2$OH, FeAlOH and MgAlOH, respectively) progressively decreased in intensity, which is consistent with the gradual removal of these metals. Moreover, the intensity of the 526 cm^{-1} (AlOSi) band, which reports the linkage between the tetrahedral and octahedral layers also decreased. Finally, a band at *ca.* 937 cm^{-1}, attributed to the bending vibrations of OH groups linked to amorphous silica, increased in intensity.

The severity of these structural changes is influenced by the acid concentration, temperature and contact time. Figures 5.6 and 5.7 highlight the influence of temperature and acid contact time. The spectra of the samples prepared at 25 ºC (Figures 5.6A and 5.7A) are perfect copies of the parent material, regardless of the concentration of the acidic solution used. On the other hand, when the bentonite was treated at 95 ºC, important structural changes occur, even when using 1M HCl solution, for a short period (Figure 5.6B). This fast octahedral depletion rate is related to the presence of substantial amounts of iron in the octahedral sheet of SD; it has been shown that octahedral Fe and Mg rich bentonites are leached more readily than those containing a higher proportion of octahedral aluminium (Osthaus, 1955; Novak and Gregor, 1969; Novák and Čičel, 1978; Janek and Komadel, 1993; Vicente *et al.*, 1994; Komadel *et al.*, 1996; Breen *et al.*, 1995[a,b], 1997[a]). SD.6M.95.60 (Figure 5.7D), although heavily delaminated, still retains some clay character, as proved by the incomplete disappearance of the 525 cm^{-1} band, indicative of the presence of octahedral aluminium.
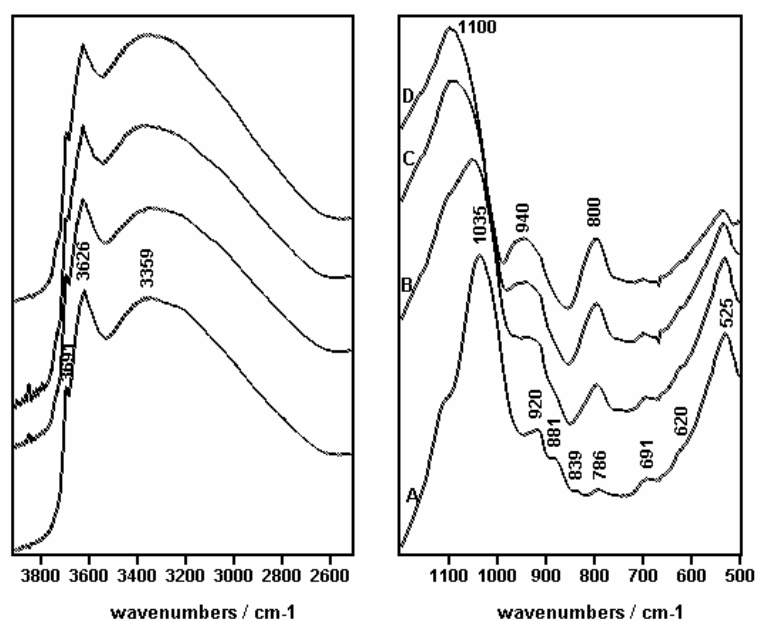
Figure 5.6 FTIR spectra of A:SD-1M-25-60, B:SD-1M-95-15, C:SD-1M-95-30 and D:SD-1M-95-60
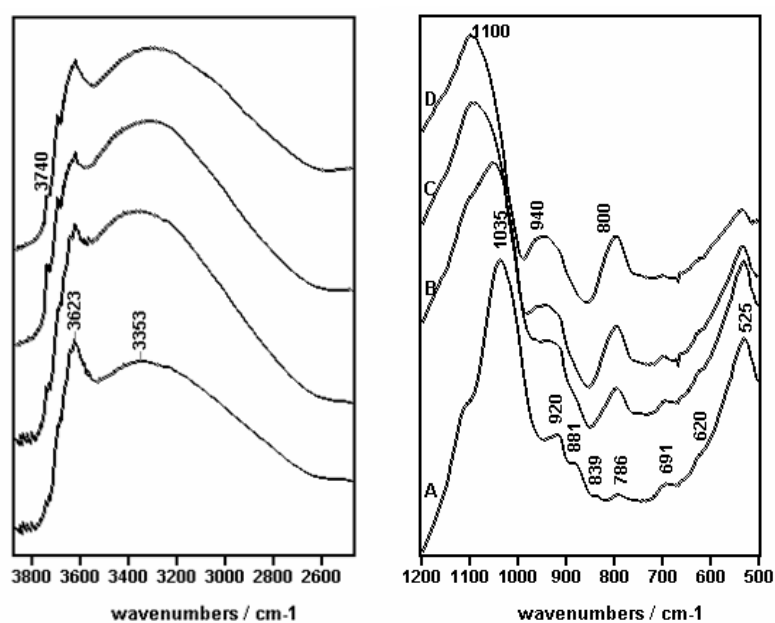
Figure 5.7 FTIR spectra of A:SD-6M-25-60, B:SD-6M-95-15, C:SD-6M-95-30 and D:SD-6M-95-60

Figure 5.8 highlights the structural transformations that occur on the clay structure as a function of the concentration of the acidic solution. The milder acid treatment does not significantly alter the clay structure, whereas the contact with 6M HCl solution significantly depletes the octahedral sheets of the SD clay minerals.
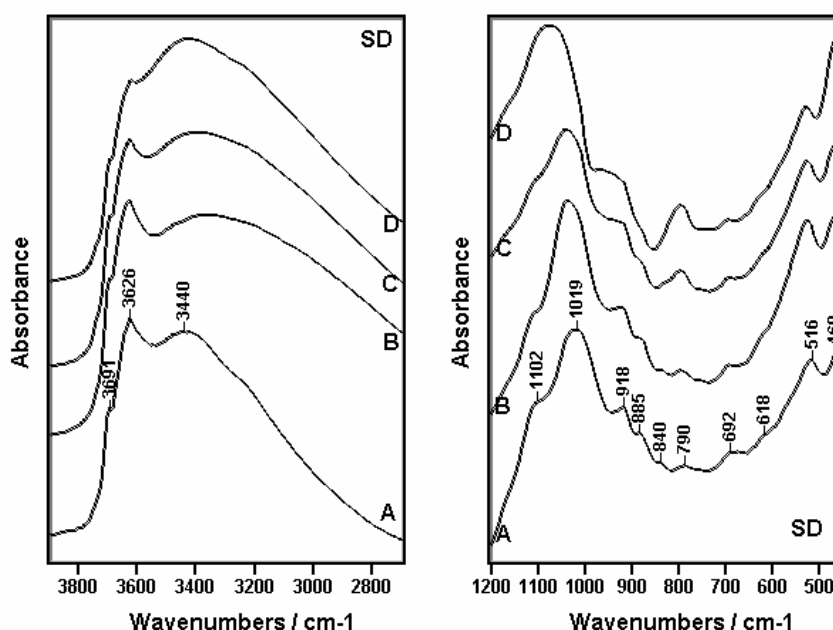
Figure 5.8 FTIR spectra of A: NaSD, B: SD-1M-95-30; C: SD-3M-95-30; D: SD-6M-95-30

The IR spectrum of untreated SAz-1 (Figure 5.9A) showed all the absorption bands expected for a Mg-rich montmorillonite with very low octahedral iron content (Farmer, 1974, 1979; cf. Chapter 3). The spectra of the acid leached SAz-1 materials (Figures 5.9B, C and D) revealed different extents of structural modification, in direct correlation with the concentration of the acidic solution. As expected, the materials obtained resemble selected samples prepared by Komadel et al. (1997) and Breen et al. (1995[a,b], 1997[a]). No significant changes were observed in the IR spectrum of SAz.1M.95.30 (Figure 5.9B), besides a slight decrease in the intensity of both OH bending vibrations (918 and 840 cm^{-1}), which reflects the reduction in content of the octahedral cations. The acidic treatment with 3M (Figure 5.9C) and 6M HCl (Figure 5.9D) solutions produces increasingly more severe changes in the clay structure. The OH bending vibrations continue to decrease in intensity for the former, and are undetectable for the latter. The 516 cm^{-1} band, which is the most sensitive indicator of the presence/absence of octahedral aluminium in acid-treated montmorillonites, decreased in intensity for SAz.3M.95.30 and almost disappeared for SAz.6M.95.30.
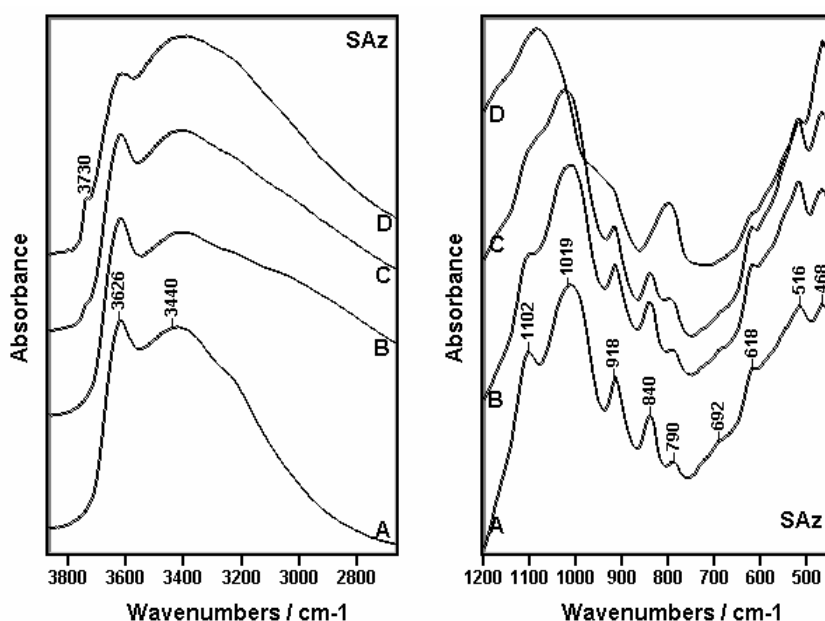
Figure 5.9 FTIR spectra of A: SAz-1, B: SAz-1M-95-30; C: SAz-3M-95-30; D: SAz-6M-95-30

The Si-O environment was concurrently affected by the acid treatment, as revealed by the changes in the position and shape of the complex Si-O stretching band in the 900-1200 cm^{-1} region. The milder acid treatments produced slight shifts of the 1019 cm^{-1} band to higher wavenumbers and the development of a band near 1085 cm^{-1}, assigned to Si-O vibrations of amorphous silica with a three-dimensional framework (Moenke, 1974). The spectrum of the most harshly treated sample (Figure 5.9D) exhibits a band at 1100 cm^{-1}, attributed to the presence of free silica. The Si-O stretching band of the tetrahedral layer was absent from the spectra of SAz.6M.30.95.

The presence of an increased amorphous content was further evidenced by the increase in intensity of the band near 800 cm^{-1} and the development of a broad band near 974 cm^{-1}, due to Si-O stretching of SiOH groups, present in the three-dimensional product formed as the octahedral sheet in the aluminosilicate layer becomes substantially depleted.

Extensive leaching of the parent material is further demonstrated by the appearance of a band at 3730 cm^{-1} (Figures 5.9C and D), attributed to the presence of free[24] silanol groups (Haffad *et al.*, 1998).

---

[24] not hydrogen bonded or inaccessible to a H-bond

Overall, the acid treatments produced three significantly different materials: the milder treatment caused minor structural change in the parent clay, whereas the most severe procedure destroyed the clay structure. The contact with 3M HCl solution caused important octahedral depletion of SAz-1 maintaining, however, an important fraction of the clay structure present in the original material.

When comparing the structural transformations that occur on the SD and SAz-1 under similar acid treatments (Figures 5.8 and 5.9), it can be seen that the latter suffers more extensive leaching than the former; this result is consistent with the accepted idea that Mg-rich clays (SAz-1) are less resistant to acid attack than Fe-rich counterparts (SD).

5.3.1.4 NITROGEN ADSORPTION-DESORPTION ISOTHERMS

Representative nitrogen adsorption-desorption isotherms of acid activated samples and that corresponding to the parent material (NaSD) are presented in Figure 5.10A. The adsorption isotherm for N_2 on Na-SD presents type I character at low relative pressures. This suggests the presence of primary micropores, while at high relative pressures the isotherm was close to type IIb and exhibited a hysteresis loop which is usually associated with adsorption of nitrogen on the walls of mesopores formed between plate-like particles (Rouquerol et al, 1999). The sample activated at room temperature and those activated using low acid concentrations at 95 ºC exhibited the same type of isotherm and hysteresis loop as the parent material. In contrast, the isotherms for the more harshly treated samples tended towards type IV and exhibited a different type of hysteresis loop which indicated that alterations in the mesoporosity had occurred.
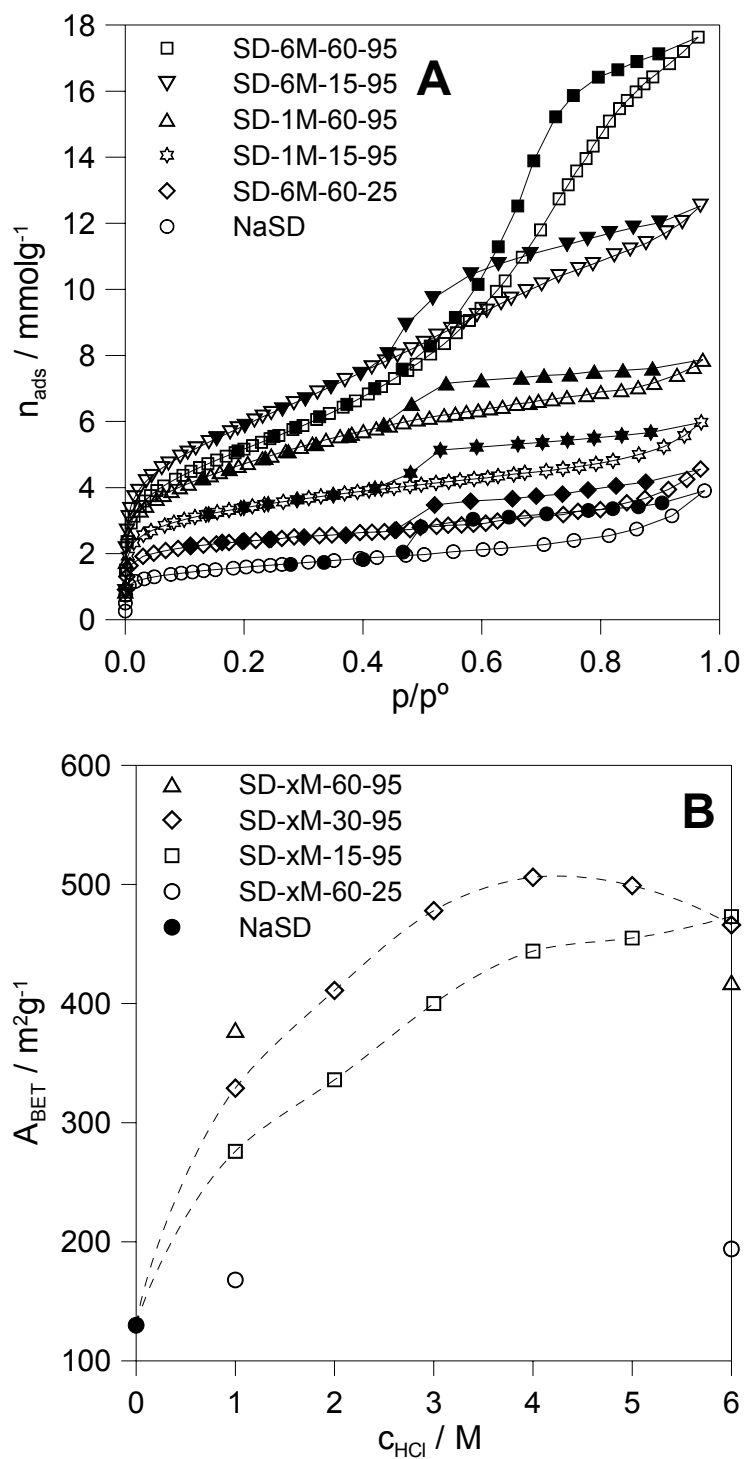
Figure 5.10 A. Nitrogen adsorption isotherms, at –196ºC, of NaSD and some acid activated samples (empty symbols: adsorption, filled symbols: desorption); B. Specific surface area (BET method) of NaSD and acid activated SD samples

The values of specific surface area of the samples under investigation, obtained by applying the Brunauer-Emmett-Teller (BET) method to the N_2 adsorption isotherms at –196ºC, are plotted as a function of the acid concentration used in Figure 5.10B. As anticipated, the

sample prepared at room temperature only displayed a slight increase in surface area when compared to that for untreated Na-SD, even after activation with 6 M acid for 60 min. Acid activation at 95ºC resulted in a significant increase in surface area, with the effects depending on both the acid concentration and the contact time. The surface area increased with treatment time in 1M acid at 95 ºC, whereas treatment with 4M acid for 30 min maximised the measured surface area. Increasing the acid concentration to 5M and 6M at 95ºC caused a downturn in surface area. Indeed, increasing the treatment time, using 6M acid at 95 ºC, to 60 min resulted in a surface area some 50 $m^2 g^{-1}$ less than the maximum. It was noted that the surface area values displayed different trends if the samples were grouped according to the time of contact at different acid concentration. For the samples prepared using the shorter contact time (15 minutes), the surface areas of the resulting materials increased in the same order as the acid concentration used in the treatment. However, for longer contact time (30 minutes), this trend was only observed up to a concentration of 4M, and with higher acid concentration lower surface area materials were produced. The downturn in surface area was not pursued further because it has been noted previously by others (Novak and Gregor, 1969; Rhodes and Brown, 1994[a]) and is generally attributed to the onset of a 3D silica structure caused by bond formation between the silica fronds which are generated as the octahedral sheet is excessively depleted.

5.3.1.5 THERMOGRAVIMETRIC STUDIES

The thermal desorption of cyclohexylamine has been frequently used to evaluate the number of acid sites on clay catalysts (Ballantine *et al.*, 1987). Despite the drawbacks that affect the method (cf. Chapter 4), it provides reasonable estimates of the number of protons if acid-leached clays are exposed to cyclohexylamine vapour within one day of acid treatment. The quantities of CHA desorbed in the appropriate temperature interval (Table 5.1) show, as anticipated from earlier work (Breen *et al.*, 1997[a]), that the estimated acidity values decreased as the severity of the acid treatment increased.

Table 5.1 Quantities of CHA desorbed in the 280 and 440 ºC temperature interval

Sample	CHA desorbed / mmol g^{-1}
SD-1M-25-60	0.63
SD-1M-95-15	0.62
SD-1M-95-30	0.52
SD-1M-95-60	0.29
SD-2M-95-15	0.50
SD-2M-95-30	0.42
SD-3M-95-15	0.42
SD-3M-95-30	0.26
SD-4M-95-15	0.21
SD-4M-95-30	0.11
SD-6M-25-60	0.60
SD-6M-95-15	0.15
SD-6M-95-30	0.10
SD-6M-95-60	0.03

5.3.2 CATALYTIC TESTS – LIMONENE CONVERSION

In the presence of acid or, in this case, acidic sites available at the clay surface, limonene reacted to form a mixture of products (cf. Scheme 4.1, Chapter 4). Similar to the ion exchanged clays catalytic results described in the previous chapter, the reaction mixture consisted of a volatile fraction, containing GC-quantifiable components (p-menthenes - two main isomers, α-terpinene, γ-terpinene, p-cymene, terpinolene and isoterpinolene) and a non-volatile fraction (high-molecular weight compounds). A few additional small peaks were present in the chromatogram but their low concentration precluded their identification by GC-MS, so they were neglected. They accounted for 4-6 % (wt) of the total reaction mixture. At the end of the process, when all the terpenes are consumed, the non-volatile fraction dominated the product distribution, reaching yields of up to 55 % (wt) (Figure 5.11).

Figure 5.12 uses the catalytic test results obtained over SD-3M-95-30, following pre-treatment at 150 ºC, to illustrate how the total conversion and the product distribution varied with time. The overall shape of the curves was the same (including the results obtained with the ion exchanged materials – cf. Chapter 4), although differing in time and yield (Figure 5.13[25]), depending on the severity of leaching to which Na-SD was subjected. Preliminary scoping studies revealed that the evolution of the reaction products with time conformed with the results for typical acid catalysts including those reported for several liquid and solid acids, including silica and acid forms of ion-exchange resins (Thomas and Bessière, 1989).
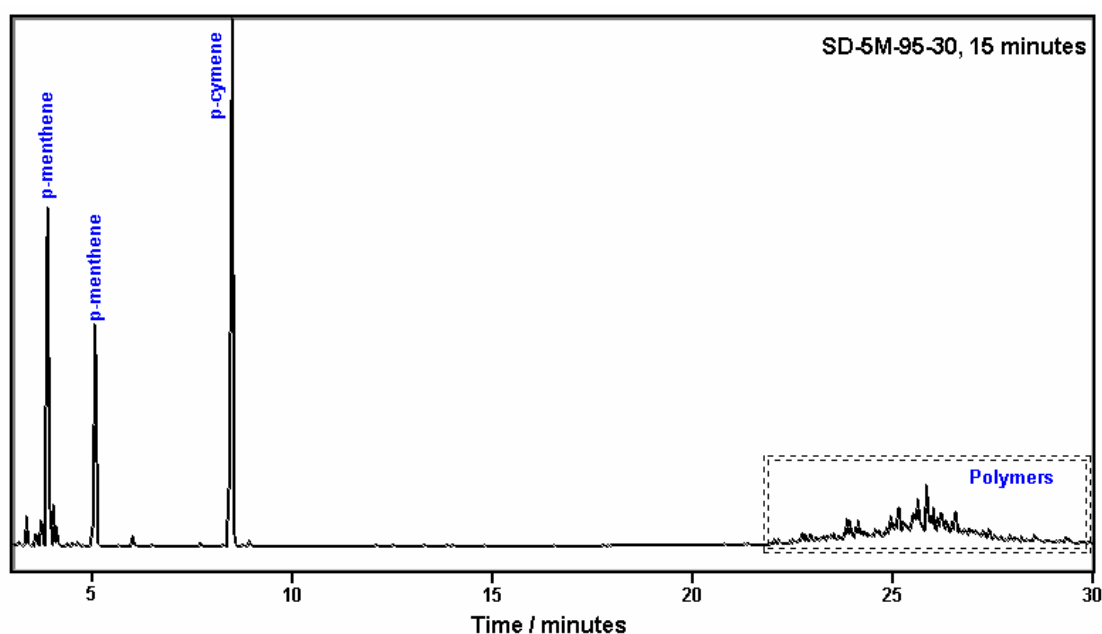
Figure 5.11 Chromatogram of the reaction mixture (15 minutes, end point) of SD-5M-95-30

The process could be formally divided into three stages (cf. Chapter 4). In this case (SD-3M-95-30; Figure 5.12), the duration of each stage is severely shortened when compared to the ion exchanged clays (cf. Figure 4.5, Chapter 4): stage I - 60 s reaction time; stage II – 120 s and stage III – from 120 s (≥ 90% limonene conversion) up to 15 minutes (complete disappearance of all dienes).

---

[25] Although the product distribution was similar for all acid activated SD catalysts, the reaction rates where markedly different. Figure 13 demonstrates how the reaction rate increased when using catalysts activated at 95ºC, during 30 minutes with A: 1M and B: 3M HCl solutions.
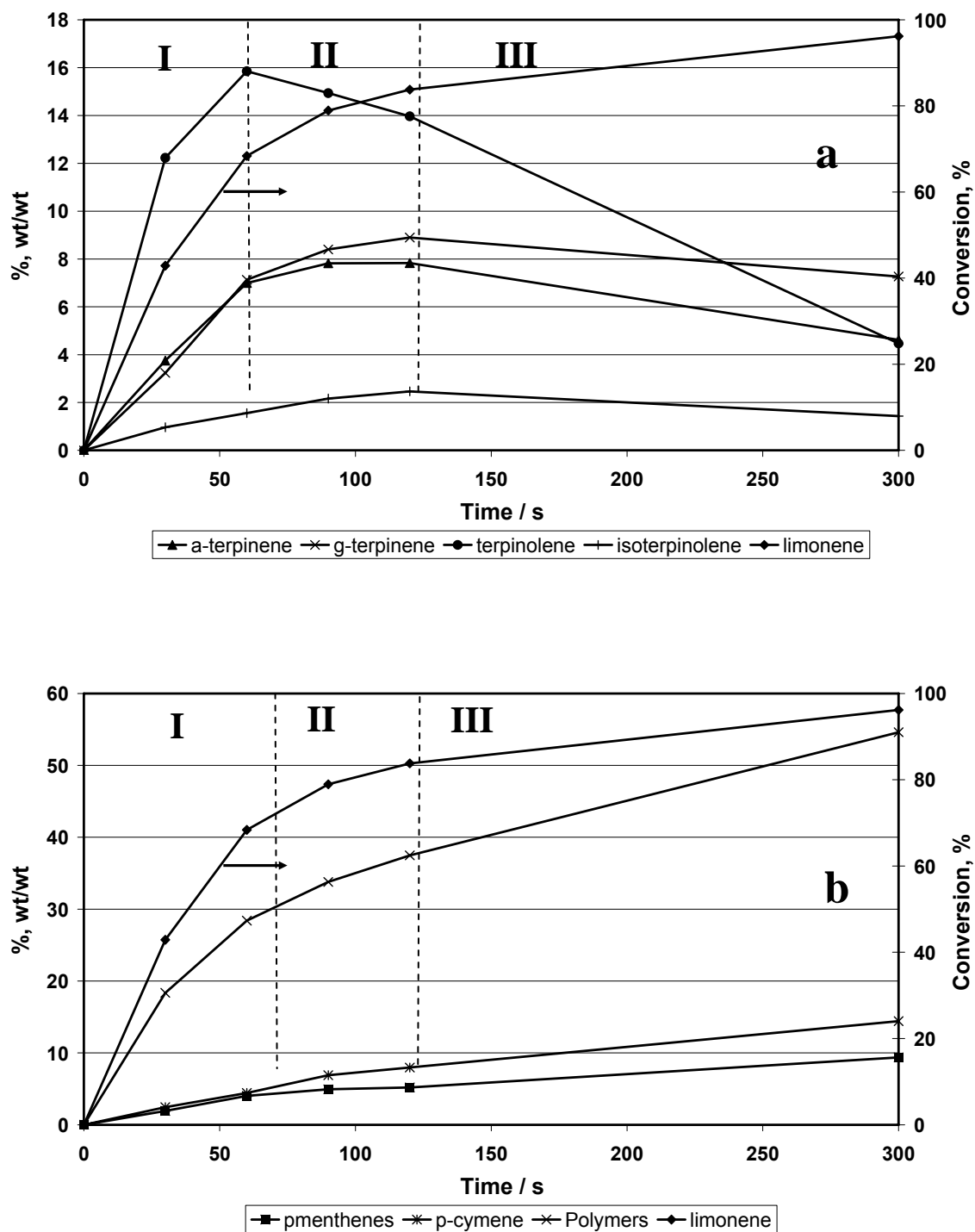
Figure 5.12 Product distribution during the conversion of limonene at a reaction temperature of 80 ºC using SD-3M-95-30 thermally activated at 150 ºC for 16 hrs. (a) Isomerisation products, (b) other products (disproportionation, polymerisation)
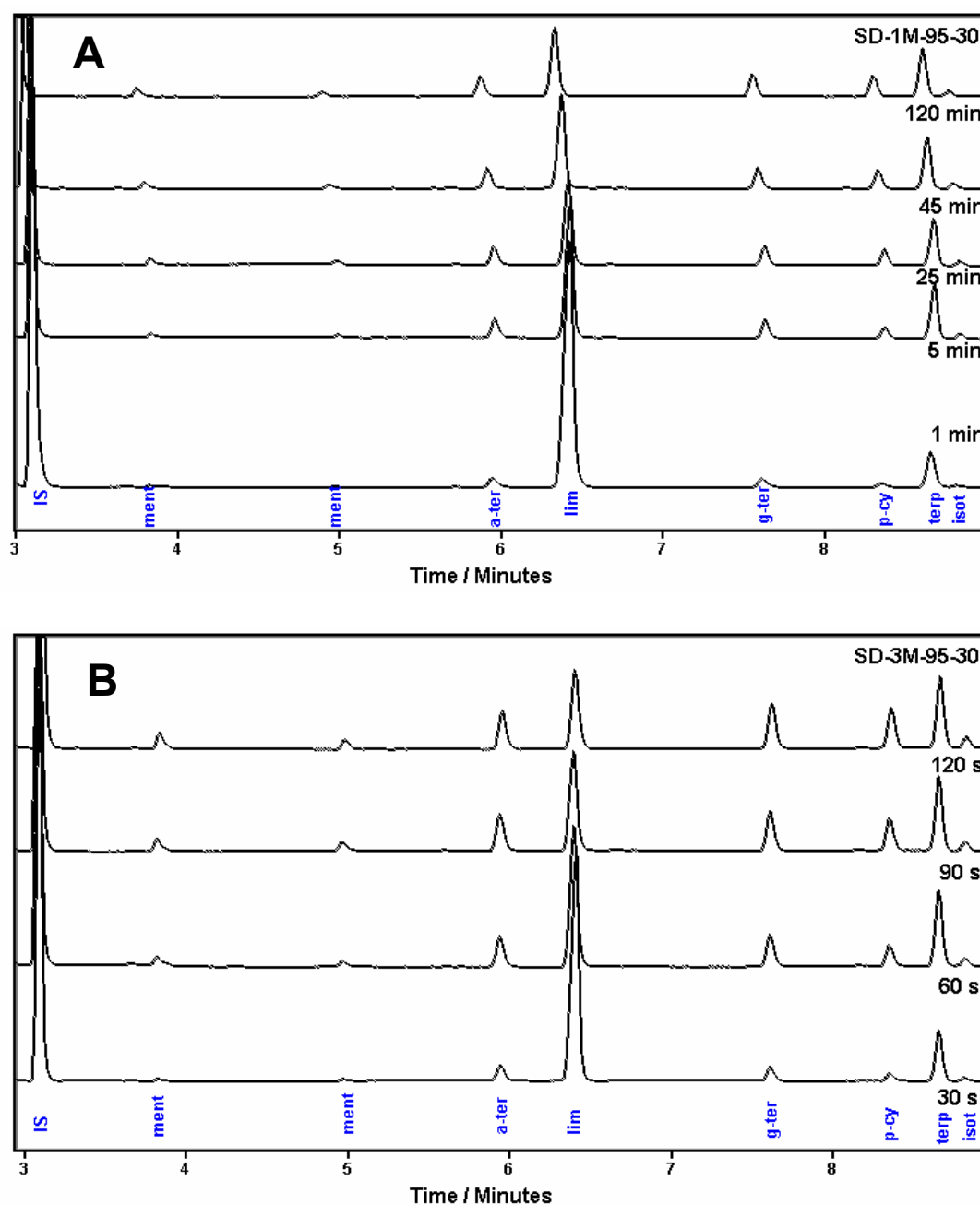
Figure 5.13 Chromatograms of the reaction mixtures at selected reaction times using A: SD-1M-95-30 and B: SD-3M-95-30

Figure 5.14 illustrates the distribution of products obtained over the range of acid-treated SD samples. The crosses present the limonene conversion values which provide a visual indication of the progress of the reaction (in conjunction with Figure 5.12). Na-SD was completely inactive under these conditions and required longer times at higher temperatures to effect any conversion of limonene. The much higher limonene conversion values over the acid-leached clays confirmed that the reaction had progressed much further during the 15

min reaction time and was in stage II (with the possible exception of the clays treated with 1M HCl). Hence the reaction rate over the individual catalysts increased from left to right in Figure 5.14. It is evident from the product yields and distributions that the catalytic activity, expressed as limonene conversion, increased with the severity of the acid activation treatment and maximised over samples SD-3M-95-30 and SD-4M-95-15 in direct correlation with the measured surface areas. This behaviour appeared to be incompatible with the acidities estimated from the desorption of cyclohexylamine (Table 5.1) but there is a complex interplay between the acidity and surface area that will be further explored below. The production of polymers reached a maximum over SD-3M-95-30 and SD-4M-95-15. These two catalysts also provided the highest yield of, and greatest selectivity towards the target species, p-cymene. Note that the yield of p-cymene decreased over SD-4M-95-30, and over the samples prepared using 6M acid, and the yield of terpinolene increased.

The catalysts prepared under mild conditions displayed a higher total number of acid sites, but a lower limonene conversion than the severely-leached clays. Hence, it seems that, for mildly treated clays, only a fraction of the acid sites was accessible for reaction, and the available surface area coupled with the accessibility of the active (acid) sites plays an important role in controlling the catalytic process. These results agree with the previous findings of Breen *et al.* (1997[a]) and Vaccari (1999) who explained that the acid-treatment conditions required to maximize the catalytic activity depends on the precise reaction of interest. Reactions involving polar molecules can be efficiently catalysed by mildly treated clays because the large number of acid sites available on the internal surface is accessible to the polar reactant. In contrast, non-polar molecules are only able to react at the accessible external face and edge sites on the surfaces of the clay platelets. Consequently, the reactions involving non-polar reagents require more harshly treated clays, and the activity depends on the complex interrelation between available surface area and accessible acidity. Similar observations have been reported by Rhodes and Brown (1994[a]) for the isomerisation of α–pinene to camphene and limonene.
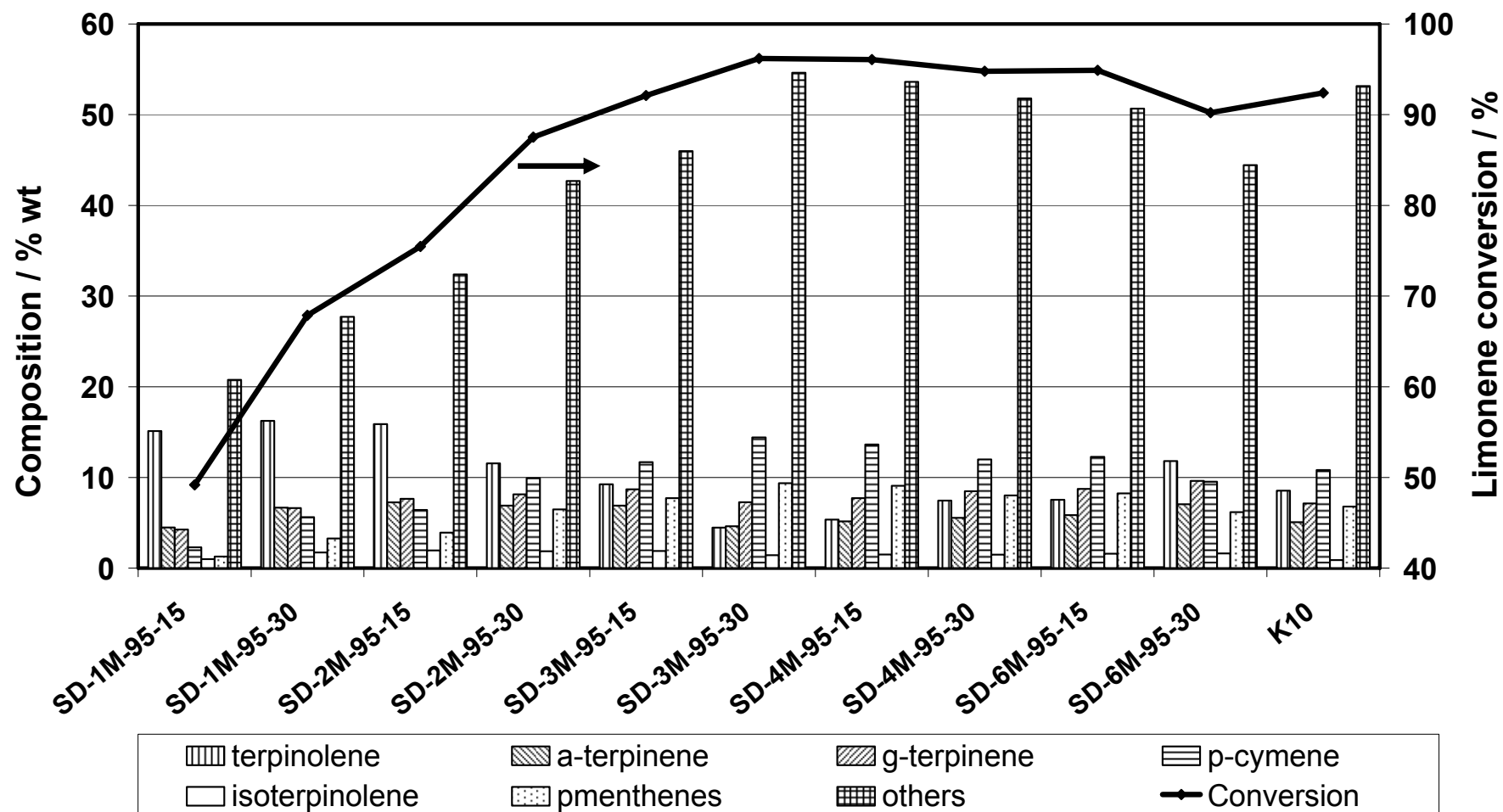
Figure 5.14 Distribution of products over SD leached using the given acid contents for 15 minutes at 80 ºC. The acid treated clays were pre-treated at 150 oC for 16 hr prior to their use in the reaction

Figure 5.15 demonstrates the effect of these two variables (surface area and total acidity) on the conversion of limonene (A) and production of p-cymene (B). Samples are ordered as a function of decreasing total acidity (cf. Table 5.1, Section 5.3.1.5). It can be seen that neither the selectivity towards p-cymene nor the limonene conversion percentages at the given reaction time follow this order, since both parameters maximise in the materials with the 'medium-low' acidity. Although surface area apparently seems to offer a better correlation with the catalytic data, the trend does not hold for all materials, the discrepancies being more obvious for the less harshly depleted materials.
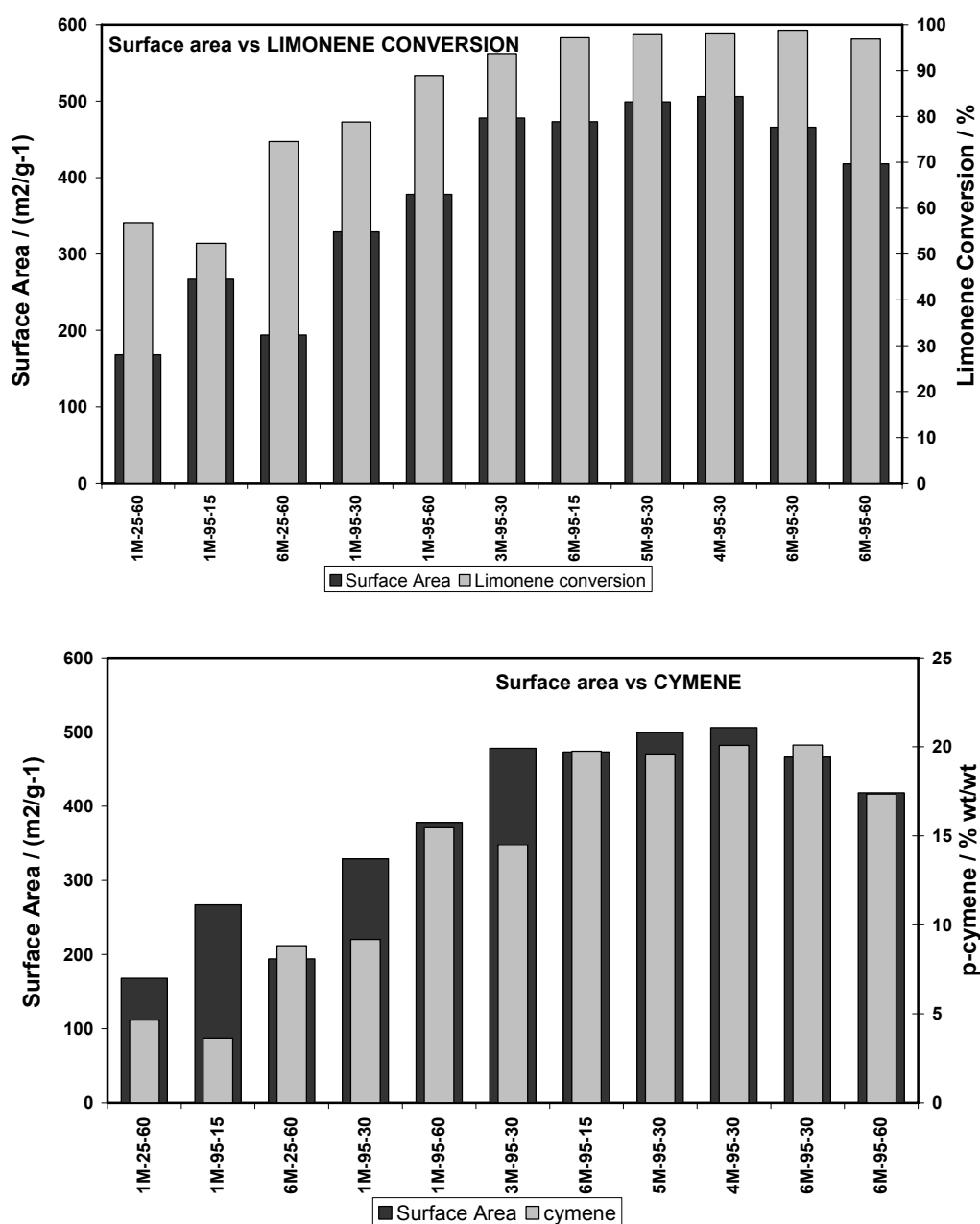
Figure 5.15 Comparison between surface area and A. limonene conversion and B. p-cymene production after 15 minutes of reaction at 80 °C (the samples are ordered in terms of decreasing total acidity)

Thus, the number of available acid sites on the external surfaces is most likely to be responsible for the observed order in the catalytic activity. It is reasonable to assume that the most active catalysts for the production of p-cymene (within the current constraints of reaction time and temperature), i.e. SD-3M-95-30 and SD-4M-95-15, offer the most appropriate combination of available surface and accessible acidity for the transformation of limonene. The number of acid sites estimated from cyclohexylamine desorption are 0.26 and 0.21 mmol (g clay)$^{-1}$. This may not reflect the number of acid sites available to the limonene molecules because cyclohexylamine is a very polar reagent which will be able to access those galleries still remaining beyond the progress of the acid leaching process. Thus, it is a considerable challenge to determine the number of acid sites available to non-polar reagents because the most commonly used probes of acidity are very polar and can access acid sites not available to the non-polar reagents.

In an attempt to evaluate the number of acid sites contributing to the catalytic activity a representative catalyst was poisoned using increasing amounts of pyridine. In an additional experiment, using the same catalyst, the protons (generated during acid activation) were replaced by back exchanging the catalysts with Na-ions. This approach was adopted to ascertain whether the acid treatment generated any sites, acidic or otherwise, which were not removed or poisoned by the Na-back exchange procedure. One particular target was to ascertain whether there were any active Lewis sites produced during the acid leaching and subsequent thermal pre-treatment. The product yields and distributions obtained using these two different approaches are presented in Figure 5.16. Clearly, increasing the amount of pyridine to amounts in excess of 0.2 mmol / 100 (g clay)$^{-1}$ completely destroyed the catalytic activity. This value is in good agreement with the acidity value (0.26 mmol.g^{-1}) estimated from CHA desorption (Table 5.1) but may indicate that only *ca.* 80% of the sites estimated using CHA were accessible and/or active in the transformation process. Like cyclohexylamine, pyridine is not selective and will poison both Brönsted and Lewis acid sites. Therefore, the Na-back exchanged samples may provide further evidence for the presence or otherwise of

Lewis acid sites. If the Lewis sites are part of the structure, rather than an adsorbed cation such as Al, Mg or Fe generated during the leaching process, then the Na-ions should not have a significant influence on their activity. The quantities of limonene converted, together with the amount of polymers formed indicated that the Na-back exchanged samples were relatively unreactive and resided in stage I of the conversion process where comparatively large amounts of terpinolene, α- and γ-terpinene would be anticipated. Nonetheless, the product profiles were equivalent to those obtained using Na-SD treated with 1M acid (SD-1M-95-15) indicating the presence of a small number of accessible acid sites – which on balance must be considered to be Lewis acidic in nature. The moderately enhanced surface area of the Na-back exchanged sample may be increasing the accessible surface near to the Lewis acid sites present in Na-SD.
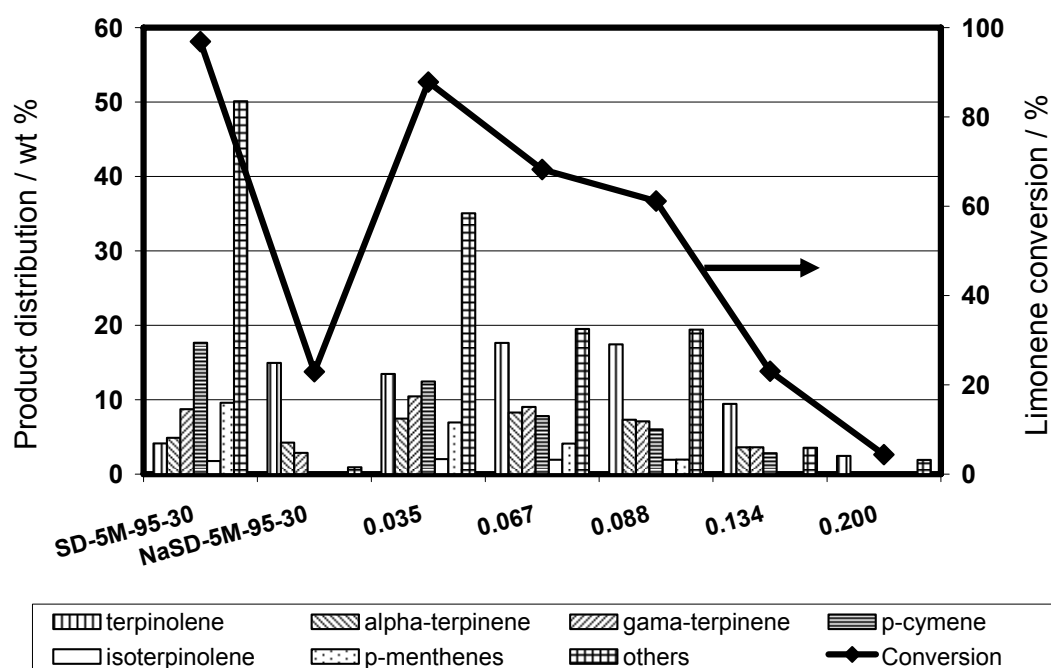
Figure 5.16 The influence of back exchange with Na-ions and poisoning with increased amounts of pyridine on the product distribution over SD-5M-95-30 (the numbers on the X-axis refer to mmol of pyridine per gram of clay)

SAz-1 is a well known montmorillonite of relatively high CEC (120 meq / 100 g clay) and low structural iron content (Fe_2O_3 = 1.6 wt %). SAz-1 also has a high octahedral magnesium content which means that, under the same acid activation conditions, it was more extensively

leached than the samples derived from SD (cf. Section 5.3.1.3). The Al- and Ni-exchanged forms of SAz-1 were compared to the same cation-exchanged forms of SD in the transformation of limonene to p-cymene (cf. Chapter 4). Al- and Ni-SD were significantly more active than Al- and Ni-SAz-1, in that the conversion of limonene over SD was > 80% but < 5% over SAz. A similar comparison has been undertaken here using samples of SAz-1 leached using 1, 3 and 6M HCl at 95 ºC for 30 min producing samples designated as SAz-1M-95-30, SAz-3M-95-30 and SAz-6M-95-30. These leaching times were selected (Breen *et al.*, 1997[a]) to produce catalysts of similar octahedral depletion to the SD samples.

Figure 5.17 shows, as anticipated, that the conversion of limonene over the acid activated products derived from SAz-1 maximised and then dropped off as the extent of leaching increased. It was clear that increasing the surface area and acidity of SAz had a tremendous influence on its catalytic activity compared with simple ion-exchange with acidic cations, e.g. Al^{3+}. Unfortunately, the activity of the SAz-derived catalysts was directed towards the polymerisation reaction and not p-cymene, the desired product. This data together with that obtained using the Al- and Ni-exchanged forms of SAz-1 clearly indicates that surface area and acidity alone are not sufficient to produce usable quantities of p-cymene.
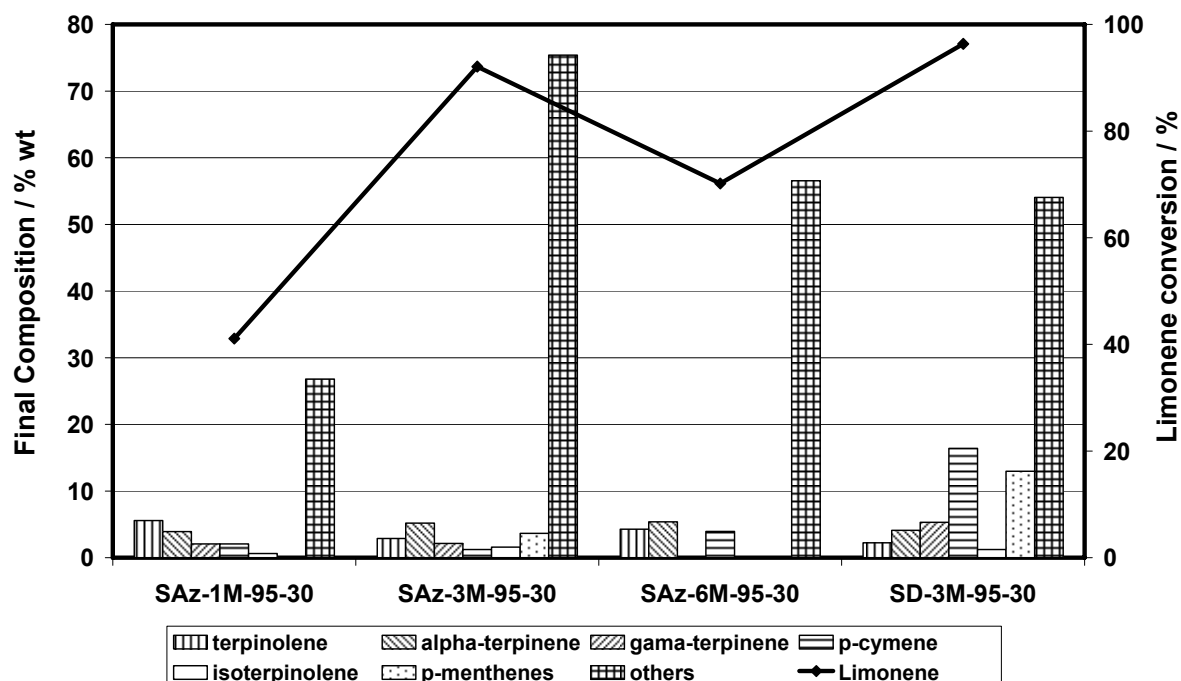
Figure 5.17 Comparison of the distribution of products obtained over SAz-1 leached using 1M, 3M and 6M HCl for 30 min at 95 ºC with that over SD.3M.30.95. The acid treated SAz-1 was pre-treated at 150 ºC for 16 hr prior to its use in the reaction

The transformation of limonene (and other terpenes) is usually attributed to Brönsted sites, which protonate the unsaturated molecule, thus initiating a network of reactions, including dehydrogenation and polymerisation. However, the p-cymene production over SAz-1 was very low perhaps suggesting, together with the moderately enhanced yield over the Na-back exchanged sample, Na.SD-5M-30-95 that structural Lewis acid sites may be involved in the catalytic conversion of limonene. As previously noted, there is some evidence (Crockett and Roduner, 1994) that the conversion of some terpenes (α-pinene, *trans*-isolimonene and α-terpinene) over zeolites is probably not catalysed by Brönsted acid sites. These authors used deuterated mordenite as the catalyst but were unable to find any deuterium incorporated in the starting terpene leading them to suggest that the rearrangements occurred over Lewis acid sites. Moreover, electron paramagnetic resonance (EPR) studies, have shown that the incorporation of the three terpenes (listed above) in mordenite give rise to the same radical cation, i.e. that of α-terpinene. Thus, a Lewis acid site could behave as an "electron hole" and accept one electron from the electron-rich terpene, giving rise to the corresponding radical cation, which undergoes further conversion to the more stable α-terpinene radical cation. Furthermore, de Stefanis *et al.* (1995) have also shown that α-pinene and limonene are readily converted over zeolites and PILCs, under Lewis acid conditions, with USY exhibiting a high selectivity (>40 %) towards p-cymene, the oxidation product of limonene. Finally, it has been shown (Hart and Brown, 2004) that the non-exchangeable acid sites (defect sites on the clay surface and coordinatively unsaturated edge sites in the lattice) are predominantly Lewis acidic and exhibit some catalytic activity in Friedel-Crafts alkylations.

The results presented here, for the catalysts derived from SD, could suggest that the reaction also proceeds over Lewis acid sites which are able to steer the reaction via two possible mechanisms. The first involves the adsorption of the exocyclic double-bound with formation of a primary carbonium ion, followed by a proton shift leading to a tertiary carbonium ion, from which terpinolene could be formed. The second possible explanation is that the Lewis site behaves as an "electron hole" and accepts one electron from the electron-rich α-

terpinene, giving rise to the radical cation of α-terpinene. Afterwards, the radical cation dehydrogenates to p-cymene via an allylic radical. The formation of radical cations is known to promote the polymerisation of dienes, and could explain the high content of polymers formed in the process (Cativiela *et al.*, 1993).

It was demonstrated in the previous chapter (Figure 4.8, Section 4.3.2) that the gallery cation, and hence the nature of the acidity (Brönsted and/or Lewis), exerted little influence on the yield of p-cymene. The amount of p-cymene produced by both Al- and Ni-exchanged forms at the different limonene conversion values was identical thus testifying to the thermodynamic control of the process. Those results are combined with the catalytic data presented in this chapter (Figure 5.18). Although the reaction conditions are different (mainly in terms of temperature) it is obvious that, despite the significant structural changes that occur in some of the acid activated materials (including increased accessibility and, eventually, creation of new types of acidic sites) with direct effects in the reaction rates, the processes that occur during the reaction remain basically the same. The amount of p-cymene produced proved to be a function of the degree of limonene conversion and not of the amount or nature of the acidic sites available. Further evidence was obtained using K10, a commercially available acid activated clay (ca. 2.3 wt % Fe_2O_3, A_{BET} 220 $m^2.g^{-1}$, Jang *et al.*, 2005), used as a reference catalyst. The amount of p-cymene produced over K10 did not differ from the amounts produced using SD based catalysts. Acid activated SAz however, did not follow the same trend: the amount of p-cymene generated by SAz-3M-95-30 (highlighted in Figure 5.18), the surface area-acidity 'well balanced' catalyst, was much lower than would have been anticipated by the degree of limonene converted, when considering the process described above.
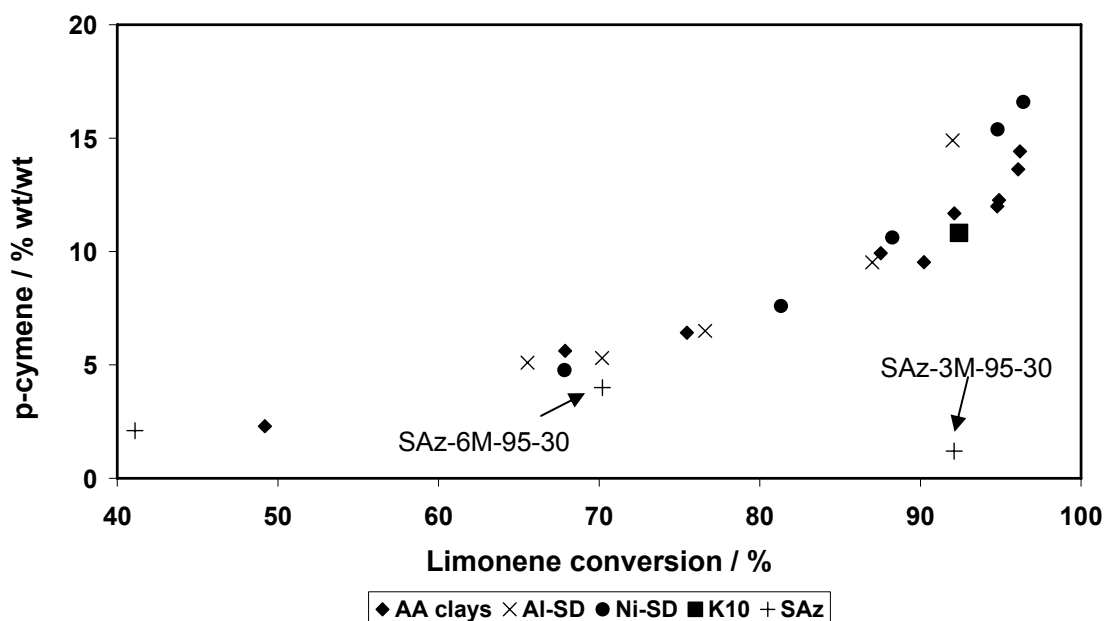
Figure 5.18 p-Cymene content in the final mixture over AlSD, NiSD, K10 and several acid activated SD and SAz materials presented as a function of limonene conversion

5.3.3 TG-MS DATA

Simple thermogravimetric CHA desorption profiles can provide an estimate of the number of acid sites (Table 5.1), but are unable to elucidate any differences that may exist between the different decomposition pathways over different materials. Real time TG-MS analysis of the decomposition products contributes to a more complete picture of the decomposition of CHA. Generally, CHA decomposition can be represented by scheme 2.1 (cf. Chapter 2).

Figure 5.19 illustrates the information obtained from a typical real time mass spectrum for CHA desorption from SD-1M-95-15. The total ion count is assigned to the left hand axis while the intensities of the single ion species are given on the right hand axis. Generally, two peaks were present in the desorption profile. The lower temperature peak arises mainly from the desorption of CHA and water whereas the peak at higher temperature has been routinely associated with the acidity and hence catalytic activity of the clay catalyst under scrutiny (Ballantine *et al.*, 1987; Bovey and Jones, 1995; Breen *et al.*, 1997[a]). This higher temperature peak arises from the desorption of decomposition/transformation products in

addition to some unmodified CHA. CH, CHD and benzene were evolved at successively higher temperatures.
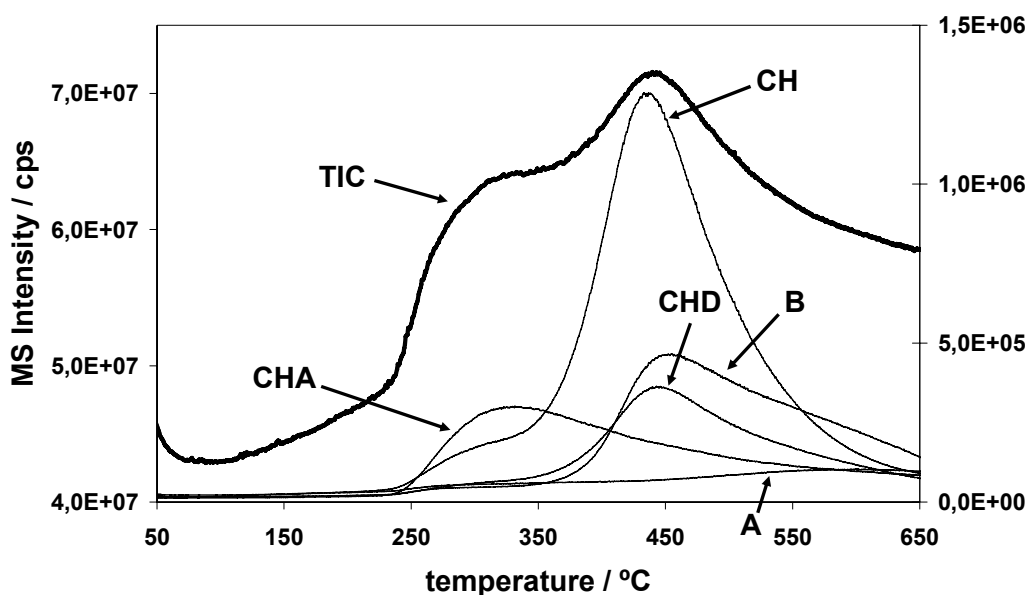
Figure 5.19 Real time MS ion chromatograms for the desorption of CHA (m/z = 99), CH (m/z = 54), CHD (m/z = 77), B (m/z = 78) and aniline (m/z = 93) from SD-1M-15-95 after a 7 day incubation period with CHA

Figure 5.20 presents the single ion profiles for the evolution of CHA, CH, CHD and B from the samples treated with 6M HCl (as a function of acid activation temperature and treatment time). The amount of unmodified CHA desorbed under the lower temperature peak increased as the severity of acid treatment increased, which was attributed to the increased surface area available (Figure 5.10) to accommodate more CHA. Moreover, the temperature at which the peak maximum occurred, T_{max}, decreased suggesting that, at least some of, the CHA was more loosely held. In contrast the quantity of all the decomposition products (CH, CHD and B) evolved under the higher temperature peak diminished, which was consistent with the decrease in the total amount of CHA desorbed in the 280 to 440 °C region (Table 5.1) as the depopulation of the octahedral sheet progressed. The characterisation data discussed above (XRD, XRF, FTIR spectra and surface area) confirmed that all the samples treated with 6M HCl at 95 °C exhibited high degrees of structural decomposition. As the extent of leaching increased, the samples became more open which should perhaps facilitate the evolution of

gas at lower temperatures. However, the T_{max} values for CH, CHD and B increased as the extent of leaching increased. This increase in T_{max} may represent an increase in binding strength of the CHA to the acid sites and/or a slower diffusion of the evolved gases out of the sample. A plausible explanation, given that the amount desorbed also decreases, is that the CH, CHD and B are generated in the (decreasing) amounts of layered material remaining and then the molecules have to negotiate a more tortuous route to the gas phase through the silica fronds generated during acid leaching. Indeed, in SD-6M-95-60 the desorption maximum for benzene at 450 ºC appears to have been removed. This could be attributed to the particular site associated with benzene production at this temperature having been dissolved away or rendered inaccessible as the silica fronds collapse together. Note that the samples prepared at 95 ºC all display a small 'prepeak' for the evolution of CH and CHD which diminishes with acid attack. This could mean that either the low temperature site responsible has been etched away or that the silica fronds are severely restricting access to it.

Once again the amount of unmodified CHA desorbed by the samples prepared using 1M HCl increased with the severity of acid treatment in line with the increase in surface area (Figures 5.10 and 5.21). Indeed the sample treated at 20 ºC for 120 min contained virtually no physisorbed CHA. Sample SD-1M-95-60 produced less CH, but more B, than the other samples whereas all the samples produced similar quantities of CHD. This dissimilarity is reflected in the lower weight loss displayed by SD-1M-95-60 in the 280 to 440 ºC (0.29 mmol g^{-1}) compared with the other samples (0.65, 0.62 and 0.52 mmol g^{-1} for SD-1M-25-120, SD-6M-95-15 and SD-6M-95-30, respectively). Unlike the samples discussed in the context of Figure 5.20, the values of T_{max} for CH, CHD and B (Figure 5.21) were unaffected by treatment of Na-SD with 1M HCl. Moreover, the low temperature desorption peak for B, at 450 ºC, has not been removed/blocked in these less extensively leached samples, perhaps providing support for the view that CH, CHD and B were generated in the galleries associated with the undamaged layers.
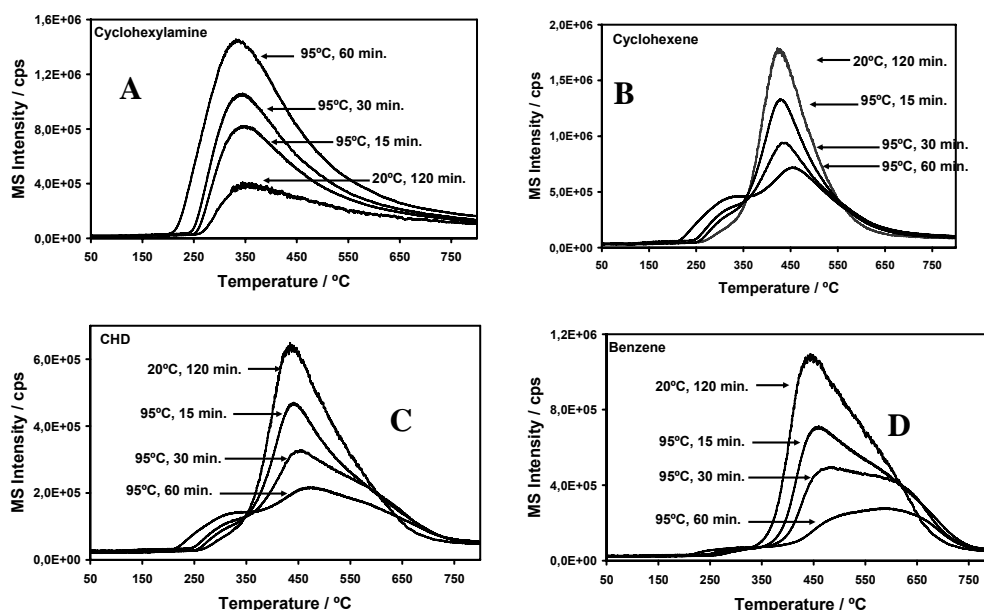
Figure 5.20 Comparative MS single ion chromatograms for SD treated with 6M HCl solutions at 25ºC during 120 minutes and at 95ºC during 15, 30 and 60 minutes. A: CHA (m/z 99); B: CH (m/z 54); C: CHD (m/z) 77 and B (m/z 78)
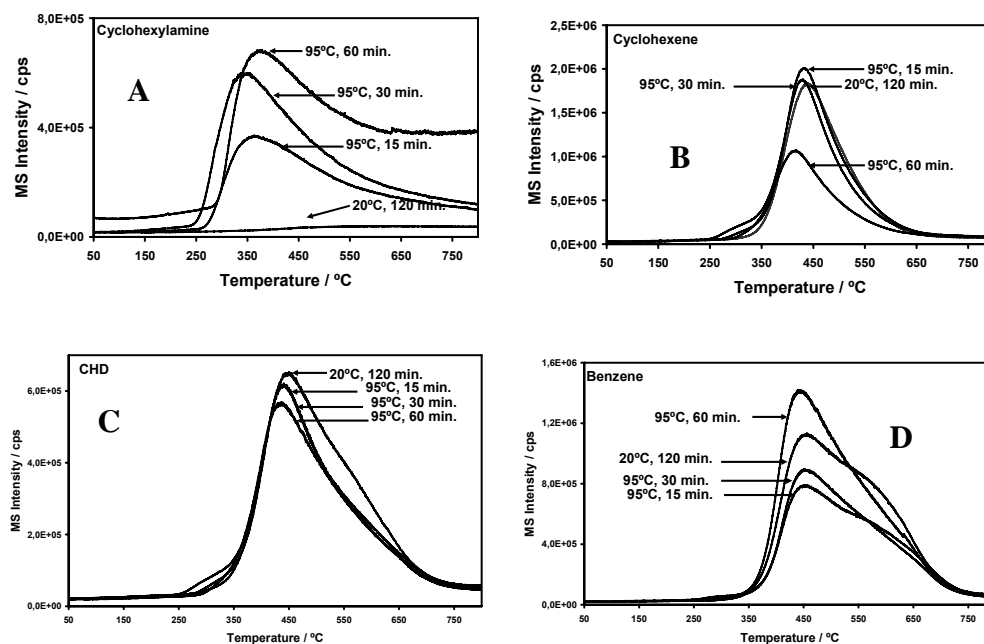
Figure 5.21 Comparative MS single ion chromatograms for SD treated with 1M HCl solutions at 25ºC during 120 minutes and at 95ºC during 30 and 60 minutes. A: CHA (m/z 99); B: CH (m/z 54); C: CHD (m/z 77 and B (m/z 78)

The materials activated with HCl at the low temperature 25 ºC (Figures 5.20 and 5.21)

displayed similar behaviour as anticipated from the characterisation data presented above.

The EGA data for Na-SD activated for 30 min at 95 ºC but with different acid concentrations is presented in Figure 5.22. Two types of behaviour were evident and can be related to structural/acidity features of the leached materials. The samples produced using weaker acids (1, 2 and 3 M) evolved the same amount of CHA, as SD-6M-95-30 but more CH, CHD and B which reflects the pronounced decrease in the total number of acidic sites on the sample treated with 6M HCl (0.1 mmol g^{-1}). Note that SD-6M-95-30 also evolved a larger amount of unmodified CHA in line with the data in Figure 5.20.
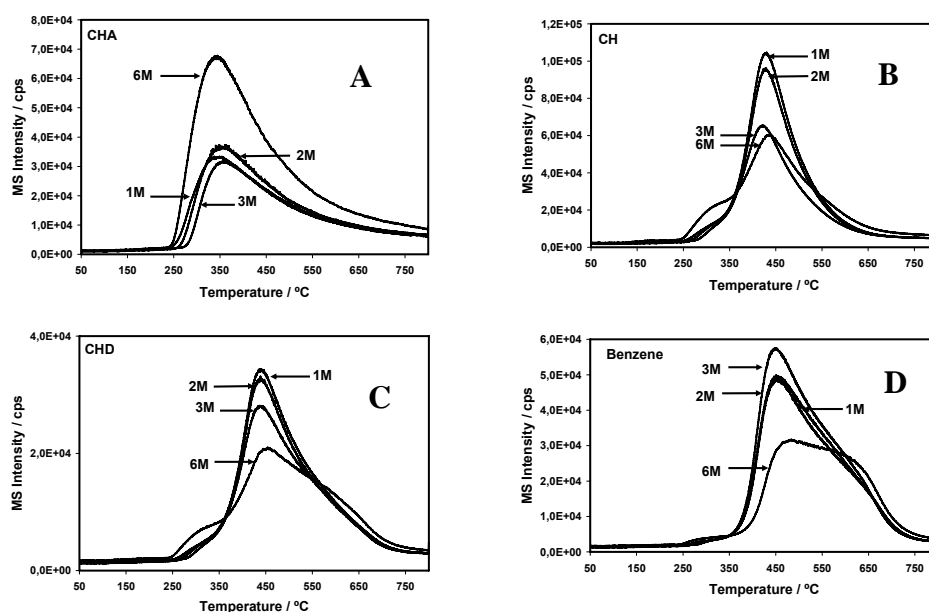
Figure 5.22 Comparative MS single ion chromatograms for SD treated with 1, 2, 3 and 6M HCl solutions at 95ºC, during 30 minutes. A: CHA (m/z 99); B: CH (m/z 54); C: CHD (m/z) 77 and D: B (m/z 78)

It is interesting to note, in the context of the catalytic results, that SD-3M-95-30, which was very effective at producing p-cymene, exhibited properties which are a combination of those produced under mild and severe leaching conditions. This material released similar amounts of CH to SD-6M-95-30 (i.e. less than samples produced using 1M and 2M acid), similar amounts of CHD to SD-1M-95-30 and SD-2M-95-30 yet more B than all the other acid activated materials. This may be of particular relevance given that dehydrogenation of a

cyclohexadiene ring to an aromatic ring is critical in the formation of p-cymene from the terpinenes.

Controlled acid activation of clays offers materials with enhanced surface areas and total acidities yet a balance must be reached where the optimum levels of surface area and acidity for a particular process produces the maximum yield of the desired product. SD-3M-95-30 and SD-4M-95-15 seem to exhibit the required balance of these conflicting features. They have a high surface area together with a significant acidity combined with the ability to dehydrogenate ring compounds as shown by the generation of more benzene than the other leached materials.

5.4 CONCLUSIONS

The variables introduced in the acid treatments applied to SD bentonite (temperature, contact time and acid concentration) generated materials with a wide range of chemical, structural and textural properties, differing between each other in a stepwise, controlled fashion. Even under the most severe conditions used all SD based catalysts retained some clay-like character. On the other hand, the same acid activation conditions applied to SAz-1 produced more extensively depleted materials than the SD counterparts, which is a consequence of the high magnesium content of the former.

Acid leaching of SD bentonite produces a very active catalyst which converts 90% of limonene in 15 min at 80 ºC. Similar transformation activity over Al^{3+}- and Ni^{2+}-exchanged SD requires 15 min at 150 ºC. The yield of p-cymene maximised near 15% over SD-3M-95-30 and SD-4M-95-15 when the surface area was near 450 m^2 g^{-1} and the acidity was relatively low but readily accessible to the reagent limonene. The yield of polymeric and non-volatile

products was high at 50 – 55% which was two or three times the yield over the Al^{3+}- and Ni^{2+}- exchanged SD catalysts. It is difficult to compare the production of non-volatile products with those of other catalysts because few authors provide relevant data.

The lack of isomerisation and dehydrogenation activity over the acid-treated samples of the low iron SAz-1 clay strongly suggests that the structural iron present in SD is responsible for the dehydrogenation role. This structural iron was most exposed/active when the surface area was at its highest. The catalytic data obtained with K10 montmorillonite provided further evidence of the role of iron in the dehydrogenation process.

The information combined in this chapter was published in two papers under the following references:

Fernandes, C., Catrinescu, C., Castilho, P., Russo, P. A., Carrott, M. R. and Breen, C. (2007) Catalytic conversion of limonene over acid activated Serra de Dentro (SD) bentonite. *Appl. Catal. A Gen.*, 318, 108-120.

Fernandes, C., Catrinescu, C., Castilho, P., Russo, P., Carrott, M. and Breen, C. (2006) Acid activated *Serra de Dentro* bentonite: chemical, structural, textural and catalytic properties. in: *Materiales Arcillosos: de la Geología a las Nuevas Aplicaciones* (Suárez, M., Vicente, M.A., Rives, V. and Sánchez, M.J., eds.). Sociedad Española de Arcillas, Salamanca, 111-122.

CHAPTER 6. PILLARED CLAYS

6. PILLARED CLAYS

6.1 INTRODUCTION

Pillared clays are obtained by calcination of the intercalated compounds prepared by exchange of the interlayer cations of layered clays with bulk inorganic oxyhydroxy oligomers. These oligomers are obtained by partial hydrolysis of multivalent cations such as Al^{3+}, Cr^{3+}, Ti^{4+} or Fe^{3+}. The pillaring process improves the surface area, imparts permanent porosity and maintains the thermal stability of the induced porosity of the clays at temperatures where the natural porosity would have been destroyed. Pillaring, gives the obtained solids important catalytic properties, namely in 'fine chemistry' applications.

6.1.1 PILLARING SOLUTIONS

The metallic oligomer most widely used in smectite pillaring studies is $[Al_{13}O_4(OH)_{24}(H_2O)_{12}]^{7+}$, usually designated as Keggin Al_{13} polycation (Gil *et al.*, 2000). The pillaring of montmorillonites and saponites with chromium polycations (formed by partial hydrolysis of Cr^{3+} solutions) has also been reported by different authors (Brindley and Yamanaka, 1979; Pinnavaia *et al.*, 1985; Carrado *et al.*, 1986; Tzou and Pinnavaia, 1988; Bornholdt *et al.*, 1991; Drljaca *et al.*, 1992; Volzone *et al.*, 1993, 1995, 2001; Sychev *et al.*, 1994; Krajovic *et al.*, 1995; Toranzo *et al.*, 1997), including their use as catalysts in reactions such as isomerisation and disproportionation of o-xylene (Krajovic *et al.*, 1995), dehydrogenation of cyclohexane (Pinnavaia *et al.*, 1985), decane cracking (Pinnavaia *et al.*, 1985; Carrado *et al.*, 1986; Tzou and Pinnavaia, 1988), cumene cracking (Zhao *et al.*, 1995; Mishra and Parida, 1998), alcohol dehydration (Mishra and Parida, 1998) and conversion of 1,2,4-trimethylbenzene (Zhao *et al.*, 1995).

It was previously noted that Cr based catalysts are frequently reported as being used in several catalytic applications. It has been shown (Breen *et al.*, 1987) that Cr containing clays

offer a combination of both Lewis and Brönsted acid sites and that they may present higher acidities than their Al counterparts (Auer and Hofmann, 1993; Cañizares *et al.*, 1999).

Chromium-pillared clays are thermally much less stable than their aluminium counterparts and the collapse of their structure provokes a decrease in the surface area and accessible porosity (Toranzo *et al.*, 1997). For this reason, mixed Cr-Al pillaring solutions were used in this work in an attempt to improve the thermal stability of the Cr-solids and to obtain solids with high surface area and high porosity.

6.1.2 REFERENCE CLAY

SapCa-1 is a saponite obtained at the Source Clay Repository, under the Special Clay Minerals Section. It originates from Ballarat, California. The chemical composition and CEC of the material is presented in Table 6.1 and the half-unit formula in Table 6.2 (Volzone, 2001). SapCa-1 contains up to 3% diopside which accounts for the high CaO content. The isomorphic substitution occurs mainly in the tetrahedral sheet.

Table 6.1 Chemical composition and CEC of SapCa-1 saponite

	Chemical Composition / %							CEC / meq.(100g) $^{-1}$
	SiO_2	Al_2O_3	Fe_2O_3	MgO	CaO	Na_2O	K_2O	
SapCa-1	47.9	4.17	0.66	26.1	0.9	2.73	0.39	92

Table 6.2 Half-unit-cell formula of SapCa-1 (Volzone, 2001)

Tetrahedral Sheet			Octahedral Sheet				Total Charge	Interlayer			
Si_{IV}^{4+}	Al_{IV}^{3+}	Charge	Al_{VI}^{3+}	Fe^{3+}	Mg^{2+}	Charge		K^+	Na^+	Ca^{2+}	Mg^{2+}
3.82	0.18	-0.18	0.20	0.02	2.50	-0.19	-0.37	0.06	0.12	0.10	---

The choice of this material as the reference clay derived from the fact that the methods used to pillar the materials in the present work were previously applied on a saponite from a different origin (Toranzo *et al.*, 1997). Characterisation data for chromium pillared SapCa-1 was also available (Volzone, 1993, 1995, 2001).

6.2 EXPERIMENTAL

The pillaring methods employed (vide infra) are similar to those reported by Toranzo *et al.* (1997 – single metal) and Pálinkó *et al.* (1997 – mixed metal), except for the time of maturation of the single Al-oligomer containing solutions and, in some cases, the relative proportions of Cr and Al in the pillaring solutions. Initially, the protocol reported by Toranzo *et al.* (1997) was used to prepare all samples, but characterisation data of the solid samples showed that the pillaring with mixed metal pillaring solutions was not successful. Na-SD and SapCa-1 were used to prepare all the pillared samples (Al, Cr and mixed Al/Cr PILCs). Each solution was prepared in order to offer different Al^{3+}/Cr^{3+} ratios. Considering the relative amount of these cations, solutions of the following stoichiometries were prepared: $Al_{1.0}$, $Al_{0.7}Cr_{0.3}$, $Al_{0.5}Cr_{0.5}$, $Al_{0.3}Cr_{0.7}$ and $Cr_{1.0}$.

In the $Al_{1.0}$ series, the aluminum polycation was prepared by addition of aqueous NaOH to a solution of $AlCl_3.6H_2O$, with the concentration ratio OH^-/Al^{3+} being 2.2. The solution was matured at 60 ºC for 2 h and at room temperature for 12 h, prior to being used. The volume of the pillaring solution was 600 mL. The solution obtained was slowly added to suspensions of 8 g of clay in 733 mL of water and maintained under stirring for 24 h. In the $Cr_{1.0}$ series, the Cr polycation was prepared by basic hydrolysis of $Cr(NO_3)_3.9H_2O$ (NaOH solution), in which the relative amounts of OH^-/Cr^{3+} was 2.0, and by aging the solution at room temperature for 10 days, i.e. the protocol used by Brindley and Yamanaka (1979). Previously, the clay samples had been in suspension for 16 h. The Al^{3+} or Cr^{3+} concentration

in the final suspensions was 0.03 M, and the Al^{3+} or Cr^{3+}/clay ratio was 5.0 mmol.g^{-1}. The final suspensions were then centrifuged, introduced into dialysis bags, and washed by dialysis until chloride or nitrate anions were absent. At this point, the samples (suspensions of about 50 mL) were centrifuged and the resulting solids dried at 50 °C, thus providing the intercalated compounds. Their calcination at 200, 300, 400 and 500 ºC for 4 h, at a heating rate of 1 °C/min from room temperature up to the calcination temperatures, gave the corresponding pillared compounds. The polyoxometalate ion solutions were prepared from mixtures of the relevant amounts of $AlCl_3.6H_2O$ and $Cr(NO_3)_3.9H_2O$ in order to produce solutions with the following proportions of metallic cations: $Al_{0.7}Cr_{0.3}$, $Al_{0.5}Cr_{0.5}$ and $Al_{0.3}Cr_{0.7}$. These solutions were hydrolysed until a ratio OH/metal of 2 was reached, using NaOH solution (1 mol.dm^{-3}). The concentration of each solution was 0.25 mol.dm^{-3}. Mixing was performed at room temperature and the solutions were aged overnight at 330 K. Pillared clay samples were prepared using 10 g of the relevant clay and 300 cm^3 of polyoxometalate solution. A 5% suspension of clay was produced using double-distilled water (preswelling the clay at room temperature with overnight stirring) and the polyoxometalate solution was added dropwise at room temperature under vigorous stirring. Stirring was maintained for 8 h at 353K. The clay mineral samples were washed and calcined following the procedure described above. The relevant preparation data is summarised in Table 6.3.

The materials obtained were labelled as follows: **clay – PILAl$_x$Cr$_{1-x}$temperature**. For example, the samples labelled SD-PrePILAl$_{0.7}$Cr$_{0.3}$ and SD-PILAl$_{0.7}$Cr$_{0.3}$500 are SD clay intercalated with the species formed from a solution containing initially 70% of Al^{3+} ions and 30% of Cr^{3+} ions, before and after calcinating at 500ºC, respectively.

Besides using the 'conventional' pillaring techniques, two single metal oxide pillared SD materials (Al and Cr) were prepared, using the methods described by Katdare et al. (1997, 1999, 2000), for which the intercalation step was performed in ultrasonic conditions (important time reduction in the overall pillaring process). Typically, 5 g of clay were mixed

with 50 cm^3 of the relevant hydrolysed metal salt solution (typically 20 mequiv metal ion per gram of clay). The mixture was immediately submitted to ultrasonification (operating frequency 50 kHz) for 20 min at ambient temperature. The product was filtered, washed several times until the filtrate was free of chlorides or nitrates, then air dried at room temperature. The calcination of the materials obtained was performed under the same conditions described above. Samples were labelled SD-PILAIUS500 and SD-PILCrUS300 corresponding to the Al- and Cr-PILCs, respectively.

Table 6.3 PILC preparation data

| Catalyst | Pillaring solution | | | | Clay Suspension | Intercalation | | |
	Metal Salt	OH$^-$/Al^{3+}	Maturation	Vol., cm^3		Time	$C_{Al3+, Cr3+}$, M	$C_{Al3+,Cr3+}/m_{clay}$, mmol.g^{-1}
Al$_{1.0}$	AlCl$_3$.6H$_2$O	2.2	60ºC/2h r.t./12h	600	8 g/ 733 mL 16h	24h stir	0.03	5.0
Al$_{0.7}$Cr$_{0.3}$	AlCl$_3$.6H$_2$O Cr(NO$_3$)$_3$.9H$_2$O	2.0	60ºC/12h	---	10 g/200 mL 12h	8h Stir 80ºC	0.15	7.5
Al$_{0.5}$Cr$_{0.5}$	AlCl$_3$.6H$_2$O Cr(NO$_3$)$_3$.9H$_2$O	2.0	60ºC/12h	---	10 g/200 mL 12h	8h Stir 80ºC	0.15	7.5
Al$_{0.3}$Cr$_{0.7}$	AlCl$_3$.6H$_2$O Cr(NO$_3$)$_3$.9H$_2$O	2.0	60ºC/12h	---	10 g/200 mL 12h	8h Stir 80ºC	0.15	7.5
Cr$_{1.0}$	Cr(NO$_3$)$_3$.9H$_2$O	2.0	r.t./10 days	600	8 g/ 733 mL 16h	24h stir	0.03	5.0

The intercalating solutions were studied by visible spectroscopy. Chemical Composition (XRF), XRD, VT-DRIFTS, BET surface area analysis, thermal desorption of cyclohexylamine (CHA) and real time mass spectrometry of the evolved gases were used to evaluate the properties of the prepared catalysts.

6.3 RESULTS AND DISCUSSION

6.3.1 UV-VIS SPECTROSCOPY

It has been shown (Finholt *et al.*, 1981; Thompson and Connick, 1981; Stünzi and Marty, 1983; Spiccia *et al.*, 1987, 1988) that when adding OH⁻ to a solution of Cr^{3+}, the dimer $[Cr_2(OH)_2(H_2O)_8]^{4+}$, the trimer $[Cr_3(OH)_4(H_2O)_9]^{5+}$, the tetramers $[Cr_4(OH)_6(H_2O)_{11}]^{6+}$ and $[Cr_4(OH)_5O(H_2O)_{10}]^{5+}$ and eventually a pentameric and a hexameric polycation may coexist.

The Cr solution is initially blue, presenting two peaks in the visible spectrum at 408 and 576 nm. The hydrolysis of this solution makes it change to green with a concurrent shift of the absorption peaks to higher wavelength. The position of the two d-d band maxima and the ratio between their extinction coefficients provide information about the extent of polymerisation of the chromium species (Stünzi and Marty, 1983, Gil *et al.*, 1998) – cf. Table 6.4.

The spectroscopic data of the pillaring solutions used in this work (Table 6.5) are similar to those reported by Toranzo *et al.* (1997) and Gil *et al.* (1998), including the mixed metal solutions prepared using the methods described by Pálinkó *et al.* (1997). The results suggest that the trimeric form dominates the solutions with higher Cr content, whereas in the $Al_{0.7}Cr_{0.3}$ solution, chromium does not polymerise extensively. The mixed metal equimolar solution seems to produce a mixture of Cr trimeric and dimeric oligomers. Gil *et al.* (1998) explained these observations in terms of the amount of Al^{3+} present in the solution. This ion is a much harder acid than Cr^{3+} and exhibits a higher tendency to form hydroxyl bridged polynuclear species than Cr^{3+}. Additionally, the formation of Al_{13} polycations involves a greater number of OH⁻ groups than the formation of chromium polymeric cations (2.46 OH⁻ per aluminium ion and 1.0 and 1.33 OH⁻ per chromium ion for the dimer and trimer, respectively). Therefore, in a solution containing both Al^{3+} and Cr^{3+} cations, the former polymerises first and only when

the polymerisation of this cation is complete, does the polymerisation of chromium begin. In the $Al_{0.7}Cr_{0.3}$, solution, the large amount of Al^{3+} in the solution consumes a large fraction of the available hydroxyl groups preventing Cr^{3+} from polymerising to any significant extent. On the other hand, the $Al_{0.5}Cr_{0.5}$ solution provides enough hydroxyl groups to dimerise chromium, but does not permit further polymerisation of this cation.

Table 6.4 Relationship between the degree of polymerisation of chromium species and the position of the d-d maxima and the respective ratio between extinction coefficients (Stünzi and Marty, 1983)

Chromium oligomer	λ_1 / nm	λ_2 / nm	$\varepsilon_1/\varepsilon_2$
$[Cr(H_2O)_6]^{3+}$	408	575	1.17
$[Cr_2(OH)_2(H_2O)_8]^{4+}$	417	582	1.18
$[Cr_3(OH)_4(H_2O)_9]^{5+}$	425	584	1.60
$[Cr_4(OH)_6(H_2O)_{11}]^{6+}$ $[Cr_4(OH)_5O(H_2O)_{10}]^{5+}$	426	580	1.95
Hexamer	426	585	1.5-1.56

Table 6.5 Wavelength of maximum absorption in the visible spectra and the ratio between the extinction coefficients of the two peaks for chromium nitrate and the different Cr-intercalating solutions

Solution	λ_1 / nm	λ_2 / nm	$\varepsilon_1/\varepsilon_2$	Species present
$Cr(NO_3)_3.9H_2O$	408	575	1.17	Monomer
$Al_{0.7}Cr_{0.3}$	409	578	1.18	Monomer
$Al_{0.5}Cr_{0.5}$	415	580	1.25	Dimer
$Al_{0.3}Cr_{0.7}$	422	583	1.48	Trimer
$Cr_{1.0}$	421	582	1.49	Trimer

6.3.2 XRF ANALYSIS

The chemical composition data is presented in Figures 6.1 (SD series) and 6.2 (Sap series). For both smectites, important uptakes of aluminium and/or chromium are reported (e.g. in the case of aluminium, a maximum value of about 10% of Al_2O_3 was fixed).

It can be seen that in both series, the amount of aluminium fixed decreases and that of chromium fixed increases in line with the increasing Cr content of the pillaring solutions. The

amounts of Cr fixed for the $Al_{0.7}Cr_{0.3}$ pillared materials (Cr apparently does not polymerise – cf. previous section) may be attributed to its adsorption on the clay surface and on the Al_{13} pillars (Kiricsi *et al.*, 1997; Toranzo *et al.*, 1997).
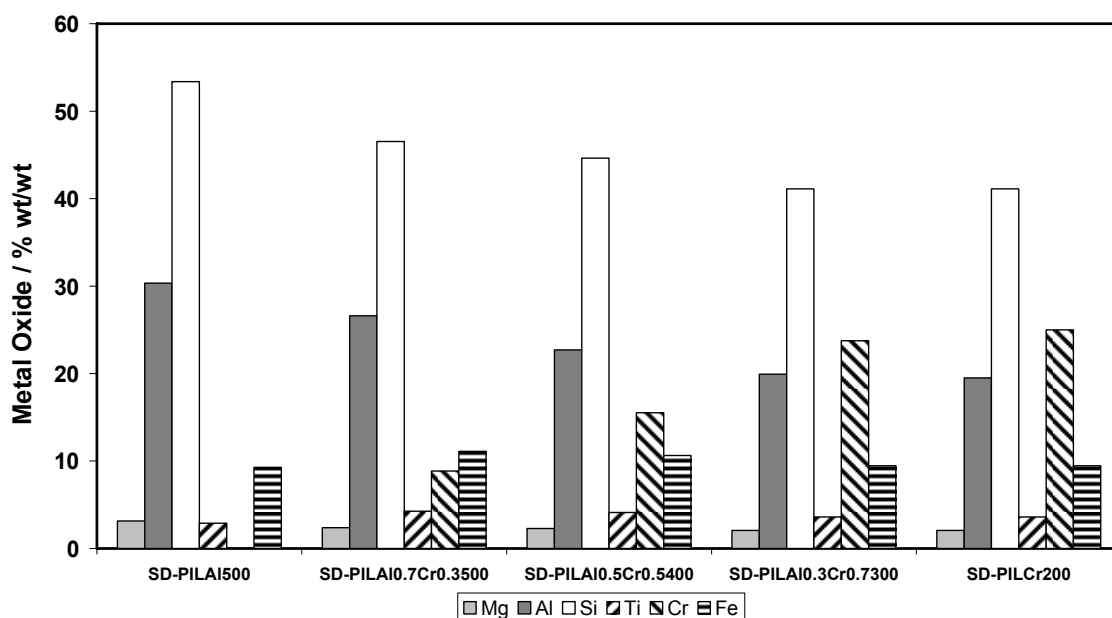
Figure 6.1 Chemical composition of SD pillared materials
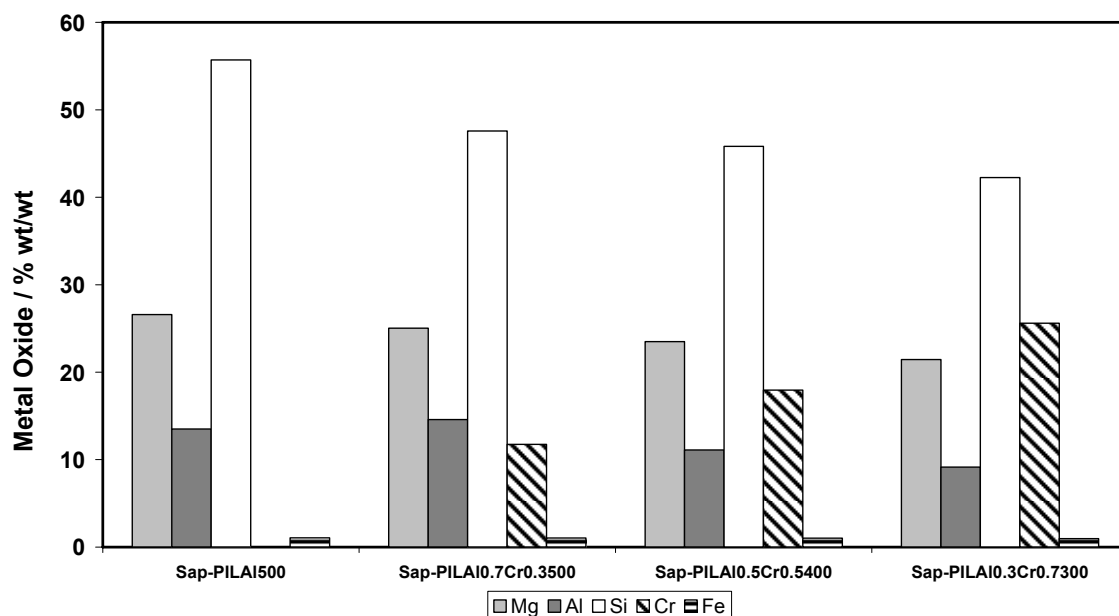
Figure 6.2 Chemical composition of Sap pillared materials

Single Cr oxide and $Al_{0.3}Cr_{0.7}$ pillared SD samples exhibit similar chemical compositions, which correlates well with the visible spectroscopy data reported in the previous section, which showed similar degrees of Cr polymerisation for the two pillaring solutions (cf. Table 6.5).

Figure 6.3 compares the chemical composition of the aluminium pillared SD clay using the conventional and the ultrasonic methods. It can be seen that Al incorporation is similar in both cases.
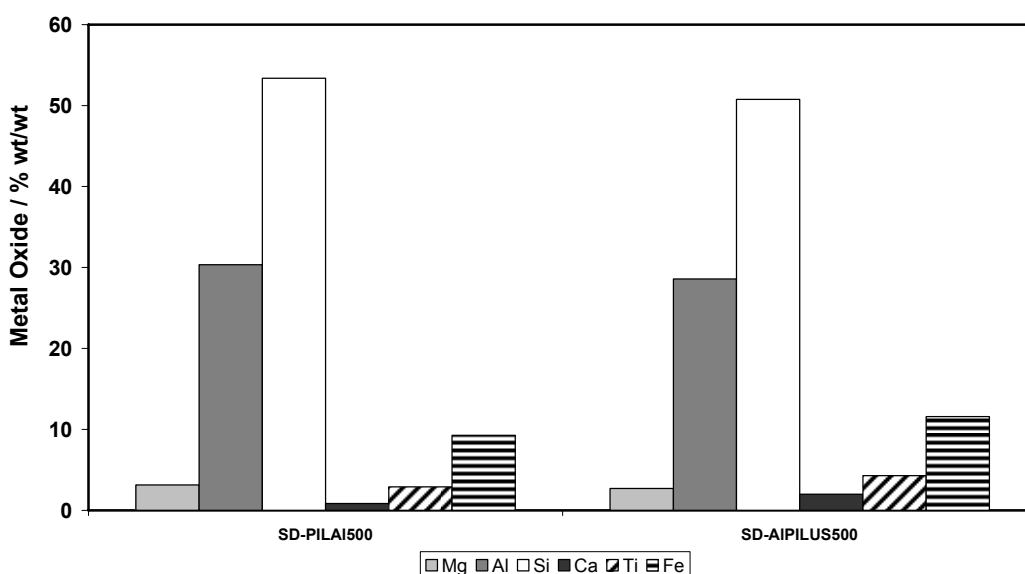
Figure 6.3 Chemical composition of conventional and ultrasound Al1.0 pillared SD

6.3.3 XRD ANALYSIS

The d_{001} values of unheated and calcined pillared materials are summarised in Table 6.6[26]. All unheated samples exhibit d spacing values comparable to other reported results (Brindley and Yamanaka, 1979; Bornholdt *et al.*, 1991; Toranzo *et al.*, 1997; Volzone, 2001) which indicate that the pillaring procedures were partially successful. However, all mixed metal unheated materials proved to be incompletely intercalated, as deduced by the presence of unresolved shoulder peaks at ca. 10 Å (ca. 8.80 $^o2\theta$, Figure 6.4).

---

[26] All XRD traces display a high scattering background, which can arise from poor ordering of the scatterers in the sample and clearly affects the determination of the exact position of the maxima.

Table 6.6 d spacing values of unheated and calcined intercalated materials

Sample	d_{001} (Å) (unheated)	d_{001} (Å) (calcined[27])
SD-PILAl500	18.6	17.8
SD- PIL $Al_{0.7}Cr_{0.3}$500*	18.9	17.0
SD- PIL $Al_{0.5}Cr_{0.5}$400*	19.5	16.2, 10.0
SD- PIL $Al_{0.3}Cr_{0.7}$300*	19.1	15.7
SD-PILCr200	17.8	16.8
Sap-PILAl500	18.7	17.3
Sap- PIL $Al_{0.7}Cr_{0.3}$500*	18.8	16.8
Sap- PIL $Al_{0.5}Cr_{0.5}$400*	18.2	16.0, 10.1
Sap- PIL $Al_{0.3}Cr_{0.7}$300*	18.3	16.0
Sap-PILCr200	18.2	16.1
SD-PILAlUS500	18.6	18.3
SD-PILCrUS300	18.1	17.3

* presence of an unresolved shoulder at ca. 10 Å
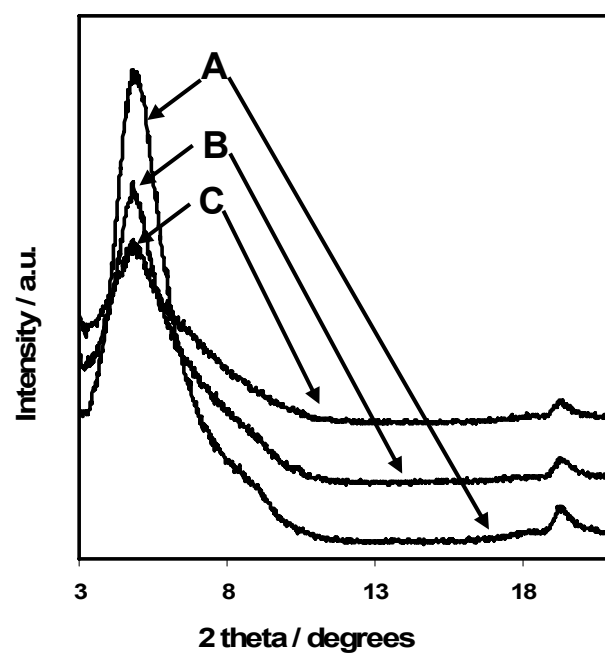
Figure 6. 4 XRD diffractograms of A: SD-PrePIL$Al_{0.7}Cr_{0.3}$, B: SD-PrePIL$Al_{0.5}Cr_{0.5}$ and SD-PrePIL$Al_{0.3}Cr_{0.7}$

---

[27] Indicated temperature

As expected, the basal spacing values decrease upon heating, but at the indicated temperatures (cf. sample labels – Table 6.6), the materials still exhibit an increased interlayer distance. However, the thermal stabilities of the pillared materials are dramatically different. It can be seen that the thermal stability of the intercalated materials decreases as the Cr content increases. $Al_{1.0}$ and $Al_{0.7}Cr_{0.3}$ are thermally stable up to, at least, 500 ºC, the materials prepared from the equimolar intercalating solution are partially stable at 400 ºC, whereas $Al_{0.3}Cr_{0.7}$ materials collapse above 300 ºC. The single Cr oxide pillared materials retain there two dimensional porous structure only up to 200 ºC.

SD generally produces materials with slightly higher d spacings than their saponite counterparts, a behaviour that has been observed before (Volzone, 2001).

The XRD data is consistent with the visible spectra data presented in Section 6.3.1. The Al-PILCs exhibit basal spacing values typical of smectites intercalated with the Al_{13} cation, whereas the Cr-PILCs exhibit basal spacing values consistent with the intercalation of trimeric Cr species, previously detected in solution. The d-spacing values and thermal stabilities exhibited by the mixed metal pillared materials (Figures 6.5 and 6.6) correlate with the presence of the Keggin ion ($Al_{0.7}Cr_{0.3}$ series), the Cr trimer ($Al_{0.3}Cr_{0.7}$ series) and a mixture of Al_{13} and Cr oligomers ($Al_{0.5}Cr_{0.5}$) series. The possible 'mixed character' of the later materials is reinforced by the presence of two d_{001} peaks (ca. 16.2 and 10.0 Å) in both $Al_{0.5}Cr_{0.5}$ materials after heating at 400 ºC, assigned to the thermally resistant Al_{13} pillar and the more fragile Cr pillar, respectively. When Cr is added in 'small' quantities to the Al_{13} oligomeric solution ($Al_{0.7}Cr_{0.3}$), the thermal stability of the pillared material is not severely affected (still stable up to, at least, 500 ºC), but the basal spacing values decrease when compared to their Al-pillared counterparts (Table 6.6).
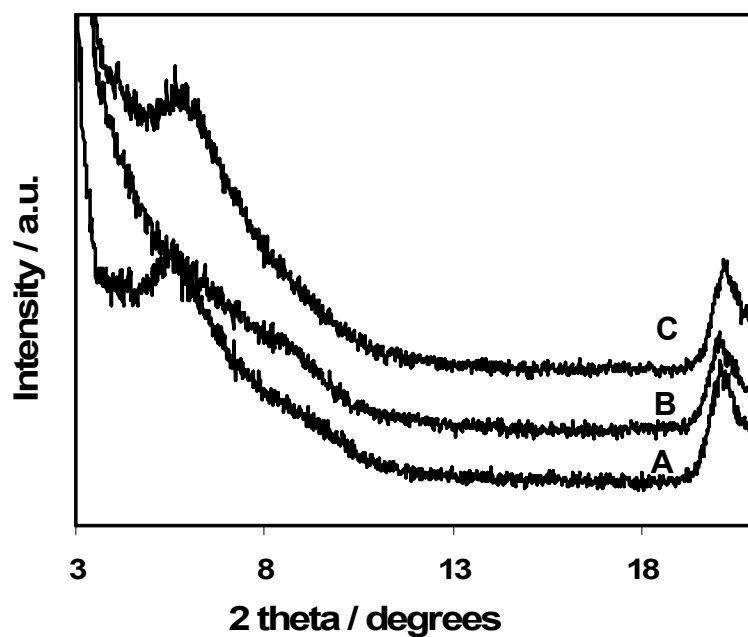
Figure 6.5 XRD diffractograms of A: SD-PILAl$_{0.7}$Cr$_{0.3}$500, B: SD-PILAl$_{0.5}$Cr$_{0.5}$400 and SD-PILAl$_{0.3}$Cr$_{0.7}$300
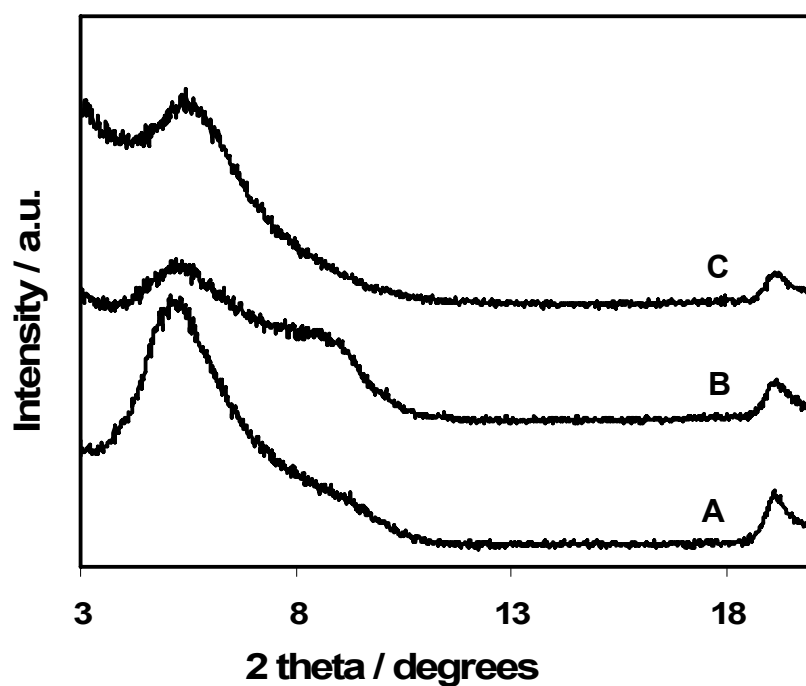
Figure 6.6 XRD diffractograms of A: Sap-PILAl$_{0.7}$Cr$_{0.3}$500, B: Sap-PILAl$_{0.5}$Cr$_{0.5}$400 and Sap-PILAl$_{0.3}$Cr$_{0.7}$300

According to Zhao *et al.* (1995) the presence of diffraction bands near d values of 2.67, 2.48 and 1.67 Å may be assigned to the presence of α-Cr$_2$O$_3$. All the materials with Cr/Al ≥ 1 submitted to calcination at 500 ºC exhibited these peaks, which is indicative of the

conversion of the Cr pillars. As anticipated, based on the previous sections, the chromium oxide peaks were absent from the $Al_{0.7}Cr_{0.3}$ PILCs diffractograms, reinforcing the idea of the absence of pure Cr pillars in these materials.

The samples intercalated ultrasonically seem to produce thermally more stable materials than their 'conventional' counterparts (Table 6.6). The ultrasonically prepared pillared Cr-SD material is stable up to 300 °C, which is a relevant increase when compared to the less resistant SD-PILCr200, which collapses above 200 °C (Figure 6.7). On the other hand, with the conditions used, complete Al oligomer intercalation does not occur[28], as demonstrated by the presence of a low d spacing value peak in the SD-PILAlUS500 diffractogram (Figure 6.8).
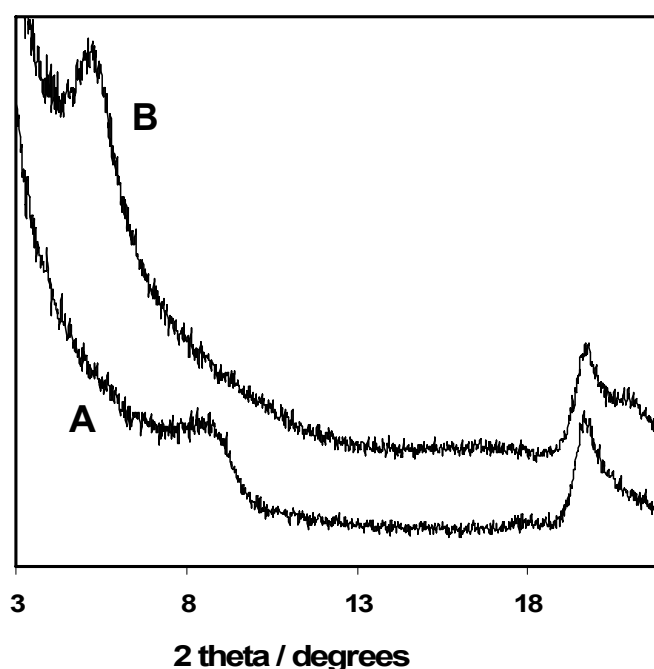
Figure 6.7 XRD diffractograms of A: SD-PILCr300 (collapsed structure) and B: SD-PILCrUS300

6.3.4 SURFACE AREA

Nitrogen adsorption-desorption isotherms of the pillared solids correspond to the type II of IUPAC classification, with a type H3 hysteresis loop in the same classification (Rouquerol *et*

---

[28] This problem can easily be resolved by employing longer sonication times or more concentrated pillaring solutions.

al., 1999), behaviour characteristic of samples with slit-shaped pores (Figure 6.9). The specific surface area of selected pillared solids was calculated by application of the BET method to these isotherms and the results obtained are summarised in Table 6.7.
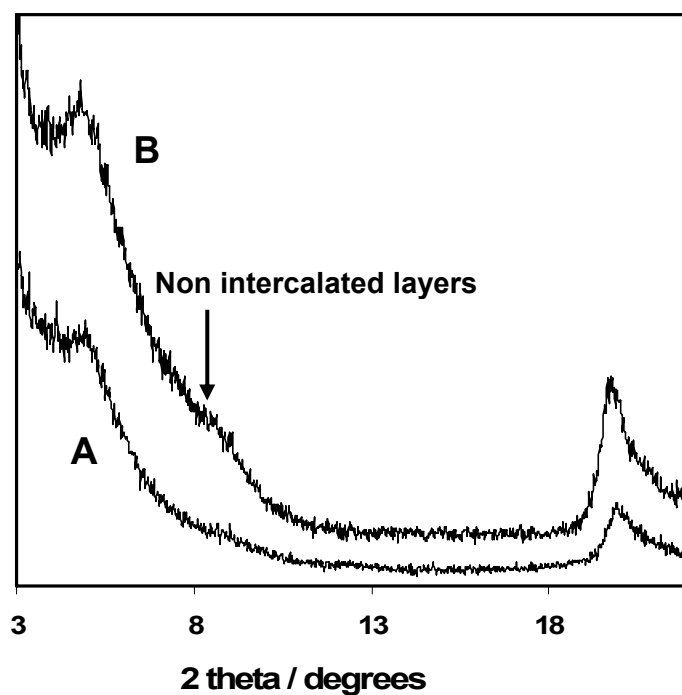
Figure 6.8 XRD diffractograms of A: SD-PILAl500 and B: SD-PILAlUS500
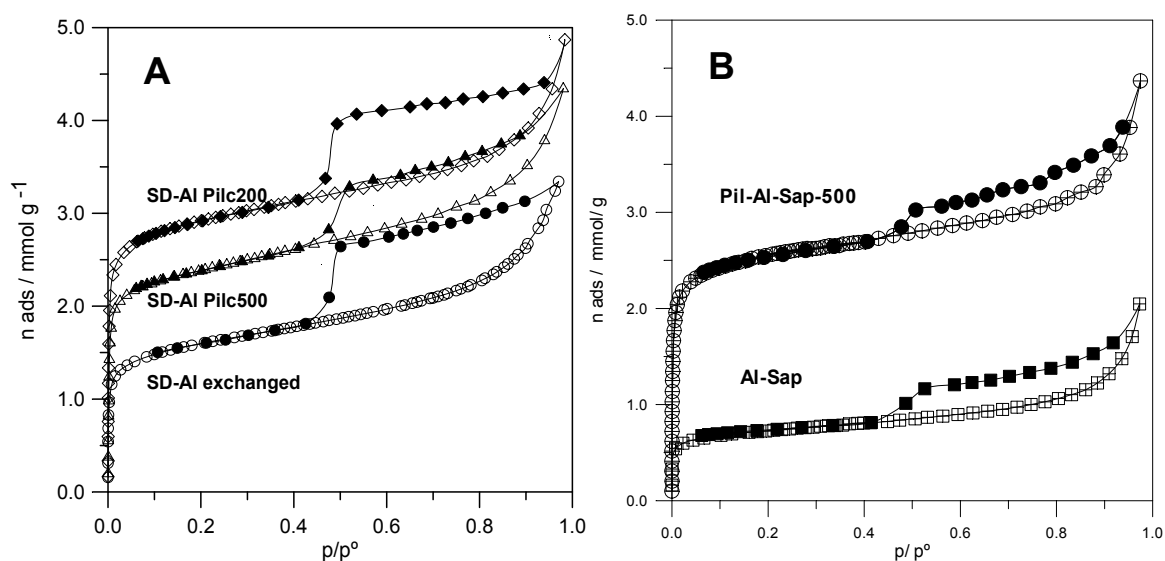
Figure 6.9 Nitrogen adsorption-desorption isotherms of A: Al-SD, SD-PILAl200 and SD-PILAl500 and B: Al-Sap and Sap-PILAl500

Table 6.7 BET surface area of selected pillared materials

PILC	BET surface area ($m^2.g^{-1}$)
Al-SD	130
SD-PILAl200	252
SD-PILAl500	202
SD-PILAl$_{0.7}$Cr$_{0.3}$500	184
SD-PILAl$_{0.5}$Cr$_{0.5}$400	176
SD-PILAl$_{0.3}$Cr$_{0.7}$300	172
SD-PILCr200	252
Al-Sap	60
Sap-PILAl500	216

BET surface areas of the pillared materials show that the procedures were successful in terms of effective increase of the accessible areas, although lower than would be expected for mixed oxide PILCs. These results are certainly related to the thermal stability of the materials, mainly in the case of SD-PILAl$_{50}$Cr$_{50}$400. The XRD trace showed a partial collapse of the pillared structure when the material was heated at 400 °C resulting in a smaller area accessible to the nitrogen molecules. The fact that intercalation was not complete in the mixed metal intercalated materials (cf. section 6.3.3) also affected the surface area values. Ageing of the materials could also result in a partial collapse of the structures (the nitrogen adsorption-desorption isotherms were obtained ca. 3 months after their preparation) (Chevalier *et al.*, 1994). The surface areas of the single oxide PILCs are comparable to those reported by Toranzo *et al.* (1997).

6.3.5 DRIFTS STUDIES

There is a general agreement that the Lewis acid sites of an Al pillared clay are located in the pillars, while the location of Brönsted sites is more controversial. It was proposed that Brönsted acid sites in the PILCs are dependent on the parent clay and are situated partly on the pillars and partly on the tetrahedral layer (Occelli and Tindwa, 1983; Occelli and Lester,

1985; Plee et al, 1985[b]; Tichit *et al.*, 1985; Poncelet and Schutz, 1986, Lambert and Poncelet, 1997).

The VT-DRIFTS spectra of SD-PILAl500 (Figure 6.10A) and SD-PILAl$_{50}$Cr$_{50}$400 (Figure 6.10B) exhibit diagnostic bands associated with Brönsted and Lewis acidity diagnostic bands, confirming the presence of both types of acidic sites in these materials.
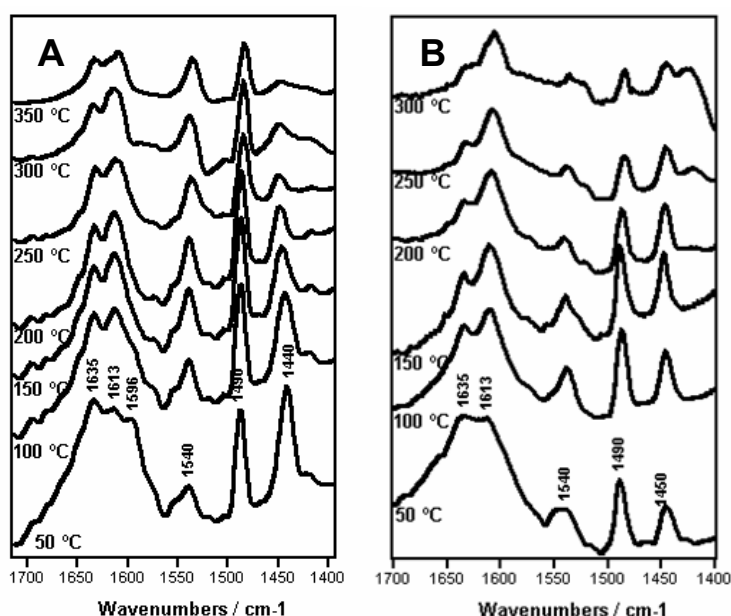
Figure 6.10 VT-DRIFTS spectra of A: SD-PILAl500 and B: SD-PILAl$_{0.5}$Cr$_{0.5}$400

As anticipated, the Lewis/Brönsted acid ratio is higher on the mixed pillared material than on the Al-PILC, due to the higher inherent Lewis acidity of Cr. It can also be seen that even at 350ºC, SD-PILAl500 still retains important amounts of pyridine bound to Brönsted acidic sites, whereas the mixed pillared material has lost most of the Brönsted bonded pyridine at 300ºC. It was previously suggested that both Al$_{13}$ and Cr oligomeric pillars populate the SD-PILAl$_{0.5}$Cr$_{0.5}$400 material. The DRIFTS results agree with this proposition, because although the number of Brönsted sites seems to be inferior in the mixed metal PILC (intensity ratio), their strength is similar to the Brönsted acidic sites of the Al-PILC (stable up to 350 ºC). However, definitive conclusions cannot be drawn because of the possible contribution from

the inherent Brönsted acidity in the parent clay (cf. DRIFTS studies, Chapter 4). The opposite trend is observed for Lewis bound pyridine. The results obtained with the saponite-based equivalents are similar to those presented here for the Serra de Dentro bentonite.

6.3.6 TG-MS Studies

Representative MS ion chromatograms are presented in Figure 6.11. The behaviour of the Al pillared bentonite and saponite are quite distinct. The saponite clearly desorbs more untransformed CHA than the bentonitic counterpart and the ratios of transformed products released are significantly different, except for the CH/CHD ratios that are similar for both clays. The CH/B and CH/A ratios are higher on the pillared saponite. This result shows that most of the transformed CHA is released as CH, produced by the deamination reaction, and suggests the absence of a significant number of dehydrogenation sites on the saponite. Another important difference is the presence of a high temperature peak (ca. 500 ºC) of untransformed CHA in the chromatogram of Sap-PILAl500. This peak does not appear in the trace for SD-PILAl500. The desorption of aniline from SD PILC exhibits several maxima, which are more intense than that for CHD[29], which suggests the presence of a significant amount of dehydrogenation sites. Aniline is released under a single peak when desorbed from Sap-PILAl500. Both these findings, together with the TG-MS data presented in previous chapters, reflects the existence of a significant number of dehydrogenation sites on the bentonitic material. The ion chromatograms of Cr pillared SD are quite similar to the Al counterpart chromatograms, revealing the release of appreciable amounts of dehydrogenation products. It is interesting to note that an inversion of the relative maximum intensities of B and CHD occurred, which reflects, probably, different strengths of the active sites.

---

[29] This does not mean that more aniline than CHD is produced, because there is no cross relationship between peak intensities and the amounts of different released products.
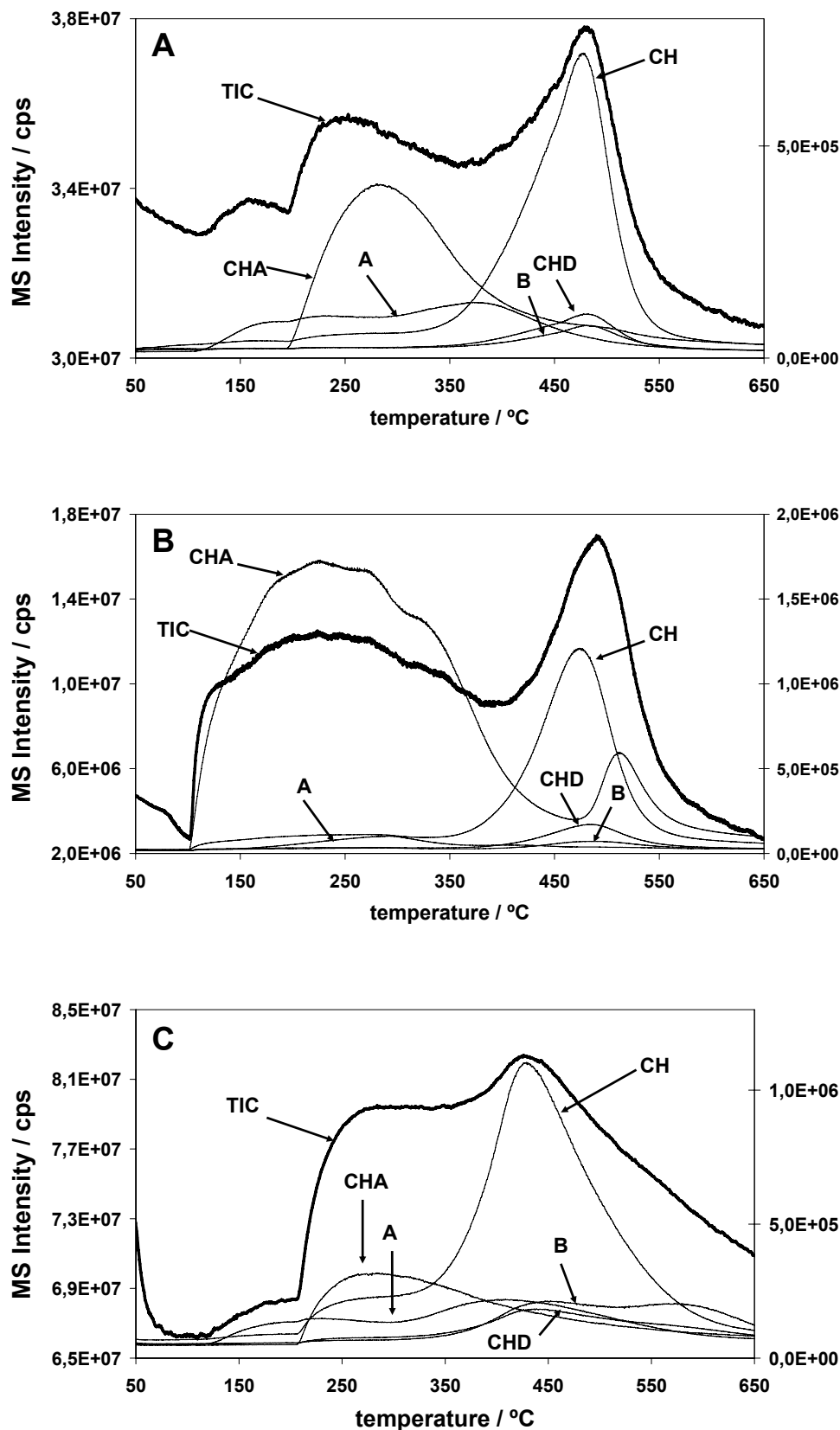
Figure 6.11 Real time MS ion chromatograms for the desorption of CHA (m/z = 56), CH (m/z = 54), CHD (m/z = 77), B (m/z = 78) and aniline (m/z = 93) from A. SD-PILAl500, B. Sap-AlPIL500 and C. SD-PILCr200 after a 7 day incubation period with CHA

The wide range of temperatures at which aniline is released from Al pillared SD, opposed to the narrow range, low temperature maximum observed for Sap-PILAl500 may be a reflection of the slightly lower basal spacing and surface area of the former, which create more hindrance to the release of the moderately bulky aniline molecules.

6.3.7 THERMOGRAVIMETRIC STUDIES

The acidity values obtained by thermal desorption of CHA saturated PILCs are resumed in Table 6.8. The first feature that arises from these values is the big difference of acidities obtained for the ion exchanged materials (ca. 1.3 mmol $CHA.g^{-1}$) and the pillared materials (ca. 0.6 mmol $CHA.g^{-1}$). The lower values for the pillared samples probably reflects the fact that a proportion of the protons produced in the firing process enter the aluminosilicate sheet and cannot be coerced back into the gallery even by a base as strong as ammonia (Purnell, 1991).

Table 6.8 Quantities of CHA desorbed in the 280 and 440 ºC temperature interval

Material	CHA desorbed / mmol g^{-1}
AlSD	1.35
CrSD	1.33
SD-PILAl500	0.60
SD-PILAl$_{0.7}$Cr$_{0.3}$500	0.58
SD-PILAl$_{0.5}$Cr$_{0.5}$400	0.60
SD-PILAl$_{0.3}$Cr$_{0.7}$300	0.63
SD-PILCr200	0.66
Sap-PILAl500	0.82
Sap-PILAl$_{0.7}$Cr$_{0.3}$500	0.78
Sap-PILAl$_{0.5}$Cr$_{0.5}$400	0.66
Sap-PILAl$_{0.3}$Cr$_{0.7}$300	0.58
Sap-PILCr200	0.62
SD-PILAlUS500	0.63
SD-PILCrUS300	0.64

Another interesting feature is that the total acidity decreases with increasing Cr content in the pillared saponite series, whereas for the SD PILCs the values are very similar, and no effective trend can be identified, given the experimental error range. The reasons for this behaviour are not clearly understood.

In terms of acidity, the 'conventional' PILC and its sonicated counterpart exhibit similar values.

6.3.8 CATALYTIC TESTS

Initially, the catalytic tests were performed at 150ºC, following activation of the PILCs at the same temperature. Under these conditions (data not shown), the materials exhibited very poor catalytic activity, except for the Al-PILCs which converted about 50% limonene after 2 hours of reaction time. The reaction and activation temperatures were raised up to 170 ºC (close to the boiling point of limonene) in order to improve the catalytic activities of the catalysts. Figures 6.12A (15 minutes reaction time) and 6.12B (2 h reaction time) summarise the catalytic results obtained for the SD series and Figure 6.12C (2 h reaction time) the results for the pillared saponite samples. For comparison purposes, the previously presented results obtained for Al- and Cr-SD (cf. Chapter 4) are reprinted in Figure 6.12A (reaction temperature: 150 ºC; activation temperature 150 ºC).

The product distribution profiles during the conversion of limonene at a reaction temperature of 170 ºC using PILCs are apparently similar in shape to the results presented for ion-exchanged (Figure 4.5, Chapter 4) and acid activated (Figure 5.12, Chapter 5) catalysts, but the reaction mixture compositions are significantly different, when PILCs and ion-exchanged clays are compared and between the PILCs obtained from two different parent materials. This issue will receive further discussion below. The reaction rate, however, is noticeably slower for all PILCs when compared to Al-SD, at 150 ºC, which may be partially explained by the fact that, although the pillared materials exhibited both Brönsted and Lewis acidities (Section 6.3.5), the total acidity (CHA thermal desorption data – cf. Section 6.3.7) was lower than for Al- and Cr-exchanged SD.
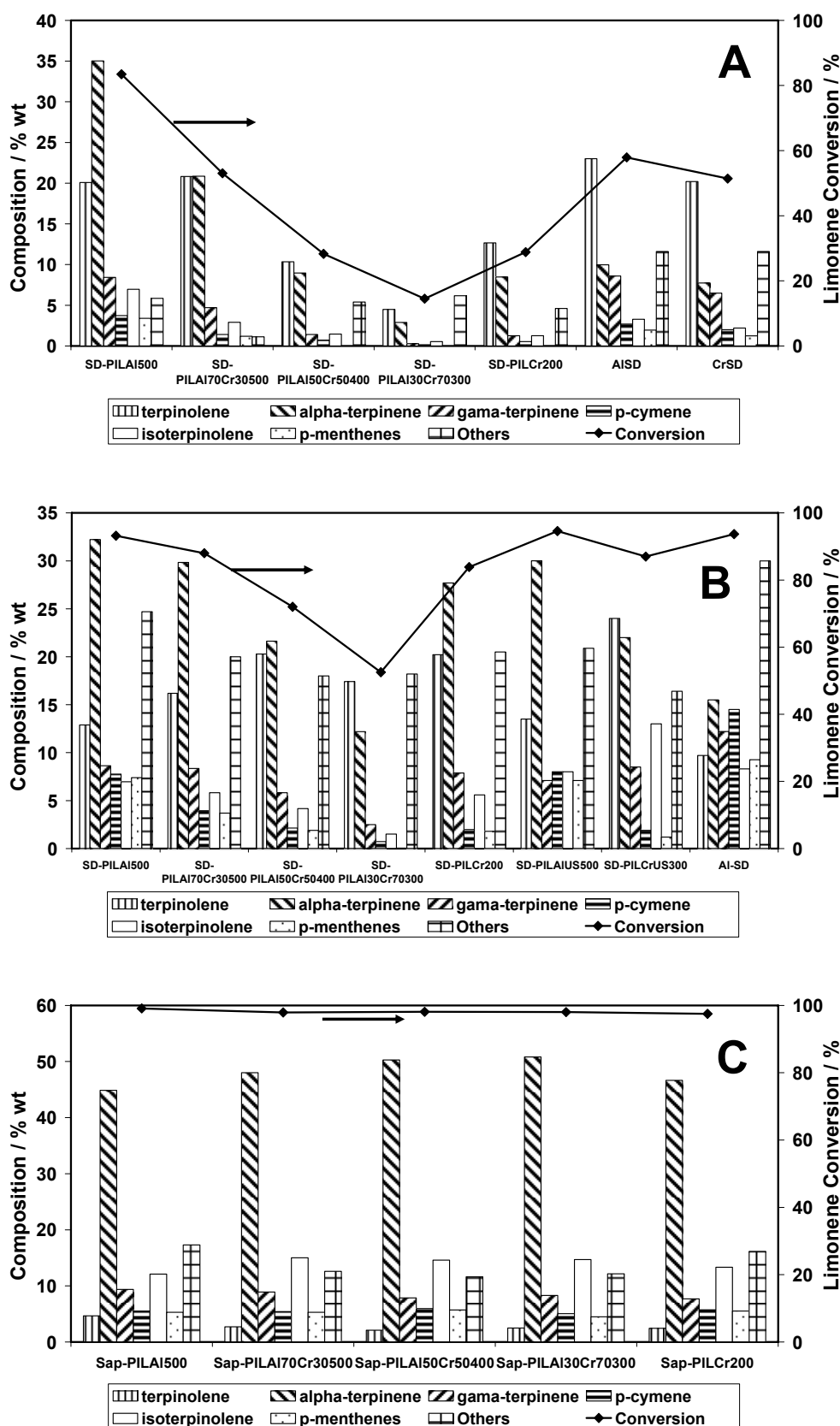
Figure 6.12 Distribution of products over SD pillared materials after A. 15 minutes and B. 2h reaction times and C. SapCa-1 pillared materials after 2 h reaction time, at 170 ºC. The pillared clays were pre-treated at 170 ºC for 2 hr prior to their use in the reaction. The results presented previously (Chapter 4) for AlSD and CrSD are repeated in Figure 6.12A for comparison purposes (reaction temperature: 150 ºC; activation temperature 150 ºC)

In the 15 min reaction time series, it can be seen that the activities (limonene conversion) of the SD based PILCs (Figure 6.12A) decreases with increasing chromium content, with the noticeable exception of the single Cr oxide PILC, the activity of this material surpassing the activity of its $Al_{0.3}Cr_{0.7}$ counterpart. However, besides SD-PILAl500, all the other materials are still in stage I of the reaction (steep decrease in limonene concentration and formation of the main reaction intermediates). After 15 minutes, the Al-pillared material has entered stage II of the reaction. The catalytic results after 2h reaction time (Figure 6.12B) show that only the single oxide aluminium PILC and the $Al_{0.7}Cr_{0.3}$ PILC have entered stage III of the reaction (> 90% limonene conversion), despite not having produced as much p-cymene and polymers as Al-SD. The reaction rate decreased with increasing Cr content of the catalysts, with the repeated exception of the single Cr pillared material. Besides poorer activity than the other modified materials, the pillaring procedures did not produce materials with added value in terms of preventing formation of polymers nor increased selectivity towards p-cymene. The activity decrease with increasing Cr content cannot be explained based upon the available total acidity data (cf. Section 6.3.7), which was similar for all SD pillared materials. However, Al-PILC exhibited stronger Brönsted acidic sites than the mixed metal PILCs (VT-DRIFTS data – Section 6.3.5). In this case, besides total and specific acidities, the accessibility to the active sites may be an important issue. In fact, single Al and Cr SD-pillared materials exhibit higher surface areas and basal spacings than the mixed pillared materials, which partially corroborates with the activity variation trend. The fact that SD-PILAl$_{0.5}$Cr$_{0.5}$400, despite presenting partial structural collapse (cf. Figure 6.4, Section 6.3.3), is still more active than SD-PILAl$_{0.3}$Cr$_{0.7}$300 (fully expanded) indicates that part of the catalytic processes may occur outside the clay galleries or that the acidity of the 'few' Al_{13} pillars present in the $Al_{0.5}Cr_{0.5}$ derived material are catalytically more active than the 'pure' Cr pillars of SD-$Al_{0.3}Cr_{0.7}$300. Following the same path, it is possible to explain the higher catalytic activity of SD-PILCr200, when compared to the $Al_{0.3}Cr_{0.7}$ counterpart: the pillar composition of these two materials is similar, but the accessible area of the single metal PILC is higher than for the mixed metal

PILC. The bulkiness of the different pillars may also affect the accessibility of the reactant molecules to the interlayer active sites. These results show that total acidity, nature of acidity and accessibility to the active sites play equally important roles in this particular reaction.

The saponite based pillared catalysts (Figure 6.12C) proved to be more active than the SD based catalysts, when evaluated exclusively from limonene conversion data. All pillared saponite catalysts converted almost all the limonene, after two hours of reaction with a marked selectivity towards α-terpinene. Unfortunately, this increased activity was not reflected in better selectivity for p-cymene, although the amounts of polymerisation products formed are lower for these materials. The different intercalation solutions used for pillaring the saponite did not produce materials with markedly different catalytic behaviours neither in terms of activity nor selectivity. The reasons for this homogeneous behaviour are not clear, but may be related to a shorter time stability of the saponite pillared materials (unlikely, because major structural collapse would render these materials almost inactive) or to structural features of the saponite clay layer (e.g. absence of transition metals). The TG-MS data (section 6.3.6) showed that, although Sap-PILAl500 released a clearly higher amount of decomposition products than its SD counterpart, the amount of B and CHD produced was relatively low, indicating the absence of a significant number of dehydrogenation sites. This behaviour is qualitatively reproduced in the catalytic results, where the 'very' active saponitic materials, produce relatively low amounts of p-cymene, the aromatisation product.

Figure 6.13 represents the relationship between the amounts of p-cymene produced and the degree of limonene conversion for three general types of modified clays: the ion-exchanged materials (cf. Chapter 4) and the pillared saponite and bentonite materials. It becomes clear that three types of catalytic behaviour are present after stage I of the reaction has been completed. The saponite pillared materials (highlighted in Figure 6.13) reached a similar stage in the reaction, in which the final composition clearly differs from the final stages over both the ion-exchanged and pillared SD materials. The amount of p-cymene produced in the

saponite catalysed reactions is clearly inferior, indicating the lack of a substantial number of dehydrogenation sites. On the other hand, the content of isomerisation products is relatively high (Figure 6.12C), which indicates the presence of substantial isomerisation (probably Brönsted) sites. With regard to the SD based materials, the behaviour of the ion-exchanged and pillared materials is also markedly different, at least during stages II (limonene conversion between 70 and 90%) and III (limonene conversion > 90%) of the reaction. It is interesting to note that also the SD PILCs are less selective towards p-cymene than the ion-exchanged counterparts. Apparently, the pillaring process removes some of the sites that promote the aromatisation of limonene or the partial loss of Brönsted acidity upon calcination exerts a negative influence on the catalytic behaviour of the PILCs.
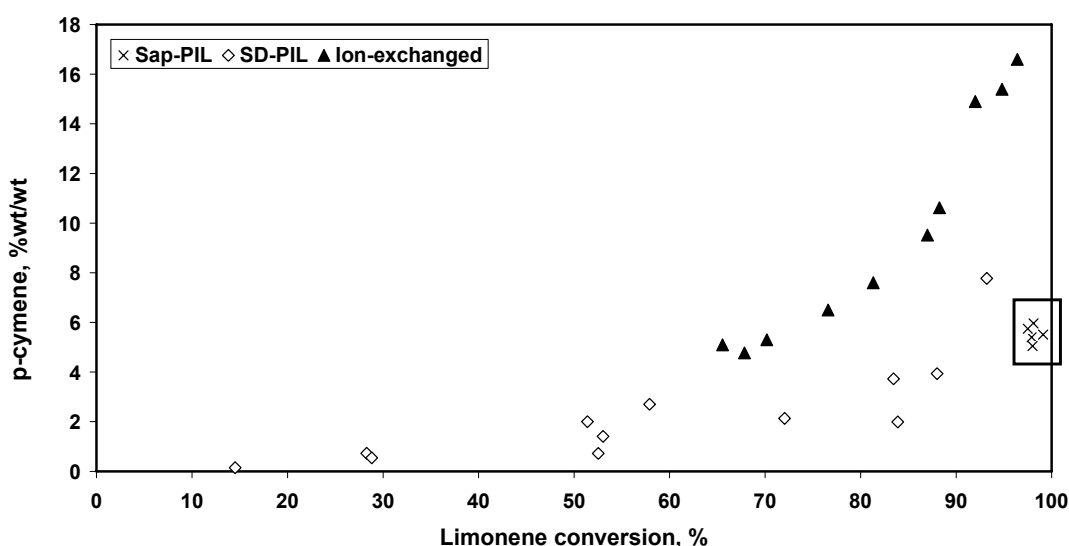
Figure 6.13 p-Cymene content in the final mixture over pillared and ion-exchanged clays presented as a function of limonene conversion. The pillared materials are grouped in series based on the parent material and not on the nature of the intercalating solutions

The catalytic results obtained for the PILCs prepared using ultrasound are presented in Figure 6.12B. The catalytic behaviours of these materials do not differ substantially from the conventional PILCs. However, the tendency to produce polymers seems to be slightly lower for the US PILCs. No increased selectivity towards p-cymene was detected. It is worth to recall that the ultrasound Cr intercalated material was thermally stable up to 300 ºC (compared to the conventional Cr-PILC which was collapsed at this temperature) and that

SD-AlPILUS500, although incompletely pillared, exhibited a higher basal spacing than its non-sonicated counterpart. These features (increased thermal stability and better structural organisation) may be the key issues behind the slightly better behaviour of the US PILCs in terms of the lower amounts of polymers formed.

6.4 FINAL COMMENTS

In this chapter, the chemical, structural, textural and catalytic properties of Al and/or Cr PILCs were described, intercalated via conventional and ultrasounds procedures. Two parent materials were used. Some important characterisation data is absent (e.g. determination of surface areas of the remaining saponite pillared materials or more extensive acidity measurements) due to problems associated with instrumentation operationally and availability, which hindered a more complete interpretation of the catalytic results. However, it was possible to draw some important conclusions from the available characterisation results.

XRD, XRF and N_2 adsorption-desorption data proved that both types of pillaring procedures were successful. All materials exhibited important uptakes of Al and/or Cr and increased basal spacings and surface areas, when compared to the unpillared parent clays. The thermal stability of the materials decreases with increasing Cr content of the intercalating solutions. Al- and $Al_{0.7}Cr_{0.3}$-pillared materials are stable up to 500 ºC, $Al_{0.5}Cr_{0.5}$-PILCs partially collapse at 400ºC and the $Al_{0.3}Cr_{0.7}$- and Cr-pillared materials are stable up to 300 and 200ºC, respectively. SD-PILAlUS500 exhibits a higher basal spacing than the conventional Al pillared material, although intercalation was incomplete. SD-PILCrUS300 proved to be thermally more stable than the SD-PILCr200 material.

The overall acidity of the PILCs is significantly lower than the ion-exchanged materials, although VT-DRIFTS data provided evidence of the existence of both Brönsted and Lewis acidic sites. Increasing Cr contents increased the Lewis to Brönsted acid sites ratio. SD-

pillared materials did not exhibit major acidity differences when prepared using different intercalating solutions, whereas for the saponite based PILCs, the total acidity decreased with increasing Cr content, with the exception of the Cr PILC.

Different decomposition profiles in terms of relative amounts of dehydrogenation and isomerisation products (TG-MS data of CHA saturated materials) were registered for different parent clay based materials and different intercalating solutions. Saponitic materials produced smaller amounts of dehydrogenation products than their SD counterparts.

Catalytically, the PILCs were less active than their ion-exchanged counterparts, at the same reaction temperature. Increasing the reaction temperature from 150 ºC to 170 ºC increased the activity of all the PILCs. The activity of SD-PILAl500 at this temperature was similar to Al-SD. The activity and selectivity towards p-cymene decreases with increasing Cr content (with a slight inversion for the Cr PILC) when SD based catalysts are considered. All the pillared saponites exhibited similar catalytic behaviour in terms of activities and selectivities. The relative amounts of reaction products produced by PILCs and ion-exchanged materials differ appreciably, namely in terms of selectivity towards p-cymene. The catalytic behaviour of pillared SD and SapCa-1 based materials is also significantly different.

CHAPTER 7. CONCLUSIONS AND PERSPECTIVES

7. CONCLUSIONS AND PERSPECTIVES

The development and implementation of environmentally friendly industrial processes is one of the major priorities in the field of catalysis science. In this work, indigenous clay based catalysts were prepared, characterised and tested in the limonene aromatisation reaction, a good example of gaining value from renewable feedstocks.

The parent clay used for the catalyst preparation originates from Serra de Dentro, Porto Santo Island. The choice of this particular material was based on purity, availability and compositional criteria, following the collection and characterisation of several bentonites from different Porto Santo deposits.

The major component in the SD bentonite is an Al rich dioctahedral smectite, with partial isomorphic substitution of Al by Mg and Fe and Si by Al or Fe in the octahedral and tetrahedral sheets, respectively. Anatase, kaolin, quartz, plagioclase and apatite are the main contaminants; they account for ca. 8-10% of the bentonite composition. Iron is present in both the clay mineral structure and external phases. A CEC value of ca. 80 meq.$(100 \text{ g})^{-1}$ and a BET surface area of 130 $m^2.g^{-1}$ were experimentally obtained for the sodium homoionic form of the SD material (NaSD). In terms of acidity, infrared spectroscopy of adsorbed pyridine on NaSD revealed the presence of acidic sites on the materials surface, Lewis and Brönsted in nature.

Three general types of modification were performed on NaSD. Ion exchange with selected cations was used to produce materials with specific Brönsted and/or Lewis acidic properties. Acid activation aimed to produce materials with a) increased acidity and b) increased exposed surface area. Finally, pillaring procedures were performed to obtain catalysts with better accessibility to the interlayer galleries and enhanced/modified acidity due to the

presence of different active sites in the Al and/or Cr pillars. Selected catalysts were prepared using either reference or commercially available clays for comparison purposes.

7.1 MODIFIED CLAYS: CHARACTERISATION

7.1.1 ION EXCHANGED CLAYS

Besides the Na-exchanged material, Al-, Ni- and Cr-exchanged catalysts were prepared. The first two are considered model Brönsted and Lewis acid catalysts, respectively, whereas the latter exhibits both types of acidity. A second set of catalysts was prepared using SAz-1 as the parent material. The choice was based on the following criteria: i) 'normal' surface area, ii) low amount of structural iron and iii) high CEC, i.e. property values that differ significantly from those of the SD material.

The acidity data (CHA thermal desorption method) obtained from these materials showed that the SAz-1 based materials were more acidic than the SD counterparts (in direct correlation with the difference in CEC values), with the noticeable exception of the Na-exchanged forms. As anticipated, NaSAz exhibited very low acidity, whereas NaSD desorbed much more CHA than normally expected for a Na-exchanged clay. Adsorbed pyridine spectroscopic data demonstrated that the intended types of acidity were present in the Al- (mainly Brönsted), Ni- (mainly Lewis) and Cr-(both Brönsted and Lewis) exchanged clays. TG-MS data obtained from CHA saturated clays proved the existence of more dehydrogenation sites on SD than on SAz, which was attributed to the existence of structural iron in the octahedral sheets of the former.

7.1.2 ACID ACTIVATED CLAYS

Three main variables were considered for the acid treatments applied to the parent material: temperature, acid concentration and contact time. The acid treatments that involved low concentration solutions, performed at room temperature produced materials in the H^+-

homoionic form, whereas more aggressive conditions produced materials with enhanced surface areas.

For SD based materials, even the harshest treatment did not completely destroy the clay structure. SAz-1 (used as a reference clay, together with the commercially available K10) proved to be more susceptible to acid treatment than the SD counterparts, when the same conditions were used, a consequence of its higher Mg content.

The surface area evolution of the acid activated SD materials followed the trend reported in the literature. In a first stage, the surface area gradually increased with increasingly higher acid concentrations, longer contact times and higher temperatures until it reached a maximum (ca. 500 $m^2.g^{-1}$ for SD-4M-95-30). On prolonged acid treatment, the fragile silica structure remaining after dissolution of soluble lattice metal ions gradually collapsed, and the surface area fell.

Acidity measurements showed that the estimated acidity values decreased as the severity of the acid treatment increased. This is a direct consequence of the depletion of the octahedral sheet and the attendant drop in the CEC caused by the acid leaching treatments. TG-MS data corroborated these observations, the quantity of all CHA decomposition products diminishing with progressive octahedral depopulation.

7.1.3 PILLARED CLAYS

Pillared clays (including SapCa-1 based materials) were prepared from Al-, Cr- and mixed Al/Cr pillaring solutions. The intercalation step was performed by conventional means and employing ultrasound.

The Cr-containing intercalation solutions were analysed by visible spectroscopy. The solution with the highest Al/Cr ratio did not provide evidence of the presence of oligomerised Cr, whereas in the cases of the solution with lowest Al/Cr ratio and the pure Cr solution, the trimeric form of Cr seems to dominate. The equimolar solution produced a mixture of dimeric and trimeric Cr species.

PILCs characterisation data proved the intercalation procedure was partially successful: although the basal spacing reached values typical of intercalated smectites, some evidence of non intercalated layers was present. Thermal stabilities tended to decrease with increasing Cr content. Surface areas of the single metal PILCs are comparable to literature data, but the surface areas of the mixed metal PILCs was lower than would be normally anticipated.

In terms of acidity, both Lewis and Brönsted sites were detected in the pillared materials, although the relative ratios exhibited important differences. Lewis-to-Brönsted acid sites ratio is higher on the mixed metal PILCs than on Al-PILC. Total acidity values for all PILCs were clearly lower than the ion exchanged counterparts. No direct correlation was obtained between pillar composition and acidity values.

TG-MS data of the pillared saponites and bentonites showed differences in terms of the total amounts of desorbed CHA decomposition products, but the relative ratios of dehydrogenated -to-non dehydrogenated products released by the SD-PILCs is clearly higher than for the saponite counterparts.

Ultrasonication significantly reduced the time needed to prepare the PILCs. The Cr-PILC exhibited better thermal stability than its conventional counterpart, but incomplete intercalation was observed for the US Al-PILC. No major differences were observed either in terms of acidity or in catalytic performance.

7.2 CATALYTIC RESULTS

7.2.1 LIMONENE CONVERSION

Regardless of the catalyst used, three competitive reactions took place during the limonene conversion experiments: isomerisation, disproportionation and polymerisation. Furthermore, in most cases, three reaction stages were identified, based on the degree of transformed limonene and the relative amounts of p-menthadienes:

i) stage I (up to 70 % limonene conversion): steep decrease in limonene concentration accompanied by the production of the main reaction intermediates (terpinolene, α-terpinene, γ-terpinene and isoterpinolene). The end of this stage is marked by the maximum amount of terpinolene produced.

ii) stage II (up to 90 % limonene conversion): terpinolene consumption follows zero-order kinetics, and the concentrations of α-terpinene and γ-terpinene remain essentially constant.

iii) stage III (above 90 % limonene conversion): the content of all dienes in the mixture decreased continuously, until their complete disappearance.

Both disproportionation and polymerisation processes begin during stage I and the yields of p-cymene, menthenes and polymeric species kept increasing throughout stages II and III. The relative amounts of p-cymene and menthenes was similar in the initial reaction stage, but at the end of the reaction the amount of the former surpassed that of the latter, suggesting that besides disproportionation, an additional oxidation mechanism was involved, promoted by Lewis acid sites. Polymerisation clearly dominated the third stage (60 % at the end of the reaction). The maximum content in dienes with conjugated double bonds in this

stage favoured their condensation via a Diels-Alders process, although a radical cation mechanism may also be involved.

7.2.2 CATALYSTS

The catalytic results obtained in this work showed that four major factors influence both activity and selectivity towards p-cymene: total acidity, accessibility to the acid sites, nature of the acid sites and existence of dehydrogenation sites (e.g. structural iron).

7.2.2.1 ACTIVITY: LIMONENE CONVERSION

All SD catalysts proved to be active in the limonene aromatisation reaction, although the degree of activity was strongly dependent on the type of modification produced on the parent bentonitic material. In terms of activity, the catalysts may be roughly ordered as: AAC >> IEC > PILCs > NaSD. For example, complete limonene conversion was achieved after 6 minutes at 80ºC using SD-3M-95-30, whereas when AlSD was used, more than 180 minutes were necessary to convert all the limonene at 150 ºC. PILCs, on the other hand, proved to be rather inactive in this particular reaction. Comparable results to those provided by IEC were obtained after increasing the reaction temperature to 170 ºC.

Limonene is a non polar molecule and can only react on sites that exist at the periphery of the gallery or on the external surface of the clay. Ion exchanged SD catalysts, despite providing lower acidity values than the SAz-1 equivalents, exhibit high surface areas (measured from N_2 – non polar molecule – adsorption isotherms) and therefore, more acid sites are available to the non-swelling reactant. This feature justifies the dramatically reduced activity of ion-exchanged SAz-1 catalysts when compared to the SD counterparts. The importance of site accessibility for reactions in non-polar media is further demonstrated when the SD based AACs were used. As the depopulation of the octahedral sheets increased, the activity of the catalyst also increased, in parallel to the increase in surface area. Although the

total acidity values decreased from sample to sample, the number of sites made accessible to limonene increased and hence enhanced activity was observed. The reduced activity of the PILCs may be attributed to two factors: i) low total acidity when compared to IEC and ii) hindered access to the active sites in the galleries and pillars. The reduced acidity values probably reflect the fact that a proportion of the protons produced in the firing process enter the aluminosilicate sheet. Despite presenting low acidity values when compared to their IEC counterparts, the PILCs exhibit similar acidity values to some of the AACs and larger interlayer spacing (and consequently, surface area) than the IEC. However, it is possible that the presence of bulky pillars in the galleries constrain the access of the reasonably large limonene molecules to the active sites present in these regions. The N_2 diagnostic probe molecules are smaller and these accessibility issues are minimised, therefore not being reflected in the surface area measurements. The involvement of Lewis acid sites in the catalysts activity was demonstrated via three separate experiments: i) the enhanced activity over AlSD pre-treated at 250 ºC (generation of Lewis acidity) when compared to the same catalyst activated at 150 ºC (predominant Brönsted acidity), ii) the fact that both Ni-exchanged clays (model Lewis catalysts) were more active than the other ion-exchanged counterparts and iii) the very high p-cymene-to-p-menthenes ratio in the final reaction mixture of a NaSD catalysed reaction (the acidity of Na-exchanged clays is Lewis in nature and is associated with non-exchangeable sites that exist on the clay surface).

7.2.2.2 SELECTIVITY: P-CYMENE

In most cases, p-cymene was obtained primarily by a disproportionation mechanism. In the later stages of the reaction, however, the p-cymene content surpassed that of the p-menthenes. This result suggests that the reaction also proceeds over Lewis acid sites which are able to steer the reaction via two possible mechanisms: i) adsorption of the exocyclic double-bond with the formation of a primary carbonium ion, followed by a proton shift leading to a tertiary carbonium ion and consequent formation of terpinolene or ii) a Lewis site accepts

one electron from α-terpinene, generating the respective radical cation; its dehydrogenation via an allylic radical produces p-cymene. The reaction referred to in the previous paragraph (using NaSD as catalyst) reinforces the idea of a Lewis based p-cymene formation mechanism.

SD ion-exchanged and acid activated catalysts produce similar amounts of p-cymene at similar limonene conversion percentages, although at clearly different rates. This result, which testifies to the thermodynamic control of the process, demonstrated that: i) the nature of the exchangeable cations exerted little influence in the yield of p-cymene and ii) acid activation did not alter the nature of the acidic sites responsible for the dehydrogenation reaction. K10, an iron containing acid activated catalyst, produced similar results in terms of selectivity towards p-cymene. On the other hand, SAz-1 acid activated catalysts produced reduced amounts of p-cymene at similar limonene conversion percentages. Therefore, the role of structural iron in the yields of p-cymene formation was demonstrated. The results obtained with the PILCs corroborate these results. Although both series of materials produced less p-cymene at similar limonene conversion levels than the ion-exchanged and acid activated SD counterparts, the SD PILCs still produced more p-cymene than the 'iron-free' pillared saponite. The reasons for the poorer selectivity of SD-PILCs towards p-cymene maybe related to heating issues or, more probably, to the distribution of pillars on anchoring points on the exposed external surface of the clay[30], which complicates the access of limonene and/or its derivatives to the dehydrogenation sites.

Overall, the yield in p-cymene was low for all catalysts (under 20%), except for the reaction catalysed by NaSD, at a higher temperature and after a prolonged reaction time (ca. 35 %).

---

[30] It was previously noted that the contribution of edge sites to the CEC may reach 20%, depending strongly on the size of the clay particle. As the particle size decreases, the contribution of broken sites to the edge exchange capacity and hence reactivity of the clay particle becomes significant. It was suggested (cf. Chapter 3) that the average size of SD clay particles is smaller than normally observed for smectites.

The content in polymers dominated the final reaction mixture (ca. 60 % at 100% limonene conversion).

7.3 PERSPECTIVES

The initial goal of this project was to create an active and selective catalyst for the aromatisation of limonene. Although a wide range of active catalysts were produced, the yields in p-cymene were poor and independent of the modifications produced (thermodynamic control of the process). Furthermore, limonene, despite being a cheap raw material, has recently become a biodegradable solvent in high demand and probably will not be produced in enough quantities to be used as an economically interesting commercial reactant. Therefore, further investigation on the potential of SD based catalysts for this particular reaction, including the use of flow reaction conditions or other terpenes and mixtures of these as reactant feedstocks or scaling-up studies, may not be actively pursued. On the other hand, an interesting detail may be further investigated. The presence of iron in the clay structure was revealed to be an important aspect in order to obtain higher yields of p-cymene. It is uncertain if higher amounts and/or different organisation of structural iron will improve the selectivity towards p-cymene. In Chapter 3, evidence for 'pure' octahedral iron domains were detected in the Vale do Touro bentonites and, hence, these could be considered good catalysts to elucidate this particular aspect. Of course, other nontronite-type clays could and should be considered.

Previously it was explained that this project is integrated in a wider strategy of gaining value from natural products of vegetable and mineral origin. Therefore, the catalysts prepared and characterised in this thesis are presently being tested in several reactions based on renewable feedstock, aiming towards the production of fine chemicals of industrial importance. From the reactions under preliminary survey, the following two have provided the most promising results:

A. Alkoxylation of monoterpenes: several catalysts have been tested and reported in the literature, but owing to corrosion, toxicity and environmental problems, almost all of the catalysts used are unacceptable for industrial purposes.

B. Synthesis of nopol: Nopol is an optically active bicyclic primary alcohol used in the agrochemical industry to produce pesticides and also in the manufacture of soaps, detergents, polishes and other household products. In the conventional process monocyclic isomers and other side products are obtained, besides nopol.

Another approach for the use of Porto Santo bentonites is currently under consideration. Nature and a clean environment are major attractive features of Madeira as a tourism destination and the golf market, in particular, has become one of the main targets of the Portuguese tourism strategy. On the other hand, the use of pesticides, in general, and of herbicides on golf courses, in particular, raises concerns for the protection of the environment, because only a part of the amount of the chemical applied exerts its effect (certain amounts remain attached to the soil or are absorbed by dust particles, are leached out, migrate into the ground water or are distributed by surface runoff). In order to minimize these health and environmental problems, several approaches may be undertaken, namely: the design of formulations which combine an optimum of bioactivity with a minimum amount of pesticides and studies into stabilisation against decomposition. For the latter, the study of pesticide-clay interactions with environmental aspects in view is particularly relevant.

CHAPTER 8. REFERENCES

8. REFERENCES

– ACEMAN, S., Lahav, N. and Yariv, S. (2000) *Appl. Clay Sci.*, **17**, 99-126.

– ADAMS, J. M. (1987) In: *Preparative Chemistry using Supported Reagents* (Laszlo, P., Ed.) Academic Press, London, 509-528.

– ADAMS, J. M., Bylina, A. and Graham, S. H. (1981) *Clay Miner.*, **16**, 325-332.

– ADAMS, J. M., Bylina, A. and Graham, S. H. (1982) *J. Catal.*, **75**, 190-195.

– Am. Cyanamid Co. (1942) U.S. 2,272,711.

– ANTUNES, J., Galhano, C., Martins, N., Naudin, J., Silva, J., Almeida, F., Rocha, F. and Gomes, C. (1998) *Geology and Technological properties of bentonite from Porto Santo Island (Madeira Archipelago, Portugal)* 2nd Mediterranean Clay Meeting M.C.M.'98, Extended Abstracts, vol. 2, September, Aveiro, pp. 186-190.

– ANTUNES, J., Martins, N., Naudin, J., Silva, J., Rocha, F., Almeida, F. and Gomes, C. (1999[a]) *Caracterização e ensaios tecnológicos de bentonite do Porto Santo, Região Autónoma da Madeira*, Materiais 99, 9º Encontro da Sociedade Portuguesa de Materiais, 333-338.

– ANTUNES, J., Naudin, J. M., Martins, N., Silva, J. B., Gomes, C., Almeida, F. and Rocha, F. (1999[b]) *Avaliação preliminar das reservas e da aplicabilidade da bentonite do Porto Santo (R. A. M.)*, Relatório, Departamento de Geociências, Universidade de Aveiro.

– ATKINS, M. P., Smith, D. J. H. and Weslake, D. J. (1983) *Clay Miner.*, **18**, 423-429.

– AUER, H. and HOFMANN, H. (1993) *Appl. Catal. A Gen.*, **97**, 23-38.

– BAEYER, A. and VILLIGER, V. (1898) *Ber.*, **31**, 1401.

– BAIN, D. C. and SMITH, B. F. L. (1994) In: *Spectroscopic and Chemical determinative methods* (Wilson, M. J., Ed.), Chapman Hall, Oxford, 300-332.

– BAIN, D. C., McHardy, W. J. and Lachowski, E. E. (1994) In: *Spectroscopic and Chemical determinative methods* (Wilson, M. J., Ed.), Chapman Hall, Oxford, 260-299.

– BAKSH, S., Kikkinides, E. S. and Yang, R. T. (1992) *Ind. Eng. Chem. Res.*, **31**, 2181-2189.

– BALLANTINE, J. A., Davies, M., Purnell, H., Rayanakorn, M. and Thomas, J. M. (1981[a]) *J. Chem. Soc. Chem. Commun.*, 427-428.

− BALLANTINE, J. A., Davies, M., Purnell, H., Rayanakorn, M., Thomas, J. M. and Williams, K. J. (1981[b]) *J. Chem. Soc. Chem. Commun.*, 8-9.

− BALLANTINE, J. A., Graham, P., Patel, I., Purnell, J. H., Williams, K. J. and Thomas, J. M. (1987) in *Proc. Int. Clay Conf.* (Schultz, L.G., van Olphen, H. and Mumpton, F.A., eds.), Denver, 1985, The Clay Minerals Society, Bloomington, IN, 311-318.

− BALOGH, M. and LASZLO, P. (1993) *Organic Chemistry using Clay*, Springer Verlag, New York.

− BAR, A. L. and TENDERLOO, H. J. (1936) *Kolloid-Beihefter*, **44**, 97.

− BARRAULT, J., Abdellaoui, M., Bouchoule, C., Majeste, A., Tatibouet, J. M., Louloudi, A., Papayannakos N. and Gangas, N. H. (2000) *Appl. Catal. B Environ.*, **27**, L225-L230.

− BARTH, R. T. and BALLOU, E. V. (1961) *Anal. Chem.*, **33**, 1080-1084.

− BASF (1967), US 3,555,103.

− BELLAOUI, A., Plee, D. and Meriaudeau, P. (1990) *Appl. Catal.*, **63**, L7-L10.

− BENESI, H. A. (1956) *J. Am. Chem. Soc.*, **78**, 5490-5494.

− BENESI, H. A. and WINQUIST, H. C. (1978) *Adv. Catal.*, **27**, 98-176.

− BERGAOUI, L., Lambert, J. F., Franck, R., Suquet, H. and Robert, J. L. (1995) *J. Chem. Soc. Faraday Tran*s. **91**(4), 2229-2239.

− BERNIER, A., Admaiai, L. F. and Grange, P. (1991) *Appl. Catal.*, **77**, 269-281.

− BONDT, N., Deiman, J. R., van Troostwyk, P. and Lowrenberg, A. (1797) *Ann. Chim. Phys.*, **21**, 48-71.

− BOOIJ, E., Kloprogge, J. T. and van Veen, J. A. R. (1996) *Clays Clay Miner.*, **44**, 774-782.

− BOOTH, A. B. and AUTENTRIETH, J. S. (1969) *Kirkothmer, Encyclopaedia of Chemical Technology*, 3rd Ed., **19**, 803-838.

− BORDEN, D. & GIESE, R. F. (2001) *Clays Clay Miner.*, **49**(5), 444-445.

− BORNHOLDT, K., Corker, J. M., Evans, J. and Rummey, J. M. (1991) *Inorg. Chem.,* **30**, 1-2.

− BOVEY, J. and JONES, W. (1995) *J. Mater. Chem.*, **5**, 2027-2035.

− BRADLEY, S. M. and KYDD, R. A. (1991) *Catal. Lett.*, **8**, 185-192.

− BRADLEY, S. M., Kydd, R. A. and Yamgagui, R. (1990) *Magn. Reson. Chem.*, **28**, 746-750.

− BRADLEY, S. M., Lehr, C. R. and Kydd, R. A. (1993) *J. Chem. Soc. Dalton Trans.*, 2415-2420.

− BRADLEY, W. F. and Grim, R. E. (1951) *Am. Miner.*, **36**, 182-201.

− BREEN, C. (1991[a]) *Clay Miner.,* **26**, 487-496.

− BREEN, C. (1991[b]) *Clay Miner.*, **26**, 473-484.

− BREEN, C. and MORONTA, A.J. (2000) *J. Phys. Chem. B*, **104**, 2702-2708.

− BREEN, C. and MORONTA, A.J. (2001) *Clay Miner.*, **36**, 467-472.

− BREEN, C., Deane, A.T., Flynn, J.J. (1987) *Clay Miner.*, **22**, 169-178.

− BREEN, C., Forsyth, J., Yarwood, J. and Hughes, T. (2000) *Phys. Chem. Chem. Phys.*, **2**, 3887-3892.

− BREEN, C., Madejová, J. and Komadel, P. (1995[a]) *Appl. Clay Sci.*, **10**, 219-230.

− BREEN, C., Madejová, J. and Komadel, P. (1995[b]) *J. Mater. Chem.*, **5**(3), 469-474.

− BREEN, C., Watson, R., Komadel, P., Madejova, J. and Klapyta, Z. (1997[b]) *Langmuir*, **13**, 6473-6497.

− BREEN, C., Zahoor, F. D., Madejova, J. and Komadel, P. (1997[a]) *J. Phys. Chem. B*, **101**, 5324-5331.

− BRINDLEY, G. W. and BROWN, G. (1984) *Crystal Structure of Clay Minerals and their X-Ray Identification*, Mineralogical Society, London.

− BRINDLEY, G. W. and YAMANAKA, S. (1979) *Am. Miner.* **64**, 830-835.

− BROWN, C. A. (1973) *J. Am. Chem. Soc.*, **95**, 982-983.

− BROWN, D. R. (1994) *Geol. Carpathica Ser. Clays*, **3**(1), 45-56.

− BROWN, D. R. and RHODES, C. N. (1997) *Catal. Lett.*, **45**, 35-40.

− BRUNAUER, S., Emmett, P. H. and Teller, E. (1938) *J. Am. Chem. Soc.*, **60**, 309-318.

− BUHL, D., Roberge, D.M. and Hölderich, W.F. (1999) *Appl. Catal. A*, **188**, 287-299.

− BUHL, D., Weyrich, P.A., Sachtler, W.M.H. and Hölderich, W.F. (1998) *Appl. Catal. A,* **171,** 1-11.

− BUJDÁK, J. and SLOSIARIKOVÁ , H. (1992) *Appl. Clay Sci.*, **7**, 263-269.

− BURCH, R. and WARBURTON, C. I. (1986) *J. Catal.*, **97**, 503-511.

− CAMPBELL, I. (1988) *Catalysis at surfaces*. Chapman and Hall, London.

− CAÑIZARES, P., Valverde, J. L., Sun Kou, M. R. and Molina, C. B. (1999) *Microporous Mesoporous Mat.*, **29**, 267-281.

− CARRADO, K. A. (2004), in *Handbook of Layered Materials* (Auerbach, S. M, Carrado, K. A. and Dutta, P. K., eds.), Marcel Dekker, New York, 1-37.

− CARRADO, K. A., Suib, S. L., Skoularikis, N. D. and Coughlin, R. W. (1986) *Inorg. Chem.*, **25**, 4217-4221.

– CATIVIELA, C., Figueras, F., Fraile, J. M., Garcia, J. I., Gil, M., Mayoral, J. A., de Menorval, L. C. and Pires, E. (1993) *Stud. Surf. Sci. Catal., Vol. 78, Heterogeneous Catalysis and Fine Chemicals III.* (Guisnet, M. *et al.*, Eds.) Elsevier, The Netherlands, 495.

– CATRINESCU, C., Teodosiu, C., Macoveanu, M., Miehe-Brendlé, J. and Le Dred, R. (2003) *Water Research*, **37**, 1154-1160.

– CHENG, S. (1999) *Catal. Today,* **49** (1-3), 303-312.

– CHEVALIER, S., Franck, R., Suquet, H., Lambert, J. F. and Barthomeuf, D. (1994) *J. Chem. Soc. Faraday Trans.*, **90**(4), 667-674.

– CHIPERA, S. J. and BISH, D. L. (2001) *Clays Clay Miner.*, **49**(5), 398-409.

– CHIPERA, S. J., Guthrie, G. D. and Bish, D. L. (1993) in: *Health Effects of Mineral Dusts* (G. D. Guthrie and B. D. Mossman, Eds) *Reviews in Mineralogy*, 28, Mineralogical Society of America, Washington, D. C., 235-249.

– CHRISTIDIS, G. E., Scott, P. W. and Dunham, A. C. (1997) *Appl. Clay Sci.*, **12**, 329-347.

– CLARK, J. H. (1994) In: *Catalysis of Organic Reactions by Supported Inorganic Reagents*. VCH Publishers, USA.

– CLARK, J. H., Kybett, A. P. and Macquarrie, D. J. (1992) In: *Supported Reagents. Preparations Analysis and Applications*. VCH Publishers, USA.

– CLARK, J. H.; Cullen, S. R.; Barlow, S. J. and Bastok, T. W. (1994) *J. Chem. Soc., Perkin Trans.* 2, 1117-1130.

– CONNERTON, J., Joyner, T. W. and Padley, M. B. (1995) *J. Chem. Soc. Faraday Trans.*, **91**, 1841-1844.

– COOL, P. and VANSANT, E. F. (2004) In: *Handbook of Layered Materials* (Auerbach, S. M, Carrado, K. A. and Dutta, P. K., eds.), Marcel Dekker, New York, 261-311.

– COSTA, A. M. and LOURENÇO, J. A. A. (1982) *Tecnologia dos Resinosos*, LNETI.

– CROCKETT, R. and RODUNER, E. (1994) *J. Chem. Soc. Perkin Trans.*, **2**, 347-350.

– CZARNECKI, J. and THUMIN, D. (1995) *NATAS Conference Proceedings*, Toronto, Canada.

– de CARVALHO, A. M. G. and BRANDÃO, J. M. (1991) *Geologia do Arquipélago da Madeira*, Museu Nacional de História Natural (Mineralogia e Geologia) da Universidade de Lisboa, Lisboa.

− de CARVALHO, M. B., Pires, J. and Carvalho, A. P. (1996) *Microporous Mater.,* **6**, 65-77.

− de STEFANIS, A., Perez, G., Ursini, O. and Tomlinson, A.A.G. (1995) *Appl. Catal. A,* **132**, 353-365.

− DOGAN, A.U., Dogan, M., Onal, M., Sarikaya, Y., Aburub, A. and Wurster, D.E. (2006) *Clays Clay Miner.,* **54**, 62-66.

− DRLJACA, A., Anderson, J. R., Spiccia, L. and Turney, T. W. (1992) *Inorg.Chem.,* **31**, 4894-4897.

− DRLJACA, A., Anderson, J. R., Spiccia, L. and Turney, T. W. (1997) *Inorg. Chim. Acta* **256**, 151-154.

− EMEIS, C. A. (1993) *J. Catal.,* 141, 347-354.

− FALARAS, P., Kovanis, I., Lezou, F. and Seiragakis, G. (1999) *Clay Miner.,* **34**, 221-232.

− FARMER, V. C. (1974) *Infrared Spectra of Minerals. (Farmer, V. C., ed.)* Mineralogical Society, London, 331.

− FARMER, V. C. (1979) *Data Handbook for Clay Materials and other Non-Metallic Minerals* (van Olphen, H. and Fripiat, J. J., eds.) Pergamon Press, England, 285.

− FERREIRA, M. and SERRANO, L. (1971) *O Problema das Esmectites na Ilha de Porto Santo,* I Congresso Hispano-Luso-Americano de Geologia Económica, Secção 6, Lisboa-Madrid, 225-244.

− FETTER, G., Heredia, G., Maubert, A. M. and Bosch, P. (1996) *J. Mater. Chem.,* **6**, 1857-1858.

− FETTER, G., Heredia, G., Valázquez, L. A., Maubert, A. M. and Bosch, P. (1997) *Appl. Catal. A Gen.,* **162**, 41-45.

− FIEGE, H. (1987) In: *Ullmann's Encyclopedia of Industrial Chemistry,* 5th Ed., **A8**, 25-59.

− FIGUEIREDO, J. L. and RIBEIRO, F. R. (1989) *Catálise heterogénea.* Fundação Calouste Gulbenkian, Porto.

− FIGUERAS, F. (1988) *Catal. Rev.—Sci. Eng.,* **30**, 457-499.

− FIGUERAS, F., Klapyta, Z., Massiani, P., Mountassir, Z., Tichit, D.,Fajula, F., Gueguen, C., Bosquet, J. and Auroux, A. (1990) *Clays Clay Miner.,* **38**, 257-264.

− FIGUERAS, F., Mattrod-Bashi, A., Fetter, G., Thrierr, A. and Zanchetta, J. V. (1989) *J. Catal.,* **119**, 91-96.

8. References

− FINHOLT, J. E., Thompson, M. E. and Connick, R. E. (1981) *Inorg. Chem.*, **20**, 4151-4155.

− FORSYTH, J. (2001) *Characterisation of Minerals by Evolved Gas Analysis and Infrared Spectroscopy*. PhD Thesis, Materials Research Institute, Sheffield Hallam University.

− FOUCAUD, A. (1987) In: *Preparative Chemistry using Supported Reagents*, (Laszlo, P., Ed.), Academic Press, London, 503 - 508.

− FRASER, D. J. J. and GRIFFITHS, P. R. (1990) *Appl. Spec.*, **44**, 193-199.

− FRENKEL, M. (1974) *Clays Clay Miner.*, **22**, 435-441.

− FRENKEL, M. and HELLER-KALLAI, L. (1983) *Clays Clay Miner.*, **31**, 92-96.

− FRIPIAT, J. J. (1988) *Catal. Today*, **2**, 281-295.

− FULLER, M. P. and GRIFFITHS, P. R. (1978) *Anal. Chem.*, **50**, 1906-1910.

− GANDÍA, L. M., Toranzo, R., Vicente, M. A. and Gil, A. (1999) *Appl. Catal. A: General,* **183**, 28-33.

− GARCIA, H. and ROTH, H. D. (2002) *Chem. Rev.*, **102**, 3947-4008.

− GATES, W. P. (2005) In: *The Application of Vibrational Spectroscopy to Clay Minerals and Layered Double Hydroxides*, CMS Workshop Lectures Vol. 13, ed. J. T. Kloprogge, Clay Minerals Society, 125-168.

− GIL, A., Gandía, L. M. and Vicente, M. A. (2000) *Catal. Rev. Sci. Eng.*, **42** (1&2), 145-212.

− GIL, A., Vicente, M. A., Toranzo, R., Banares, M. A. and Gandía, L. M. (1998) *J. Chem. Technol. Biotechnol.*, **72**, 131-136.

− GOMES, C. F. (1988) *Argilas: O que são e para que servem*, Fundação Calouste Gulbenkian, Lisboa, 1988.

− GREGORY, R., Smith, D. J. H. and Westlake, D. J. (1983) *Clay Miner.*, **18**, 431-435.

− GRIFFITHS, P.R. and FULLER M. P. (1982), *Advances in Infrared and Raman Spectroscopy*, **9** (Clark, R. J. H. and Hester, R. E., Eds) Heyden and Son Ltd, London.

− GRIM, R. E. (1962) Applied Clay Mineralogy, McGraw-Hill, New York, 1962.

− GRIM, R. E. (1968) *Clay Mineralogy*, 2nd ed, McGraw Hill, New York,.

− GRIM, R. E. and BRADLEY, W. F. (1940) *J. Am. Ceram. Soc.*, **23**, 242-248.

− GRIM, R. E. and BRAY, R. H. (1936) *Am. Ceram. Soc.*, **19**, 307-315.

− GRIM, R. E. and KULBICKI, G. (1961) *Am. Miner.*, **46**, 1329-1369.

− GRIMSHAW, R. W. (1971) *Chemistry and Physics of Clays*, Benn, London.

− GUGGENHEIM, S. and MARTIN, R. T. (1995) *Clays Clay Miner.*, **43**, 255-256.

− GUGGENHEIM, S. and van GROOS, A. F. K. (2001) *Clays Clay Miner.*, **49**(5), 433-443.

− GUIL, J. M., Mélon, J. A. P., de Carvalho, M. B., Carvalho, A. P., Pires, J. (2002) *Microporous and Mesoporous Mater.*, **51**, 145-154.

− HAFFAD, D., Chambellan, A. and Lavalley, J. C. (1998) *Catal. Lett.*, **54**, 227-233.

− HAMADEH, I. M., Yeboah, S. A., Trumbull, K. A. and Griffiths, P. R. (1984) *Appl. Spec.* **38**, 486-492.

− HARRIS, J. R. (1988) In: *American Chemical Society Symp. Ser*, **375** (Occelli, L., Ed.), American Chemical Society, Washington, DC, 253.

− HART, M. P. and BROWN, D. R. (2004) *J. Molec. Catal. A*, **212**, 315-321.

− HELSEN, J. J. (1970) *Bull. Groupe Fr. Argiles*, **22**, 139-155.

− HENDRICKS, S. B. (1942) *J. Geol.*, **50**, 276-290.

− Hercules Powder Co. (1946) U.S. 2,402,898.

− HEYDING, R. D, Ironside, R., Norris, A. R. and Prysiazniuk, T. Y. (1960) *Can J. Chem.*, **38**, 1003-1016.

− HO, T. (1987) *Chemistry and Industry*, 295.

− HOFMANN, U., Endell, K. and Wilm, D. (1933) *Z. Krist.*, **86**, 340-348.

− HOJABRI, F. J. (1971) J. *Appl. Chem. Biotechnol.*, **21**, 87-89.

− HÖLDERICH, W. F. (2000) *Catal. Today*, **62**, 115-130.

− HUTSON, N. D., Gualdoni, D. J. and Yang, R. T. (1998) *Chem. Mater.*, **10**, 3707-3715.

− JANEK, M. and KOMADEL, P. (1993) *Geol. Carpath. Ser. Clays*, **44**, 59-64.

− JANG, B-S., Cho, K-H., Kim, K-H. and Park, D-W. (2005) *React. Kinet. Catal. Lett.*, **86**(1), 75-82.

− JASRA, R. V. (2003) *Bull. Catal. Soc. India*, **2**, 157–183.

− JAYNES, W. J. and BOYD, S. A. (1991) *Clays Clay Miner.*, **39**, 428-436.

− JOHANSSON, G. (1960) *Acta Chem. Scand.*, **14**, 771-773.

− JOHNSTON, C. T. (1996) In: *Organic Pollutants in the Environment* (Sawhney, B. L., Ed.) Clay Minerals Society Workshop, Lectures 8, Boulder, CO, USA, 1-44.

− JOUSSEIN, E., Petit, S. and Decarreau, A. (2001) *Comptes Rendus de l'Academie des Sciences*. Paris, **332**, 83-89.

− JOVANOVIĆ, N., Brezovska, S., Burevski, D., Boevska, V., Panova, B. and Vuković, Z. (1996) *J. Serbian Chem. Soc.*, **61**, 453-460.

− KAISERSBERGER, E. and POST, E. (1997) *Thermochim. Acta*, **295**, 73-93.

− KAPLAN, H. (1966) U.S. Patent 3,287,422.

− KATDARE, S. P., Ramaswamy, V. and Ramaswamy, A. V. (1997) *J. Mater. Chem.,* **7**(11), 2197-2199.

− KATDARE, S. P., Ramaswamy, V. and Ramaswamy, A. V. (1999) *Catal. Today*, **49**, 313-320.

− KATDARE, S. P., Ramaswamy, V. and Ramaswamy, A. V. (2000) M*icroporous Mesoporous Mater.*, **37**, 329-336.

− KAVIRATNA, H. and PINNAVAIA, T. J. (1994) *Clays Clay Miner.*, **42**, 717-723.

− KELLENDONK, F. J. A., Heinerman, J. J. L. and van Santen, R. A. (1987) In: *Preparative Chemistry using Supported Reagents* (Laszlo, P., Ed.), Academic Press, London, 455-468.

− KHEOK, S. C. and LIM, E. E. (1982) *J. Am. Oil. Chem. Soc.*, **59**, 129-131.

− KIRICSI, I., Molnár, A., Pálinkó, I., Fudala, A. and Nagy, J. B. (1997) *Sol. State Ionics*, **101-103**, 793-797.

− KLOPROGGE, J. T. (1998) *J. Porous Mater.,* **5**, 5-41.

− KLOPROGGE, J. T., Frost, R. L. and Fry, R. (1999) *Analyst,* **124**, 381-384.

− KOLOMAI, I. (1990) Czech. CS 276,120, 3rd June.

− KOMADEL, P. (2003) *Clay Miner.*, **38**, 127-138.

− KOMADEL, P., Janek, M., Madejova, J., Weekes, A. and Breen, C. (1997) *J. Chem. Soc. Faraday Trans.*, **93**, 4207-4210.

− KOMADEL, P., Madejová, J., Janek, M., Gates, W. P., Kirkpatrick, R. J. and Stucki, J.W. (1996) *Clays Clay Miner.*, **44**, 228-236.

− KOOLI, F. and JONES, W. (1998) *J. Mater. Chem.*, **8**, 2119-2124.

− KRAJCOVIC, J., Hudec, P. and Grejtak, F. (1995) *React. Kinet. Catal. Lett.*, **54**, 87-97.

− KRISHNASAMY, V. and YEDDANAPALLI, L.M. (1976) *Can. J. Chem.,* **54**, 3458-3463.

− KRIVACSY, Z. and HLAVAY, J. (1994) *Talanta*, **41**, 1143-1149.

− KUBOKAWA, Y. (1963) *J. Phys. Chem.,* **67**, 769-771.

− KUMAR, P., Jasra, R. V. and Bhat, S. G. T. (1997) *Indian J. Chem.,* **36A**, 667-671.

− LAGALY, G. (1981) *Clay Miner.*, **16**, 1-21.

- LAMBERT, J. F. and PONCELET, G. (1997) *Topics Catal.*, **4**, 43-56.

- LAMBERT, J. F., Chevalier, S., Franck, R., Suquet, H. and Bartomeuf, D. (1994) *J. Chem. Soc. Faraday Trans.,* **90**(4), 675-682.

- LEE, J. F., Mortland, M. M., Chiou, C. T., Kile, D. E. and Boyd, S. A. (1990) *Clays Clay Miner.*, **38**, 113-120.

- LENARDA, M., Storaro, L., Ganzerla, R. and Bertoncello, R. (1999) *J. Molecular Catal. A: Chemical,* **144**, 151-158.

- LOPES, C. (1996) *Conversão de Limoneno em p-Cimeno*, Tese de Mestrado, INETI, Lisbon.

- LOULOUDI, A., Michelopoulos, J., Gangas, N.-H. and Papayannakos, N. (2003) *Appl. Catal. A Gen.*, **242**, 41-49.

- LOURENÇO (1999) *Personnel Communication*.

- LOURENÇO, J. A. A. and CASQUILHO, M. S. (1988) In: *Proceedings of Encontro sobre o Pinheiro Manso*, Sociedade Portuguesa de Ciências Florestais, Tróia.

- LOW, P. F., Ravina, I. and White, J. L. (1970) *Nature*, **226**, 445-446.

- MADEJOVÁ, J. (2003) *Vibrational Spec.*, **31**, 1–10.

- MADEJOVÁ, J. and KOMADEL, P. (2001) *Clays Clay Miner.*, **49** (5), 410–432.

- MADEJOVÁ, J. and KOMADEL, P. (2005) In: *The Application of Vibrational Spectroscopy to Clay Minerals and Layered Double Hydroxides*, CMS Workshop Lectures Vol. 13, ed. J. T. Kloprogge, Clay Minerals Society, 65-98.

- MADEJOVÁ, J., Bujdák, J., Janek, M. and Komadel, P. (1998) *Spectrochim. Acta A*, **54**, 1397-1406.

- MADEJOVÁ, J., Keckés, J., Pálková, H. and Komadel, P. (2002) *Clay Minerals*, **37**, 377-388.

- MADEJOVÁ, J., Kraus, I. and Komadel, P. (1995) *Geologica Carpathica – Ser Clays*, **4**(1), 23-32.

- MAEGDEFRAU, E. and HOFMANN, U. (1937) *Z. Krist.*, **98**, 299-323.

- MAIRELES-TORRES, P., Olivera-Pastor, P., Rodriguez-Castellon, E., Jimenez-Lopez, A. and Tomlinson, A. A. G. (1991) *J. Mater. Chem.*, **1**, 739-746.

- MARSHALL, C. E. (1935) *Z. Krist.*, **91**, 433-449.

- MATSUDA, Y., Nakai, K., Ebara, H. and Momoi, K. (1993ª) Jpn. Kokai Tokkyo Koho JP 06,253,741 to Honshu Kosan Kk, 3rd March.

− MATSUDA, Y., Nakai, K., Ebara, H. and Momoi, K. (1993[b]) Jpn. Kokai Tokkyo Koho JP 06,256,792 to Honshu Kosan Kk, 8th March.

− MCCABE, R. W. (1996) In: *Inorganic Materials* (Bruce, D. W. and O'Hare, D., Eds.) John Wiley and Sons, England, 314-363.

− MCCONNELL, D. (1950) *Am. Mineralogist*, **35**, 166-172.

− MCGEE, T., Subramanian, S. and Yeager, C. E. (1993) PCT Int. Appl. WO 95 12,379 to Givaudan-Roure (International) S.A., 2nd November.

− MCKILLOP, A. and CLISSOLD, D. W. (1987) In: *Preparative Chemistry using Supported Reagents* (Laszlo, P., Ed.), Academic Press, London, 469-482.

− MENDIOROZ, S. and PAJARES, J. A. (1987) *Langmuir*, **3**, 676-681.

− MERMUT, A. R. and CANO, A. F. (2001) *Clays Clay Miner.*, **49**(5), 381-386.

− MICHOT, L. J., Villiéras, F., Lambert, J. F., Bergaoui, L., Grillet, Y. and Robert, J. L. (1998) *J. Phys. Chem. B,* **102**(18), 3566-3476.

− MILLS, G. A., Holmes, J. and Cornelius, E. B. (1950) *J. Phys Colloid Chem.*, **54**, 1170-1185.

− MISHRA, T. and PARIDA, K. (1998) *Appl. Catal. A Gen.*, **166**, 123-133.

− MITCHELL, P. W. D. and SASSLER, D. E. (1993) Eur. Pat. Appl. EP 522839, 13th January.

− MITRE, R. P. and SINDHU, P. S. (1971) *Clays Clay Miner.*, **19**, 391-397.

− MOENKE, H. H. W. (1974) *Infrared Spectra of Minerals. (Farmer, V. C., ed.)* Mineralogical Society, London, 365.

− MOKAYA, R. and JONES, W. (1994) *J. Chem. Soc. Chem. Commun.*, **8**, 929-930.

− MOKAYA, R. and JONES, W. (1995) *J. Catal.*, **153**, 76-85.

− MOKAYA, R., Jones, W., Davies, M. E. and Whittle, M. E. (1993) *J. Mater. Chem.*, **3**, 381-387.

− MOLINA, R., Shutz, A. and Poncelet, G. (1994) *J. Catal.*, **145**, 79-85.

− MOORE, D.M. and REYNOLDS, R.C., Jr. (1989) *X-Ray Diffraction and the Identification and Analysis of Clay Minerals*. Oxford University Press, New York.

− MORADI, K., Depecker, C. and Corset, J. (1994) *Appl. Spec.*, **48**, 1491-1497.

− MORENO, S., Sun Kou, R. and Poncelet, G. (1997) *J. Phys. Chem. B,* **101**, 1569-1578.

− MORTLAND, M. M. and RAMAN, K. V. (1968) *Clays Clay Miner.,* **16**, 393-398.

− MORTLAND, M. M., Fripiat, J. J., Chaussidon, J. and Uytterhoeven, J. (1963) *J. Phys. Chem.*, **67**, 248-258.

− MULLER, F., Besson, G., Manceau, A. and Drits, V.-A. (1997) *Phys Chem Minerals*, **24**, 159-166.

− MURRAY, H. H. (1998) In: *Industrial inorganic chemicals and products, Vol. II* [Ullmann's Encyclopedia]. Wiley-VCH, Germany, 1389-1434.

− MURRAY, H. H. (1999) *Clay Miner.*, **34**, 39-49.

− NORVAK, J. and GREGOR, M. (1969) *Proc. Int. Clay Conf. Tokyo*, 851-857.

− NOVÁK, I. and ČÍČEL, B. (1978) *Clays Clay Miner.*, **26**, 341-344.

− OCCELLI, M. L. and TINDWA, R. M. (1983) *Clays Clay Miner.*, **31**, 22-28.

− OCCELLI, M. L., Huggins, F. E., Dominguez, J. M., Stencel, J. M., Gould, S. A. (1995) *Microporous Mater.*, **4**, 291-300.

− OCELLI, M. L. and LESTER, J. E. (1985) *Ind. Eng. Chem. Prod. Res. Dev.*, **24**, 27-32.

− OH, S. J., Cook, D. C. and Townsend, H. E. (1998) *Hyperfine Interact. Ions*, **112**, 59-65.

− OHTSUKA, K. (1997) *Chem. Mater.*, **9**, 2039-2050.

− OKKERSE C. and van BEKKUM H. (1999) *Green Chem.*, **2**, 107-114.

− OSTHAUS, B. B. (1955) *Clays Clay Miner.*, **4**, 301-321.

− PAGE, J. B. (1943) *Soil Sci.* **56**, 273-281.

− PÁLINKÓ, I., Molnár, A., Nagy, J. B., Bertrand, J. C., Lázár, K., Valyon, J. and Kiricsi, I. (1997) *J. Chem. Soc., Faraday Trans.*, **93**(8), 1591-1599.

− PARRY, E. P. (1963) *J. Catal.*, **2**, 371-379.

− PEREIRA, P. R., Pires, J. and de Carvalho, M. B. (1998) *Langmuir*, **14**, 4584-4588.

− PEREIRA, P. R., Pires, J. and de Carvalho, M. B. (2001) *Sep. Pur. Tech.*, **21**, 237-246.

− PINNAVAIA, T. J. (1983) *Science*, **220**, 365-371.

− PINNAVAIA, T. J. (1987) In: *Preparative Chemistry using Supported Reagents* (Laszlo, P., Ed.), Academic Press, London, 483 - 502.

− PINNAVAIA, T. J. (1995) In: *Advances in Chemistry Series*, **245** (Interrante, L. V., Caspar, L. A. and Ellis, A. B., eds.), American Chemical Society, Washington, DC, 283-300.

− PINNAVAIA, T. J., Tzou, M. S. and Landau, S. D. (1985) *J. Am. Chem. Soc.*, *107*, 4783-4785.

− PIRES J., de Carvalho, M. B., Carvalho, A. P., Guil, J. M. and Perdigón-Melón, J. A. (2000) *Clays Clay Miner.*, **48** (3), 385 – 391.

− PIRES, J. and de CARVALHO, M. B. (1997) *J. Mater. Chem.*, **7**(9), 1901-1904.

− PIRES, J., de Carvalho, M. B. and Carvalho, A. P. (1997) *Zeolites*, **19**, 107-113.

− PIRES, J., Machado, M. and de Carvalho, M. B. (1998) *J. Mater. Chem.*, **8**(6), 1465-1469.

− PIRES, J., Pinto, M., Carvalho, A. and de Carvalho, M. B. (2003) *Adsorption*, **9**, 303-309.

− PLEE, D., Borg, F., Gatineau, L. and Fripiat, J. J. (1985[a]) *J. Am. Chem. Soc.*, **107**, 2362-2369.

− PLEE, D., Gatineau, L and Fripiat, J. J. (1987) *Clays Clay Miner.*, **35**, 81-88.

− PLEE, D., Schutz, A., Poncelet, G. and Fripiat, J. J. (1985[b]) In: *Catalysis by Acids and Bases* (Imelik, B., Naccache, C., Goudurier, G., Ban Taarit, Y. and Vedrine, J. C., Eds.), Elsevier, Amsterdam, 343-350.

− PLISKIN, W. A. and EISCHENS, R. P. (1955) *J. Phys. Chem.*, **59**, 1156-1159.

− PONCELET, G. and SCHUTZ, A. (1986) In: *Chemical Reactions in Organic and Inorganic Constrained Systems* (Setton, R., Ed.) Reidel, Dordrecht, 165-178.

− PURNELL, J. H., Williams, J. and Yun, L. (1991) *Catal. Lett.*, **10**, 63-70.

− REGGEL, L., Friedman, S. and Wender, I. (1958) *J. Org. Chem.*, **23**, 1136-1139.

− RHODES, C. N. and BROWN, D. R. (1994[b]) *Clay Miner.*, **29**, 799-801.

− RHODES, C. N. and BROWN, D. R. (1992) *J. Chem. Soc., Faraday Trans.*, **88**, 2269-2274.

− RHODES, C. N. and BROWN, D. R. (1993) *J. Chem. Soc. Faraday Trans.*, **89**, 1387–1391.

− RHODES, C. N. and BROWN, D. R. (1994[a]) *Catal Lett.*, **24**, 285-291.

− RHODES, C.N., Franks, M., Parkes, G.M.B. and Brown, D.R. (1991) *J. Chem. Soc. Chem. Commun.,* 804–807.

− ROBERGE, D. M., Buhl, D., Niederer, J. P. M. and Hölderich, W. F. (2001) *Appl. Catal. A Gen.*, **215**, 111-124.

− ROUQUEROL, F., Rouquerol, J. and Sing, K. S. W. (1999) *Adsorption by Powders & Porous Solids*, Academic Press, London.

− RUSSELL, J.D. and FRASER, A.R. (1994) in: *Clay Mineralogy: Spectroscopic and Chemical Determinative Methods* (M.J. Wilson, editor). Chapman & Hall, London, 11-67.

− RUSSO, P. and CARROTT, M. R. (2004) *Personnel communication*.

− RYLAND, L. B., Tamele, M. W. and Wilson, J. N. (1960) In: *Catalysis* (Emmett, P. H., ed.) New York.

− SANTOS, P. S. (1989) *Ciência e Tecnologia de Argilas.* 2ª edição. Edgard Blücher, São Paulo.

− SATO, H., Kato, K. and Shimizu, H. (1993) Jpn. Kokai Tokkyo Koho JP 06,340,559 to Sumitomo Chemical Co., 5th April.

− SCHOONHEYDT, R. A. and LEEMAN, H. (1992) *Clay Miner.,* **27**, 249-252.

− SCHOONHEYDT, R. A., van der Eynde, J., Tubbax, H., Leeman, H., Stuyckens, M., Lenotte, I. and Stone, W. E. E. (1993) *Clays Clay Miner.*, **41**(5), 598-607.

− SERRATOSA, J. M. (1960) *Am. Miner.*, **45**, 1101-1104.

− SHABTAI, J. (1979) *Chim. Ind.*, **61**, 734-741.

− SHELDRICK, B. H. and WANG, C. (1993) In: *Soil sampling and methods of analysis* (Carter, M. R., ed.) Boca Raton, FL, Lewis Publishers, 499-511.

− SHIMAKAVA, K and SASAMI, M. (1993) Jpn. Kokai Tokkyo Koho JP 07,126,152 to Nikka Chemical Ind Co Ltd, 1st November.

− SHIRATO, K. and INOE, T. (1994) Jpn. Kokai Tokkyo Koho JP 08 13,335 to Kao Corp, Japan, 5th June.

− SILVA, J., Naudin, J., Gomes, C., Rocha, F. and Almeida, F. (2000) *Study on the potentialities of smectitic clays from Porto Santo island (Madeira archipelago) to be used in geomedicine*, in Proceedings ISCREI 2000, Annamalai University, India.

− SOLIN, S. A. (1997) *Annu. Rev. Mater. Sci.*, **27**, 89-115.

− SPICCIA, L., Marty, W. and Giovanoli, R. (1988) *Inorg. Chem.*, **27**, 2660-2666.

− SPICCIA, L., Stoeckli-Evans, H., Marty, W. and Giovanoli, R. (1987) *Inorg. Chem.*, **26**, 474-482.

− STÜNZI, H. and MARTY, W. (1983) *Inorg. Chem.*, **22**, 2145-2150.

− SUZUKI, K. and MORI, T. (1989) *J. Chem. Soc. Chem. Commun.*, 7-8.

− SUZUKI, K., Mori, T., Kawase, K., Sakami, H., Iida, S. (1988) *Clays Clay Miner.*, **36**, 147-152.

− SWIFT, K.A.D. (2004) *Top. Catal.,* **27**, 143-155.

− SWOBODA, A. R. and KUNZE, G. W. (1964) *Clays Clay Miner.*, **13**, 277-288.

− SYCHEV, M., de Beer, V. H. J., van Santen, R. A., Prihodko, R. and Goncharuk, V. (1994) In *Zeolites and related microporous materials: State of the Art 1994*; (Weitkamp,

J., Karge, H. G., Pfeifer, H. and Hoelderich, W., Eds.) Elsevier: Amsterdam; *Stud. Surf. Sci. Catal.*, **84**, 267-274.

− SYCHEV, M., Shubina, T., Rozwadowski, M., Sommen, A. P. B., de Beer, V. H. J. and van Santen, R. A. (2000) *Microporous Mesoporous Mater.*, **37**, 187-200.

− TAKAHASHI, K. and MIZOGUCHI, I. (1994) Jpn. Kokai Tokkyo Koho JP 07,309,968 to Achilles Corp, Japan, 25th March.

− TANABE, K. and HÖLDERICH, W. F. (1999) *Appl. Catal. A: General,* **181**, 399-434.

− TAYLOR, D. R. and JENKINS, D. B. (1986) *Soc. Min. Eng. AIME Trans.*, **282**, 1901-1910.

− TENNAKOON, D. T. B., Schlögl, R., Rayment, T., Klinowski, J. Jones, W. and Thomas, J. M. (1983) *Clay Miner.*, **18**, 357-371.

− THENG, B. K. G. (1974) *The Chemistry of Clay-Organic Reactions* (Hilger, A., Ed.) London.

− THOMAS, A. F. and BESSIERE, Y. (1989) *Natural Product Reports*, 291-309.

− THOMAS, J. M. and THEOCHARIS, C. R. (1992) In: P*erspectives in Catalysis, a Chemistry for the 21st Century (IUPAC)* (Thomas, J. M. and Zamaraev, K. I., eds.), Blackwell Scientific, Oxford, 465-488.

− THOMAS, J. M. and THOMAS, W. J. (1997) *Principles and Practice of Heterogeneous Catalysis*. VCH Publications, Germany.

− THOMAS, S. M. and OCCELLI, M. L. (2000) *Clays Clay Miner.*, **48**, 304-308.

− THOMPSON, M. and CONNICK, R. E. (1981) *Inorg. Chem.*, **20**, 2279-2285.

− TICHIT, D., Fajula, F., Figueras, F., Bosquet, J. and Guegen, C. (1985) In: *Catalysis by Acids and Bases* (Imelik, B., Naccache, C., Goudurier, G., Ban Taarit, Y. and Vedrine, J. C., Eds.), Elsevier, Amsterdam, 351-367.

− TORANZO, R., Vicente, M. A. and Bañares-Muñoz, M. A. (1997) *Chem. Mater. B,* **9**, 1829-1836.

− TSAI, S., Jing, S., Du, L., Liu, S. and Cheng, S. (1994) *Microporous Mater.*, **2**, 185-196.

− TZOU, M. S. and PINNAVAIA, T. J. (1988) *Catal. Today*, **2**, 243-259.

− VACCARI, A. (1998) *Catal. Today*, **41**, 53 – 71.

− VACCARI, A. (1999) *Appl. Clay Sci.*, **14**, 161-198.

− VALENZUELA-DIAZ, F. R. and SANTOS, P. S. (2001) *Química Nova*, **24**, 345-353.

− VALVERDE, J. L., Cañizares, P., Kou, M. R. S. and Molina, C. B. (2000) *Clays Clay Miner.*, **48**, 424-432.

− VAN OLPHEN, H. (1977) *An Introduction to Colloid Clay Chemistry*. 2nd edition. Interscience, New York.

− VARMA, R.S. (2002) *Tetrahedron*, **58**, 1235-1255.

− VAUGHAN, D. E. W. (1990) *Perspectives in Molecular Sieve Science* (Flank, W. H. and Whyte, Jr. T. E., eds.), *ACS Symp. Series* **368**, American Chemical Society, Washington, DC, 308.

− VELDE, B. (1995) In: *Origin and Mineralogy of Clays, Clays and the Environment*, Springer, Berlin.

− VELGHE, F., Schoonheydt, R.A. and Uytterhoeven, J.B. (1977) *Clay Clay Miner.*, **25**, 375-380.

− VICENTE, M. A. and LAMBERT, J. F. (1999) *Phys. Chem. Chem. Phys.*, **1**, 1633-1639.

− VICENTE, M. A., Bañares-Muñoz, M. A., Suárez, M., Pozas, J. M., López-González, J. D., Santamaría, J. and Jiménez-López, A. (1996[b]) *Langmuir,* **12**, 5143-5147.

− VICENTE, M. A., Meyer, A., Gonzalez, E., Bañares-Muñoz, M. A., Gandía, L. M. and Gil, A. (2002) *Catal. Lett.*, **78**, 99-103.

− VICENTE, M. A., Suárez, M., López-González, J. D. and Banares-Munoz, M. A. (1994) *Clays Clay Miner.*, **44**, 724-730.

− VICENTE, M. A., Suárez, M., López-González, J. D. and Bañares-Muñoz, M. A. (1996[a]) *Langmuir*, **12**, 566-572.

− VIJAYAKUMAR, S., Vijaya, C., Rengaraj, K. and Sivasankar, B. (1994) *Bull. Chem. Soc. Jpn.*, **67**, 3107-3111.

− VLASBOM, J. and DOTOLO, V. A. (1994) U.S. Patent 5,415,789 to Citra Science, 20th September.

− VOGELS, R. J. M. J., Kloprogge, J. T. and Geus, J. W. (2005) *J. Catal.*, **231**, 443-452.

− VOLZONE, C, Cesio, A. M., Torres Sánchez, R. M. and Pereira, E. *(1993) Clays Clay Miner.*, **41**, 702-706.

− VOLZONE, C, Cesio, A. M., Torres Sánchez, R. M. and Pereira, E. *(1995) Clays Clay Miner.*, **43**, 377-382.

− VOLZONE, C. (2001) *Microporous Mesoporous Mater.*, **49**, 197-202.

− VUKOVIĆ, Z., Milutinović-Nikolić, A., Krstić, J., Abu-Rabi, A., Novaković, T. and Jovanović, D. (2005) *Mater. Sci. For.*, **494**, 339-344.

− WALLING, C. (1950) *J. Am. Chem. Soc.*, **72**, 1164-1168.

– WARD, J. W. (1968) *J. Colloid Interf. Sci.*, **28**, 269-277.

– WEYRICH, P. A. and HÖLDERICH, W. F. (1997[a]) *Appl. Catal. A*, **158**, 145-162.

– WEYRICH, P. A., Trevino, H., Hölderich, W. F. and Sachtler, W. M. H. (1997[b]) *Appl. Catal. A*, **163**, 31-44.

– WHITE, R. L. (1992) *Anal. Chem.*, **64**, 2010-2013.

– WILLIAMS, W. A. (1993) PCT Int. Appl. WO 93 02,169 to PPG Industries, Inc., 4th November.

– WILSON, M. J. (1994) *Clay Mineralogy: Spectroscopic and Chemical Determinative Methods*, Chapman and Hall, UK, 1994.

– YADAV, M. K., Chudasama, C. D. and Jasra, R. V. (2004) *J. Mol. Catal. A: Chem.*, **216**, 51–59.

– YANG, R. T., Tharappiwattananon, N. and Long, R. Q. (1998) *Appl. Catal. B: Environ.*, **19**, 289-304.

– YANG, X. (1999) U. S. Patent 5883035 to Engelhard Corporation, 16th March.

– YARIV, S. and MICHAELIAN, K. H. (2002) In: *Organo-Clay Complexes and Interactions* (Yariv, S. and Cross, H., eds) New York, Marcel Dekker, 1-38.

– YEBOAH, S. A., Wang, S. H. and Griffiths, P. R. (1984) *Appl. Spect*, **38**, 259-264.

– YOKUSUKA, M., Makino, Y. and Nakazawa, Y. (1992) Jpn. Kokai Tokkyo Koho JP 06,108,011 to Kao Corp, Japan, 1st October.

– ZHAO, D., Yang, Y. and Guo, X (1995) *Zeolites*, **15**, 58-66.

– ZHU, H. Y. and LU, G. Q. (1998) *J. Porous Mater.*, **5**, 227-239.

– ZHU, H. Y., Zhu, Z. H. and Lu, G. Q. (2000) *J. Phys. Chem. B,* **104**, 5674-5680.